Higher Order QCD Studies of Semi-Inclusive Deep-Inelastic Scattering

Dissertation

der Mathematisch-Naturwissenschaftlichen Fakultät
der Eberhard Karls Universität Tübingen
zur Erlangung des Grades eines
Doktors der Naturwissenschaften
(Dr. rer. nat.)

vorgelegt von
Maurizio Abele
aus Zürich/Schweiz

Tübingen
2023

Gedruckt mit Genehmigung der Mathematisch-Naturwissenschaftlichen Fakultät der Eberhard Karls Universität Tübingen.

Tag der mündlichen Qualifikation:	18.07.2023
Dekan:	Prof. Dr. Thilo Stehle
1. Berichterstatter:	Prof. Dr. Werner Vogelsang
2. Berichterstatter:	Prof. Dr. Thomas Gutsche

ZUSAMMENFASSUNG

In der vorliegenden Dissertation habe ich mich intensiv mit der Berechnung von Beiträgen zu Wirkungsquerschnitten der semi-inklusiven tiefinelastischen Streuung[1] (SIDIS) beschäftigt. Die gewonnenen Ergebnisse können verwendet werden, um Informationen über die Partonverteilungsfunktionen und Fragmentationsfunktionen aus SIDIS-Daten zu erhalten. Sie tragen somit zur genaueren Bestimmung der Nukleonenstruktur bei. Insbesondere führen diese Erkenntnisse auch zu Informationen über die Spinstruktur des Protons.

Im Rahmen der perturbativen Quantenchromodynamik wurden Beiträge zur Störungsreihe der transversalen Strukturfunktion in SIDIS untersucht, welche in allen Ordnungen der laufenden starken Kopplung auftreten. Dieses Phänomen, bekannt als *threshold resummation*, taucht in der Region des Phasenraums auf, in der logarithmische Beiträge zu einer festen Ordnung divergieren. Das Summieren jener logarithmischen Beiträge in allen Ordnungen liefert schließlich endliche Beiträge zur Strukturfunktion. Das Wissen über den Aufbau solcher Beiträge ermöglicht, sie zu einer beliebigen festen Ordnung vorherzusagen. Somit ist eine Näherung der Strukturfunktion in einer festen Ordnung durch sogenannte threshold-Logarithmen möglich. Ziel der vorliegenden Dissertation ist, es eine Näherung der transversalen Strukturfunktion in übernächst-führender Ordnung durch threshold-Logarithmen zu erhalten. Dabei wurden außerdem (führende) Beiträge berücksichtigt, welche in der threshold-Region des Phasenraums unterdrückt sind.

Im letzten Teil der Dissertation wird das Verhalten der SIDIS Strukturfunktionen zur Streuung von longitudinal polarisierten Protonen mit unpolarisierten Elektronen bei kleinen Transversalimpulsen untersucht. In diesem Bereich können SIDIS-Daten besonders gut durch transversalimpulsabhängige Partonverteilungsfunktionen beschrieben werden. Hier wird der Kontakt zu jenen Verteilungsfunktionen von Seiten der kollinearen Faktorisierung hergestellt und die sogenannte T-odd-Asymmetrie im Limes kleiner Transversalimpulse betrachtet.

1 Semi-inclusive deep-inelastic scattering.

PUBLICATIONS

JOURNAL PAPERS

[i] Maurizio Abele, Daniel de Florian, Werner Vogelsang,
Approximate NNLO QCD corrections to semi-inclusive DIS,
Phys.Rev.D 104, 094046 (2021); arXiv: 2109.00847

[ii] Maurizio Abele, Daniel de Florian, Werner Vogelsang,
Threshold resummation at N^3LL accuracy and approximate N^3LO corrections to semi-inclusive DIS,
Phys.Rev.D 106, 014015 (2022); arXiv: 2203.07928

[iii] Maurizio Abele, Matthias Aicher, Fulvio Piacenza,
Andreas Schäfer, Werner Vogelsang,
T-odd proton-helicity asymmetry in semi-inclusive DIS in perturbative QCD,
Phys.Rev.D 106, 014020 (2022); arXiv: 2204.13967

CONTENTS

1 INTRODUCTION 1
- 1.1 Experimental and theoretical discoveries 1
- 1.2 Motivation & outline 8

2 PERTURBATIVE QUANTUM CHROMODYNAMICS 11
- 2.1 Lagrangian 11
- 2.2 Renormalization & asymptotic freedom 13
- 2.3 Quark form factor 17

3 SEMI-INCLUSIVE DEEP-INELASTIC SCATTERING 23
- 3.1 Introduction 23
- 3.2 Cross section 24
- 3.3 Factorization & evolution 26
  - 3.3.1 Leading order coefficient functions 29
  - 3.3.2 Next-to leading order coefficient functions 30
  - 3.3.3 Evolution equations 32
- 3.4 Resummation 35
  - 3.4.1 Next-to leading order coefficient functions in Mellin space 36
  - 3.4.2 Resummation at next-to leading logarithmic accuracy 38
  - 3.4.3 Mellin inversion 40

4 THRESHOLD APPROXIMATIONS 43
- 4.1 Introduction 43
- 4.2 The Drell-Yan process 44
  - 4.2.1 Change of integration order 45
  - 4.2.2 The hard factor 49
- 4.3 Semi-inclusive e^+e^- annihilation 51
  - 4.3.1 Single integration 51
  - 4.3.2 The hard factor 55
- 4.4 Deep-inelastic Scattering 56

5 APPROXIMATE NNLO CORRECTIONS 59
- 5.1 Introduction 59
- 5.2 Perturbative SIDIS cross section 61
- 5.3 Threshold resummation 64
  - 5.3.1 Structure of resummation for Drell-Yan and SIDIS 64
  - 5.3.2 The hard factor H_{qq}^{SIDIS} 66
- 5.4 Subleading contributions near threshold 69
- 5.5 Expansion to NNLO 73

5.6 Phenomenological predictions 76
5.7 Conclusions and outlook 80
6 THRESHOLD RESUMMATION AT N^{3}LL ACCURACY 83
6.1 Introduction 83
6.2 Perturbative SIDIS cross section 84
6.3 Threshold resummation at N^{3}LL accuracy 86
6.4 The hard factor at three loops 89
6.5 Expansion to N^{3}LO 93
6.6 Phenomenological predictions 94
6.7 Conclusions and outlook 100
7 T-ODD PROTON-HELICITY ASYMMETRY 103
7.1 Introduction 103
7.2 Perturbative SIDIS cross section 105
7.3 T-odd single-spin asymmetry at lowest order 108
7.4 Analytical results 112
7.5 Low-q_T limit 113
7.6 Phenomenological results 117
7.7 Conclusions 123
A APPENDIX 125
B APPENDIX 127
B.1 Coefficients for resummation 127
B.2 Near-threshold results in x, z-space 131
C APPENDIX 135
C.1 Derivation of Eq. (7.27) 135
C.2 Perturbative results for the beam-spin asymmetry A_{LU} 136

ACKNOWLEDGEMENTS 139

BIBLIOGRAPHY 141

1

INTRODUCTION

1.1 EXPERIMENTAL AND THEORETICAL DISCOVERIES

Here we introduce the unfamiliar reader to the major discoveries which led to the theory of the strong interaction in order to motivate key concepts used in the theory. We stress that what follows is a short introduction. The vast field of particle physics[1] entails numerous studies in plenty directions. It is a huge scientific enterprise on the theoretical part as well as on the experimental side.

At the end of the first half of the 20th century the proton with a positive electromagnetic charge and the neutron were recognized as the constituents of the atomic nucleus. Experiments showed that these particles, are bound strongly by some other force than the electromagnetic force, named *strong* force. On very small length scales ($\sim 10^{-15}$ m or 1 fm (femtometer)) protons which ought to repulse each other having the same electric charge, seemed very attracted to each other. Hence, at this scale the strong force had to dominate the electromagnetic one. Furthermore the neutron being bound with protons while having no electromagnetic charge encouraged Physicists to investigate this new force.

Likewise, the concept of quantum-mechanical spin was established and Physicists described the observed symmetry between these particles – having roughly the same mass – as isospin. Both particles, proton and neutron, seemed to be two configurations of the same quantum mechanical system (like the spin of an electron) which was called a nucleon. This lead to a precursor of the theory of the strong force. In 1935 Hideki Yukawa proposed a field theoretical approach [4] with particle interaction by exchange of a particle predicting the existence of a new "heavy quantum which has the elementary charge [...] and which obeys Bose's statistics" under the condition that "the interaction [...] should be far greater than that with the light particle." The exchange particle proposed by Yukawa is named pion (written as π^+, π^-, π^0). Indeed, after some time of confusion it was definitively identified by a group around Cecil Frank Powell [5] in 1947 while analyzing emulsion

1 The interested reader is referred to [1, 2], an immensely copious collection of knowledge about particle physics. Of course, Ref. [3] is a great introduction into the field.

photographs of cosmic radiation at high altitudes. Cosmic radiation was the only source of much more energetic particles (order of magnitude: ~ 1 Giga electronvolt, GeV) than artificially generated ones by experiments at the time.

The confusion stemmed from another newly detected particle: the muon having a similar mass as the pion predicted by Yukawa. Powell and collaborators found that the pions decayed into the muons and the latter into electrons (see top left of Fig. 1 for a sketch of the π-μ-e decay) clarifying the prevailing misunderstanding. Here is an example for a negatively charged pion decay:

$$\begin{aligned} \pi^- &\longrightarrow \mu^- + \bar{\nu}_\mu \\ &\hookrightarrow e^- + \bar{\nu}_e \,, \end{aligned} \tag{1.1}$$

where each lepton is accompanied with the corresponding anti-neutrino. A similar process occurs for the π^+ decay while the neutral pion π^0, a superposition of π^+ and π^-, is very short lived and primarily decays by the emission of two photons which can generate a cascade of electron positron pairs and photons.

In a later measurement [6] in 1949 by analyzing electron sensitive plates exposed to cosmic radiation at the Hochalpine Forschungsstation Jungfraujoch[2] Powell's group found even more massive charged particles decaying into three pions:

$$? \longrightarrow 2\pi^+ + \pi^- \,, \tag{1.2}$$

which were not expected to exist. Similar particles were detected in another experiment. Of course this was not yet known. Meanwhile George Rochester and Clifford Butler [7] also detected *strange* particles in cloud chambers induced by the strong force. They selected a series of events "from five thousand photographs taken in an effective time of operation of 1500 hours" as they state in their paper. The decay of these particles or their creation could not be explained by the methods available. The newly found particles triggered V-shaped tracks indicating reactions with at least one neutral particle and two charged particles. They identified different kinds of "forked tracks" where, for example, neutral strange particles decayed into

$$? \longrightarrow \pi^- + p \quad \text{and} \quad ? \longrightarrow \pi^+ + \pi^- \,. \tag{1.3}$$

These particles were not anticipated as opposed to the pion and partially due to this declared as strange. The isospin symmetry between proton and neutron suggested a unique way to distinguish them so there was no explanation for such additional, more massive particles. Furthermore it was not clear at all why such particles interacted strongly and decayed weakly. They appeared rather frequently

2 The astronomical observatory is located on a glacier saddle on the upper snows of the Great Aletsch Glacier and is also referred to as Sphinx Observatory

indicating a fast production which is typical for the strong force while generating very long visible tracks in cloud chambers. Such visible tracks have their origin in longer decay times compared to the ones expected for strongly interacting particles. In fact, they fitted with weakly interacting particles. The decay must have been prevented by some conservation law which was only slightly broken, so that they could decay eventually.

In 1953 Murray Gell-Mann and later in the same year Kazuhiko Nishijima showed this violation of conservation and proposed to consider an additional quantum number to isospin, namely strangeness[3]. It would always be conserved in strong interactions but not conserved under the weak force. This would prevent the particles from decaying at a fast rate but then give rise to a more slow and therefore visible decay through the weak force. As one can see in both "slow", i.e. weak decays in (1.3) strangeness is not conserved whereas if two strange particles interact, strangeness must be conserved which for example is the case in

$$\pi^- + p \longrightarrow \Lambda^0 + K^0 \,. \tag{1.4}$$

Here Λ^0 has strangeness -1 and K^0 has strangeness $+1$. The process is depicted on the top right side of Fig. 1, where each strange particle after being produced through strong interactions, decays through the weak force as observed in (1.3). The inventors of strangeness then postulated a new charge, *hypercharge*, which connects strangeness, isospin and electric charge. One needs further classification since it is not directly obvious how to connect these properties. The particles interacting strongly are referred to as *hadrons* and within this group of particles we discern *mesons* and *baryons*. This distinction originates from the fact that baryons tend to be heavier and mesons tend to be lighter than the proton. We will come back to this distinction below.

Then, more and more hadrons were detected at Cosmotron (3 GeV) in Brookhaven and at Bevatron (6 GeV) in Berkeley. This raised the question: what are the fundamental ones? Hypercharge was a very successive way of categorizing newly found particles but it would not describe the structure of theses particles. At least two fundamental spin $1/2$ particles were needed to build all hadrons but how to account for the strange ones? An additional one being strange should be sufficient. In 1956 Shoichi Sakata proposed proton, neutron and the newly discovered Λ^0. Their masses were – very roughly – the same, hence the idea of an approximate symmetry. This model could explain the nine lightest mesons correctly and introduced a mathematical tool to find such combinations of particles starting from fundamental ones: group theory. Unfortunately this model was not able to correctly predict the lightest eight baryons.

3 A year earlier this was already anticipated by Abraham Pais.

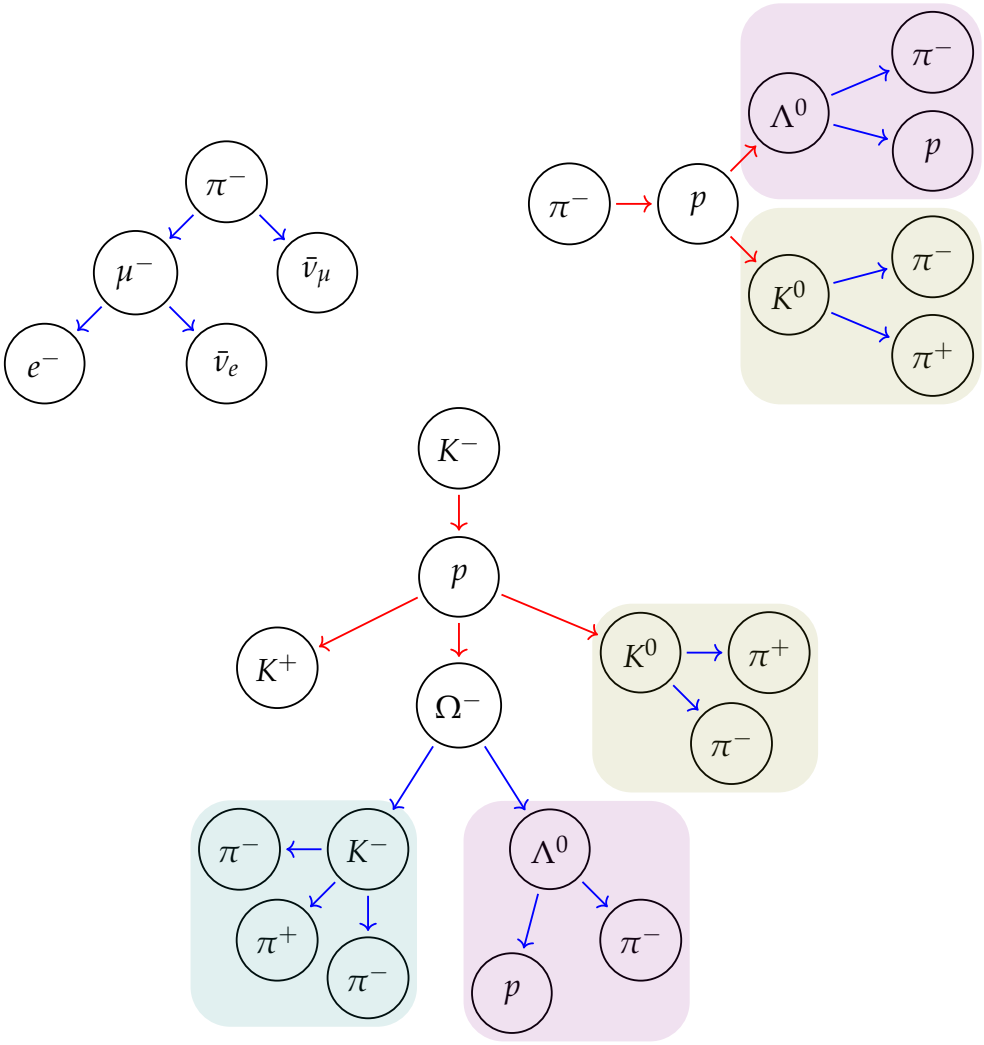

Figure 1: Top-Left: π-μ-e decay. Top-Right: strange particle production (red arrows indicate the strong force) and decay (blue arrows indicate the weak force), here the proton is at rest. Bottom: Ω^- production. The sketches have been adapted from photographs in [8–10].

A few years later, Yuval Ne'eman and Gell-Mann used the available mathematical tools as well and proposed the *eightfold way* [11] where they could effectively describe the detected mesons and baryons. A huge success for the eightfold way was the discovery of the Ω^- baryon in Brookhaven since it was predicted before its existence was known. In a letter [12] to the editors of the Physcial Review BNL physicists pronounced the detection of a negatively charged isospin singlet particle with strangeness -3. It turned out to be the suggested particle. Several months later [10] they confirmed its existence from two events captured in the BNL 80″ hydrogen bubble chamber selected from 120 000 photographs. The Ω^- production was found in the interaction of a K^- and a proton which could be explained by

$$K^- + p \to \Omega^- + K^+ + K^0\,, \tag{1.5}$$

where its decay can be seen in Fig. 1. The two previously mentioned strange decays are part of the Ω^- decay. The K^+ decay is not indicated since it was not included within the frame of the photograph. We stress that this was all found without the knowledge of what kind of fundamental things would build up these measured particles. As Gell-Mann states in Ref. [13] it was discussed "by abstracting the properties from a formal field theory model based on fundamental entities from which baryons and mesons are built up." From the group theoretical arguments it was imposed that at least three fundamental blocks were necessary. In this paper he then proposes to consider a unitary spin $1/2$ triplet consisting of an isospin singlet s with non-integer electric charge $-1/3$ (in units of the elementary charge e) and an isospin doublet (u,d) with electric charges $2/3$ and $-1/3$ respectively. He named these fundamental things "quarks". Around that time George Zweig had different thoughts about this topic as well leading to similar conclusions as Gell-Mann. It was the quark-picture that prevails in the literature to this day. In this picture the composition of the proton would be: two u quarks and one d quark. In general, the anti-quarks were denoted by $\bar{q}$. Furthermore, baryons could be identified as (qqq) and mesons as $(q\bar{q})$ compositions. Of course, the s quark would account for strangeness. We then obtain the following compositions:

$$\begin{aligned}
&\pi^+ : (u\bar{d})\,,\ \pi^- : (\bar{u}d)\,,\ \pi^0 : (u\bar{u} - d\bar{d})\,,\\
&K^0 : (d\bar{s})\,,\ K^+ : (u\bar{s})\,,\ K^- : (\bar{u}s)\,,\\
&\Lambda^0 : (uds)\,,\ \Omega^- : (sss)\,,\ \Delta^{++} : (uuu)\,.
\end{aligned} \tag{1.6}$$

The actual detection of these quarks will be explained below. Three other kinds of quarks have been detected since then: the *charm*, *bottom* and *top* quarks. Their discovery was a lengthy process over a time span of several decades. Since in this dissertation we will concentrate more on the first three quarks, also named *light* quarks, we refrain from introducing the others properly which however should not diminish the importance of their discovery. It is also worth mentioning that

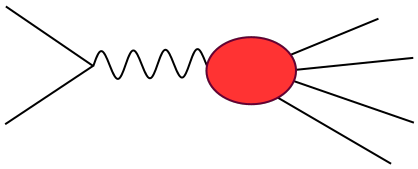

Figure 2: $e^+e^- \to$ hadrons

only after the discovery of the charm quark the whole picture as described here was accepted in the community of theoretical physics. Each type is named "flavor" of the considered quark.

The doubly positively charged Δ^{++} was already known for quite some time. It was found by a group around Herbert Anderson and Enrico Fermi [14] in 1951 in pion nucleon spectroscopy before strangeness or even quarks were discussed widely. It could be reasonably explained within the framework of isospin. But Fermi had pointed out earlier in the 1920s that particles with half-integer spin – named *fermions* – obey a certain statistic where the underlying wave function must be antisymmetric. This could not hold true for a Δ^{++} since it was symmetric in flavor with three u type quarks but simultaneously was a spin $3/2$ particle with symmetric spin wave function. Furthermore, it was expected that the system had vanishing orbital angular momentum. This meant that an additional degree of freedom had to be introduced to make the total wave function antisymmetric. The new charge, named *color*, can have three values, e.g. red, blue and green. Since all observed hadrons are neutral with respect to this charge the name seemed convenient.

An example of one of the most prominent strong interacting processes is electron positron annihilation, also known as $e^+e^- \to$ hadrons. It is an example of an *inclusive* process since it includes every possible product of the collision in the final state. In other words: no specific final state is observed exclusively. In Fig. 2 one can see a scheme of the process where a virtual photon created by the annihilation can induce a complicated final state of multiple color neutral hadrons. The red blob signifies the strong-interacting part. The first approach to this problem is to approximate the decay of the virtual photon into a pair of quarks $\gamma^* \to q\bar{q}$. This is achieved by considering the cross section for $e^+e^- \to \mu^+\mu^-$, as described for example in Ref. [15]

$$\sigma(e^+e^- \to \mu^+\mu^-) = \frac{4\pi}{3}\frac{\alpha^2}{Q^2}\,, \tag{1.7}$$

where α is the fine structure constant and Q is the center of mass energy. Replacing the final state with a quark-antiquark pair we obtain

$$\sigma(e^+e^- \to q\bar{q}) = N_c\,\frac{4\pi}{3}\frac{\alpha^2}{Q^2}\,e_q^2\,, \tag{1.8}$$

where the factor N_c comes from the sum over all possible colors of the quark, i.e. $N_c = 3$, and e_q is the quarks fractional electric charge. The total cross section reads

$$\sigma(e^+e^- \to \text{hadrons}) = \frac{4\pi}{3}\frac{\alpha^2}{Q^2} N_c \sum_q e_q^2 \left(1 + \frac{\alpha_s}{\pi}\right) \equiv \sigma_{\text{tot}}\,, \tag{1.9}$$

where we have included the first correction in α_s, the strong coupling which however is not important here but will be used at a later stage. The ratio of the total cross sections is then given by

$$R^{e^+e^-} = \frac{\sigma(e^+e^- \to \text{hadrons})}{\sigma(e^+e^- \to \mu^+\mu^-)} = N_c \sum_q^{N_f} e_q^2\,, \tag{1.10}$$

where we neglected the α_s contribution and N_f is the number of considered flavors $u, d, s, \ldots$ that could be produced as a quark-antiquark pair. For instance, in the case of a center-of-mass energy $\sqrt{s} < 2m_c$ we obtain $R^{e^+e^-} = 2$ which is confirmed experimentally (see e.g. [16]).

In the late 1960s Bjorken scaling (at high energies) was experimentally confirmed at Stanford Linear Accelerator Center (SLAC) indicating that the proton had a substructure made out of partons, i.e. point-like particles. We will explain Bjorken scaling in more detail in Sec. 3.3. The experimental tool enabling these findings was electron proton scattering $e^- p \to e^- X$. When going to higher energies, i.e. higher momentum transfer, the elastic scattering becomes inelastic and is therefore referred to as deep-inelastic scattering (DIS). The scattering process is sketched out on Fig. 3(d). It was only after the theoretical discovery of asymptotic freedom in the early 1970s, which is the subject of Sec. 2.2, that the full theory of the strong force *quantum chromodynamics* (QCD) was established and partons could safely be associated with quarks and gluons. The gluon being the exchange particle of the strong force comparable to the photon in quantum electrodynamics (QED). QCD as a field theory will be introduced in Sec. 2.1.

As already mentioned we will consider some of the basic concepts of QCD in later Chapters. During the investigation of the structure of nucleons another striking principle appears: factorization. Since hadrons are colorless objects, the bounded state remains hidden to *direct* observation and therefore the mechanisms that confine partons are not yet understood. In DIS the high energetic electron probes the Lorentz contracted proton as a system of almost "free" partons since interactions within the proton are time dilated. Factorization assumes this incoherence and enables the separation of a priori unknown but universal long distance effects and short distance scattering calculable in perturbation theory. In Sec. 3.3 we will explain factorization in more detail. The non-perturbative parts of the observables

in the case of an initial and final hadron are named parton distribution function (PDF) and fragmentation function (FF), respectively. In this picture the compositions in (1.6) do not seem appropriate over a wide kinematical range. This is the reason the quarks in these compositions are named "valence" quarks.

1.2 MOTIVATION & OUTLINE

Extraction of PDFs and FFs from the data needs calculated short distance scattering input. The method for calculating these contributions is perturbation theory. Higher order perturbative QCD calculations are very cumbersome and collective effort of many theoretical physicists lead to remarkable achievements in this field. Nowadays the goal of global PDF and FF analysis has become to be ruled out at next-to-next-to leading order (NNLO) accuracy since perturbative calculations of the short distance scattering are known to that order in the strong coupling. In this dissertation we focus on these perturbative QCD (pQCD) calculations. Some of these perturbative contributions are known to *all* orders in the strong coupling which will be studied in the framework of threshold resummation. This framework will be introduced in Sec. 3.4. Our main focus lies upon such all-order contributions since they may be used to approximate a fixed-order result after expansion in the strong coupling.

In recent years *polarized* PDFs elucidating the protons spin structure gained more attention since polarized short distance cross sections and its corresponding data became available. The decomposition of the proton spin into contributions of quarks, anti-quarks, gluons and orbital motion is an exciting but hard task. The measurement of precise data and perturbative calculations are very involved. In this dissertation we consider two types of polarized semi-inlcusive deep-inelastic scattering (SIDIS) cross sections that can each contribute to better extract polarized PDFs: the more inclusive cross section depending on two kinematical variables x and z and the more differential cross section depending on the transverse momentum $P_{h\perp}$ of the produced hadron. In the seminal works of the de Florian-Sassot-Stratmann-Vogelsang (DSSV) group [17, 18] such spin-dependent PDFs have been extracted. The perturbative input therein was taken at NLO accuracy, where data used in the analysis came from DIS, SIDIS and proton-proton scattering. SIDIS data plays an important role within these studies since it enables a separation of different flavor contributions. Appropriate results of unpolarized and polarized cross sections for SIDIS at NNLO are still missing, while they are available for the remaining processes. As discussed above, NNLO being the new "standard" of perturbative accuracy, a new attempt to upgrade the DSSV PDFs to this level is a natural task

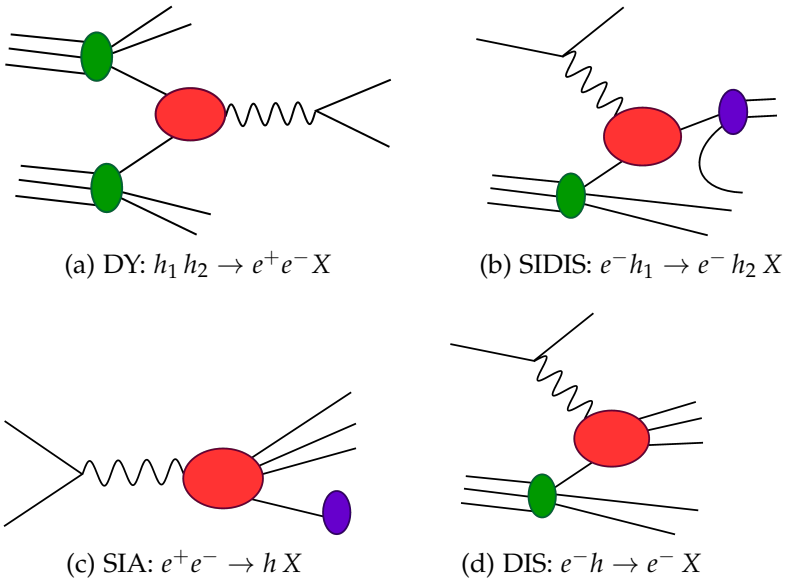

(a) DY: $h_1\, h_2 \to e^+ e^- X$ (b) SIDIS: $e^- h_1 \to e^-\, h_2\, X$

(c) SIA: $e^+ e^- \to h\, X$ (d) DIS: $e^- h \to e^-\, X$

Figure 3: In the left column are processes with a timelike virtual photon, whereas on the right the involved virtual photon is spacelike. The DY process (a) and SIDIS (b) are characterized by two identified hadrons during the scattering process, while in SIA (c) and DIS (d) only one hadron is considered.

to pursue. It becomes even more attractive in light of the Electron-Ion Collider. Currently under construction it will be able to measure polarized SIDIS data at an unprecedented energy range and precision.

The major achievement of this dissertation is the derivation of approximate NNLO, and even N^{3}LO, corrections to unpolarized and polarized SIDIS, enabling a global analysis of (polarized) PDFs or FFs at NNLO accuracy. The unpolarized approximation has recently been included in a global analysis of fragmentation functions [19]. We furthermore significantly improved the threshold resummed SIDIS cross section from [20, 21] including N^{3}LL corrections. The strategy for the derivation of these results is based on the application of several all-order resummation methods to processes that are *known* to NNLO accuracy. In Figure 3 we show theses processes. The green and purple blobs represent PDFs and FFs, respectively.

DY · The Drell-Yan process $h_1\, h_2 \to e^+ e^- X$ is named after Sidney Drell and Tung-Mow Yan. It is shown on Fig. 3(a). The $\mathcal{O}(\alpha_s^2)$ corrections have been derived in Ref. [22]. The threshold resummed contribution to this process bears resemblance with the one for SIDIS.

DIS · Deep-inelastic scattering $e^- h \to e^- X$ is sketched out on Fig. 3(d). The $\mathcal{O}(\alpha_s^2)$ corrections were calculated in Ref. [23].

SIA · Semi-inclusive electron positron annihilation $e^+e^- \to h\,X$ is depicted on Fig. 3(c). The $\mathcal{O}(\alpha_s^2)$ corrections were derived in Ref. [24].

SIDIS · Fig. 3(b) shows semi-inclusive DIS $e^- h_1 \to e^- h_2\,X$. The main focus of this dissertation is placed on SIDIS since its $\mathcal{O}(\alpha_s^2)$ corrections are not yet available. The process involves both PDF *and* FF, an advantage that is used to separate different flavor contributions to the cross section.

Before we present the Outline of this dissertation we want to explain the content of Chapter 7, which does not follow the same thread of the remaining Chapters. Therein we present the single spin asymmetry of unpolarized electrons and polarized protons in SIDIS. At high transverse momentum of the final hadron, i.e. in standard collinear factorization, the lowest order calculation is presented, which has been derived in [25]. Being a T-odd observable these findings may be interesting in itself, in Chapter 7 however we extend this work by considering its *low* transverse momentum behavior. Here we present new results, where we make contact to the framework of transverse-momentum dependent parton distribution functions (TMDs). The transition of these two realms is topic of ongoing research and is still not sufficiently well understood. The "matching" of observables in intermediate regions of the transverse momentum spectrum are summarized e.g. in [26]. We fill the missing spots in Table 2 therein.

After a short introduction to perturbative QCD in Chapter 2, we introduce the SIDIS process in more detail in Chapter 3. The methods used for obtaining approximate fixed-order results from threshold resummed contributions are outlined and illustrated in Chapter 4. Chapter 5 is based on publication [i], where we derive approximate NNLO results to SIDIS. Next to that we extend the threshold formalism for SIDIS in Chapter 6, based on publication [ii], where we perform threshold resummation at $\mathrm{N^3LL}$ accuracy. We also give approximate $\mathrm{N^3LO}$ results to SIDIS in this Chapter. Finally, we introduce the T-odd proton-helicity asymmetry in Chapter 7 which is based on publication [iii]. We show the calculation of the leading order correction to the asymmetry at high transverse momentum based on Ref. [25] and extend this work to the small transverse momentum limit.

2

PERTURBATIVE QUANTUM CHROMODYNAMICS

2.1 LAGRANGIAN

QCD has the structure of a Yang-Mills gauge theory [27]. This implies a specific set of rules for constructing the theory. We will briefly sketch out the main characteristics of the theory by following Chapter 2 in [28] and Chapter 14 in [3]. The Lagrange density $\mathcal{L}_{QCD}$ of the theory must be invariant under local gauge transformations (D dimensional continuous group of transformations) such as

$$\phi'(x) = U(\theta^A)\phi(x) \qquad (A = 1, 2, \ldots, D) \tag{2.1}$$

with

$$U(\theta^A) = \exp\left(ig \sum_{A=1}^{D} \theta^A T^A\right) \sim 1 + ig \sum_{A=1}^{D} \theta^A T^A + \ldots \tag{2.2}$$

Here, the transformation parameters are the quantities θ^A, where for infinitesimal values of θ^A the right hand side is valid. The value g is the coupling of the theory and T^A are the generators of the group[1] of transformations defined by (2.1). The coupling g is often expressed like the fine structure constant in Quantumelectrodynamics (QED) as

$$\alpha_s \equiv \frac{g^2}{4\pi} \,. \tag{2.3}$$

The free quark fields ψ_f are classically described by the following Lagrange density

$$\mathcal{L}_0 = \sum_{f=1}^{N_f} \bar{\psi}_f \left(i\partial\!\!\!/ - m_f\right) \psi_f \tag{2.4}$$

N_f is the number of different flavours. Similar to the case of QED the Lagrangian is invariant under global phase transformation of the quark fields. However, *local* gauge invariance of the Lagrangian yields to a totally different structure than in the case of QED. The N_f independent quark fields each have three components $\psi_f = (\psi_f^R, \psi_f^G, \psi_f^B)^T$: red (R), green (G), blue (B) sometimes also numerated 1,2 & 3

1 A great introduction into group theory and its applications in modern physics can be found in [29] (Section 7.8 therein discusses the $SU(3)$ symmetry)

since the total number of color charges is $N_c = 3$. We impose not only global gauge invariance on the Lagrangian in (2.4) but especially invariance under local phase transformations of the form

$$\psi_f(x) \to U\psi_f(x) \equiv \exp\left(ig\boldsymbol{\theta}(x)\right)\psi_f(x) = 1 + ig\boldsymbol{\theta}(x)\psi_f(x) + \mathcal{O}(\boldsymbol{\theta}^2(x))\,, \tag{2.5}$$

with

$$\boldsymbol{\theta}(x) \equiv \sum_{a=1}^{N_c^2-1} \theta^a(x) T^a\,, \tag{2.6}$$

where $U \in SU(N_c)$ and T^a are the eight $(N_c^2 - 1)$ hermitian and traceless generators of the $SU(N_c = 3)$ group. Usually one takes the matrices $T^a = \lambda^a/2$ first introduced by Gell-Mann [11]. By imposing this *internal* symmetry we need to adjust the derivative in (2.4) since it spoils the invariance of the Lagrange density. This is done by introducing eight gauge fields

$$D_\mu \equiv \partial_\mu + igT^a G^a_\mu\,. \tag{2.7}$$

At first sight, the gauge fields G^a_μ transform as

$$G^a_\mu \;\to\; G^a_\mu - \frac{1}{g}\partial_\mu\theta^a \tag{2.8}$$

in order to compensate the non invariant term from the simple derivative in (2.4) leading to the following Lagrangian with the covariant derivative

$$\mathcal{L}_0 = \bar\psi_f\left(i\not{D} - m_f\right)\psi_f = \bar\psi_f\left(i\not{\partial} - m_f\right)\psi_f - g\bar\psi_f(\gamma^\mu T^a G^a_\mu)\psi_f\,. \tag{2.9}$$

However, the last term on the right hand side is not invariant

$$g\bar\psi_f\gamma^\mu T^a\psi_f \to g\bar\psi_f\gamma^\mu T^a\psi_f - gf^{abc}\theta^b\left(\bar\psi_f\gamma^\mu T^c\psi_f\right)\,, \tag{2.10}$$

because of the non-abelian nature of the $SU(3)$ group:

$$[T^a, T^b] = if^{abc}T^c \neq 0\,. \tag{2.11}$$

By imposing a further restriction to the transformation of the gauge fields

$$G^a_\mu \to G^a_\mu - \frac{1}{g}\partial_\mu\alpha_a - \theta^b f^{abc}G^c_\mu \tag{2.12}$$

the invariance of the Lagrangian is guaranteed. The non-abelian *field strength* in its gauge invariant form is then given by

$$F^a_{\mu\nu} = \underbrace{\partial_\mu G^a_\nu - \partial_\nu G^a_\mu}_{\text{analog. to QED}} - \underbrace{gf^{abc}G^b_\mu G^c_\nu}_{\text{SU(3) non-abelian}}\,. \tag{2.13}$$

What in QED is sometimes referred to as "kinetic" term now additionally contains a gluon self-interacting term responsible for the three and four gluon vertex in the Feynman rules of perturbative QCD. The complete invariant Lagrange density writes

$$\mathcal{L}_{invar} = \bar{\psi}_f \left(i\not{D} - m_f \right) \psi_f - \frac{1}{4} F^a_{\mu\nu} F^{a,\mu\nu} \tag{2.14}$$

Quantization leads to "gauge-fixing" terms from which we describe one method: the *covariant* gauges

$$\mathcal{L}_{gauge} = -\frac{1}{2\xi} \left(\partial^\mu G^a_\mu \right)^2 \tag{2.15}$$

the most prominent ones are: $\xi = 1$ the *Feynman gauge* and $\xi \to 0$ the *Landau gauge*. While using covariant gauges, one needs the introduction of so called *ghost* fields which ensure the unitarity of the "physical" S-matrix used in perturbation theory

$$\mathcal{L}_{ghost} = \partial_\mu \bar{\eta}^a \, \partial^\mu \eta^a + g f^{abc} \, \partial_\mu \bar{\eta}^a \, G^{b,\mu} \eta^c \,, \tag{2.16}$$

where $\eta^a(x)$ are the *Faddeev-Popov* ghost fields. In conclusion we obtain the full Lagrange density

$$\begin{aligned} \mathcal{L}_{QCD} &= \mathcal{L}_{invar} + \mathcal{L}_{gauge} + \mathcal{L}_{ghost} \\ &= \bar{\psi}_f \left(i\not{D} - m_f \right) \psi_f - \frac{1}{4} F^a_{\mu\nu} F^{a,\mu\nu} - \frac{1}{2\xi} \left(\partial^\mu G^a_\mu \right)^2 \\ &\quad + \partial_\mu \bar{\eta}^a \, \partial^\mu \eta^a + g f^{abc} \, \partial_\mu \bar{\eta}^a \, G^{b,\mu} \eta^c \,. \end{aligned} \tag{2.17}$$

This Lagrangian can be used in perturbation theory to derive the Feynman rules of the theory, a helpful system of rules illustrating the calculation of amplitudes by simple diagrams in momentum space. They are presented in Appendix A. In (2.4) we introduced quark masses m_f. Throughout this dissertation we will work in the framework of massless QCD and therefore neglect mass terms in (2.17) in the following. As a consequence we will only need to renormalize the strong coupling which is explained in the next Section.

The main conclusion from this Section is to fully appreciate the fact that QCD does not exclude self interactions as it is the case in QED. This far reaching difference will be clarified in the next Section as the difference in sign of the beta functions of these theories.

2.2 RENORMALIZATION & ASYMPTOTIC FREEDOM

In the last Section we discussed the non-abelian nature of QCD. In this Section we focus on another feature of QCD as a gauge field theory, namely that it is

renormalizable. In calculations of radiative corrections one encounters loop (virtual) contributions, where the integral over the loop momentum includes, a priori, regions at arbitrary high momenta. As a renormalizable theory QCD ensures these divergences, called ultraviolet (UV) divergences, to be removed by a renormalization procedure. This program is justified since we do not expect the theory to accurately predict observables at arbitrary high energies.

Renormalization of the theory implies the assumption that the coupling introduced in (2.2), appearing in the Lagrangian, is not the physical coupling measured in an experiment. Eq. (2.3) is interpreted as the *bare* coupling α_s^b without any physical meaning. The before mentioned UV divergencies are then absorbed into the bare coupling in order to define the physical coupling.

Following Ref. [30], we first sketch out this procedure with help of a more traditional method of regularization: the momentum cut-off. We consider the sum of Born and one-loop contribution in pQCD

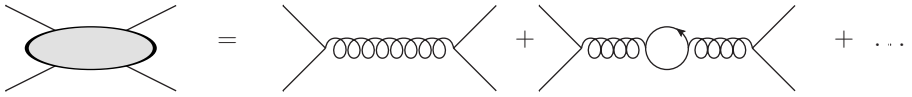

$$\sim \quad \alpha_s^b \left\{ \; 1 \; + \; \alpha_s^b \, b_0 \int_{p^2}^{\Lambda^2} \frac{dk^4}{(k^2)^2} \; + \; \mathcal{O}(\alpha_s^{b\,2}) \; \right\} , \tag{2.18}$$

where Λ^2 is an arbitrary UV scale that serves as a cut-off in the loop integration. The prefactor b_0 is the coefficient of the one-loop amplitude, while p is some external momentum depending on the scattering process. We can rewrite the logarithm of the loop integration by introducing a new scale μ, the renormalization scale, as follows

$$\sim \alpha_s^b \left\{ \; 1 \; + \; \alpha_s^b \, b_0 \left(\ln \frac{\Lambda^2}{\mu^2} + \ln \frac{\mu^2}{p^2} \right) \; + \; \mathcal{O}(\alpha_s^{b\,2}) \; \right\} . \tag{2.19}$$

The physical coupling α_s is then obtained by absorbing the UV divergent term through a redefinition of the bare coupling so that we end up with a finite and cut-off independent expression

$$\sim \alpha_s(\mu) \left\{ \; 1 \; + \; \alpha_s(\mu) \, b_0 \, \ln \frac{\mu^2}{p^2} \; + \; \mathcal{O}(\alpha_s^2(\mu)) \; \right\} , \tag{2.20}$$

where

$$\alpha_s(\mu) \equiv \alpha_s^b \left\{ 1 + \alpha_s^b \, b_0 \ln \frac{\Lambda^2}{\mu^2} + \mathcal{O}(\alpha_s^{b\,2}) \right\} \tag{2.21}$$

is the finite, scale dependent physical coupling[2]. It is universal, i.e. cut-off and process independent. This procedure can be extended to higher orders of the power

2 The bare coupling in (2.19) is expressed through the physical coupling at the scale μ making the contribution cut-off independent, i.e. UV finite.

expansion in α_s so that eventually the renormalization can be achieved by redefining the bare coupling in the Lagrange density. Subtracting only divergent contributions is referred to as *minimal subtraction* renormalization scheme which we will use throughout this dissertation with a slight modification of subtracting an additional finite factor $S^\epsilon = e^{-\epsilon\gamma_E}(4\pi)^\epsilon$, named $\overline{\text{MS}}$ scheme[3].

Commonly one chooses the method of dimensional regularization instead of a cut-off, where the 4 space-time dimensions are extended to $d = 4 - 2\epsilon$ dimensions. By using this method the UV divergences appear as poles $1/\epsilon$ that diverge when taking the limit $\epsilon \to 0$, i.e. going back to four dimensions. Such poles also appear in later Chapters as infrared divergences, another class of divergences that can be made manifest in dimensional regularization. After introducing d dimensions the bare coupling is not a dimensionless quantity anymore. In order to stay a bare quantity a new scale μ, the renormalization scale, must be introduced $\alpha_s^b = \alpha_s'^b\,\mu^{2\epsilon}$. From now on we work in the framework of dimensional regularization and name the bare quantity α_s^b (not $\alpha_s'^b$).

The scale dependence of the physical coupling $\alpha_s(\mu)$, also referred to as *running* coupling, seems appropriate since in an experiment we measure observables at a certain scale which we mostly identify with the momentum transfer of the particle collision. From this perspective we observe that the theory does not make a prediction of the actual size of the coupling. However, its scale dependence is unambiguously predicted which is reflected by the renormalization group equation

$$\frac{d\ln\alpha_s}{d\ln\mu^2} = \beta(\alpha_s) = \alpha_s\left(-b_0 - \alpha_s\, b_1 - \alpha_s^2\, b_2 - \alpha_s^3\, b_3 + \dots\right)\,, \tag{2.22}$$

where $\beta(\alpha_s)$ is the QCD beta-function with its coefficients b_i given in (B.1). Solving this equation up to $\mathcal{O}(\alpha_s^4)$, see e.g. [31, 32], leads to the connection of the coupling at scale μ with the coupling at another scale μ_R

$$\begin{aligned}
\alpha_s(\mu) = {}& \frac{\alpha_s(\mu_R)}{X} - \left(\frac{\alpha_s(\mu_R)}{X}\right)^2 \frac{b_1}{b_0}\ln X \\
&+ \left(\frac{\alpha_s(\mu_R)}{X}\right)^3 \left(\frac{b_1^2}{b_0^2}\left(\ln^2 X - \ln X + X - 1\right) - \frac{b_2}{b_0}(X-1)\right) \\
&+ \left(\frac{\alpha_s(\mu_R)}{X}\right)^4 \left(\frac{b_1^3}{b_0^3}\left(X - \frac{1}{2}X^2 - \ln^3 X + \frac{5}{2}\ln^2 X + 2(1-X)\ln X - \frac{1}{2}\right)\right. \\
&\qquad \left. + \frac{b_1 b_2}{b_0^2}(-X(1-X) + 2X\ln X - 3\ln X) + \frac{b_3}{2b_0}\left(1 - X^2\right)\right)\,,
\end{aligned} \tag{2.23}$$

3 γ_E is the Euler-Mascheroni constant.

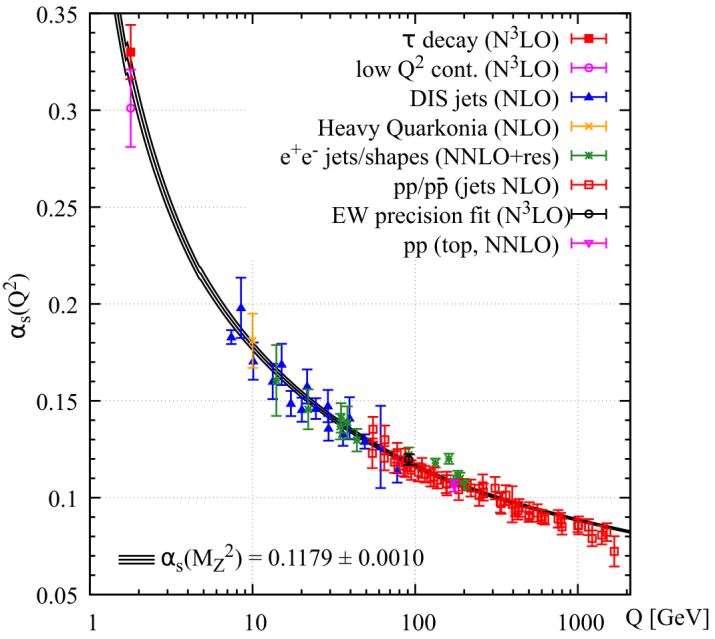

Figure 4: Collection of measurements of the running strong coupling taken from [35]. Since the scales in (2.23) always appear as logarithms of the square of scales, it is common to write $\alpha_s(\mu^2)$ instead of $\alpha_s(\mu)$.

where

$$X \equiv 1 + b_0 \alpha_s(\mu_R) \ln \frac{\mu^2}{\mu_R^2} . \tag{2.24}$$

If we consider the lowest order contribution in (2.23) at a scale Q with a reference scale $\mu_R = M_Z \sim 90$ GeV

$$\alpha_s(Q) \;=\; \frac{\alpha_s(M_Z)}{1 + b_0\, \alpha_s(M_Z)\, \ln \frac{Q^2}{M_Z^2}} , \tag{2.25}$$

where $b_0 = \left(11 C_A - 2N_f\right)/12\pi$ with $C_A = N_c$, the coupling decreases at higher scales Q for positive values of b_0. As long as N_f, the number of active flavours, is less than 16 this is fulfilled in QCD[4]. It is now possible to measure the strong coupling in an experiment at momentum scale $\sim M_Z$ and predict its value at other scales. Fig. 4 shows experimental measuring of the running strong coupling compared to its theoretical scale dependence prediction $\alpha_s(Q)$. The phenomenon of the decreasing running strong coupling at higher energies is called *asymptotic freedom*, a central property of QCD. It justifies the use of perturbation theory at high energies. Asymptotic freedom was derived in [33, 34].

It is worth discussing to which point asymptotic freedom is sensible and hence the use of perturbation theory is justified to make predictions. A scale with the

4 So far, only $N_f = 6$ has been observed in nature as discussed in Sec. 1.1.

property $\mu \to \mu_L$ is called a *Landau pole* $\Lambda_{\rm QCD}$ which is experimentally confirmed by the so called *Confinement* property of QCD. By Confinement we mean the fact that quarks and gluons do not appear as free particles but only as bound, colorless composites. Since $\Lambda_{\rm QCD} < 1$ GeV, it is suitable to make perturbative predictions for $Q > 2$ GeV which is confirmed by Fig. 4 where the running strong coupling remains a small parameter with $\alpha_s(2\text{GeV}) \sim 0.3$.

As mentioned above within perturbative calculations of cross sections infrared (IR) divergent terms appear. In dimensional regularization they are manifested by $1/\epsilon$ poles. As was shown in [36, 37], it is possible to define observables within pQCD that are infrared *safe*. They do not depend on the long distance behavior of the theory. The cancellation of these divergences is expected in general and known as Kinoshita-Lee-Nauenberg theorem [38, 39].

2.3 QUARK FORM FACTOR

Since Sudakov[5] exponentiation or resummation, is one of the main topics in this dissertation we give an example by introducing the dimensionally regulated electromagnetic form factor of a massless quark following Ref. [41]

$$\Gamma_\mu \;=\; i\, e_q\, \bar{u}(p')\, \gamma_\mu\, u(p)\, \mathcal{F}^q(\alpha_s, Q^2, \epsilon), \tag{2.26}$$

with $Q^2 = (p' - p)^2$. Perturbative QCD corrections to this amplitude have been studied for a long time and are nowadays known to four loops [42]. The discussion of the quark form factor (QFF) here should not be seen as an introduction to resummation. We rather want to make contact with a fundamental pQCD amplitude exhibiting contributions that are known to all orders in the strong coupling. A more suitable introduction to resummation for the purpose of this dissertation will be given at later stage. Figure 5 shows some Feynman diagrams that contribute to Γ_μ. The quark form factor $\mathcal{F}^q$ is a fundamental quantity in pQCD and has multiple applications. For example, in inclusive DIS it collects all virtual higher-order corrections of the hard scattering coefficient function. The infrared divergences from the QFF then cancel in combination with the real emission contributions.

The quark form factor exponentiates as

$$\mathcal{F}^q(Q^2, \epsilon) = \exp\left\{ \frac{1}{2} \int_0^{Q^2} \frac{d\eta^2}{\eta^2} \left[K(\alpha_s(\mu), \epsilon) + G\left(\frac{\eta^2}{\mu^2}, \alpha_s(\mu), \epsilon \right) \right] \right\}, \tag{2.27}$$

5 First introduced by V.V. Sudakov in 1956 [40].

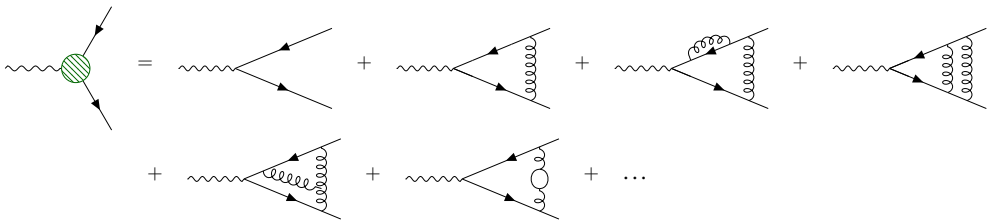

Figure 5: The LO and some higher order diagrams contributing to the $\gamma^* qq/\gamma^* q\bar{q}$ vertex, also known as electromagnetic quark form factor with spacelike or timelike virtual photon. The NLO to NNLO contributions were calculated in [43–49]. The three loop contributions were calculated in [50–52]. The explicite coefficients are given in Chapters 5 & 6.

since it obeys the following evolution equation [41, 53–56]

$$Q^2 \frac{\partial}{\partial Q^2} \ln \mathcal{F}^q \left(\alpha_s(\mu), \frac{Q^2}{\mu^2}, \epsilon \right) = \frac{1}{2} \left[K(\alpha_s(\mu), \epsilon) + G \left(\frac{Q^2}{\mu^2}, \alpha_s(\mu), \epsilon \right) \right] . \tag{2.28}$$

The function K contains all infrared singularities manifested by poles in ϵ, whereas G is infrared finite and includes the scale dependence on Q^2, i.e. it summarizes ultraviolet behavior and has at most a single logarithm in Q^2/μ^2. Both are perturbative functions. We can find explicit expressions for K and G by using (2.28) and the QFF to a specific order, e.g. for a spacelike photon ($-q^2 = Q^2$) at one loop [45, 57–59]

$$\mathcal{F}^q(Q^2, \epsilon) = 1 + \frac{\alpha_s}{\pi} \left(\frac{Q^2}{\mu^2} \right)^{-\epsilon} C_F \left\{ -\frac{1}{2\epsilon^2} - \frac{3}{4\epsilon} + \frac{\pi^2}{24} - 2 \right.$$
$$\left. + \left(\frac{7\zeta(3)}{6} + \frac{\pi^2}{16} - 4 \right) \epsilon + \mathcal{O}\left(\epsilon^2\right) \right\} . \tag{2.29}$$

We can then read of the coefficients

$$K^{(1)} = C_F \frac{1}{\epsilon} , \tag{2.30}$$

$$G^{(1)} = C_F \left(\frac{\mu^2}{Q^2} \right)^{\epsilon} \left\{ \frac{1}{\epsilon} + \frac{3}{2} + \left(4 - \frac{\pi^2}{12} \right) \epsilon \right.$$
$$\left. + \left(8 - \frac{7\zeta(3)}{3} - \frac{\pi^2}{8} \right) \epsilon^2 + \mathcal{O}\left(\epsilon^3\right) \right\} - C_F \frac{1}{\epsilon} . \tag{2.31}$$

When taking the limit $\epsilon \to 0$, i.e. going back to the ordinary four dimensions, we find

$$G \left(\frac{Q^2}{\mu^2}, \alpha_s(\mu), \epsilon \right) = -\frac{\alpha_s}{\pi} C_F \left(\ln \frac{Q^2}{\mu^2} - \frac{3}{2} \right) + \mathcal{O}(\alpha_s^2) , \tag{2.32}$$

which is known as leading-logarithmic (LL) contribution to the QFF. The expression fixates the leading behavior of the momentum transfer dependence of the QFF to all orders of the power expansion in the running strong coupling.

The full solution of (2.28) in dimensional regularization is more involved than what we have shown so far. In the following we sketch out a solution of (2.28) following [56]. First, we notice that the QFF is independent of the renormalization scale:

$$\mu \frac{d}{d\mu}(K+G) = 0\,. \tag{2.33}$$

We therefore know that G and K each have renormalization group equations

$$\left(\mu^2\frac{\partial}{\partial\mu^2} + \beta(\alpha_s,\epsilon)\frac{\partial}{\partial\alpha_s}\right) G\left(\frac{Q^2}{\mu^2},\alpha_s,\epsilon\right) = A_q(\alpha_s)\,, \tag{2.34}$$

$$\left(\mu^2\frac{\partial}{\partial\mu^2} + \beta(\alpha_s,\epsilon)\frac{\partial}{\partial\alpha_s}\right) K\left(\alpha_s,\epsilon\right) = -A_q(\alpha_s)\,, \tag{2.35}$$

where A_q is a perturbative function

$$A_q(\alpha_s) = \frac{\alpha_s}{\pi}A_q^{(1)} + \left(\frac{\alpha_s}{\pi}\right)^2 A_q^{(2)} + \dots \tag{2.36}$$

with

$$A_q^{(1)} = C_F\,, \qquad A_q^{(2)} = \frac{1}{2}\,C_F\left[C_A\left(\frac{67}{18}-\frac{\pi^2}{6}\right)-\frac{5}{9}N_f\right]\,, \tag{2.37}$$

where $C_F = 4/3$, $C_A = 3$ and N_f is the number of active flavours. Its higher-order coefficients are given in (B.4). The ϵ dependent β function introduced above is given by

$$\beta(\alpha_s,\epsilon) = \frac{d\ln\bar{\alpha}_s}{d\ln\mu^2} = -\epsilon + \bar{\alpha}_s\left(-b_0 - \bar{\alpha}_s b_1 + \dots\right)\,, \tag{2.38}$$

which is solved (in the lowest nontrivial order) by

$$\bar{\alpha}_s\left(Q,\alpha_s,\epsilon\right) = \alpha_s(\mu_R)\left(\frac{Q^2}{\mu_R^2}\right)^{-\epsilon}\left[1-\frac{b_0\,\alpha_s(\mu_R)}{\epsilon}\left(\left(\frac{Q^2}{\mu_R^2}\right)^{-\epsilon}-1\right)\right]^{-1}\,, \tag{2.39}$$

where $\bar{\alpha}_s(Q=\mu_R) = \alpha_s(\mu_R)$ is the boundary condition and higher order contributions to the running strong coupling in d dimension are given[6] in [47]. We observe that the expression from (2.25) is reproduced in the low ϵ limit. A solution of Eq. (2.34) is now obtained by [47, 56, 60]

$$G\left(\frac{Q^2}{\mu^2},\alpha_s(\mu),\epsilon\right) = G\left(1,\bar{\alpha}_s\left(Q,\alpha_s,\epsilon\right),\epsilon\right) + \int_{Q^2}^{\mu^2}\frac{d\lambda^2}{\lambda^2}A_q\left(\bar{\alpha}_s\left(\lambda,\alpha_s,\epsilon\right)\right)\,. \tag{2.40}$$

6 Eq.(2.8) in [47] seems to be missing a factor λ^ϵ compared to Eq.(2.7) in [56], where $\lambda = Q^2/\mu_R^2$.

Inserting this into (2.27) yields the exponentiation of the QFF

$$\mathcal{F}^q\left(\alpha_s(\mu), \frac{Q^2}{\mu^2}, \epsilon\right) = \exp\left\{\frac{1}{2}\int_0^{Q^2}\frac{d\eta^2}{\eta^2}\left[K(\alpha_s(\mu),\epsilon) + G\left(1, \bar{\alpha}_s\left(\eta, \alpha_s, \epsilon\right), \epsilon\right)\right.\right.$$
$$\left.\left. + \int_{\eta^2}^{\mu^2}\frac{d\lambda^2}{\lambda^2} A_q\left(\bar{\alpha}_s\left(\lambda, \alpha_s, \epsilon\right)\right)\right]\right\}, \quad (2.41)$$

where the counter term function K can be determined recursively [56]. The computation of the integrals in (2.41) involves nested sums, and is more involved when considering higher order contributions to (2.39). We refer the reader to Ref. [47, 56], where the steps during the integration are explained in more detail. In the one-loop approximation we presented so far, the QFF is compactly expressed in terms of an analytic function

$$\ln \mathcal{F}^q(Q, \alpha_s, \epsilon) = -\frac{2}{4\pi b_0}\left[\frac{1}{\epsilon}A_q^{(1)}\mathrm{Li}_2\left(\frac{b_0\,\alpha_s(Q)}{b_0\,\alpha_s(Q)+\epsilon}\right) + G^{(1)}\ln\left(1+\frac{b_0\,\alpha_s(Q)}{\epsilon}\right)\right]. \quad (2.42)$$

After expansion in the strong coupling and inserting the coefficients for $A_q^{(1)}$ and $G^{(1)}$, we obtain the first order result from (2.29), where we set $Q = \mu$.

The quark form factor will be an essential ingredient when determining the hard virtual contributions in SIDIS at NNLO or N^{3}LO. We therefore need $\mathcal{F}_q$ up to α_s^3 which was found in [47]. There, the QFF was extracted from the third-order computation of DIS structure functions. Since it is a fundamental quantity and therefore different renormalzation schemes may be of interst, the QFF is usually given as a bare quantity expanded in the bare coupling α_s^b which is related to α_s by

$$\alpha_s^b \;=\; Z_{\alpha_s}\,\alpha_s\,. \quad (2.43)$$

We work in the $\overline{\mathrm{MS}}$ scheme with the renormalization constant

$$Z_{\alpha_s} = 1 - \frac{b_0}{\epsilon}\alpha_s + \left(\frac{b_0^2}{\epsilon^2} - \frac{b_1}{2\epsilon}\right)\alpha_s^2 - \left(\frac{b_0^3}{\epsilon^3} - \frac{7}{6}\frac{b_1 b_0}{\epsilon^2} + \frac{1}{3}\frac{b_2}{\epsilon}\right)\alpha_s^3 + \mathcal{O}(\alpha_s^4)\,. \quad (2.44)$$

The bare (unrenormalized) spacelike QFF, where $q^2 < 0$, is then expressed by

$$\mathcal{F}_b^q(\alpha_s^b, Q) \;=\; 1 + \sum_{n=1}^{\infty}\left(\frac{\alpha_s^b}{\pi}\right)^n\left(\frac{Q^2}{\mu^2}\right)^{-n\epsilon}\mathcal{F}_q^{(n)}\,. \quad (2.45)$$

The *timelike* ($q^2 > 0$, both quarks are in the initial or final state) and *spacelike* ($q^2 < 0$, one quark in the initial and one quark in the final state) QFFs differ by an imaginary part from the ϵ expansion of $(q^2)^{-\epsilon}$ which is gathered in the following factor[7]

$$\Delta(q^2) = \begin{cases} (-1 - i0)^{-\epsilon} & \text{for} \quad q^2 > 0 \\ 1 & \text{for} \quad q^2 < 0 \end{cases} \tag{2.46}$$

with

$$(-1 - i0)^{-\epsilon} = 1 - i\pi\epsilon - \frac{\pi^2\epsilon^2}{2} + \frac{1}{6}i\pi^3\epsilon^3 + \frac{\pi^4\epsilon^4}{24} + \mathcal{O}\left(\epsilon^5\right) \tag{2.47}$$

for small ϵ. The bare timelike quark form factor, where $q^2 > 0$, is then given by

$$\mathcal{F}_b^q(\alpha_s^b, Q) \;=\; 1 + \sum_{n=1}^{\infty} \left(\frac{\alpha_s^b}{\pi}\right)^n \left(\frac{Q^2}{\mu^2}\right)^{-n\epsilon} \Delta(q^2)\, \mathcal{F}_q^{(n)} \,. \tag{2.48}$$

The renormalized coefficients $F_q^{(i)}$ are obtained by [47, 51]

$$\begin{aligned} F_q^{(1)} &= \mathcal{F}_q^{(1)}\, \Delta(q^2) \,, \\ F_q^{(2)} &= \mathcal{F}_q^{(2)}\, (\Delta(q^2))^2 - \frac{\pi b_0}{\epsilon} \mathcal{F}_q^{(1)}\, \Delta(q^2) \,, \\ F_q^{(3)} &= \mathcal{F}_q^{(3)}\, (\Delta(q^2))^3 - \frac{2\pi b_0}{\epsilon} \mathcal{F}_q^{(2)}\, (\Delta(q^2))^2 - \left(\frac{\pi^2 b_0^2}{\epsilon^2} - \frac{\pi^2 b_1}{2\epsilon}\right) \mathcal{F}_q^{(1)}\, \Delta(q^2) \,. \end{aligned} \tag{2.49}$$

Explicit expressions of the renormalized coefficients can be found in Sec. 5.3 and Sec. 6.4.

The QFF will be used to determine the hard virtual factor H_{qq}^{SIDIS} appearing in the refactorized hard scattering function in Chapters 5 & 6. For this we will subtract all divergences from F_q by a method that will be explained in Chapter 4. It is therefore a vital ingredient for the approximate NNLO corrections to SIDIS. Before we use the QFF, we introduce the SIDIS process in more detail.

7 This factor corresponds to Eq. (4.1) in [47], where it is written in terms of Γ functions.

3

SEMI-INCLUSIVE DEEP-INELASTIC SCATTERING

3.1 INTRODUCTION

In this Chapter, we give an introduction to the characteristics of semi-inclusive deep-inelastic scattering, formerly known as one-particle (or hadron) inclusive leptoproduction [61, 62]. As the name suggests it is based on inclusive deep-inelastic lepton proton scattering (DIS). Since in SIDIS a hadron is detected in the final state, it is named *semi*-inclusive. As already mentioned in Chapter 1, it is part of the QCD sensitive processes and hence gives insights into the structure of nucleons. In particular, parton distribution *and* fragmentation functions can be extracted simultaneously from SIDIS observables. This is not the case for e^+e^- annihilation. So far data used for global analyses of fragmentation functions is largely based on e^+e^- annihilation data and hence SIDIS data plays an important role within these studies being an additional source of information about the fragmentation of hadrons.

We will consider SIDIS in the so called *current* fragmentation region, where standard collinear factorization can be applied. During the particle collisions secondary hadron fragmentation can occur in the beam or target remnants that do not have their origin in the hard scattering. We do not include such target fragmentation and assure current fragmentation by considering a cut on the fragmentation scaling variable ($z > 0.2$) which will be defined below. This excludes target fragmentation, where fracture functions have to be involved.

SIDIS also provides insights into the spin structure of the proton. In the works of the DSSV group [17, 18] measurements of SIDIS asymmetries have been used in a global analysis to extract the nucleon's helicity distribution. The uncertainties in SIDIS data used there are still large. A new experiment, the Electron-Ion-Collider currently under construction in the USA, brings the prospect of more precise data calling for even more precise pQCD calculations which is the main motivation for higher order studies in SIDIS.

The contents of Chapters 5 & 6 rely on the findings of Refs. [20, 21] which we want to outline in the present Chapter. The latter can be seen as the preparing work for

the application of the methods developed in Chapter 4 to SIDIS in Chapters 5 & 6, where we take significant steps further. We not only extend resummation in SIDIS from NLL to N^{3}LL accuracy but also investigate its all-order structure including the hard factor in the threshold limit in order to give approximate NNLO or even N^{3}LO corrections. In the following we introduce the SIDIS cross section in Section 3.2 and its factorization in Section 3.3 from the perspective of Refs. [20, 21]. Section 3.4 addresses NLL resummation in Mellin space.

3.2 CROSS SECTION

Semi-inclusive deep-inelastic scattering is characterized by

$$\ell(k)\; p(P) \;\to\; \ell'(k')\; h(P_h)\; X\,, \tag{3.1}$$

where ℓ denotes the beam lepton, p the proton target and h the observed hadron in the final state. The momenta of these particles are given in parentheses and are depicted in Fig. 6, where we show the virtual photon as exchange particle for the electromagnetic interaction between the proton and the lepton. By X we mean everything else produced in the collision which is not detected. The blobs with different colors schematically illustrate the separation of the long distance interactions within the initial proton (green) or the detected hadron (purple) and the short distance interactions (red) which will be addressed in the next Section. Both the incoming lepton as well as the target proton may be polarized. The final-state hadron however is, in our case, restricted to be unpolarized, although there have been studies for polarized Λ Production [63, 64] in SIDIS. That case offers the opportunity to study spin transfer reactions as opposed to spinless mesons like pions and kaons for which usually one studies the SIDIS process. Another "invaluable" feature of SIDIS, as mentioned in Ref. [64], is flavor separation of fragmentation functions. In contrast to other processes involving FFs, SIDIS is unique in separating information of the different flavors present in hadrons.

The electromagnetic interaction between the lepton and the proton is approximated by the exchange of a virtual photon γ^* with momentum transfer $q = k - k'$ and virtuality $Q^2 = -q^2$. The kinematic variables used in SIDIS are defined by

$$\begin{aligned} Q^2 \;&=\; -q^2 \;=\; -(k-k')^2\,, \quad x \;=\; \frac{Q^2}{2P\cdot q}\,, \\ y \;&=\; \frac{P\cdot q}{P\cdot k}\,, \quad z \;=\; \frac{P\cdot P_h}{P\cdot q}\,, \end{aligned} \tag{3.2}$$

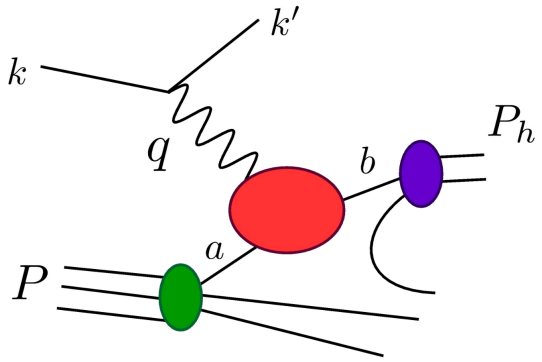

Figure 6: SIDIS process with labeled momenta

where x is the Bjorken variable known from DIS. The newly introduced variable z is called fragmentation variable. The unpolarized SIDIS cross section differential in these variables may be written as [61, 62, 64–67]:

$$\frac{d^3\sigma^h}{dxdydz} = \frac{4\pi\alpha^2}{Q^2}\left[\frac{1+(1-y)^2}{2y}\mathcal{F}_T^h(x,z,Q^2)+\frac{1-y}{y}\mathcal{F}_L^h(x,z,Q^2)\right], \tag{3.3}$$

where α is the fine structure constant. $\mathcal{F}_T^h$ and $\mathcal{F}_L^h$ are the transverse and the longitudinal structure functions; they are related to the more customary structure functions F_1^h and F_L^h by $\mathcal{F}_T^h \equiv 2F_1^h$ and $\mathcal{F}_L^h \equiv F_L^h/x$.

As we already saw in the case of electron-positron annihilation in Section 1.1, experimentally it is common to measure ratios of cross sections. In the case of SIDIS one usually measures the SIDIS hadron multiplicity

$$R_{\text{SIDIS}}^h \equiv \frac{d^3\sigma^h/dxdydz}{d^2\sigma/dxdy}, \tag{3.4}$$

where $d^2\sigma/dxdy$ is the cross section for inclusive DIS, $\ell p \to \ell X$, given by

$$\frac{d^2\sigma}{dxdy} = \frac{4\pi\alpha^2}{Q^2}\left[\frac{1+(1-y)^2}{2y}\mathcal{F}_T(x,Q^2)+\frac{1-y}{y}\mathcal{F}_L(x,Q^2)\right], \tag{3.5}$$

where the structure functions are defined as $\mathcal{F}_T = 2F_1$ and $\mathcal{F}_L = F_L$.

The SIDIS structure functions $\mathcal{F}_i^h$ with $i \in \{T, L\}$, but in particular the transverse one, are the central objects of our interest in this work. The pioneering work in [61] obtained next-to leading order (NLO) corrections to these structure functions. We show in the next Section how to calculate such theoretical predictions using standard pQCD techniques. A key principle that enables this calculation is factorization.

3.3 FACTORIZATION & EVOLUTION

The parton model, introduced by Richard Feynman, James Bjorken and Emmanuel A. Paschos [68, 69] assumes[1] free quarks within the hadron interacting weakly at high energies $Q \gg 2$ GeV, i.e. short distances $\sim 1/Q$. It was originally formulated in the framework of DIS, not in SIDIS. The remaining dynamics in the hadron happen at greater distances and hence lower energies. A natural consequence is to *factorize* the long distance and short distance physics

$$\mathcal{F}_T \sim \omega_f^T \otimes f \,, \tag{3.6}$$

where f is a non-perturbative function and ω_f^T is a perturbative function in the strong coupling, also named hard scattering coefficient function. The parton model predicts the scaling of the structure function, named Bjorken scaling [70], meaning that at high momentum transfer Q the structure function becomes scale independent. Its success reinforced the picture of a nucleon containing point-like constituents, namely partons. This can be understood by the the fact that at higher energies higher spatial resolution is expected which implies a pointlike structure, i.e. no structure at all, if the structure function is independent of the resolution scale. However, Bjorken scaling is approximate and does not hold in general. Its violation could only be fully understood in the framework of QCD involving quark-gluon *and* gluon-gluon interactions as an asymptotically free gauge theory, where the scale dependence of the non-perturbative function f governed by its *evolution* equation is taken into account[2]. Nevertheless, the parton model, as a precursor to QCD, and the corresponding experimental findings of Bjorken scaling achieved to correctly forecast a non trivial substructure of the proton.

In Subsection 3.3.2 the perturbative part of the cross section will exhibit initial and final state collinear divergences when calculating Feynman diagrams including higher order pQCD corrections, i.e. gluonic interactions. These collinear singularities may be interpreted as sensitivity to the factorization of long-distance and short-distance physics. The question of how to remove that sensitivity then arises. As we will see below universal factorization of collinear singularities assures to obtain a finite short distance function. Factorization can also be understood by exploiting the analogy to renormalization in Sec. 2.2. While absorbing collinear divergences into the *bare* parton density one assumes it to be the physical density. This introduces a new scale μ_F, called factorization scale.

By universal factorization, as described in [71], we mean the factorization of long distance effects into *universal* functions describing the distribution of partons in a

1 Asymptotic freedom was not yet discovered.
2 This is sometimes referred to as the QCD improved parton model.

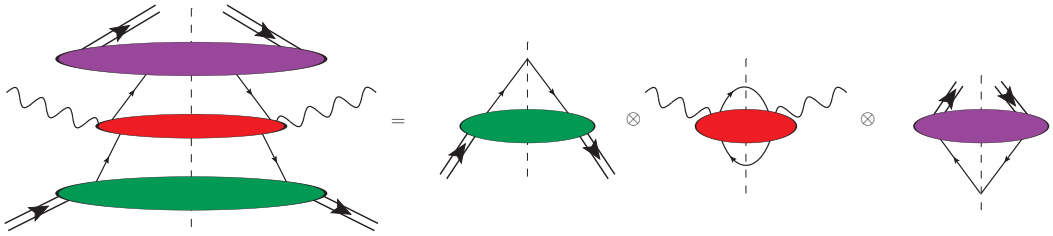

Figure 7: Collinear factorization for the SIDIS process, adapted from [62]

hadron or the fragmentation of partons into a hadron. It is sketched out diagrammatically for SIDIS in Fig. 7. Universality in this context means that the distribution and fragmentation functions are independent of the high energy process. Thus, these functions are an intrinsic property of the hadron. Being universal, these functions may be extracted in a number of experiments. The remaining perturbative short distance function then becomes independent of the hadron structure. In practice, the densities can be extracted in one experiment at a certain scale, then evolved to another scale in order to predict the cross section in a different experiment at that new scale, while using the appropriate short distance function. Combining a wide range of data from different processes for these distributions leads to, so called, *global* analyses.

In this Section we focus on the calculation of the structure functions $\mathcal{F}_T^h$ and $\mathcal{F}_L^h$ using factorization, following Refs. [71, 72][3]. They are expressed by the following factorization formula

$$\mathcal{F}_i^h(x,z,Q^2) = \sum_{f,f'} \int_x^1 \frac{d\hat{x}}{\hat{x}} \int_z^1 \frac{d\hat{z}}{\hat{z}} D_{f'}^h\left(\frac{z}{\hat{z}},\mu_F\right) \omega_{f'f}^i\left(\hat{x},\hat{z},\alpha_s(\mu_R),\frac{\mu_R}{Q},\frac{\mu_F}{Q}\right) f\left(\frac{x}{\hat{x}},\mu_F\right) . \tag{3.7}$$

for partons $f, f' = q, \bar{q}, g$. and where $i \in \{L, T\}$. $f(\xi, \mu_F)$ is the distribution of finding parton f with momentum fraction ξ in the nucleon with total momentum P. The fragmentation function $D_{f'}^h(\zeta, \mu_F)$ describes the fragmentation of the parton f' into the observed hadron h. The factorization formula (3.7) only considers contributions to the cross section that are not suppressed by higher powers of $1/Q^2$ or $1/Q$. Within this thesis such contributions, also known as power corrections, are neglected. This is referred to as leading *twist*.

Once this separation is effected, the *hard* scattering coefficient function $\omega_{f'f}^i$ is calculable in pQCD. It describes the interaction of the involved particles in the framework of perturbation theory. It is named "hard" scattering since the typical energies involved are high compared to the proton mass.

3 Ref. [72] provides a detailed calculation of the NLO contribution to the unpol. SIDIS cross section, as well as significant steps towards a full NNLO calculation, a major progress since the calculations in [61].

In principle, Eq. (3.7) contains all orders in α_s if the hard scattering function is known at each order. Since this is an extremely non-trivial task, theoretical predictions of the structure functions rely on perturbative fixed-order results, where the hard scattering function is a perturbative series in the strong coupling

$$\omega^i_{f'f} = \omega^{i,(0)}_{f'f} + \frac{\alpha_s(\mu_R)}{\pi}\,\omega^{i,(1)}_{f'f} + \left(\frac{\alpha_s(\mu_R)}{\pi}\right)^2 \omega^{i,(2)}_{f'f} + \mathcal{O}(\alpha_s^3)\,. \tag{3.8}$$

In the following we are interested in the leading order (LO) contribution and next-to-leading order (NLO) correction. Nevertheless, as we will see in Sec. 3.4 there are methods of finding some contributions to the hard scattering function to all orders.

The PDF and FF are independent of the underlying hard process and hence the hard scattering function is independent of the external state. It can therefore be obtained by calculating the partonic cross section, assuming external partons in the initial and final states and using factorization again:

$$\frac{d^2\sigma_k^{\gamma^* f\to f'}}{d\hat{x}d\hat{z}} = \int_{\hat{x}}^1 \frac{d\tilde{x}}{\tilde{x}} \int_{\hat{z}}^1 \frac{d\tilde{z}}{\tilde{z}}\, d_{f'/i}\left(\frac{\hat{z}}{\tilde{z}}, \mu_F, \epsilon\right) \omega^k_{ij}\left(\tilde{x}, \tilde{z}, \alpha_s, \frac{\mu_R}{Q}, \frac{\mu_F}{Q}\right) f_{j/f}\left(\frac{\hat{x}}{\tilde{x}}, \mu_F, \epsilon\right), \tag{3.9}$$

where $d_{f'/i}$ and $f_{j/f}$ are the corresponding partonic analogues of the distributions in (3.7). For better readability we name the transverse partonic structure function as follows

$$\frac{d^2\sigma_k^{\gamma^* f\to f'}}{d\hat{x}d\hat{z}} \equiv G^k_{f'f}\left(\hat{x}, \hat{z}, \alpha_s, \frac{\mu_R}{Q}, \frac{\mu_F}{Q}, \epsilon\right), \tag{3.10}$$

which is also a perturbative series in α_s

$$G^k_{f'f} = G^{k,(0)}_{f'f} + \frac{\alpha_s(\mu_R)}{\pi}\, G^{k,(1)}_{f'f} + \mathcal{O}(\alpha_s^2)\,. \tag{3.11}$$

Here we introduced the characteristic partonic scaling variables

$$\hat{x} = \frac{Q^2}{2p_a\cdot q} \quad \text{and} \quad \hat{z} = \frac{p_a\cdot p_b}{p_a\cdot q}\,, \tag{3.12}$$

where p_a and p_b are the momenta of the incoming parton and the fragmenting parton, respectively. One can now calculate the perturbative contributions of the partonic cross section to the desired order.

For simplicity we only consider the partonic channel $\gamma^* q \to q$. The methods described here are, of course, also valid in the case of an initial or final gluon. The parton-in-parton distributions can be calculated in perturbation theory. After UV renormalization in the $\overline{\text{MS}}$ scheme we have up to NLO [71]

$$d_{q/q}(\hat{y}) = f_{q/q}(\hat{y}) = \delta_y - \frac{\alpha_s}{\pi}\frac{1}{\epsilon} S^\epsilon\, P^{(0)}_{qq}(\hat{y}) + \mathcal{O}(\alpha_s^2)\,. \tag{3.13}$$

with

$$S^\epsilon \equiv \left(4\pi e^{-\gamma_E}\right)^\epsilon \tag{3.14}$$

and the leading order $q \to q$ splitting function

$$P_{qq}^{(0)}(\hat{y}) \;=\; C_F\left(\frac{1}{2}(1+\hat{y}^2)\mathcal{D}_y^0 + \frac{3}{4}\delta_y\right) \;\equiv\; C_F\,\bar{P}_{qq}^{(0)}(\hat{y})\,, \tag{3.15}$$

where we used the following abbreviations:

$$\delta_y \;\equiv\; \delta(1-\hat{y})\,, \quad \mathcal{D}_y^i \equiv \left[\frac{\ln^i(1-\hat{y})}{1-\hat{y}}\right]_+\,, \quad \ell_y^i \equiv \ln^i(1-\hat{y})\,. \tag{3.16}$$

The singular behavior of the $\mathcal{D}_y^i$ functions when $\hat{y} \to 1$ was regularized with help of the "plus" prescription

$$\int_0^1 dy\,\big(f(y)\big)_+\,g(y) \;\equiv\; \int_0^1 dy\,f(y)\,\big(g(y)-g(1)\big)\,. \tag{3.17}$$

Inserting the parton-in-parton distributions from (3.13) into (3.9) and expanding both sides in α_s we get

$$\begin{aligned} G_{qq}^{T,(0)} + \frac{\alpha_s}{\pi}G_{qq}^{T,(1)} + \mathcal{O}(\alpha_s^2) = \omega_{qq}^{T,(0)} + \frac{\alpha_s}{\pi}\omega_{qq}^{T,(1)} - \frac{\alpha_s}{\pi}\frac{1}{\epsilon}S^\epsilon \int_x^1 \frac{d\hat{x}}{\hat{x}}\omega_{qq}^{T,(0)}(\hat{x})\,P_{qq}^{(0)}\left(\frac{x}{\hat{x}}\right) \\ - \frac{\alpha_s}{\pi}\frac{1}{\epsilon}S^\epsilon \int_z^1 \frac{d\hat{z}}{\hat{z}}\omega_{qq}^{T,(0)}(\hat{z})\,P_{qq}^{(0)}\left(\frac{z}{\hat{z}}\right) + \mathcal{O}(\alpha_s^2)\,. \end{aligned} \tag{3.18}$$

By comparing the coefficients at each order we will obtain finite expressions for the hard scattering functions at LO and NLO.

3.3.1 *Leading order coefficient functions*

In LO, the red blob in Fig. 7 corresponds to a QED vertex with no gluon emission which is shown by the first diagram in Fig. 8. Comparing the LO expressions in (3.18) we see that at LO the hard coefficient and the partonic contribution coincide

$$\omega_{qq}^{T,(0)}(\hat{x},\hat{z}) \;=\; G_{qq}^{T,(0)}(\hat{x},\hat{z}). \tag{3.19}$$

Inserting this into (3.7) reproduces the parton model since the LO coefficient function is given by

$$\begin{aligned} \omega_{qq}^{T,(0)}(\hat{x},\hat{z}) &= e_q^2\,\delta(1-\hat{x})\delta(1-\hat{z}), \\ \omega_{qq}^{L,(0)}(\hat{x},\hat{z}) &= 0, \end{aligned} \tag{3.20}$$

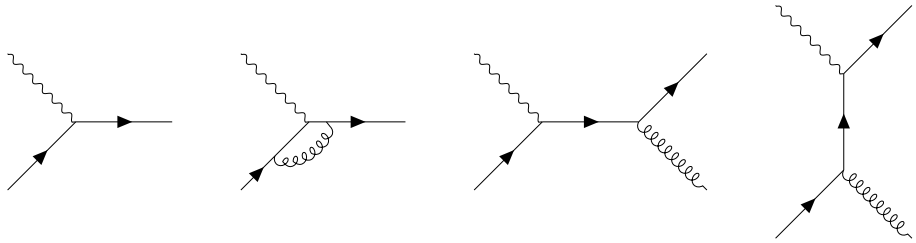

Figure 8: The first diagram from the left is the LO contribution to SIDIS. The diagrams including gluonic interaction are virtual and real NLO corrections for the partonic process $\gamma^* q \to q$.

By parton model we mean the approximation of free quarks in the proton as described after (3.6). One can see that the LO contribution to the transverse structure function leads to flavor separation of fragmentation and parton distribution function

$$\mathcal{F}_T^h(x,z) \;=\; \sum_q e_q^2\, D_q^h\,(z)\; q\,(x)\;. \tag{3.21}$$

This is quite a unique feature of SIDIS. It is used in global analyses of PDFs and FFs. In Eq. (3.21) we observe a similar behavior as Bjorken scaling in DIS, where PDF and FF are scale independent at LO.

3.3.2 *Next-to leading order coefficient functions*

Inspecting Eq. (3.18) at NLO we need to subtract the following terms from the partonic coefficient function to obtain the hard scattering function

$$\omega_{qq}^{T,(1)}(\hat{x},\hat{z}) = G_{qq}^{T,(1)}(\hat{x},\hat{z},\epsilon) + e_q^2 \frac{1}{\epsilon} S^\epsilon \left(\delta_z\, P_{qq}^{(0)}\,(\hat{x}) + \delta_x\, P_{qq}^{(0)}\,(\hat{z})\right)\,, \tag{3.22}$$

where we have used the LO coefficients from Eq. (3.20). We want the transverse part of the structure function which is given by [64, 72]

$$\mathcal{F}_\Sigma^h \;=\; \mathcal{F}_T^h - \frac{1}{2}\mathcal{F}_L^h\,. \tag{3.23}$$

This leads to

$$G_{qq}^{T,(1)} = G_{qq}^{\Sigma,(1)} + \frac{1}{2} G_{qq}^{L,(1)}\;. \tag{3.24}$$

The NLO contributions to the partonic cross section from the real and virtual diagrams in Fig. 8 can be calculated using the Feynman rules (see Appendix A), they are given by [72]

$$G_{qq,\,\text{virtual}}^{L,(1)} \;=\; 0\,, \tag{3.25}$$

$$G^{L,(1)}_{qq,\,\text{real}} = 2e_q^2\, C_F\, \hat{x}\, \hat{z}\,, \tag{3.26}$$

$$G^{\Sigma,(1)}_{qq,\,\text{virtual}} = e_q^2 C_F \left(\frac{\mu_F^2}{Q^2}\right)^{\epsilon} S^{\epsilon}(1-\epsilon)\, \delta_x\, \delta_z \left[-\frac{1}{\epsilon^2} - \frac{3}{2\epsilon} - 4\right]\,, \tag{3.27}$$

$$\begin{aligned} G^{\Sigma,(1)}_{qq,\,\text{real}} &= e_q^2 C_F \left(\frac{\mu_F^2}{Q^2}\right)^{\epsilon} S^{\epsilon}(1-\epsilon) \\ &\times \left\{ \frac{1}{\epsilon^2}\,\delta_x\,\delta_z - \frac{1}{\epsilon}\,\delta_x\,\frac{1}{2}(1+\hat{z}^2)\mathcal{D}_z^0 - \frac{1}{\epsilon}\,\delta_z\,\frac{1}{2}(1+\hat{x}^2)\mathcal{D}_x^0 \right. \\ &+ \delta_x\,\frac{1}{2}\left[(1+\hat{z}^2)\mathcal{D}_z^1 + (1+\hat{z}^2)\ell_z^1 + 1 - \hat{z}\right] \\ &+ \delta_z\,\frac{1}{2}\left[(1+\hat{x}^2)\mathcal{D}_x^1 - (1+\hat{x}^2)\ell_x^1 + 1 - \hat{x}\right] \\ &+ \left. \mathcal{D}_x^0\mathcal{D}_z^0 - \frac{1}{2}(1+\hat{z})\mathcal{D}_x^0 - \frac{1}{2}(1+\hat{x})\mathcal{D}_z^0 + 1 \right\}\,. \end{aligned} \tag{3.28}$$

We observe that the IR-structure from the QFF (up to normalization) in (2.29) reappears in the virtual contributions. If we now add real and virtual contributions the double poles cancel. The cancellation of these soft divergences was discussed in Sec. 2.2, and anticipated by the Kinoshita-Lee-Nauenberg theorem. The initial and final state *collinear* divergences, however, remain as we pointed out earlier while introducing factorization,

$$\begin{aligned} G^{\Sigma,(1)}_{qq} &= e_q^2 C_F \left(\frac{\mu_F^2}{Q^2}\right)^{\epsilon} S^{\epsilon}(1-\epsilon) \\ &\times \left\{ -4\,\delta_x\,\delta_z - \frac{1}{\epsilon}\left(\delta_x\,\bar{P}^{(0)}_{qq}(\hat{z}) + \delta_z\,\bar{P}^{(0)}_{qq}(\hat{x})\right) \right. \\ &+ \delta_x\,\frac{1}{2}\left[(1+\hat{z}^2)\mathcal{D}_z^1 + (1+\hat{z}^2)\ell_z^1 + (1-\hat{z})\right] \\ &+ \delta_z\,\frac{1}{2}\left[(1+\hat{x}^2)\mathcal{D}_x^1 - (1+\hat{x}^2)\ell_x^1 + (1-\hat{x})\right] \\ &+ \left. \mathcal{D}_x^0\mathcal{D}_z^0 - \frac{1}{2}(1+\hat{z})\mathcal{D}_x^0 - \frac{1}{2}(1+\hat{x})\mathcal{D}_z^0 + 1 \right\}\,, \end{aligned} \tag{3.29}$$

where we identified the leading order splitting functions from (3.15) (written as $\bar{P}_{qq}^{(0)}$ since it was divided by a factor of C_F) in the second line of Eq. (3.28). We can now apply Eq. (3.22) in order to obtain the transverse hard coefficient at NLO

$$\begin{aligned}\omega_{qq}^{T,(1)}(\hat{x},\hat{z}) &= e_q^2 C_F \Big\{ -4\,\delta_x\,\delta_z + \mathcal{D}_x^0\mathcal{D}_z^0 - \frac{1}{2}(1+\hat{z})\mathcal{D}_x^0 - \frac{1}{2}(1+\hat{x})\mathcal{D}_z^0 + (1+\hat{x}\hat{z}) \\ &+ \delta_x \frac{1}{2}\left[(1+\hat{z}^2)\mathcal{D}_z^1 + (1+\hat{z}^2)\ell_z^1 + (1-\hat{z}) - 2\bar{P}_{qq}^{(0)}(\hat{z})\ln\frac{\mu_F^2}{Q^2}\right] \\ &+ \delta_z \frac{1}{2}\left[(1+\hat{x}^2)\mathcal{D}_x^1 - (1+\hat{x}^2)\ell_x^1 + (1-\hat{x}) - 2\bar{P}_{qq}^{(0)}(\hat{x})\ln\frac{\mu_F^2}{Q^2}\right]\Big\}\,,\end{aligned} \tag{3.30}$$

which is now free of any divergences. The NLO coefficient function is almost symmetrical for $\hat{x} \leftrightarrow \hat{z}$ except for the different sign in the $\delta_x\ell_z^1$ and $\delta_z\ell_x^1$ terms. Furthermore it should be noted that contributions like $\mathcal{D}_x^1$ become large in the limit $\hat{x},\hat{z} \to 1$. This behavior is also present in the splitting function (3.15). The question of how to deal with these large contributions will be addressed in Sec. 3.4.

3.3.3 *Evolution equations*

The scale dependence of (polarized) PDFs and FFs is given by the Dokshitzer-Gribov-Lipatov-Altarelli-Parisi (DGLAP) evolution equations which we illustrate in the case of polarized PDFs, i.e. proton spin dependent PDFs. Since in the next Section we will mainly work in Mellin space, we introduce the double Mellin transform $\mathcal{M}$ defined by

$$\mathcal{M}[\mathcal{F}](N,M) = \int_0^1 dx\, x^{N-1} \int_0^1 dz\, z^{M-1}\mathcal{F}(x,z) \equiv \tilde{\mathcal{F}}(N,M)\,. \tag{3.31}$$

It is used to factorize the structure function in (3.7) into three separate integrals (instead of the rather inconvenient double convolutions). This can be seen by taking the double Mellin transform of (3.7) (for simplicity we omit the scale dependencies)

$$\tilde{\mathcal{F}}_i(N,M) = \sum_{f,f'} \tilde{f}(N)\ \cdot\ \tilde{\omega}_{f'f}^i(N,M)\ \cdot\ \tilde{D}_{f'}(M)\,, \tag{3.32}$$

where we rewrite the integral over $\hat{x}$ (or $\hat{z}$) as

$$\int_0^1 d\hat{x}\, f\left(\frac{x}{\hat{x}}\right)\omega_{f'f}^i(\hat{x}) = \int_0^1 dy \int_0^1 d\hat{x}\, f(y)\,\omega_{f'f}^i(\hat{x})\,\delta\left(y - \frac{x}{\hat{x}}\right)\,. \tag{3.33}$$

An example of a simple Mellin transform, i.e. with only one variable, is the transform of the LO splitting function $P_{qq}^{(0)}$ from (3.15), given by

$$P_{qq}^{N,(0)} = \int_0^1 d\hat{y}\, \hat{y}^{N-1}\, P_{qq}^{(0)}(\hat{y}) = C_F \left(-S_1(N) + \frac{3}{4} - \frac{1}{2N(N+1)} \right) , \tag{3.34}$$

where

$$S_1(N) = \sum_{k=1}^{N} \frac{1}{k} = \ln \bar{N} + \mathcal{O}\left(\frac{1}{N}\right) , \tag{3.35}$$

where $\bar{N} = Ne^{\gamma_E}$. We will show a more detailed calculation of such a transform in Sec.3.4. We observe that in Mellin space the singular behavior of the distribution $\mathcal{D}_y^1$ for $\hat{y} \to 1$ corresponds to large values of N. If not stated otherwise we will only consider terms not suppressed like the inverse power of a Mellin variable indicated in (3.35).

To explain evolution we introduce the helicity case, although the same reasoning applies to the unpolarized case. The factorization formula in (3.32) can also be applied in the case of longitudinally polarized incoming leptons and protons with helicity parton distribution functions

$$\Delta\tilde{f}\,(N,\mu_F) \equiv \tilde{f}^{+}\,(N,\mu_F) - \tilde{f}^{-}\,(N,\mu_F) \qquad (f = u,d,s,\bar{u},\bar{d},\bar{s},g)\,, \tag{3.36}$$

where $\tilde{f}^{+}$ or $\tilde{f}^{-}$ are the the number densities of partons in Mellin space with the same or opposite helicity with respect to the nucleon's helicity. The spin-dependent structure function then takes the form [21]

$$\mathcal{G}_1^h(N,M,Q^2) \;=\; \sum_{f,f'} \tilde{D}_{f'}^h\,(M,\mu_F)\,\Delta\tilde{\omega}_{f'f}\left(N,M,\alpha_s(\mu_R),\frac{\mu_R}{Q},\frac{\mu_F}{Q}\right)\Delta\tilde{f}\,(N,\mu_F)\;, \tag{3.37}$$

where $\mathcal{G}_1^h = 2g_1$ and $\Delta\tilde{\omega}_{f'f}$ is the spin dependent hard scattering function. A more detailed description of $\mathcal{G}_1^h$ and its cross section is given in Sec. 5.2. Here we only want to focus on its general structure which is similar to the unpolarized case. As discussed in the beginning of this Chapter, the structure function $\mathcal{G}_1^h$ is independent of the factorization scale μ_F, and thus

$$\frac{d\,\mathcal{G}_1^h}{d\ln\mu_F^2} = 0\,. \tag{3.38}$$

Since (3.37) is valid to all orders in the strong coupling, the μ_F dependency on the right hand side must cancel. But at a fixed order this is not the case. The scale dependence of the PDF is then given by the spin dependent DGLAP evolution [73, 74]

$$\frac{d}{d\ln\mu^2}\begin{pmatrix}\Delta\tilde{q}(N,\mu)\\ \Delta\tilde{g}(N,\mu)\end{pmatrix} \;=\; \underbrace{\begin{pmatrix}\Delta\mathcal{P}_{qq}^N(\alpha_s) & \Delta\mathcal{P}_{qg}^N(\alpha_s)\\ \Delta\mathcal{P}_{gq}^N(\alpha_s) & \Delta\mathcal{P}_{gg}^N(\alpha_s)\end{pmatrix}}_{=\Delta\mathcal{P}^N} \times \begin{pmatrix}\Delta\tilde{q}(N,\mu)\\ \Delta\tilde{g}(N,\mu)\end{pmatrix}\,. \tag{3.39}$$

The $\Delta\mathcal{P}_{ij}^N$ are the entries of the matrix $\Delta\mathcal{P}^N$ containing the spin-dependent splitting functions [73–77]

$$\Delta\mathcal{P}_{ij}^N = \frac{\alpha_s}{\pi}\left(\Delta P_{ij}^{N,(0)} + \frac{\alpha_s}{\pi}\Delta P_{ij}^{N,(1)} + \dots\right) \tag{3.40}$$

In the calculation of these polarized splitting functions special care has to be taken in dimensional regularization to the Dirac matrix

$$\gamma_5 \equiv \frac{i}{4!}\epsilon^{\mu\nu\rho\sigma}\gamma_\mu\gamma_\nu\gamma_\rho\gamma_\sigma \,, \tag{3.41}$$

where $\epsilon^{\mu\nu\rho\sigma}$ is the Levi-Civita symbol, which is true in general when performing helicity dependent calculations. The Levi-Civita symbol is a uniquely four-dimensional object, it is therefore not clear how to extend it to d dimensions [78]. As pointed out in [76], dimensional regularization so far seems to be the only viable method to regularize spin dependent amplitudes. An algebraically consistent prescription of treating γ_5, appearing in the helicity projectors, in d dimensions is the HVBM scheme [79, 80]. In the unpolarized case the framework of Refs. [81, 82] is an established way of obtaining splitting functions in $\mathcal{P}^N$. This was adopted in [76, 77] to the polarized case, while using the mentioned HVBM scheme.

We give the LO splitting functions in the large N limit, where the helicity evolution kernels $\Delta\mathcal{P}_{ij}$ are (at this order) equivalent to the unpolarized ones from [83]

$$\Delta P_{qq}^{N,(0)} = P_{qq}^{N,(0)} = C_F\left(-\ln\bar{N} + \frac{3}{4} - \frac{1}{2N}\right) \,, \quad \Delta P_{qg}^{N,(0)} = P_{qg}^{N,(0)} = \frac{1}{4N} \,, \tag{3.42}$$

$$\Delta P_{gq}^{N,(0)} = P_{gq}^{N,(0)} = \frac{C_F}{2N} \,, \quad \Delta P_{gg}^{N,(0)} = P_{gg}^{N,(0)} = -C_A\ln\bar{N} - \frac{C_A}{2N} + \pi b_0 \,. \tag{3.43}$$

Three loop contributions to $\Delta\mathcal{P}_{ij}$ were calculated in [84]. The unpolarized splitting functions in $\mathcal{P}^N$ are known up to three loops as well [85, 86]. Steps towards a four-loop result have recently been made in [87, 88].

As already mentioned, the evolution in the unpolarized case is similar to the evolution above. Furthermore, the fragmentation also has an evolution as the one described above but with unpolarized *timelike* splitting functions which are equivalent to the ones in (3.43) as well when taking the large M limit. As we will explore in Chapter 5, DGLAP evolution will generate a certain type of *threshold* enhanced contributions to the hard scattering function which are suppressed by one Mellin variable, which is the reason we did not omit the suppressed terms in (3.43). This leads us to threshold resummation, the main topic of this thesis.

3.4 RESUMMATION

Resummation in SIDIS is known in the literature up to NLL in the unpolarized [20] and polarized case [21]. The appearance of logarithms that spoil the perturbative series is known for many different pQCD processes, e.g. DY, SIA,... In general, the threshold region is characterized by the fact that most of the phase space is used to produce the partonic reaction ($\hat{x}, \hat{z} \to 1$). The remaining phase space becomes small leading to arbitrary soft gluon radiation, which is sometimes referred to as an incomplete cancellation of real and virtual contributions. From [89] we know that in the case of SIDIS, where we have two scaling variables, the energy of radiated gluons, with total momentum $\bar{k}$, becomes completely soft for $\hat{x}, \hat{z} \to 1$

$$(1-\hat{x}) + (1-\hat{z}) \approx \frac{2\bar{k}^0}{Q} \,. \tag{3.44}$$

The perturbative series is spoiled as the gluons become softer and softer. In the coefficient function this is reflected by the terms $\propto \alpha_s^k [\ln^n(1-\hat{y})/(1-\hat{y})]_+$ (where $\hat{y}$ can be $\hat{x}$ or $\hat{z}$), so called *threshold* logarithms, which in turn have to be summed to all orders in the strong coupling since they diverge at fixed order. We stress that these terms are generally not problematic. It is near the phase space boundary where they diverge and hence need special attention. Exponentiation of eikonal diagrams in color-singlet processes systematically deals with the all-order resummations of theses logarithms [90–94]. We will follow the approach given in theses References. Although being an extremely interesting subject by itself we will not enlarge upon the foundations of resummation, we rather focus on its consequences and structure in SIDIS and several other processes. The essential points from these works we rely upon in the following are: the factorization of the QCD matrix element for n-gluon emissions into the product of n single *soft* gluon emissions. Furthermore we require the phase space to factorize as well which can be done in Mellin space.

At NLO the most singular terms near the phase space boundary are given by double distributions, i.e. terms containing a plus- and a delta-distribution, e.g. $\delta_z \mathcal{D}_x^1$ from (3.16), called leading-logarithms (LL). The NLO coefficient function in (3.30) receives large corrections when $\hat{x}, \hat{z} \to 1$, given by the double distribution terms

$$\omega_{qq'}^{T,(1)}(\hat{x},\hat{z}) \;=\; e_q^2 C_F \Big\{ \delta_x \, \mathcal{D}_z^1 + \delta_z \, \mathcal{D}_x^1 + \mathcal{D}_x^0 \mathcal{D}_z^0 - 4\, \delta_x \, \delta_z \Big\} \,, \tag{3.45}$$

where we set $\mu_F = Q$ for simplicity. In the following we will explain how to obtain these contributions to all orders in perturbation theory. Before we turn to the actual resummed cross section, we will treat the NLO coefficient function in Mellin space.

3.4.1 *Next-to leading order coefficient functions in Mellin space*

We calculate the Mellin moments of the NLO transverse coefficient function for the $\gamma^* q \to q$ channel $\omega_{qq}^{T,(1)}(\hat{x},\hat{z},1)$ in Eq. (3.30), where we set $\mu_F = Q$. Let us first consider double distribution terms, e.g. $\sim \delta_x\,\delta_z$ or $\sim \delta_x\,\mathcal{D}_z^1$. The terms containing two delta distributions render simple constants in Mellin space. As an example we calculate the Mellin transform of the second kind using the definitions in (3.16):

$$\mathcal{M}[\delta_x\,(1+\hat{z}^2)\mathcal{D}_z^1](N,M) = \int_0^1 d\hat{x}\;\hat{x}^{N-1}\delta(1-\hat{x})\int_0^1 d\hat{z}\;\hat{z}^{M-1}(1+\hat{z}^2)\left[\frac{\ln(1-\hat{z})}{(1-\hat{z})}\right]_+ . \tag{3.46}$$

Applying the definition of the $+$ distribution from (3.17) in the $\hat{z}$-integration leads to

$$\begin{aligned} &-\int_0^1 d\hat{z}\;\left(\frac{1-\hat{z}^{M-1}}{1-\hat{z}}+\frac{1-\hat{z}^{M+1}}{1-\hat{z}}\right)\ln(1-\hat{z}) \\ &= -\int_0^1 d\hat{z}\;\sum_{k=0}^{M-2}\hat{z}^k\ln(1-\hat{z}) - \int_0^1 d\hat{z}\;\sum_{j=0}^{M}\hat{z}^j\ln(1-\hat{z})\,, \end{aligned} \tag{3.47}$$

where we identify an integral representation of the n-th harmonic number

$$\int_0^1 x^k\ln(1-x)\,dx = -\frac{1}{k+1}H_{k+1}\,, \qquad H_n \equiv \sum_{k=1}^{n}\frac{1}{k}\,. \tag{3.48}$$

This leads to the following expression in Mellin space

$$\begin{aligned} \mathcal{M}[\delta_x\,(1+\hat{z}^2)\mathcal{D}_z^1](N,M) &= \sum_{k=1}^{M-1}\frac{1}{k}H_k + \sum_{j=1}^{M+1}\frac{1}{j}H_j \\ &= S_1^2(M) - \frac{S_1(M)}{M(M+1)} + S_2(M) + \frac{1}{(M+1)^2}\,, \end{aligned} \tag{3.49}$$

where we have used

$$\sum_{k=1}^{n}\frac{1}{k}H_k = \frac{1}{2}\left(S_1^2(n)+S_2(n)\right)\,, \qquad S_k(n) = \sum_{j=1}^{n}\frac{1}{j^k}\,. \tag{3.50}$$

After performing likewise the Mellin transform of the full NLO coefficient function in (3.30), we obtain the following expression[4] in accordance with [20, 95]

$$\begin{aligned}
&\tilde{\omega}_{qq}^{T,(1)}(N,M) \\
&= e_q^2 C_F \frac{1}{2}\left\{-8 - \frac{1}{M^2} + \frac{2}{(M+1)^2} + \frac{1}{N^2} + \frac{(1+N+M)^2+1}{M(M+1)N(N+1)} + 3S_2(M) - S_2(N)\right. \\
&\quad + (S_1(M)+S_1(N))\left(S_1(M)+S_1(N) - \frac{1}{M(M+1)} - \frac{1}{N(N+1)}\right) \\
&\quad \left. + \left(2(S_1(N)+S_2(M)) - 3 - \frac{1}{N(N+1)} - \frac{1}{M(M+1)}\right)\ln\frac{\mu_F^2}{Q^2}\right\} . \qquad (3.51)
\end{aligned}$$

Here we calculated the exact Mellin transform. For the purpose of threshold resummation this is not necessary when working in the phase space region for large values of N and M since most terms are suppressed. However, the exact expression in (3.51) will serve as a valuable comparison to our approximate results developed in Chapter 4. Let us now expand this result for large values of N and M. This corresponds to the limits $\hat{x} \to 1$ and $\hat{z} \to 1$ since the Mellin integrand x^{N-1} becomes a step function for large N. Furthermore, we use

$$S_1(N) = \ln \bar{N} + \mathcal{O}(1/N) , \qquad (3.52)$$

$$S_2(N) = \frac{\pi^2}{6} + \mathcal{O}(1/N) , \qquad (3.53)$$

where, as before, $\bar{N} = Ne^{\gamma_E}$ and $\bar{M} = Me^{\gamma_E}$. If we insert these approximations into (3.51) and neglect suppressed contributions, we obtain

$$\tilde{\omega}_{qq}^{T,(1)}(N,M) = e_q^2 C_F\left\{\frac{1}{2}(\ln\bar{M}+\ln\bar{N})^2 - 4 + \frac{\pi^2}{6} + \mathcal{O}\left(\frac{1}{N},\frac{1}{M}\right)\right\} . \qquad (3.54)$$

This expression is analogous to (3.45) in the sense that we disregard suppressed terms. Although the Mellin transform is unique, the approximations in Mellin or x,z-space, Eqs. (3.54) and (3.45) respectively, are not readily comparable. Special care has to be taken to suppressed terms when comparing expressions in the threshold limit since they need not be the same in both spaces. In other words, suppressed terms in Mellin space do not correspond single distribution (or non-distribution) terms in x,z space. It appears that Mellin moments provide a better approximation of the full NLO coefficient in (3.51). A more detailed picture about this difference will be given in Sec. 5.6.

It is of considerable interest to find a way to manage the logarithms in Eq. (3.54) for large values of N and M. In general, the leading logarithms at kth order in perturbation theory (for xz-space or Mellin space)

$$\alpha_s^k\left(\delta_x\,\mathcal{D}_z^{2k-1} + \delta_z\,\mathcal{D}_x^{2k-1}\right) + \ldots \qquad \text{or} \qquad \alpha_s^k(\ln\bar{M}+\ln\bar{N})^{2k-1} + \ldots \qquad (3.55)$$

4 From this point on we use the more compact notation $\mathcal{M}[\omega](N,M) \equiv \tilde{\omega}(N,M)$.

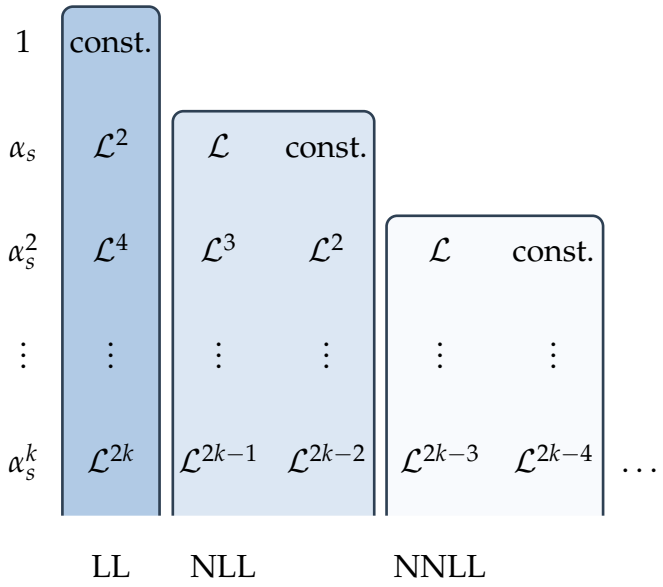

Figure 9: All-order threshold logarithmic structure, where $\mathcal{L} = \frac{1}{2}(\ln \bar{N} + \ln \bar{M})$

may be obtained in threshold resummation. We will find that such logarithms follow a certain hierarchy which is displayed on Fig. 9, where the left-most column corresponds to the leading logarithms. The kth row indicates the fixed-order logarithmic structure. We additionally show the NLL and NNLL "towers". In Chapter 6 we will even find N^{3}LL contributions, i.e. the seven leading towers of logarithms.

3.4.2 *Resummation at next-to leading logarithmic accuracy*

We follow Refs. [20, 21] to perform NLL resummation in SIDIS. Exponentiation of the eikonal hard-scattering function [89, 90, 94, 96, 97] leads to the following structure of the resummed part of the transverse hard scattering function

$$\ln \tilde{\omega}_{qq}^{T,\mathrm{res}}(N, M, \alpha_s(Q)) \propto \int_0^{Q^2} \frac{d\mu^2}{\mu^2} A_q\left(\alpha_s(\mu)\right) \left\{ \int_{\frac{\mu^2}{Q^2}}^1 \frac{d\xi}{\xi} \left[e^{-N\xi - M\frac{\mu^2}{\xi Q^2}} - 1 \right] + \ln \bar{N} + \ln \bar{M} \right\}, \tag{3.56}$$

which is valid to next-to-leading logarithmic (NLL) accuracy. Here, $A_q(\alpha_s)$ is the perturbative function from Eq. (2.36). Neglecting contributions that are exponentially suppressed we may write the ξ-integration as follows

$$\int_{\frac{\mu^2}{Q^2}}^1 \frac{d\xi}{\xi} \left[e^{-N\xi - M\frac{\mu^2}{\xi Q^2}} - 1 \right] + \ln \bar{N} + \ln \bar{M} \approx 2 \left[K_0\left(\sqrt{NM}\, \frac{2\mu}{Q} \right) + \ln\left(\frac{\mu}{Q} \sqrt{\bar{N}\bar{M}} \right) \right], \tag{3.57}$$

where K_0 is a Bessel function. At this point we can make a crucial observation that will be more developed in Sec. 4.2. The inclusive Drell Yan process is characterized by one scaling variable instead of two. The analog expression to (3.57) is given by [89, 94, 97]

$$\int_{\frac{\mu^2}{Q^2}}^1 \frac{d\xi}{\xi}\left[e^{-N\left(\xi-\frac{\mu^2}{\xi Q^2}\right)}-1\right]+2\ln\bar{N} \;\approx\; 2\left[K_0\left(N\frac{2\mu}{Q}\right)+\ln\left(\frac{\mu}{Q}\bar{N}\right)\right]. \quad (3.58)$$

It is now possible to obtain the SIDIS expression by substituting $\bar{N}\to\sqrt{\bar{N}\bar{M}}$. Furthermore we recognize the all-order subtraction of collinear divergences in the initial and the final state by $\ln\bar{N}$ and $\ln\bar{M}$ respectively. In Eq. (3.22) we saw that subtraction at NLO, where the LO splitting functions in Mellin space (3.34) contain these logarithms. In DY two initial partons produce the $2\ln\bar{N}$ contribution resumming collinear divergences in the initial state.

With (3.57), the final resummed coefficient function becomes in the $\overline{\text{MS}}$ scheme:

$$\tilde{\omega}_{qq}^{T,\text{res}}(N,M,\alpha_s(Q)) \propto \exp\left[2\int_0^{Q^2}\frac{d\mu^2}{\mu^2}A_q\left(\alpha_s(\mu)\right)\left\{K_0\left(\sqrt{NM}\frac{2\mu}{Q}\right)+\ln\left(\frac{\mu}{Q}\sqrt{\bar{N}\bar{M}}\right)\right\}\right]. \quad (3.59)$$

At small argument, the Bessel function K_0 behaves as

$$K_0(x) = -\ln\left(xe^{\gamma_E}/2\right)+\mathcal{O}(x^2\ln x)\,.$$

We are now ready to expand the exponent to NLL. This is done by integrating over μ^2 using the running coupling (2.23) at $\mathcal{O}(\alpha_s^2)$. We find[5]

$$\int_{\frac{Q^2}{\bar{N}\bar{M}}}^{Q^2}\frac{d\mu^2}{\mu^2}A_q\left(\alpha_s(\mu)\right)\ln\left(\frac{\mu^2\bar{N}\bar{M}}{Q^2}\right)\approx h_q^{(1)}\left(\frac{\lambda_{NM}}{2}\right)\frac{\lambda_{NM}}{2b_0\alpha_s(\mu_R)}+h_q^{(2)}\left(\frac{\lambda_{NM}}{2}\right), \quad (3.60)$$

where $h_q^{(1)}$ and $h_q^{(2)}$ are given by

$$\begin{aligned}
\lambda_{NM} &\equiv b_0\alpha_s(\mu_R)\left(\ln\bar{N}+\ln\bar{M}\right),\\
h_q^{(1)}(\lambda) &= \frac{A_q^{(1)}}{\pi b_0\lambda}\left[2\lambda+(1-2\lambda)\ln(1-2\lambda)\right],\\
h_q^{(2)}(\lambda) &= -\frac{A_q^{(2)}}{\pi^2 b_0^2}\left[2\lambda+\ln(1-2\lambda)\right]+\frac{A_q^{(1)}b_1}{\pi b_0^3}\left[2\lambda+\ln(1-2\lambda)+\frac{1}{2}\ln^2(1-2\lambda)\right].
\end{aligned} \quad (3.61)$$

5 A more detailed description of this expansion can be found after Eq. (4.17).

As stated above, these results can be obtain as well by setting $\lambda_{\rm DY} \to \lambda_{NM}/2$ in the exponent of Ref. [98] for the DY process, where $\lambda_{\rm DY} = b_0 \alpha_s(\mu_R) \ln \bar{N}$. For simplicity we set $\mu_F = \mu_R = Q$.

Since the exponent is a function of the strong coupling we can expand it and obtain the large Mellin moments expression from (3.54)

$$\begin{aligned}\frac{1}{e_q^2}\tilde{\omega}_{qq}^{T,\text{res}} &= H_{qq}^{\text{SIDIS}}\,\widehat{C}_{qq}\,\exp\left\{\int_{Q^2/(\bar{N}\bar{M})}^{Q^2}\frac{d\mu^2}{\mu^2}A_q\big(\alpha_s(\mu)\big)\ln\left(\frac{\mu^2\bar{N}\bar{M}}{Q^2}\right)\right\}\\ &= 1+\frac{\alpha_s}{\pi}C_F\left\{\frac{1}{2}(\ln\bar{N}+\ln\bar{M})^2-4+\frac{\pi^2}{6}+\mathcal{O}\left(\frac{1}{N},\frac{1}{M}\right)\right\}+\mathcal{O}(\alpha_s^2)\,.\end{aligned} \tag{3.62}$$

Here we already inserted the constant contributions which are gathered in the product

$$H_{qq}^{\text{SIDIS}}\cdot\widehat{C}_{qq} = 1+\frac{\alpha_s}{\pi}\left(-4+\frac{\pi^2}{6}\right)+\mathcal{O}(\alpha_s^2)\,, \tag{3.63}$$

where H_{qq}^{SIDIS} and $\widehat{C}_{qq}$ each are perturbative functions. In Chapter 4 we will develop a method for systematically finding these constant contributions at higher orders. For now, we simply read them off the NLO calculation in (3.54).

The main two results from the procedure above are, of course, all-order resummation of LL and NLL contributions, but we can also approximate the hard scattering function by expanding the exponent in α_s. At NLO this method may seem superfluous, especially since the fixed-order result has been known for a long time. Nevertheless it will show to serve as a way to approximate NNLO corrections in Sec. 5.5 that are quite cumbersome to calculate as pointed out in Ref. [72].

3.4.3 *Mellin inversion*

Although being extremely useful from the perspective of soft gluon resummation, Mellin space is not used for giving phenomenological predictions. These are commonly ruled out in x, z space. The transverse structure function is then given by the inverse Mellin transforms of (3.32)

$$\mathcal{F}_T^h(x,z,Q^2) = \int_{\mathcal{C}_N}\frac{dN}{2\pi i}\,x^{-N}\int_{\mathcal{C}_M}\frac{dM}{2\pi i}\,z^{-M}\,\tilde{\mathcal{F}}_T^h(N,M,Q^2)\,. \tag{3.64}$$

The contours $\mathcal{C}_N$ and $\mathcal{C}_M$ in the complex plane are illustrated on Fig. 10 as red dashed lines. The complex integrations can be performed if all singularities, except for the Landau[6] singularity, lie to the left of the contours adopting the *minimal*

6 See the discussion after (2.25).

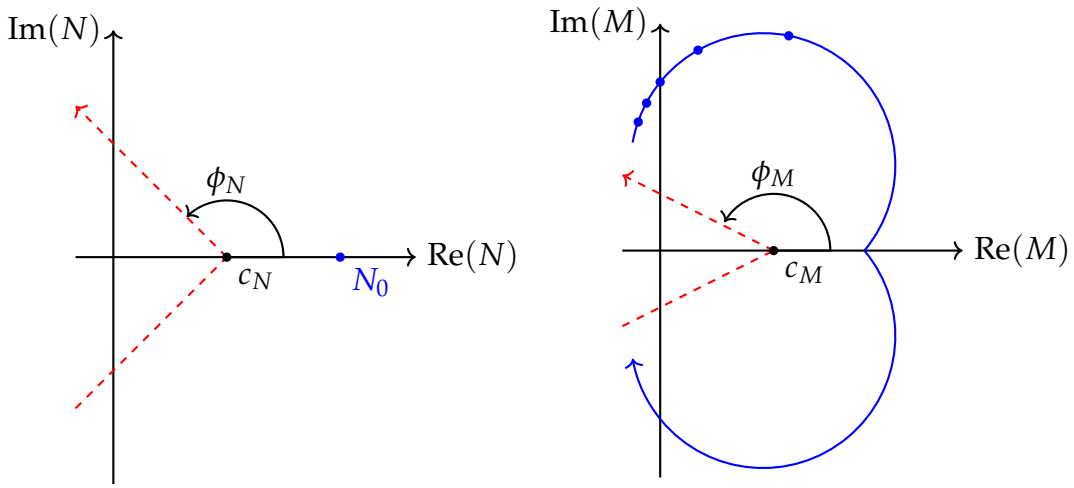

Figure 10: Contours for N and M integrations in the Mellin inversion, adapted from [20].

prescription from [98]. In passing we note that in Chapter 5 we give approximate fixed-order results, where we expand the exponent without resumming to all orders in α_s. In that case no special caution has to be exercised to the Landau singularity. It appears if the running coupling diverges for $\mu \to \Lambda_{\rm QCD}$ in the exponent of Eq. (3.59). This is related to the moments by the λ_{NM} variable approaching one in (3.60)

$$\lambda_{NM} = 1 \quad \to \quad \bar{N}\bar{M} = \exp\left(\frac{1}{\alpha_s b_0}\right) \equiv L_0 \,, \tag{3.65}$$

where N and M are complex numbers parametrized by polar coordinates

$$N = c_N \pm \zeta e^{i\phi_N} \,, \quad M = c_M \pm \xi e^{i\phi_M} \,, \quad \zeta, \xi \in (0, \infty) \,, \tag{3.66}$$

where $\phi_N \sim 3\pi/4$. We will give explicit numbers for the parameters c_N and c_M in later Chapters. Here we qualitatively show the approach of the Mellin inversion following Ref. [20]. From (3.65) we know that the position of the Landau pole in the complex M plane depends on the position of N along its contour. We therefore start with the standard contour for the N-integration chosen to be tilted towards the real axis in order to obtain a negative real part. This leads to a better convergence of the numerical integration since in (3.64) the prefactor x^{-N} , where $x \in (0,1)$, suppresses contributions with large real parts exponentially. The same is true for the M contour. Furthermore the minimal prescription requires $c_N < N_0$, where $N_0 \equiv L_0/c_M$. For different values of N on its contour, the Landau pole moves along the blue curve in the M plane

$$M_{L_0}(\zeta) = f(\zeta) + ig(\zeta) \,, \tag{3.67}$$

$$f(\zeta) = \frac{L_0(\sqrt{2}c_N - \zeta)}{\sqrt{2}(\zeta^2 - \sqrt{2}c_N\zeta + c_N^2)} \,, \quad g(\zeta) = -\frac{L_0\zeta}{\sqrt{2}(\zeta^2 - \sqrt{2}c_N\zeta + c_N^2)} \,, \tag{3.68}$$

where some of the positions are shown as blue dots. Now the M contour has to be chosen in such a way that it does not cross the Landau pole, making the angle ϕ_M depend on the position of the Landau pole. The Landau pole moves towards the real axis if $\zeta \to \pm\infty$ which would induce $\phi_M \to \pi$. As discussed above, these contributions are exponentially suppressed and we can neglect them.

4

THRESHOLD APPROXIMATIONS

4.1 INTRODUCTION

In this Chapter we will explore the fact that fixed-order calculations of the hard scattering functions of the processes SIA, DIS and DY can be approximated by re-factorized short distance functions of the following form

$$\begin{aligned} \omega^{\text{res}}(N,\alpha_s) &= H(\alpha_s)\cdot\Delta(N,\alpha_s) \\ &= H(\alpha_s)\cdot\widehat{C}(\alpha_s)\cdot\widehat{\Delta}(N,\alpha_s) \end{aligned} \tag{4.1}$$

which generally consist of three ingredients: the hard factor H and the soft-gluon exponent Δ which can be split into two parts: one part only containing threshold logarithms and an additional – rather cosmetic – function $\widehat{C}$ extracting all Mellin constant contributions from Δ. This procedure has been studied in [32, 99]. The hard virtual contributions can be obtained by using the time- or spacelike quark form factor as described in [100]. We combine the methods of these works and apply them to the before mentioned processes. We derive approximate NNLO hard scattering functions containing all threshold enhanced logarithms and all Mellin constant contributions. Exact calculations of these hard scattering functions exist in the literature up to NNLO providing powerful checks of our calculations. We stress, however, that the contributions derived here are known to all orders in the strong coupling α_s.

In Chapter 5 we derive approximate NNLO corrections to SIDIS. Since no full NNLO calculation in SIDIS exists, the natural question that arises here is: on which grounds can we give such approximation? The following Chapter stands as the foundation for our reasoning. In order to give a sensible answer to this question we will compare the *timelike* Drell Yan (at measured rapidity) with *spacelike* SIDIS which have a very close resummation structure as pointed out in Ref. [89]. In order to be confident that the crossing of these processes succeeds, we compare timelike SIA and spacelike DIS, where the resummation is equivalent but the hard factors disagree. We find that the approximation does work in these cases making an application to SIDIS possible.

Unfortunatly, the processes described here all have different historical notations and conventions used when expressing their cross sections. Since we want to introduce all of them we try to be as consistent as possible with the notation used in the Chapters so far, however respecting traditional notation when a change of it could lead to confusion.

It is clear that the resummed expressions we use here were initially derived to improve the perturbative fixed-order prediction near the threshold region of phase space. However, since we are interested in the expansion at a specific order we will primarily talk about approximated cross sections in the sense that we take the threshold limit and expand its resummed exponents to a finite order. It turns out that these approximations are quite powerful to get sensible estimations of the hard scattering function (at least up to NNLO).

This Chapter is organized as follows: In Sec. 4.2 we introduce the DY process and relate two equivalent ways of writing the soft exponents from a traditional form to a form that is more suitable for our purposes. We furthermore explain the calculation of the hard virtual factor. In Sec. 4.3 and Sec. 4.4 we apply these methods to SIA and DIS respectively.

4.2 THE DRELL-YAN PROCESS

We consider the Drell-Yan process $h_1 h_2 \to e^+ e^- X$ with its differential cross section in the factorized form as in SIDIS (3.7), first calculated to NLO in [57]

$$\frac{d\sigma}{dQ^2} = \frac{4\pi\alpha^2}{9sQ^2} \sum_{f,f'} \int_{Q^2/s}^1 \frac{d\xi_1}{\xi_1} \int_{Q^2/(s\xi_1)}^1 \frac{d\xi_2}{\xi_2}\, \omega_{ff'}\left(z, \alpha_s, \frac{\mu}{Q}\right)\, f\left(\xi_2, \mu\right)\, f\left(\xi_1, \mu\right) \,, \quad (4.2)$$

for partons $f, f' = q, \bar{q}, g$, where Q^2 is the square of the lepton pair mass q and $z = Q^2/\hat{s}$. The particle collision takes places at a center of mass energy $\sqrt{s}$ and $\hat{s} = \xi_1\xi_2 s$ is the partonic c.m.s. energy. The leading order contribution to the hard scattering function is given by $\omega^{(0)}_{q\bar{q}} = e_q^2 \delta(1-z)$. The NLO coefficient function in z-space is given by

$$\tilde{\omega}^{(1)}_{q\bar{q}} = C_F \left[2(1+z^2)\mathcal{D}^1_z - \frac{1+z^2}{1-z}\ln z + \left(-4 + \frac{\pi^2}{3}\right)\delta_z + \tilde{P}^{(0)}_{qq}(\hat{z}) \ln\frac{Q^2}{\mu^2} \right] \,, \quad (4.3)$$

where we used the notation from (3.16) for the distributions. In further Sections we will refer to these corrections as $\omega^{\mathrm{DY,incl}}_{ff'}(z)$ depending on a *single* scaling variable to differentiate them from the Drell-Yan process at measured rapidity

$$\frac{d^2\sigma}{dQ^2 dy} = \sum_{f,f'} \int_{x_1}^1 d\xi_1 \int_{x_2}^1 d\xi_2\, H_{ff'}\left(z_1, z_2, \alpha_s, \frac{\mu}{Q}\right)\, f\left(\xi_2, \mu\right)\, f\left(\xi_1, \mu\right) \,, \quad (4.4)$$

where $z_i = x_i/\xi_i$ and

$$x_1 = e^y\sqrt{\frac{Q^2}{s}}\,, \quad x_2 = e^{-y}\sqrt{\frac{Q^2}{s}}\,. \tag{4.5}$$

The rapidity is then defined as

$$y = \frac{1}{2}\ln\left(\frac{q\cdot P_1}{q\cdot P_2}\right)\,. \tag{4.6}$$

The momenta of the incoming protons h_1 and h_2 are P_1 and P_2, respectively. The hard scattering function $H_{ff'}$ is normalized as follows

$$H_{ff'} = \frac{4\pi\alpha^2}{9Q^4}\left(\omega^{(0)}_{ff'} + \frac{\alpha_s}{\pi}\omega^{(1)}_{ff'} + \left(\frac{\alpha_s}{\pi}\right)^2\omega^{(2)}_{ff'} + \mathcal{O}(\alpha_s^3)\right)\,, \tag{4.7}$$

where $\omega^{(0)}_{q\bar{q}} = e_q^2\delta(1-z_1)\delta(1-z_2)$. These hard scattering cofficients are then referred to as $\omega^{\text{DY,rap}}_{ff'}(z_1,z_2)$, depending on *two* scaling variables. Naturally, in Mellin space we write $\tilde{\omega}^{\text{DY,incl}}_{ff'}(N)$ and $\tilde{\omega}^{\text{DY,rap}}_{ff'}(N,M)$.

The Mellin transform was discussed widely in Chapter 3. The NLO correction to DY at measured rapidity in the large N, M limit is given by [101]

$$\frac{1}{e_q^2}\tilde{\omega}^{\text{DY,rap},(1)}_{q\bar{q}}(N,M) \;=\; C_F\left\{\frac{1}{2}(\ln\bar{N}+\ln\bar{M})^2 - 4 + \frac{2\pi^2}{3} + \mathcal{O}\left(\frac{1}{N},\frac{1}{M}\right)\right\}\,. \tag{4.8}$$

These corrections, as well as the NNLO corrections from [101], can be reproduced starting from the inclusive DY and rescaling its Mellin variable as $N \to \sqrt{NM}$. This can readily be seen by performing the substitution in

$$\frac{1}{e_q^2}\tilde{\omega}^{\text{DY,incl},(1)}_{q\bar{q}}(N) \;=\; C_F\left\{2\ln^2\bar{N} - 4 + \frac{2\pi^2}{3} + \mathcal{O}\left(\frac{1}{N}\right)\right\}\,. \tag{4.9}$$

4.2.1 *Change of integration order*

Traditionally, the soft-gluon resummation of the DY quark coefficient, for $q\bar{q}\to\gamma^*$, is given in the following form (with an explicit Mellin transform) at NLL accuracy [96, 102]

$$\Delta_q(N,\alpha_s) = \exp\left\{2\int_0^1 dz\frac{z^N-1}{1-z}\int_{\mu_F^2}^{(1-z)^2Q^2}\frac{d\mu^2}{\mu^2}A_q(\alpha_s(\mu))\right\}\,. \tag{4.10}$$

This exponent is usually referred to as collinear soft-gluon radiation off an initial-state quark. The factor 2 comes from the sum over both incoming quarks in DY.

Our goal in this Section is to rewrite this exponent in a more usable form. As discussed in Sec. 3.4 we want to make close contact to resummation in SIDIS which is more convenient when writing the exponent as a single integration as described in [32, 99]. We now take a closer look at the integration in (4.10). In Ref. [32] the following all order prescription to handle threshold logarithms in the z variable with its conjugate Mellin variable N is defined as

$$z^N - 1 = -\tilde{\Gamma}\left(1 - \frac{\partial}{\partial \ln N}\right)\Theta\left(1 - z - \frac{1}{\bar{N}}\right) + \mathcal{O}\left(\frac{1}{N}\right) \tag{4.11}$$

with

$$\tilde{\Gamma}(1+\epsilon) = e^{\gamma_E \epsilon}\,\Gamma(1+\epsilon) = \exp\left(\sum_{n=2}^{+\infty}(-1)^n \frac{\zeta(n)}{n}\epsilon^n\right)\,. \tag{4.12}$$

This means

$$\tilde{\Gamma}\left(1 - \frac{\partial}{\partial \ln N}\right) \approx 1 + \frac{\zeta(2)}{2}\left(\frac{\partial}{\partial \ln N}\right)^2 + \mathcal{O}\left(\left(\frac{\partial}{\partial \ln N}\right)^3\right)\,, \tag{4.13}$$

which will be used below. The full prescription in (4.11) is useful when including higher logarithmic orders which will be addressed in the following Sections. When performing threshold resummation up to NLL it is sufficient to use the first approximation of (4.11)

$$z^N - 1 = -\Theta\left(1 - z - \frac{1}{\bar{N}}\right)\,. \tag{4.14}$$

Furthermore we can interchange the integration sequence as follows. First, we split the μ^2-integration into μ_F dependent and independent parts

$$\begin{aligned}\int_0^{1-1/\bar{N}} dz \,\ldots \int_{\mu_F^2}^{(1-z)^2Q^2} d\mu^2 \,\ldots \;=\; &\int_0^{1-1/\bar{N}} dz \,\ldots \int_{\mu_F^2}^{Q^2} d\mu^2 \,\ldots \\ &+ \int_0^{1-1/\bar{N}} dz \,\ldots \int_{Q^2}^{(1-z)^2Q^2} d\mu^2 \,\ldots\end{aligned} \tag{4.15}$$

and then perform a change of integration order for each term. The first term is trivial. The change of the second term is sketched in Fig 11. We can then write it as

$$-\int_0^{1-1/\bar{N}} dz \,\ldots \int_{(1-z)^2Q^2}^{Q^2} d\mu^2 \,\cdots = -\int_{Q^2/\bar{N}^2}^{Q^2} d\mu^2 \,\ldots \int_{1-\sqrt{\mu^2/Q^2}}^{1-1/\bar{N}} dz \,\ldots \tag{4.16}$$

The z-integration is now reduced to the denominator $1-z$ without forgetting the overall minus sign and leads to

$$\ln \Delta_q = \int_{Q^2/\bar{N}^2}^{Q^2} \frac{d\mu^2}{\mu^2}\, A_q(\alpha_s(\mu))\, \ln\left(\frac{\mu^2\bar{N}^2}{Q^2}\right) + 2\ln\bar{N}\int_{Q^2}^{\mu_F^2}\frac{d\mu^2}{\mu^2}A_q(\alpha_s(\mu)) \tag{4.17}$$

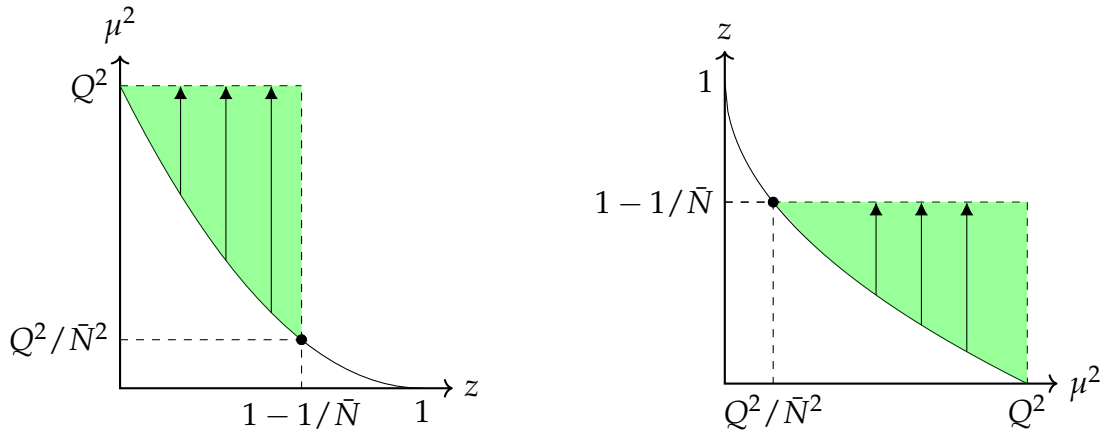

Figure 11: Change of integration order. The arrows indicate the direction and the length of the inner integration for a fixed value of the outer integration variable as in Eq. (4.16). The colored area is the total integration area.

We can take a closer look at the first integration as an example, while inserting the lowest order expressions of Eqs. (2.23) and (2.36):

$$\frac{\alpha_s(\mu_R)}{\pi} A_q^{(1)} \int_{Q^2/\bar{N}^2}^{Q^2} \frac{d\mu^2}{\mu^2} \frac{\ln \mu^2 + 2\ln \bar{N} - \ln Q^2}{1 + b_0 \alpha_s(\mu_R) \ln(\mu^2/\mu_R^2)} \,. \tag{4.18}$$

If we substitute $y = b_0 \alpha_s \ln(\mu^2/\mu_R^2)$ and omit the μ_R dependency of α_s, we obtain

$$\frac{1}{b_0 \alpha_s} \frac{A_q^{(1)}}{b_0 \pi} \int_{\bar{\lambda}-2\lambda}^{\bar{\lambda}} dy \left(1 + \frac{2\lambda - \bar{\lambda} - 1}{1+y}\right) , \tag{4.19}$$

where $\bar{\lambda} \equiv b_0 \alpha_s \ln(Q^2/\mu_R^2)$ and λ is the usual variable $\lambda \equiv \alpha_s b_0 \ln \bar{N}$. When expanding this in α_s, while keeping λ *fixed*, this leads to

$$\ln \Delta_q = \frac{A_q^{(1)}}{\pi b_0^2 \alpha_s} \left(2\lambda + (1-2\lambda)\ln(1-2\lambda)\right) + \mathcal{O}(\alpha_s^0) \,. \tag{4.20}$$

After integration of (4.17) we expand the exponent up to NLL [98]

$$\Delta_q \;=\; \exp\left\{ \frac{\lambda}{b_0 \alpha_s} h_q^{(1)}(\lambda) + h_q^{(2)}(\lambda) + \mathcal{O}(\alpha_s) \right\} . \tag{4.21}$$

This is the same NLL exponent as in SIDIS, see Eq. (3.60) where we only need to adjust the λ variable. The LL contribution is given by

$$h_q^{(1)}(\lambda) = \frac{A_q^{(1)}}{\pi b_0 \lambda} \left(2\lambda + (1-2\lambda)\ln(1-2\lambda)\right) . \tag{4.22}$$

Let us now consider corrections beyond NLL accuracy. As mentioned earlier the approximation in (4.14) is not sufficient. We have to include the derivative term from (4.13) which is given by the second derivative in λ

$$\frac{\zeta(2)}{2}\left(\alpha_s b_0 \frac{\partial}{\partial\lambda}\right)^2 \frac{\lambda}{\alpha_s b_0} h_q^{(1)}(\lambda) = \frac{\alpha_s}{\pi}\, 2\zeta(2)\, A_q^{(1)}\, \frac{1}{1-2\lambda}\,. \tag{4.23}$$

Since we only write terms proportional to logarithms, i.e. λ, within the exponent we rewrite this result before expanding the exponent in α_s

$$\frac{\alpha_s}{\pi}\, 2\zeta(2)\, A_q^{(1)}\, \frac{1}{1-2\lambda} = \frac{\alpha_s}{\pi}\, 2\zeta(2)\, A_q^{(1)} \left(\frac{2\lambda}{1-2\lambda}+1\right)\,. \tag{4.24}$$

This separates the non-logarithmic from the logarithmic part. The constant term corresponds to a shift in the hard function (after expansion in α_s). The $\widehat{C}_{qq}$ function gathers all such terms at each order in α_s

$$\widehat{C}_{qq}(\alpha_s) = 1 + \frac{\alpha_s}{\pi} 2\zeta(2) A_q^{(1)} + \mathcal{O}(\alpha_s^2)\,. \tag{4.25}$$

An all-order formula of this function is given in the Appendix B of Ref. [32]. The higher order coefficients are given in Appendix B.1. The remaining part within the exponent

$$\frac{\alpha_s}{\pi}\, 2\zeta(2)\, A_q^{(1)} \frac{2\lambda}{1-2\lambda}\,, \tag{4.26}$$

has the form of a D function term. The D function is a perturbative series as the A function (2.36). It begins at $\mathcal{O}(\alpha_s^2)$, see (B.3), and hence only appears at NNLL which is the reason we did not write it earlier in the exponent of (4.10). It has been derived in [103] without attributing it to the $\alpha_s((1-z)Q)$ contribution which was done in [31]. According to [104], it contains the contributions of soft-gluon emission at large angle. On that account the full exponent is extended by a new term as in [31]

$$\Delta_q = \exp\left\{\int_0^1 dz \frac{z^N-1}{1-z}\left(2\int_{\mu_F^2}^{(1-z)^2Q^2}\frac{d\mu^2}{\mu^2}A_q(\alpha_s(\mu)) + D_q\left(\alpha_s([1-z]Q)\right)\right)\right\}\,. \tag{4.27}$$

The remaining contribution from (4.26) can then be obtained by shifting the D function as

$$\widehat{D}_q(\alpha_s) - D_q(\alpha_s) = -\left(\frac{\alpha_s}{\pi}\right)^2 4\zeta(2)\,\pi b_0\, A_q^{(1)} + \mathcal{O}(\alpha_s^3)\,. \tag{4.28}$$

The shift at $\mathcal{O}(\alpha_s^2)$ can be generalized to all orders, see Appendix B of Ref. [32]. We will perform this generalization in the next Section in the case of SIA. In total, we rewrite the exponent (4.27) as in (4.17) with the shifted D function [32, 99]

$$\begin{aligned}\Delta_q(N,\alpha_s) &= \widehat{C}_{qq}(\alpha_s)\ \widehat{\Delta}_q(N,\alpha_s) \\ &\equiv \widehat{C}_{qq}(\alpha_s)\exp\left\{\int_{Q^2/\bar{N}^2}^{Q^2}\frac{d\mu^2}{\mu^2}\,A_q(\alpha_s(\mu))\,\ln\left(\frac{\mu^2\bar{N}^2}{Q^2}\right)-\frac{1}{2}\widehat{D}_q\left(\alpha_s(\mu)\right)\right. \\ &\qquad\left.+2\ln\bar{N}\int_{Q^2}^{\mu_F^2}\frac{d\mu^2}{\mu^2}A_q(\alpha_s(\mu))\right\}\,.\end{aligned} \tag{4.29}$$

4.2.2 *The hard factor*

So far we only considered the soft-gluon exponent of the cross section. In order to obtain an approximation of the cross section we still lack the hard virtual coefficients. In other words, we look for the remaining N-independent contributions (not coming from the resummed exponent). Fortunately, there is a method to extract precisely such contributions from the timelike quark form factor from Sec. 2.3 in the case of the Drell-Yan process. These coefficients are given by a subtraction operator $\tilde{I}_q$ [100]

$$H_{q\bar{q}}^{\mathrm{DY}}\left(\alpha_s(Q^2)\right) = \left|\left[1-\tilde{I}_q(\epsilon,\alpha_s(Q^2))\right]F_q^t\right|^2\,, \tag{4.30}$$

removing all poles from the timelike quark form factor F_q^t from Eq. (2.48). It can be written as [100]

$$1-\tilde{I}_q(\epsilon,\alpha_s(Q^2)) = \exp\left\{R_q(\epsilon,\alpha_s(Q^2))-i\Phi_q(\epsilon,\alpha_s(Q^2))\right\}\,, \tag{4.31}$$

where Φ_q is the IR divergent Coulomb phase which is not of our interest since it vanishes when taking the absolute value after the subtraction. The function R_q assures the extraction of all IR finite terms of the quark form factor. It is decomposed into a soft and collinear part:

$$R_q(\epsilon,\alpha_s) = R_q^{\mathrm{soft}}(\epsilon,\alpha_s)+R_q^{\mathrm{coll}}(\epsilon,\alpha_s)\,, \tag{4.32}$$

where

$$R_q^{\mathrm{soft}}(\epsilon,\alpha_s) = C_F\left(\frac{\alpha_s}{\pi}R_q^{\mathrm{soft}(1)}(\epsilon)+\mathcal{O}(\alpha_s^2)\right) \tag{4.33}$$

$$R_q^{\mathrm{coll}}(\epsilon,\alpha_s) = \frac{\alpha_s}{\pi}R_q^{\mathrm{coll}(1)}(\epsilon)+\mathcal{O}(\alpha_s^2)\,. \tag{4.34}$$

The all-order form of Eq. (4.31), of course, suggests that higher orders of the subtraction operator are known since higher order calculations of the quark form factor exist. In this Section, however, we only want to motivate the use of this operator and therefore refrain from showing higher order expressions. They are given in Chapters 5 & 6 when calculating approximate NNLO and N^{3}LO corrections to SIDIS. Their first order expressions read

$$R_q^{\text{soft}(1)}(\epsilon) = \frac{1}{2\epsilon^2} + R_q^{\text{fin}(1)} \,, \tag{4.35}$$

$$R_q^{\text{coll}(1)}(\epsilon) = \frac{3}{4\epsilon} C_F \,. \tag{4.36}$$

The IR-finite term $R_q^{\text{fin}(1)} = -\pi^2/8$ will be useful when distinguishing the hard factor of the Drell-Yan process from the one of SIA in the next Section. After subtraction of the IR-divergences from the timelike quark form factor we end up with the following hard factor

$$H_{q\bar{q}}^{\text{DY}}(\alpha_s) = 1 + \frac{\alpha_s}{\pi} C_F \left(-4 + \frac{\pi^2}{3} \right) + \mathcal{O}(\alpha_s^2) \,. \tag{4.37}$$

Equipped with this hard factor, we can estimate the inclusive Drell-Yan cross section with the following expression

$$\tilde{\omega}_{q\bar{q}}^{\text{DY,res}}(N, \alpha_s) = e_q^2 \, H_{q\bar{q}}^{\text{DY}}(\alpha_s) \, \widehat{C}_{qq}(\alpha_s) \, \widehat{\Delta}_q \,, \tag{4.38}$$

where we use Eq. (4.29). After expansion in the strong coupling (up to NLO) we obtain

$$\frac{1}{e_q^2} \tilde{\omega}_{q\bar{q}}^{\text{DY,res}}(N, \alpha_s) = 1 + \frac{\alpha_s}{\pi} C_F \left(2 \ln^2 \bar{N} - 4 + \frac{2\pi^2}{3} + \mathcal{O}\left(\frac{1}{N} \right) \right) + \mathcal{O}(\alpha_s^2) \,. \tag{4.39}$$

This corresponds to the large N (or $z \to 1$ in Eq. (4.3)) limit of the exact cross section from Ref. [22] in Mellin space. This approximation also holds in NNLO when comparing it with the expression found in [22]. As in the previous Chapter we obtain an approximation of the full cross section by using threshold resummation techniques. At NLO the procedure seems rather unintuitive and lengthy. We chose to not yet go to higher orders for pedagogical reasons which will be done in the case of SIDIS in Chapters 5 & 6.

This method applies also in the case of SIA and DIS. As we will see in the next Section only few adaptations have to be made in order to get approximate results for these processes as well.

4.3 SEMI-INCLUSIVE e^+e^- ANNIHILATION

In the last Section we only considered the all-order prescription (4.11) to a finite order to extract coefficients for $\widehat{C}_{qq}$ and change the exponent in the D function by hand. In the case of SIA we show the consequences of the all-order prescription at each order in the strong coupling.

We consider the SIA process $e^+e^- \to h\ X$ produced via a virtual timelike photon $\gamma^*(q)$ at c.m.s. energy $\sqrt{S}$ and $S = q^2 \equiv Q^2$ which is given by so called hadron multiplicites, calculated up to NLO in [61, 105]

$$\frac{1}{\sigma_{\rm tot}}\frac{d^2\sigma^h}{dx_E d\cos\theta} = \frac{\pi\alpha^2}{\sigma_{\rm tot}Q^2}N_c\left(\frac{1+\cos^2\theta}{2}\hat{\mathcal{F}}_T^h(x_E,Q^2) + \sin^2\theta\hat{\mathcal{F}}_L^h(x_E,Q^2)\right) \equiv R^h_{e^+e^-}\ , \tag{4.40}$$

where $\sigma_{\rm tot}$ is the total hadronic cross section for $e^+e^- \to$ hadrons as in Eq. (1.9). The characteristic scaling variable is defined as $x_E = 2P_h\cdot q/Q^2$, where P_h is the momentum of the produced hadron. The angle between h and the annihilated e^+e^- pair is named θ. In the following we are interested in the *timelike* transverse structure function

$$\mathcal{F}_T^{h,\rm SIA}(x_E,Q^2) \;=\; \sum_f \int_{x_E}^1 \frac{d\hat{z}}{\hat{z}} D_f^h\left(\frac{x_E}{\hat{z}},\mu\right)\omega_f^{\rm SIA}\left(\hat{z},\alpha_s(\mu),\frac{\mu}{Q}\right)\ . \tag{4.41}$$

As before, we sum over partons $f = q,\bar{q},g$, while D_f^h is the fragmentation function of parton f into a hadron h and $\omega_f^{\rm SIA}$ is the *transverse* hard scattering coefficient function[1] calculable in perturbation theory.

4.3.1 *Single integration*

The resummed SIA hard scattering function in the case of $\gamma^* \to q\bar{q}$ can be written as follows

$$\tilde{\omega}_q^{\rm SIA,res}(N,\alpha_s) \;=\; e_q^2\ H_q^{\rm SIA}(\alpha_s)\ \Sigma_q(N,\alpha_s)\ , \tag{4.42}$$

where $H_q^{\rm SIA}$ is the hard function collecting all constant contributions (in Mellin space) from the hard virtual diagrams. The usual way of writing the SIA exponent is [106]

$$\Sigma_q = \exp\left\{\int_0^1 dz\frac{z^N-1}{1-z}\int_{\mu_F^2}^{(1-z)Q^2}\frac{d\mu^2}{\mu^2}A_q(\alpha_s(\mu)) + B_q\left(\alpha_s\left(\sqrt{1-z}Q\right)\right)\right\}\ , \tag{4.43}$$

1 We omit the superscript T in the following since we do not discuss longitudinal contributions to SIA.

where we have a B function instead of the D function in comparison to (4.27). Equation (4.43) is often referred to as "jet function", see [106], responsible for collinear emissions from the *unobserved* final-state quark . In the context of resummation this unobserved particle is the main difference between DY and SIA. Also, the soft scale has changed which can be seen in the upper integration limit of the μ^2-integration and in the argument of the B function. This is due to a different phase space. In analogy to Eq.(34) in [32] the exponent in (4.43) may be written as

$$\Sigma_q = \widehat{C}^B_{qq}(\alpha_s) \exp\left\{ -\int_{1/\bar{N}}^1 \frac{dy}{y} \left[\int_{\mu_F^2}^{yQ^2} \frac{d\mu^2}{\mu^2} A_q(\alpha_s(\mu)) - \widehat{B}_q\left(\alpha_s\left(\sqrt{y}Q\right)\right) \right] \right\} . \tag{4.44}$$

We now show the equivalence of both representations following Ref. [32], while starting from (4.43). Substituting $y = 1 - z$ and using the all-order prescription (4.11)

$$\ln \Sigma_q(N, \alpha_s) = -\tilde{\Gamma}\left(1 - \frac{\partial}{\partial \ln N}\right) \int_{1/\bar{N}}^1 \frac{dy}{y} \left[\int_{\mu_F^2}^{yQ^2} \frac{d\mu^2}{\mu^2} A_q(\alpha_s(\mu)) + B_q\left(\alpha_s\left(\sqrt{y}Q\right)\right) \right] . \tag{4.45}$$

The modified Gamma function $\tilde{\Gamma}$ from (4.12) can also be written as

$$\tilde{\Gamma}\left(1 - \frac{\partial}{\partial \ln N}\right) = 1 - \Gamma_2\left(\frac{\partial}{\partial \ln N}\right)\left(\frac{\partial}{\partial \ln N}\right)^2 , \tag{4.46}$$

where

$$\Gamma_2(\epsilon) = \frac{1}{\epsilon^2}(1 - e^{-\gamma_E \epsilon}\Gamma(1-\epsilon)) . \tag{4.47}$$

After inserting (4.46) into (4.45) we compare Eqs. (4.45) with (4.44) to make the expressions for $\widehat{C}_{qq}$ and $\widehat{B}_q$ explicit. The comparison leads to

$$\begin{aligned} &\int_{1/\bar{N}}^1 \frac{dy}{y} \widehat{B}_q\left(\alpha_s\left(\sqrt{y}Q\right)\right) - \ln \widehat{C}^B_{qq}(\alpha_s) \stackrel{!}{=} \int_{1/\bar{N}}^1 \frac{dy}{y} B_q\left(\alpha_s\left(\sqrt{y}Q\right)\right) \\ &- \Gamma_2\left(\frac{\partial}{\partial \ln N}\right)\left(\frac{\partial}{\partial \ln N}\right)^2 \int_{1/\bar{N}}^1 \frac{dy}{y} \int_{\mu_F^2}^{yQ^2} \frac{d\mu^2}{\mu^2} A_q(\alpha_s(\mu)) + B_q\left(\alpha_s\left(\sqrt{y}Q\right)\right) . \end{aligned} \tag{4.48}$$

Let us first discuss the derivative of the last term in Eq. (4.48) in more detail

$$\begin{aligned}
&\left(\frac{\partial}{\partial \ln N}\right)^2 \int_{1/\bar{N}}^1 \frac{dy}{y} \int_{\mu_F^2}^{yQ^2} \frac{d\mu^2}{\mu^2} A_q(\alpha_s(\mu)) + B_q\left(\alpha_s\left(\sqrt{y}Q\right)\right) \\
&= \left(\frac{\partial}{\partial \ln N}\right)^2 \int_{-\ln \bar{N}}^0 dt \int_{\mu_F^2}^{e^t Q^2} \frac{d\mu^2}{\mu^2} A_q(\alpha_s(\mu)) + B_q\left(\alpha_s\left(\sqrt{e^t}Q\right)\right) \\
&= \frac{\partial}{\partial \ln N}\left[\int_{\mu_F^2}^{Q^2/\bar{N}} \frac{d\mu^2}{\mu^2} A_q(\alpha_s(\mu)) + B_q\left(\alpha_s\left(\sqrt{Q^2/\bar{N}}\right)\right)\right] \\
&= \frac{\partial}{\partial \ln N} \int_{\ln \mu_F^2}^{\ln(Q^2/\bar{N})} d\varphi A_q(\alpha_s(e^{\varphi/2})) + \frac{\partial}{\partial \ln N} B_q\left(\alpha_s\left(\sqrt{Q^2/\bar{N}}\right)\right) \\
&= -A_q\left(\alpha_s\left(\sqrt{Q^2/\bar{N}}\right)\right) + \frac{\partial}{\partial \ln N} B_q\left(\alpha_s\left(\sqrt{Q^2/\bar{N}}\right)\right), \qquad (4.49)
\end{aligned}$$

where we have substituted $t = \ln y$ and $\varphi = \ln \mu^2$. The comparison then reads

$$\begin{aligned}
&\int_{1/\bar{N}}^1 \frac{dy}{y} \widehat{B}_q\left(\alpha_s\left(\sqrt{y}Q\right)\right) - \ln \widehat{C}_{qq}^B(\alpha_s) = \int_{1/\bar{N}}^1 \frac{dy}{y} B_q\left(\alpha_s\left(\sqrt{y}Q\right)\right) \\
&- \Gamma_2\left(\frac{\partial}{\partial \ln N}\right)\left[-A_q\left(\alpha_s\left(\sqrt{Q^2/\bar{N}}\right)\right) + \frac{\partial}{\partial \ln N} B_q\left(\alpha_s\left(\sqrt{Q^2/\bar{N}}\right)\right)\right]. \qquad (4.50)
\end{aligned}$$

The derivative $\partial/\partial \ln N$ of any function f that depends on the strong coupling can be formulated with help of the QCD β function in (2.22)

$$\begin{aligned}
\frac{\partial}{\partial \ln N} f\left(\alpha_s\left(\sqrt{k/N}\right)\right) &= -\frac{1}{2}\frac{\partial}{\partial \ln u} f\left(\alpha_s(u)\right) \\
&= -\frac{\partial \ln \alpha_s(u)}{\partial \ln u^2} \frac{\partial f\left(\alpha_s(u)\right)}{\partial \ln \alpha_s(u)} \\
&= \underbrace{-\beta(\alpha_s)\,\alpha_s \frac{\partial}{\partial \alpha_s}}_{\equiv \partial_{\alpha_s}^B} f(\alpha_s), \qquad (4.51)
\end{aligned}$$

where we substituted $u = \sqrt{k/N} = \exp(\frac{1}{2}\ln k - \frac{1}{2}\ln N)$. The newly defined derivative $\partial_{\alpha_s}^B$ has a superscript B since it is half of ∂_{α_s} defined in [32] where one uses the D function at a different soft scale. The derivatives in (4.50) can now be replaced with $\partial_{\alpha_s}^B$ and we obtain

$$\begin{aligned}
&\int_{1/\bar{N}}^1 \frac{dy}{y} \widehat{B}_q\left(\alpha_s\left(\sqrt{y}Q\right)\right) - \ln \widehat{C}_{qq}^B(\alpha_s) = \int_{1/\bar{N}}^1 \frac{dy}{y} B_q\left(\alpha_s\left(\sqrt{y}Q\right)\right) \\
&+ \Gamma_2\left(\partial_{\alpha_s}^B\right)\left[A_q\left(\alpha_s\left(\sqrt{Q^2/\bar{N}}\right)\right) - \partial_{\alpha_s}^B B_q\left(\alpha_s\left(\sqrt{Q^2/\bar{N}}\right)\right)\right], \qquad (4.52)
\end{aligned}$$

which is valid for arbitrary values of N. In order to obtain an expression for $\widehat{C}_{qq}$ we choose $\bar{N} \to 1$

$$\widehat{C}^B_{qq}(\alpha_s(Q)) = \exp\left\{-\Gamma_2\left(\partial^B_{\alpha_s}\right)\left[A_q\left(\alpha_s\right) - \partial^B_{\alpha_s}\, B_q\left(\alpha_s\right)\right]\right\}\,. \tag{4.53}$$

This function collects all N independent contributions of the soft exponent. It is a perturbative function in the strong coupling

$$\widehat{C}^B_{qq}(\alpha_s) \;=\; 1 + \frac{\alpha_s}{\pi}\,\widehat{C}^{B,(1)}_{qq} + \left(\frac{\alpha_s}{\pi}\right)^2\,\widehat{C}^{B,(2)}_{qq} + \mathcal{O}(\alpha_s^3)\,, \tag{4.54}$$

with

$$\widehat{C}^{B,(1)}_{qq} \;=\; \frac{\pi^2}{12} A_q^{(1)}\,, \tag{4.55}$$

$$\widehat{C}^{B,(2)}_{qq} \;=\; \frac{\pi^4}{288}(A_q^{(1)})^2 + \pi b_0\left(\frac{1}{3}A_q^{(1)}\zeta(3) - \frac{\pi^2}{12}B_q^{(1)}\right) + \frac{\pi^2}{12}A_q^{(2)}\,. \tag{4.56}$$

By differentiating (4.52) with respect to $\ln N$ we obtain a relation for the shifted B function

$$\begin{aligned}\widehat{B}_q\left(\alpha_s\left(\sqrt{Q^2/\bar{N}}\right)\right) &= \widehat{B}_q\left(\alpha_s\left(\sqrt{Q^2/\bar{N}}\right)\right) \\ &+ \frac{\partial}{\partial \ln N}\left\{\Gamma_2\left(\partial^B_{\alpha_s}\right)\left[A_q\left(\alpha_s\right) - \partial^B_{\alpha_s}\, B_q\left(\alpha_s\right)\right]\right\}_{\alpha_s=\alpha_s\left(\sqrt{Q^2/\bar{N}}\right)}\,.\end{aligned} \tag{4.57}$$

We use the new derivative $\partial^B_{\alpha_s}$ from (4.51) for the $\ln\bar{N}$-derivative in the second line of (4.57) and the expression becomes

$$\widehat{B}_q\left(\alpha_s\right) = \widehat{B}_q\left(\alpha_s\right) + \partial^B_{\alpha_s}\left\{\Gamma_2\left(\partial^B_{\alpha_s}\right)\left[A_q\left(\alpha_s\right) - \partial^B_{\alpha_s}\, B_q\left(\alpha_s\right)\right]\right\}\,. \tag{4.58}$$

This completes the connection of the representations of Eqs. (4.43) and (4.44) to all orders in α_s and we end up with

$$\begin{aligned}\Sigma_q \;=\;& \widehat{C}^B_{qq}(\alpha_s)\,\widehat{\Sigma}_q \\ \equiv\;& \widehat{C}^B_{qq}(\alpha_s)\exp\left\{\int_{Q^2/\bar{N}}^{Q^2}\frac{d\mu^2}{\mu^2}A_q(\alpha_s(\mu))\ln\left(\frac{\mu^2\bar{N}}{Q^2}\right) - \widehat{B}_q\left(\alpha_s\left(\mu\right)\right)\right. \\ &\left. + \ln\bar{N}\int_{Q^2}^{\mu_F^2}\frac{d\mu^2}{\mu^2}A_q(\alpha_s(\mu))\right\}\,,\end{aligned} \tag{4.59}$$

where we rewrite the exponent in (4.44) as discussed in Subsec. 4.2.1 with a *single* integration. Using Eq. (4.58) we obtain

$$\begin{aligned}\widehat{B}_q^{(1)} \;&=\; B_q^{(1)}\,, \\ \widehat{B}_q^{(2)} \;&=\; B_q^{(2)} - \frac{\pi b_0}{2}\zeta(2)A_q^{(1)}\,,\end{aligned} \tag{4.60}$$

which is in accordance with Ref. [99]. The explicit expressions of the coefficients are given in (B.7).

4.3.2 *The hard factor*

The hard factor in SIA

$$H_q^{\rm SIA}\left(\alpha_s(Q^2)\right) = \left|\left[1-\tilde{I}_q^{\rm SIA}(\epsilon,\alpha_s(Q^2))\right]F_q^t\right|^2 , \tag{4.61}$$

can be obtained similarly as in the previous Section with help of a subtraction operator $\tilde{I}_q^{\rm SIA}$ and the timelike quark form factor (2.48). The only difference between $\tilde{I}_q$ and $\tilde{I}_q^{\rm SIA}$ lies in the finite contribution of the $R_q^{\rm soft}$ function in (4.33). We find the difference (up to NNLO)

$$R_q^{\rm fin,SIA(1)} - R_q^{\rm fin(1)} = \frac{7}{8} , \tag{4.62}$$

$$\begin{aligned} R_q^{\rm fin,SIA(2)} - R_q^{\rm fin(2)} &= C_F\left(-\frac{3\zeta(3)}{16}+\frac{41\pi^4}{2880}+\frac{9}{256}-\frac{41\pi^2}{384}\right) \\ &+ C_A\left(\frac{7\zeta(3)}{12}+\frac{53\pi^2}{1728}+\frac{3745}{2304}-\frac{37\pi^4}{5760}\right) \\ &+ N_f\left(-\frac{5\zeta(3)}{24}-\frac{\pi^2}{864}-\frac{305}{1152}\right) . \end{aligned} \tag{4.63}$$

Note, there is an overall prefactor of C_F in (4.33). After making these adjustements we obtain the SIA hard factor

$$H_q^{\rm SIA}(\alpha_s) = 1+\frac{\alpha_s}{\pi}H_q^{\rm SIA,(1)}+\left(\frac{\alpha_s}{\pi}\right)^2 H_q^{\rm SIA,(2)}+\mathcal{O}(\alpha_s^3) , \tag{4.64}$$

with

$$H_q^{\rm SIA,(1)} = C_F\left(-\frac{9}{4}+\frac{\pi^2}{3}\right) , \tag{4.65}$$

$$\begin{aligned} H_q^{\rm SIA,(2)} &= C_F^2\left(-\frac{33\zeta(3)}{8}+\frac{77\pi^4}{1440}-\frac{23\pi^2}{64}+\frac{331}{128}\right) \\ &+ C_FC_A\left(\frac{35\zeta(3)}{12}+\frac{215\pi^2}{288}-\frac{5465}{1152}-\frac{49\pi^4}{2880}\right) \\ &+ C_FN_f\left(\frac{\zeta(3)}{12}-\frac{19\pi^2}{144}+\frac{457}{576}\right) . \end{aligned} \tag{4.66}$$

The SIA cross section is then approximated by Eq. (4.42) using (4.59) for the exponent. After expansion in the strong coupling we obtain the coefficient functions up to NNLO from Ref. [24] in the large N limit.

4.4 DEEP-INELASTIC SCATTERING

We extend this reasoning to the case of DIS. We already introduced the process in (3.5) and here we consider the transverse *spacelike* structure function

$$\mathcal{F}_T(x,Q^2) = \sum_f \int_x^1 \frac{d\hat{x}}{\hat{x}}\, \omega_f^{\rm DIS}\left(\hat{x}, \alpha_s(\mu_R), \frac{\mu_R}{Q}, \frac{\mu_F}{Q}\right) f\left(\frac{x}{\hat{x}}, \mu_F\right), \tag{4.67}$$

where we sum over partons f and $\omega_f^{\rm DIS}$ is the transverse hard scattering function[2]. It was pointed out in [106] that the soft gluon radiation exponent is the same as in SIA and given in Eq. (4.59) since we also integrate over an unobserved final state quark. The resummed cross section in Mellin space can then be written as

$$\tilde{\omega}_q^{\rm DIS,res}(N,\alpha_s) = e_q^2\, H_q^{\rm DIS}(\alpha_s)\, \widehat{C}_{qq}^B(\alpha_s)\, \widehat{\Sigma}_q(N,\alpha_s)\,. \tag{4.68}$$

The hard factor needs to be adjusted since the quark form factor in

$$H_q^{\rm DIS}\left(\alpha_s(Q^2)\right) = \left|\left[1 - \tilde{I}_q^{\rm DIS}(\epsilon,\alpha_s(Q^2))\right] F_q\right|^2, \tag{4.69}$$

is spacelike. We find the same subtraction operator as in SIA:

$$\tilde{I}_q^{\rm DIS} = \tilde{I}_q^{\rm SIA} \equiv \tilde{I}^B \tag{4.70}$$

with the IR-finite terms

$$R_q^{\rm fin,DIS(1)} = R_q^{\rm fin,SIA(1)} \tag{4.71}$$

$$R_q^{\rm fin,DIS(2)} = R_q^{\rm fin,SIA(2)}\,. \tag{4.72}$$

We then find the following hard factor for DIS

$$H_q^{\rm DIS,(1)} = C_F\left(-\frac{9}{4} - \frac{\pi^2}{6}\right), \tag{4.73}$$

$$\begin{aligned} H_q^{\rm DIS,(2)} &= C_F^2\left(-\frac{33\zeta(3)}{8} + \frac{17\pi^4}{1440} + \frac{49\pi^2}{64} + \frac{331}{128}\right) \\ &+ C_F C_A\left(\frac{35\zeta(3)}{12} + \frac{71\pi^4}{2880} - \frac{251\pi^2}{288} - \frac{5465}{1152}\right) \\ &+ C_F N_f\left(\frac{\zeta(3)}{12} + \frac{19\pi^2}{144} + \frac{457}{576}\right). \end{aligned} \tag{4.74}$$

2 We again omit the superscript T as in (4.41).

Again, expanding the resummed cross section (4.68) in the strong coupling leads to fixed-order results in the large N limit which are in agreement with [23] up to NNLO. Table 1 summarizes the findings of this Chapter, while including the inferred consequences for SIDIS. The all-order methods described here prove to be applicable to SIDIS which is done in the following Chapters. The quark form factor combined with the corresponing soft gluon exponents lead to approximate fixed-order results. All non-suppressed logarithmic enhanced, as well as all Mellin constant contributions are found to coincide with fixed-order calculations.

So far we have not yet addressed suppressed contributions by $1/N$, which will be the subject of Sec. 5.4, where evolution-type subleading contributions are derived in SIDIS. Further improvement of the findings here can be done by including these suppressed contributions. In particular, when taking the threshold limit of only one Mellin variable (in the case of two scaling variables as in SIDIS), while keeping the other one fixed, it is possible to gain even more insights into suppressed contributions. In [107, 108] this has been studied in the case of DY at measured rapidity. We leave a more advanced study and adaption to SIDIS for future work.

TIMELIKE γ^*	SPACELIKE γ^*
$\tilde{\omega}^{\mathrm{DY,res}}_{q\bar{q}}(N) = e_q^2\, H^{\mathrm{DY}}_{q\bar{q}}\, \Delta_q(N)$	$\tilde{\omega}^{T,\mathrm{res}}_{qq}(N,M) = e_q^2\, H^{\mathrm{SIDIS}}_{q\bar{q}}\, \Delta_q(\sqrt{NM})$
$= e_q^2 \left\lvert \left[1 - \tilde{I}_q\right] F_q^t \right\rvert^2 \widehat{C}_{qq}\widehat{\Delta}_q(N)$	$= e_q^2 \left\lvert \left[1 - \tilde{I}_q\right] F_q \right\rvert^2 \widehat{C}_{qq}\widehat{\Delta}_q(\sqrt{NM})$
$\tilde{\omega}^{\mathrm{DY,rap}}_{q\bar{q}}(N,M) = \tilde{\omega}^{\mathrm{DY,incl}}_{q\bar{q}}(\sqrt{NM})$	
$\tilde{\omega}^{\mathrm{SIA,res}}_{q}(N) = e_q^2\, H^{\mathrm{SIA}}_{q}\, \Sigma_q(N)$	$\tilde{\omega}^{\mathrm{DIS,res}}_{q}(N) = e_q^2\, H^{\mathrm{DIS}}_{q}\, \Sigma_q(N)$
$= e_q^2 \left\lvert \left[1 - \tilde{I}^B_q\right] F_q^t \right\rvert^2 \widehat{C}^B_{qq}\widehat{\Sigma}_q(N)$	$= e_q^2 \left\lvert \left[1 - \tilde{I}^B_q\right] F_q \right\rvert^2 \widehat{C}^B_{qq}\widehat{\Sigma}_q(N)$

Table 1: Resummed cross sections of the DY, SIDIS, SIA and DIS processes in the threshold limit, i.e. for large Mellin variables. In the left column are the processes with timelike photon $q\bar{q} \to \gamma^*$ or $\gamma^* \to q\bar{q}$, i.e. timelike QFF (blue), whereas in the right column we show the processes with a spacelike photon $\gamma^* q \to q$ and spacelike QFF (green). In SIDIS we use the same soft radiation exponent (red) as in DY at a rescaled argument, whereas in SIA and DIS we use the exponent containing soft radiation collinear to an unobserved final state parton (cyan). The subtraction operators are the same in the case of DY and SIDIS (orange) or DIS and SIA (magenta). The DY cross section at measured rapidity (dependent on two scaling variables) is equivalent to the inclusive DY cross section when rescaling it as $N \to \sqrt{NM}$. This is used to obtain resummed corrections to the transverse coefficient functions in SIDIS. After opening the digital version of this dissertation in the portable document format, each colored box is clickable leading to the corresponding equations.

5

APPROXIMATE NNLO CORRECTIONS

We determine approximate next-to-next-to-leading order (NNLO) corrections to unpolarized and polarized semi-inclusive DIS. They are derived using the threshold resummation formalism, which we fully develop to next-to-next-to-leading logarithmic (NNLL) accuracy, including the two-loop hard factor. The approximate NNLO terms are obtained by expansion of the resummed expression. They include all terms in Mellin space that are logarithmically enhanced at threshold, or that are constant. In terms of the customary SIDIS variables x and z they include all double distributions (that is, "plus" distributions and δ-functions) in the partonic variables. We also investigate corrections that are suppressed at threshold and we determine the dominant terms among these. Our numerical estimates suggest much significance of the approximate NNLO terms, along with a reduction in scale dependence. This Chapter is based on publication [i].

5.1 INTRODUCTION

Data taken in the semi-inclusive deep-inelastic scattering (SIDIS) process $\ell p \to \ell h X$ offer powerful insights into QCD and hadronic structure. Among their main uses are extractions of fragmentation functions [109–113], (polarized) parton distributions [18, 114], or even combinations thereof [115, 116].

Today, modern "global" analyses of parton distributions are customarily carried out at next-to-next-to-leading order (NNLO) accuracy of QCD perturbation theory. Although SIDIS might in principle offer important complementary information on, for example, the flavor structure of the sea quarks, the analyses usually do not include information from SIDIS. One reason for this is the fact that the NNLO partonic hard-scattering functions for SIDIS are not yet available (a few first steps toward their calculation have been taken in [117–119]), so that computations of the SIDIS cross section are currently restricted to next-to-leading order (NLO).

The Electron Ion Collider (EIC) is now firmly on its path toward construction [120]. The past few years have seen tremendous progress on the development of the theoretical framework for describing reactions relevant at the EIC. Further improve-

ments will likely occur in the near term. Ideally, by the time the EIC will turn on, it would be hoped that the precision of theoretical calculations should be on par with what has by now been achieved for the LHC, with NNLO corrections available for many observables, and extractions of parton distributions and fragmentation functions routinely at NNLO using numerically efficient tools. As part of this, it is expected that also full calculations of the NNLO corrections to SIDIS will become available at some point. Until this is the case, it is useful to provide accurate approximations of the NNLO corrections for SIDIS. This is the main goal of this paper. The results we obtain may be used to carry out analyses of parton distributions and/or fragmentation functions using SIDIS data at (approximate) NNLO already now.

The strategy we will follow to derive approximate NNLO corrections to SIDIS is to use QCD threshold resummation. The partonic SIDIS process is characterized by two "scaling" variables, $\hat{x} = -q^2/2p\cdot q \equiv Q^2/2p\cdot q$ and $\hat{z} = p\cdot p_c/p\cdot q$, with q, p, p_c the momenta of the virtual photon, the incoming parton, and the fragmenting parton, respectively. When $\hat{x}$ and $\hat{z}$ get close to 1, the partonic hard-scattering functions develop large double-logarithmic terms. These logarithms arise since large $\hat{x}, \hat{z}$ corresponds to scattering near a phase space boundary, where real-gluon emission is suppressed. At the kth order of perturbation theory, the SIDIS quark hard-scattering function contains terms of the form $\alpha_s^k \delta(1-\hat{x}) \left(\frac{\ln^m(1-\hat{z})}{1-\hat{z}}\right)_+$, $\alpha_s^k \delta(1-\hat{z}) \left(\frac{\ln^m(1-\hat{x})}{1-\hat{x}}\right)_+$, with $m \leq 2k-1$, or "mixed" terms $\alpha_s^k \left(\frac{\ln^m(1-\hat{x})}{1-\hat{x}}\right)_+ \left(\frac{\ln^n(1-\hat{z})}{1-\hat{z}}\right)_+$ with $m+n \leq 2k-2$. Here the subscript "+" indicates the usual distribution. Threshold resummation addresses these large logarithmic terms to all orders in the strong coupling. The resummation for the case of SIDIS was discussed in Refs. [20, 21, 89, 121] to next-to-leading logarithm (NLL), which amounts to the cases $m = 2k-1, 2k-2, 2k-3$ and $m+n = 2k-2, 2k-3$ above, respectively. To NLO, this reproduces *all* double distributions, but only the three leading towers of logarithms at NNLO and beyond.

In the present paper we take a significant step further and extend the work of [20, 21] to next-to-next-to-leading logarithm (NNLL). The close correspondence of SIDIS with the Drell-Yan cross section is particularly useful in this context [89], and so is the close correspondence between the totally inclusive Drell-Yan cross section and the cross section differential in rapidity [20, 122, 123]. We use results available in the literature [48, 49, 100, 124] to determine the two-loop hard virtual contribution to the resummed expression for SIDIS. The NNLL results may then be expanded to fixed order, NNLO. The main important new result of our paper is that we derive *all* double distributions in $\hat{x}$ and $\hat{z}$ in the NNLO SIDIS quark coefficient function. We further improve our results by deriving the dominant part

of NNLO contributions that are suppressed near threshold. These terms are of the form $\ln^m(1-\hat{x})\ln^n(1-\hat{z})$, with $m+n=3$. We also show that the NNLO contributions near threshold are the same for the spin-averaged and spin-dependent cases. This is indeed expected for the terms with $+$-distributions, since these terms are associated with emission of soft gluons which does not care about spin, but it extends even to the threshold-suppressed contributions that we derive.

Our results are readily suited for phenomenology for the SIDIS cross section and spin asymmetry at (nearly) NNLO. At the very least, they provide important benchmarks for future full calculations of SIDIS at NNLO.

Our paper is organized as follows: Section 5.2 sets the stage by addressing the perturbative SIDIS cross section. In Sec. 5.3 we determine the threshold resummation for SIDIS to NNLL. Special emphasis is put on the derivation of the hard factor at two loops. Section 5.4 addresses the dominant threshold-suppressed contributions. Having determined all ingredients, we finally present the NNLO expansions in Sec. 5.5. Section 5.6 rounds off the paper by presenting some basic phenomenological results at approximate NNLO.

5.2 PERTURBATIVE SIDIS CROSS SECTION

We consider the semi-inclusive deep-inelastic scattering (SIDIS) process $\ell(k)\,p(P)\to\ell'(k')\,h(P_h)\,X$ with the momentum transfer $q=k-k'$. It is described by the variables

$$\begin{aligned} Q^2 &= -q^2=-(k-k')^2\,,\\ x &= \frac{Q^2}{2P\cdot q}\,,\\ y &= \frac{P\cdot q}{P\cdot k}\,,\\ z &= \frac{P\cdot P_h}{P\cdot q}\,. \end{aligned} \tag{5.1}$$

We have $Q^2=xys$, with $\sqrt{s}$ the center-of-mass (c.m.) energy for the incoming electron and proton. We may write the spin-averaged SIDIS cross section as (see, for example [20])

$$\frac{d^3\sigma^h}{dxdydz}=\frac{4\pi\alpha^2}{Q^2}\left[\frac{1+(1-y)^2}{2y}\mathcal{F}_T^h(x,z,Q^2)+\frac{1-y}{y}\mathcal{F}_L^h(x,z,Q^2)\right], \tag{5.2}$$

where α is the fine structure constant and $\mathcal{F}_T^h \equiv 2F_1^h$ and $\mathcal{F}_L^h \equiv F_L^h/x$ are the transverse and longitudinal structure functions. For collisions of longitudinally polarized leptons and protons we obtain the helicity-dependent cross section as

$$\begin{aligned}\frac{1}{2}\left(\frac{d^3\sigma^h_{++}}{dxdydz} - \frac{d^3\sigma^h_{+-}}{dxdydz}\right) &= \frac{4\pi\alpha^2}{Q^2}\,\frac{1-(1-y)^2}{2y}\,\mathcal{G}_1^h(x,z,Q^2) \\ &\equiv \frac{d^3\Delta\sigma^h}{dxdydz}\,, \end{aligned} \tag{5.3}$$

with $\mathcal{G}_1^h = 2g_1^h$ in the more conventional notation of Ref. [64]. The subscripts in the first expression denote the helicities of the incoming lepton and proton.

Using factorization, the unpolarized structure functions may be written as

$$\begin{aligned}\mathcal{F}_i^h(x,z,Q^2) \;=\; \sum_{f,f'}\int_x^1\frac{d\hat{x}}{\hat{x}}\int_z^1\frac{d\hat{z}}{\hat{z}}\,D_{f'}^h\left(\frac{z}{\hat{z}},\mu_F\right) \\ \times\,\omega^i_{f'f}\left(\hat{x},\hat{z},\alpha_s(\mu_R),\frac{\mu_R}{Q},\frac{\mu_F}{Q}\right) f\left(\frac{x}{\hat{x}},\mu_F\right)\,, \end{aligned} \tag{5.4}$$

for $i = T, L$. Here $f(\xi,\mu_F)$ is the distribution of parton $f = q, \bar{q}, g$ in the nucleon at momentum fraction ξ and factorization scale μ_F, while $D_{f'}^h(\zeta,\mu_F)$ is the corresponding fragmentation function for parton f' going to the observed hadron[1] h. The functions $\omega^i_{f'f}$ are the spin-averaged hard-scattering coefficient functions. In the same way, we have in the spin-dependent case:

$$\begin{aligned}\mathcal{G}_1^h(x,z,Q^2) \;=\; \sum_{f,f'}\int_x^1\frac{d\hat{x}}{\hat{x}}\int_z^1\frac{d\hat{z}}{\hat{z}}\,D_{f'}^h\left(\frac{z}{\hat{z}},\mu_F\right) \\ \times\,\Delta\omega_{f'f}\left(\hat{x},\hat{z},\alpha_s(\mu_R),\frac{\mu_R}{Q},\frac{\mu_F}{Q}\right)\Delta f\left(\frac{x}{\hat{x}},\mu_F\right)\,, \end{aligned} \tag{5.5}$$

with the proton's spin-dependent parton distribution functions Δf, and with spin-dependent hard-scattering functions $\Delta\omega_{f'f}$.

The $\omega^i_{f'f}, \Delta\omega_{f'f}$ can be computed in QCD perturbation theory. Their expansions read

$$\omega^i_{f'f} \;=\; \omega^{i,(0)}_{f'f} + \frac{\alpha_s(\mu_R)}{\pi}\,\omega^{i,(1)}_{f'f} + \left(\frac{\alpha_s(\mu_R)}{\pi}\right)^2\omega^{i,(2)}_{f'f} + \mathcal{O}(\alpha_s^3)\,, \tag{5.6}$$

and

$$\Delta\omega_{f'f} \;=\; \Delta\omega^{(0)}_{f'f} + \frac{\alpha_s(\mu_R)}{\pi}\Delta\omega^{(1)}_{f'f} + \left(\frac{\alpha_s(\mu_R)}{\pi}\right)^2\Delta\omega^{(2)}_{f'f} + \mathcal{O}(\alpha_s^3)\,. \tag{5.7}$$

1 We always use the same factorization scales in the initial and the final state.

Here the strong coupling is evaluated at the renormalization scale μ_R. To lowest order (LO), only the process $\gamma^* q \to q$ contributes, and we have

$$\begin{aligned} \omega_{qq}^{T,(0)}(\hat{x},\hat{z}) &= \Delta\omega_{qq}^{(0)}(\hat{x},\hat{z}) &&= e_q^2\,\delta(1-\hat{x})\delta(1-\hat{z}), \\ \omega_{qq}^{L,(0)}(\hat{x},\hat{z}) &= 0, \end{aligned} \tag{5.8}$$

with the quark's fractional charge e_q. Beyond LO, also gluons in the initial or final state contribute. The first-order coefficient functions $(\Delta)\omega_{f'f}^{i,(1)}$ have been known for a long time [61, 62, 64–67] (see also Ref. [20]).

In the following, it is convenient to take Mellin moments of the SIDIS cross section, for which the convolutions in Eqs. (6.3),(5.5) turn into ordinary products. We define

$$\tilde{\mathcal{F}}_i^h(N,M,Q^2) \equiv \int_0^1 dx\, x^{N-1} \int_0^1 dz\, z^{M-1}\, \mathcal{F}_i^h(x,z,Q^2)\,, \tag{5.9}$$

and in the same way for $\mathcal{G}_1^h$. One readily finds from (6.3)

$$\tilde{\mathcal{F}}_i^h(N,M,Q^2) = \sum_{f,f'} \tilde{D}_{f'}^h(M,\mu_F)\,\tilde{\omega}_{f'f}^i\left(N,M,\alpha_s(\mu_R),\frac{\mu_R}{Q},\frac{\mu_F}{Q}\right)\tilde{f}(N,\mu_F)\,, \tag{5.10}$$

where

$$\begin{aligned} &\tilde{f}(N,\mu_F) \equiv \int_0^1 dx\, x^{N-1} f(x,\mu_F), \\ &\tilde{D}_{f'}^h(M,\mu_F) \equiv \int_0^1 dz\, z^{M-1} D_{f'}^h(z,\mu_F), \\ &\tilde{\omega}_{f'f}^i\left(N,M,\alpha_s(\mu_R),\frac{\mu_R}{Q},\frac{\mu_F}{Q}\right) \\ &\quad\equiv \int_0^1 d\hat{x}\,\hat{x}^{N-1} \int_0^1 d\hat{z}\,\hat{z}^{M-1}\,\omega_{f'f}^i\left(\hat{x},\hat{z},\alpha_s(\mu_R),\frac{\mu_R}{Q},\frac{\mu_F}{Q}\right). \end{aligned} \tag{5.11}$$

We observe that the Mellin moments of the structure functions are obtained from the moments of the parton distribution functions and fragmentation functions, and the double-Mellin moments of the partonic hard-scattering functions. For the spin-dependent case we have in the same way

$$\tilde{\mathcal{G}}_1^h(N,M,Q^2) = \sum_{f,f'} \tilde{D}_{f'}^h(M,\mu_F)\,\Delta\tilde{\omega}_{f'f}\left(N,M,\alpha_s(\mu_R),\frac{\mu_R}{Q},\frac{\mu_F}{Q}\right)\Delta\tilde{f}(N,\mu_F)\,, \tag{5.12}$$

with the corresponding moments $\Delta\tilde{f}(N,\mu_F)$ and $\Delta\tilde{\omega}_{f'f}(N,M,\ldots)$ of the polarized parton distributions and hard-scattering functions, respectively.

For the perturbative expansions given in Eqs. (6.4),(5.7), we have at lowest order according to (6.5)

$$\begin{aligned} \tilde{\omega}_{qq}^{T,(0)}(N,M) &= \Delta\tilde{\omega}_{qq}^{(0)}(N,M) &&= e_q^2, \\ \tilde{\omega}_{qq}^{L,(0)}(N,M) &= 0. \end{aligned} \tag{5.13}$$

The corresponding moments of the next-to-leading order (NLO) terms $\omega_{f'f}^{i,(1)}, \Delta\omega_{f'f}^{(1)}$ may be found in Refs. [20, 95]. In the following, we address higher-order corrections to the hard-scattering functions that arise at large values of $\hat{x}$ and $\hat{z}$ or, equivalently, at large N and M.

5.3 THRESHOLD RESUMMATION

5.3.1 *Structure of resummation for Drell-Yan and SIDIS*

As has been discussed in [20, 21] (and as is familiar from numerous other situations in perturbative calculations of cross sections), in the "threshold limit" of large N and M the perturbative QCD corrections for $\tilde{\omega}_{f'f}^{T}$ and $\Delta\tilde{\omega}_{f'f}$ develop large double-logarithmic corrections in $\ln(N)$ and $\ln(M)$. These corrections exponentiate and may thus be controlled to all orders in the strong coupling, amounting to a resummation of the logarithmic corrections. The exponentiated result may be used to obtain approximate fixed-order corrections to the SIDIS cross sections.

To achieve the resummation of the threshold logarithms for SIDIS, we will use the methods developed in Refs. [20, 32, 89, 99]. Technically, the resummation for SIDIS with its two Mellin variables N and M bears much resemblance with that for the Drell-Yan or Higgs cross sections at measured rapidity, which are also described by two separate moments [102, 121–123]. This is in contrast to observables characterized by a *single* moment variable N, such as the totally inclusive Drell-Yan cross section. However, as was shown in Ref. [20] to NLL, there is a simple correspondence between the threshold-resummed expressions for the case with two Mellin moments, and those with only a single moment. To state this correspondence, let us consider the resummed $q\bar{q}$ hard-scattering function for the Drell-Yan process as an example. For the totally inclusive cross section, we denote the function by $\tilde{\omega}_{q\bar{q}}^{\mathrm{DY,incl}}(N)$, where N is the Mellin variable conjugate to $z \equiv Q^2/\hat{s}$, with Q the Drell-Yan pair mass and $\sqrt{\hat{s}}$ the partonic c.m. energy. For the rapidity-dependent cross section, we have instead $\tilde{\omega}_{q\bar{q}}^{\mathrm{DY,rap}}(N,M)$, where N and M are conjugate to $\sqrt{z}\,\mathrm{e}^{\pm y}$, respectively, with y the lepton pair's rapidity. Near threshold one then has

$$\tilde{\omega}_{q\bar{q}}^{\mathrm{DY,rap}}(N,M) = \tilde{\omega}_{q\bar{q}}^{\mathrm{DY,incl}}(\sqrt{NM})\,. \tag{5.14}$$

This correspondence is a consequence of kinematics in the exponentiation of eikonal diagrams as discussed in Refs. [20, 89, 94]. It applies to all color-singlet processes and may therefore also be exploited for the SIDIS process[2]. As a result, we may obtain resummed expressions for SIDIS by considering those for the inclusive Drell-Yan process, "rescaling" N to $\sqrt{NM}$ appropriately, and "crossing" from timelike (Drell-Yan) kinematics to spacelike (SIDIS) kinematics. This is the strategy we will pursue in this paper.

There are various (of course, equivalent) ways of writing the all-order expression for the resummed inclusive Drell-Yan hard-scattering function near threshold. Here we will follow the approaches developed in Refs. [32, 99]. We have, in the $\overline{\text{MS}}$ scheme,

$$\begin{aligned}
&\tilde{\omega}_{q\bar{q}}^{\text{DY,res}}\left(N,\alpha_s(\mu_R),\frac{\mu_R}{Q},\frac{\mu_F}{Q}\right)\\
&= e_q^2\,H_{q\bar{q}}^{\text{DY}}\left(\alpha_s(\mu_R),\frac{\mu_R}{Q},\frac{\mu_F}{Q}\right)\,\Delta_q\left(N,\alpha_s(\mu_R),\frac{\mu_R}{Q},\frac{\mu_F}{Q}\right)\\
&= e_q^2\,H_{q\bar{q}}^{\text{DY}}\left(\alpha_s(\mu_R),\frac{\mu_R}{Q},\frac{\mu_F}{Q}\right)\,\widehat{C}_{qq}\left(\alpha_s(\mu_R),\frac{\mu_R}{Q}\right)\\
&\times \exp\left\{\int_{Q^2/\bar{N}^2}^{Q^2}\frac{d\mu^2}{\mu^2}\left[A_q\big(\alpha_s(\mu)\big)\ln\left(\frac{\mu^2\bar{N}^2}{Q^2}\right)-\frac{1}{2}\widehat{D}_q\big(\alpha_s(\mu)\big)\right]\right.\\
&\qquad\left.+2\ln\bar{N}\int_{Q^2}^{\mu_F^2}\frac{d\mu^2}{\mu^2}A_q\big(\alpha_s(\mu)\big)\right\},
\end{aligned}\tag{5.15}$$

where

$$\bar{N} = N\,\mathrm{e}^{\gamma_E}\,,\tag{5.16}$$

with the Euler constant γ_E. In Eq. (5.15) each of the functions $H_{q\bar{q}}^{\text{DY}}$, $\widehat{C}_{qq}$, A_q, $\widehat{D}_q$ is a perturbative series in the strong coupling with expansion coefficients that are collected in Appendix B.1 to the order required for resummation at next-to-next-to-leading logarithmic (NNLL) accuracy. The factor Δ_q in the first line contains all soft-gluon radiation near threshold (both collinear and wide-angle), while the coefficient $H_{q\bar{q}}^{\text{DY}}$ collects hard virtual corrections to the underlying lowest-order (LO) process (here, $q\bar{q}\to\gamma^*$), which are independent of the moment variable. In the second line we have followed Refs. [32, 99] to split up the soft-gluon factor Δ_q into the term $\widehat{C}_{qq}$ that is again independent of N, and an exponential that contains all N-dependence. The latter is in fact entirely a function of $\ln(\bar{N})$ and contains no further N-independent terms.

2 As discussed in Ref. [89], one may actually define a simplified variant of SIDIS that is characterized by only a single Mellin variable, conjugate to $\tau_{\text{SIDIS}} = xz$, with x, z defined in Eq. (6.1).

The NNLL resummation formula for the SIDIS transverse structure function may now be written as follows:

$$\begin{aligned}
&\tilde{\omega}_{qq}^{T,\mathrm{res}}\left(N,M,\alpha_s(\mu_R),\frac{\mu_R}{Q},\frac{\mu_F}{Q}\right)\\
&\quad= e_q^2\,H_{qq}^{\mathrm{SIDIS}}\left(\alpha_s(\mu_R),\frac{\mu_R}{Q},\frac{\mu_F}{Q}\right)\,\Delta_q\left(\sqrt{NM},\alpha_s(\mu_R),\frac{\mu_R}{Q},\frac{\mu_F}{Q}\right)\,. \qquad (5.17)
\end{aligned}$$

As anticipated, we have "rescaled" N to $\sqrt{NM}$ in the moment-dependent part of the expression. The function Δ_q is otherwise identical to that for the Drell-Yan case in Eq. (5.15), including the function $\widehat{C}_{qq}$. The hard coefficient H_{qq}^{SIDIS} is, however, different from $H_{q\bar{q}}^{\mathrm{DY}}$, owing to the different kinematics of the two processes. It will be derived in the next subsection. Inserting Δ_q from (5.15) into Eq. (6.9) we obtain

$$\begin{aligned}
&\tilde{\omega}_{qq}^{T,\mathrm{res}}\left(N,M,\alpha_s(\mu_R),\frac{\mu_R}{Q},\frac{\mu_F}{Q}\right)\\
&\quad= e_q^2\,H_{qq}^{\mathrm{SIDIS}}\left(\alpha_s(\mu_R),\frac{\mu_R}{Q},\frac{\mu_F}{Q}\right)\,\widehat{C}_{qq}\left(\alpha_s(\mu_R),\frac{\mu_R}{Q}\right)\\
&\quad\times\ \exp\left\{\int_{Q^2/(\bar{N}\bar{M})}^{Q^2}\frac{d\mu^2}{\mu^2}\left[A_q\left(\alpha_s(\mu)\right)\ln\left(\frac{\mu^2\bar{N}\bar{M}}{Q^2}\right)-\frac{1}{2}\widehat{D}_q\left(\alpha_s(\mu)\right)\right]\right.\\
&\quad+\ \left.\ln\bar{N}\int_{Q^2}^{\mu_F^2}\frac{d\mu^2}{\mu^2}A_q\left(\alpha_s(\mu)\right)+\ln\bar{M}\int_{Q^2}^{\mu_F^2}\frac{d\mu^2}{\mu^2}A_q\left(\alpha_s(\mu)\right)\right\}\,, \qquad (5.18)
\end{aligned}$$

where (see (6.10)) $\bar{M}=Me^{\gamma_E}$. We note that the same resummation formula applies to the spin-dependent case:

$$\Delta\tilde{\omega}_{qq}^{\mathrm{res}}\;=\;\tilde{\omega}_{qq}^{T,\mathrm{res}}\,. \qquad (5.19)$$

5.3.2 *The hard factor* H_{qq}^{SIDIS}

As already mentioned, the factor H_{qq}^{SIDIS} is derived from the finite part of the virtual corrections to the LO process, which for SIDIS is $q\gamma^*\to q$. Since we want to derive the resummed formula to NNLL (and ultimately the near-threshold NNLO corrections to SIDIS), we need H_{qq}^{SIDIS} to two loops. The relevant two-loop virtual corrections are known in terms of the "quark form factor" computed to two and even three loops in Refs. [48, 49, 51]. In case of the space-like kinematics ($q^2<0$) relevant for SIDIS the renormalized spacelike quark form factor is given to two loops in dimensional regularization with $d=4-2\epsilon$ space-time dimensions as [48, 49]

$$F_q(q^2)\;=\;F_q^{(0)}+\frac{\alpha_s}{\pi}F_q^{(1)}+\left(\frac{\alpha_s}{\pi}\right)^2F_q^{(2)}+\mathcal{O}(\alpha_s^3)\,, \qquad (5.20)$$

where

$$
\begin{aligned}
F_q^{(0)} &= 1\,, \\
F_q^{(1)} &= C_F\left[-\frac{1}{2\epsilon^2}-\frac{3}{4\epsilon}+\frac{\pi^2}{24}-2+\left(\frac{7\zeta(3)}{6}+\frac{\pi^2}{16}-4\right)\epsilon\right. \\
&+ \left.\left(\frac{7\zeta(3)}{4}+\frac{47\pi^4}{2880}+\frac{\pi^2}{6}-8\right)\epsilon^2+\mathcal{O}\left(\epsilon^3\right)\right]\,, \\
F_q^{(2)} &= C_F^2\left[\frac{1}{8\epsilon^4}+\frac{3}{8\epsilon^3}+\left(\frac{41}{32}-\frac{\pi^2}{48}\right)\frac{1}{\epsilon^2}+\left(\frac{221}{64}-\frac{4\zeta(3)}{3}\right)\frac{1}{\epsilon}\right. \\
&- \left.\frac{29\zeta(3)}{8}-\frac{13\pi^4}{576}+\frac{17\pi^2}{192}+\frac{1151}{128}\right] \\
&+ C_F C_A\left[\frac{11}{32\epsilon^3}+\left(\frac{1}{9}+\frac{\pi^2}{96}\right)\frac{1}{\epsilon^2}+\left(\frac{13\zeta(3)}{16}-\frac{11\pi^2}{192}-\frac{961}{1728}\right)\frac{1}{\epsilon}\right. \\
&+ \left.\frac{313\zeta(3)}{144}+\frac{11\pi^4}{720}-\frac{337\pi^2}{1728}-\frac{51157}{10368}\right] \\
&+ C_F N_f\left[-\frac{1}{16\epsilon^3}-\frac{1}{36\epsilon^2}+\left(\frac{65}{864}+\frac{\pi^2}{96}\right)\frac{1}{\epsilon}\right. \\
&+ \left.\frac{\zeta(3)}{72}+\frac{23\pi^2}{864}+\frac{4085}{5184}\right]+\mathcal{O}\left(\epsilon\right)\,,
\end{aligned}
\tag{5.21}
$$

with N_f the number of flavors and $C_F = 4/3, C_A = 3$. In these expressions we have kept terms of order ϵ and ϵ^2 in the one-loop result since these turn out to make finite contributions in the end.

As shown in Refs. [100, 124], the hard coefficient may be extracted from the form factor in the following way. Applied to the case of SIDIS we have from [100]

$$
H_{qq}^{\text{SIDIS}}\left(\alpha_s(Q)\right) \;=\; \left|\left[1-\tilde{I}_q\left(\epsilon,\alpha_s(Q)\right)\right]F_q\right|^2\,, \tag{5.22}
$$

where $\tilde{I}_q$ is an operator that removes the poles of the form factor and makes the necessary soft and collinear adjustments needed to extract the hard coefficient. It is given in [100] in terms of a convenient all-order form:

$$
1-\tilde{I}_q(\epsilon,\alpha_s) \;=\; \exp\left\{R_q\left(\epsilon,\alpha_s\right)-i\Phi_q\left(\epsilon,\alpha_s\right)\right\}\,, \tag{5.23}
$$

with functions R_q and Φ_q that each are perturbative series. The phase Φ_q does not contribute in our case since we take the absolute square in Eq. (6.20). The function R_q effects the cancelation of infrared divergences from the quark form factor. It can be expressed in terms of a soft and a collinear part:

$$
R_q(\epsilon,\alpha_s) = R_q^{\text{soft}}(\epsilon,\alpha_s)+R_q^{\text{coll}}(\epsilon,\alpha_s)\,, \tag{5.24}
$$

where for NNLL accuracy

$$
\begin{aligned}
R_q^{\text{soft}}(\epsilon,\alpha_s) &= C_F\left(\frac{\alpha_s}{\pi}R_q^{\text{soft}\,(1)}(\epsilon)+\left(\frac{\alpha_s}{\pi}\right)^2 R_q^{\text{soft}\,(2)}(\epsilon)+\mathcal{O}(\alpha_s^3)\right)\,,\\
R_q^{\text{coll}}(\epsilon,\alpha_s) &= \frac{\alpha_s}{\pi}R_q^{\text{coll}\,(1)}(\epsilon)+\left(\frac{\alpha_s}{\pi}\right)^2 R_q^{\text{coll}\,(2)}(\epsilon)+\mathcal{O}(\alpha_s^3)\,,
\end{aligned}
\tag{5.25}
$$

with

$$
\begin{aligned}
R_q^{\text{soft}\,(1)}(\epsilon) &= \frac{1}{2\epsilon^2}-\frac{\pi^2}{8}\,,\\
R_q^{\text{soft}\,(2)}(\epsilon) &= -\frac{3\pi b_0}{8\epsilon^3}+\frac{1}{8\epsilon^2}\frac{A_q^{(2)}}{C_F}\\
&\quad-\frac{1}{16\epsilon}\left[C_A\left(7\zeta(3)+\frac{11\pi^2}{36}-\frac{202}{27}\right)+N_f\left(\frac{28}{27}-\frac{\pi^2}{18}\right)\right]\\
&\quad+C_A\left(-\frac{187\zeta(3)}{144}+\frac{\pi^4}{288}-\frac{469\pi^2}{1728}+\frac{607}{648}\right)\\
&\quad+N_f\left(\frac{17\zeta(3)}{72}+\frac{35\pi^2}{864}-\frac{41}{324}\right)\,,\\
R_q^{\text{coll}\,(1)}(\epsilon) &= \frac{3}{4\epsilon}C_F\,,\\
R_q^{\text{coll}\,(2)}(\epsilon) &= -\frac{3\pi b_0}{8\epsilon^2}C_F\\
&\quad+\frac{1}{8\epsilon}\left[C_F^2\left(6\zeta(3)-\frac{\pi^2}{2}+\frac{3}{8}\right)+C_F N_f\left(-\frac{1}{12}-\frac{\pi^2}{9}\right)\right.\\
&\qquad\left.+C_A C_F\left(-3\zeta(3)+\frac{11\pi^2}{18}+\frac{17}{24}\right)\right]\,.
\end{aligned}
\tag{5.26}
$$

The coefficient b_0 can be found in Appendix B.1. Inserting all terms into Eq. (6.20) and expanding in α_s, all poles in powers of $1/\epsilon$ cancel, and we find for an arbitrary renormalization scale μ_R, but for $\mu_F = Q$:

$$
\begin{aligned}
H_{qq}^{\text{SIDIS}}\left(\alpha_s(\mu_R),\frac{\mu_R}{Q},1\right) &= 1+\frac{\alpha_s(\mu_R)}{\pi}H_{qq}^{\text{SIDIS},(1)}\\
&\quad+\left(\frac{\alpha_s(\mu_R)}{\pi}\right)^2 H_{qq}^{\text{SIDIS},(2)}+\mathcal{O}(\alpha_s^3)\,,
\end{aligned}
\tag{5.27}
$$

with

$$
\begin{aligned}
H_{qq}^{\text{SIDIS},(1)} &= C_F\left(-4-\frac{\pi^2}{6}\right), \\
H_{qq}^{\text{SIDIS},(2)} &= C_F\left(-4-\frac{\pi^2}{6}\right)\pi b_0 \ln\frac{\mu_R^2}{Q^2} \\
&+ C_F^2\left(-\frac{15\zeta(3)}{4}+\frac{61\pi^2}{48}+\frac{511}{64}-\frac{\pi^4}{60}\right) \\
&+ C_F C_A\left(\frac{7\zeta(3)}{4}+\frac{3\pi^4}{80}-\frac{1535}{192}-\frac{403\pi^2}{432}\right) \\
&+ C_F N_f\left(\frac{\zeta(3)}{2}+\frac{29\pi^2}{216}+\frac{127}{96}\right). \qquad (5.28)
\end{aligned}
$$

The factorization scale dependence of H_{qq}^{SIDIS} is trivially determined by the DGLAP evolution kernels of the parton distributions and fragmentation functions and will be addressed later.

With all ingredients to NNLL resummation at hand we are now also in the position to expand the hard-scattering function in (5.18) to NNLO (that is, $\mathcal{O}(\alpha_s^2)$) accuracy. This expansion will be carried out in Sec. 5.5. Before turning to it, we will discuss another class of corrections near threshold that are suppressed with respect to the terms addressed by resummation, but that can be significant as well in phenomenological studies.

5.4 SUBLEADING CONTRIBUTIONS NEAR THRESHOLD

All contributions contained in Eq. (5.18) are *leading* near threshold in the sense that they carry powers of $\ln(N)$ or $\ln(M)$, never accompanied by any suppression by $1/N$ or $1/M$. Such terms are therefore often referred to as *leading-power (LP)* contributions. For the NNLL resummed cross section the LP terms contain the five "towers" $\alpha_s^n L^m$, with $m \in \{2n, \ldots, 2n-4\}$, where L^m can be any product of (in total) m logarithms in N or M. The LP terms correspond to distributions ("+"-distributions and δ-functions) in $\hat{x}, \hat{z}$ space. In the full cross section there are, of course, also terms that are suppressed near threshold. The most important among these are terms still containing logarithms, but suppressed by a single power in $1/N$ or $1/M$. Such terms are known as *next-to-leading power (NLP)* corrections. Their structure is $\alpha_s^n L^m/N$ or $\alpha_s^n L^m/M$, with $m \in \{2n-1, \ldots, 2n-3\}$, corresponding to terms of the form $\alpha_s^n \ell^m$ in $\hat{x}, \hat{z}$ space, where ℓ^m is a product of $\ln(1-\hat{x})$ and $\ln(1-\hat{z})$ with total power m.

The role of NLP terms in color-singlet hard-scattering cross sections has been addressed early on in Refs. [32, 125–128]. In recent years, the understanding of such corrections has further advanced, and numerous studies have been carried out [107, 129–151] that address the NLP contributions from various angles, such as corrections to the eikonal approximation, resummations of NLP terms to leading logarithm and beyond, and generalized factorization theorems at NLP. For especially simple processes such as the fully inclusive Drell-Yan process, the results of these studies are quite mature. For processes described by two scaling variables (or, two Mellin moments), as relevant for SIDIS, comparably fewer studies are available [107, 147]. In the present study we will derive the dominant NLP contributions at NNLL which, as described above, are of the form $\alpha_s^n L^{2n-1}/N$ or $\alpha_s^n L^{2n-1}/M$. In terms of the NNLO expansion, these are the terms $\alpha_s^2 L^3/N$ or $\alpha_s^2 L^3/M$, where $L \in \{\ln^3(N), \ln^2(N)\ln(M), \ln(N)\ln^2(M), \ln^3(M)\}$.

As discussed in [32, 125, 127], these dominant NLP terms may be incorporated to all orders via a particular treatment of the evolution of the parton distributions and fragmentation functions[3]. To this end, we consider a specific SIDIS quark channel in the spin-averaged case and include the parton distribution and fragmentation function. From Eqs. (5.10),(5.18) the corresponding resummed contribution to the transverse SIDIS structure function in moment space may be written as

$$
\begin{aligned}
&\tilde{q}(N,\mu_F)\,\tilde{D}_q^h(M,\mu_F)\,\tilde{\omega}_{qq}^{T,\mathrm{res}}\left(N,M,\alpha_s(\mu_R),\frac{\mu_R}{Q},\frac{\mu_F}{Q}\right)\\
&= e_q^2\,H_{qq}^{\mathrm{SIDIS}}\left(\alpha_s(\mu_R),\frac{\mu_R}{Q},\frac{\mu_F}{Q}\right)\exp\left\{-2\int_{\mu_F^2}^{Q^2}\frac{d\mu^2}{\mu^2}P_{q,\delta}\big(\alpha_s(\mu)\big)\right\}\widehat{C}_{qq}\left(\alpha_s(\mu_R),\frac{\mu_R}{Q}\right)\\
&\times\exp\left\{\int_{Q^2/(\bar{N}\bar{M})}^{Q^2}\frac{d\mu^2}{\mu^2}\left[A_q\big(\alpha_s(\mu)\big)\ln\left(\frac{\mu^2}{Q^2}\right)+2P_{q,\delta}\big(\alpha_s(\mu)\big)-\frac{1}{2}\widehat{D}_q\big(\alpha_s(\mu)\big)\right]\right\}\\
&\times\exp\left\{\int_{\mu_F^2}^{Q^2/(\bar{N}\bar{M})}\frac{d\mu^2}{\mu^2}\Big[-A_q\big(\alpha_s(\mu)\big)\,\ln\bar{N}+P_{q,\delta}\big(\alpha_s(\mu)\big)\Big]\right\}\tilde{q}(N,\mu_F)\\
&\times\exp\left\{\int_{\mu_F^2}^{Q^2/(\bar{N}\bar{M})}\frac{d\mu^2}{\mu^2}\Big[-A_q\big(\alpha_s(\mu)\big)\,\ln\bar{M}+P_{q,\delta}\big(\alpha_s(\mu)\big)\Big]\right\}\tilde{D}_q^h(M,\mu_F)\,,
\end{aligned}
\tag{5.29}
$$

where the function $P_{q,\delta}$ corresponds to the coefficient of $\delta(1-x)$ in the quark DGLAP splitting function and is also given in Appendix B.1.

We make the following observations concerning Eq. (5.29). We obviously have simply added and subtracted the terms involving $P_{q,\delta}$ in the exponent, so that they cancel. However, each of the individual terms serves a separate purpose. The $P_{q,\delta}$ term

3 For an alternative, but equivalent, approach in $\hat{x},\hat{z}$ space, see Ref. [143].

in the second line, when combined with $H_{qq}^{\text{SIDIS}}\big(\alpha_s(\mu_R), \mu_R/Q, \mu_F/Q\big)$, removes the factorization scale dependence of the SIDIS hard function, so that we end up with $H_{qq}^{\text{SIDIS}}\big(\alpha_s(\mu_R), \mu_R/Q, 1\big)$, precisely as given in Eq. (B.9). Thanks to factorization, this must hold true to all orders of perturbation theory. The other two $P_{q,\delta}$ terms in Eq. (5.29) combine with the terms $A_q \ln \bar{N}$ or $A_q \ln \bar{M}$ to reproduce the quark-to-quark splitting function in the large-N or large-M limit, at leading power. As a result, the last two exponential factors simply represent the DGLAP evolutions of the quark parton distribution function and the fragmentation function, respectively, from scale μ_F to scale $Q/\sqrt{\bar{N}\bar{M}}$. At leading power, this evolution is entirely diagonal, and evolution of parton distributions (spacelike) and of fragmentation functions (timelike) is identical. We can therefore carry out this evolution and write Eq. (5.29) as

$$\begin{aligned}
&\tilde{q}(N,\mu_F)\,\tilde{D}_q^h(M,\mu_F)\,\tilde{\omega}_{qq}^{T,\text{res}}\left(N, M, \alpha_s(\mu_R), \frac{\mu_R}{Q}, \frac{\mu_F}{Q}\right) \\
&\quad = e_q^2\, H_{qq}^{\text{SIDIS}}\left(\alpha_s(\mu_R), \frac{\mu_R}{Q}, 1\right) \widehat{C}_{qq}\left(\alpha_s(\mu_R), \frac{\mu_R}{Q}\right) \tilde{q}\left(N, Q/\sqrt{\bar{N}\bar{M}}\right) \tilde{D}_q^h\left(M, Q/\sqrt{\bar{N}\bar{M}}\right) \\
&\quad \times \exp\left\{\int_{Q^2/(\bar{N}\bar{M})}^{Q^2} \frac{d\mu^2}{\mu^2}\left[A_q\big(\alpha_s(\mu)\big) \ln\left(\frac{\mu^2}{Q^2}\right) + 2P_{q,\delta}\big(\alpha_s(\mu)\big) - \frac{1}{2}\widehat{D}_q\big(\alpha_s(\mu)\big)\right]\right\}. \qquad (5.30)
\end{aligned}$$

Again, this is correct to all orders. The trick now to obtain the dominant NLP corrections is to evolve the parton distributions and fragmentation functions from scale $Q/\sqrt{\bar{N}\bar{M}}$ back to scale μ_F, but now using the DGLAP evolution *including* NLP corrections [32, 125, 127]. The latter are readily obtained from the $1/N$ or $1/M$ terms in the spacelike or timelike splitting functions, respectively. As it turns out, for the *dominant* NLP terms, only the $1/N$ (or $1/M$) terms in the *leading-order* splitting kernels need to be taken into account. The related terms in the higher-order splitting functions lead to contributions that have fewer logarithms. Let us for the moment continue to consider only diagonal evolution, corresponding to the SIDIS quark channel. We write the standard LO quark-to-quark splitting function at large values of the moment variable as

$$\begin{aligned}
\mathcal{P}_{qq}^N &= \frac{\alpha_s}{\pi}\left(-A_q^{(1)} \ln \bar{N} + P_{q,\delta}^{(1)} + \frac{Q_q^{(1)}}{N}\right) + \mathcal{O}(\alpha_s^2) \\
&= \frac{\alpha_s}{\pi} C_F \left(-\ln \bar{N} + \frac{3}{4} - \frac{1}{2N}\right) + \mathcal{O}(\alpha_s^2). \qquad (5.31)
\end{aligned}$$

The term proportional to $Q_q^{(1)}$ is the NLP correction. At this order, the spacelike and timelike quark-to-quark splitting functions are identical so that also their NLP

corrections are the same. The relation between $\tilde{q}\left(N, Q/\sqrt{\bar{N}\bar{M}}\right)$ and $\tilde{q}(N,\mu_F)$ including the dominant NLP correction is now given by

$$\tilde{q}\left(N,\frac{Q}{\sqrt{\bar{N}\bar{M}}}\right) = \exp\left\{\int_{\mu_F^2}^{Q^2/(\bar{N}\bar{M})}\frac{d\mu^2}{\mu^2}\left[-A_q\big(\alpha_s(\mu)\big)\ln\bar{N} + P_{q,\delta}\big(\alpha_s(\mu)\big) + \frac{\alpha_s(\mu)}{\pi}\frac{Q_q^{(1)}}{N}\right]\right\}\tilde{q}(N,\mu_F) \tag{5.32}$$

and in the same way for the quark fragmentation functions. As we discussed, only the LO term with $Q_q^{(1)}$ is relevant for the dominant NLP corrections. The terms with A_q and $P_{q,\delta}$ remain, of course, the full all-order functions, needed to second order (NLO) for our purpose of obtaining NNLL/NNLO accuracy. We see from Eq. (5.32) that the dominant NLP corrections in the quark channel are obtained by multiplying the full resummed expression in Eq. (5.29) by the two factors

$$\exp\left\{-\int_{\mu_F^2}^{Q^2/(\bar{N}\bar{M})}\frac{d\mu^2}{\mu^2}\frac{\alpha_s(\mu)}{\pi}\frac{C_F}{2N}\right\}\exp\left\{-\int_{\mu_F^2}^{Q^2/(\bar{N}\bar{M})}\frac{d\mu^2}{\mu^2}\frac{\alpha_s(\mu)}{\pi}\frac{C_F}{2M}\right\}, \tag{5.33}$$

corresponding to the NLP terms related to diagonal evolution of the parton distribution and the fragmentation function.

As is well known, once the NLP terms are included, the evolution of parton distributions and fragmentation functions also involves quark-gluon mixing and hence is no longer diagonal, taking instead a matrix form. Transitions among quarks of different flavor turn out to be suppressed as $1/N^2$ or higher, at least through NLO in the evolution kernels which is all we need here. Including the dominant NLP corrections, the full evolution equations for the parton distributions may be cast into the form

$$\frac{d}{d\ln\mu^2}\begin{pmatrix}\tilde{q}(N,\mu)\\ \tilde{g}(N,\mu)\end{pmatrix} = \mathcal{P}_s^N\big(\alpha_s(\mu)\big)\begin{pmatrix}\tilde{q}(N,\mu)\\ \tilde{g}(N,\mu)\end{pmatrix} \tag{5.34}$$

to all orders, where $\mathcal{P}_s^N(\alpha_s)$ denotes the NLO matrix of spacelike splitting functions in moment space, which may be found in [83]. A corresponding equation holds for the fragmentation functions, with however the timelike splitting functions $\mathcal{P}_t^M$ [83].

It is interesting to explore the implications of the singlet mixing and to see what NLP effects it generates beyond the quark-to-quark channel. We will do this as part of the NNLO expansion to be discussed in the next section. For this expansion we do not need to fully solve the evolution equation (although this could be done

using the techniques of Ref. [62]). Instead, it suffices to just solve the equation to second order in the strong coupling, which may be achieved by iterating the kernel:

$$\begin{pmatrix} \tilde{q}\left(N, Q/\sqrt{\bar{N}\bar{M}}\right) \\ \tilde{g}\left(N, Q/\sqrt{\bar{N}\bar{M}}\right) \end{pmatrix} = \left(\mathbb{1} + \int_{\mu_F^2}^{\frac{Q^2}{\bar{N}\bar{M}}} \frac{dq^2}{q^2}\, \mathcal{P}_s^N\left(\alpha_s(q)\right) \right.$$
$$\left. + \int_{\mu_F^2}^{\frac{Q^2}{\bar{N}\bar{M}}} \frac{dq^2}{q^2}\, \mathcal{P}_s^N\left(\alpha_s(q)\right) \int_{\mu_F^2}^{\frac{q^2}{\bar{N}\bar{M}}} \frac{d\tilde{q}^2}{\tilde{q}^2}\, \mathcal{P}_s^N\left(\alpha_s(\tilde{q})\right) \right) \begin{pmatrix} \tilde{q}(N, \mu_F) \\ \tilde{g}(N, \mu_F) \end{pmatrix}, \tag{5.35}$$

and similarly for the fragmentation functions. This expression may then straightforwardly be expanded further in $\alpha_s(\mu_R)$. If we keep just the diagonal (quark-to-quark) contributions and their LP and lowest-order NLP parts, we recover the NLO and NNLO terms already contained in Eq. (5.32).

In the spin-dependent case the spacelike matrix in Eq. (5.34) is to be replaced by the polarized one, $\Delta\mathcal{P}_s^N(\alpha_s)$, given to NLO in [75–77]. The helicity evolution kernels $\Delta\mathcal{P}_s^N(\alpha_s)$ are identical to the unpolarized ones in the large-N limit at LP. This equality extends even to the first NLP $(1/N)$ corrections, except for a difference $\propto \ln(N)/N$ in the NLO gq splitting function [84]. This difference, however, does not affect the dominant NLP corrections for SIDIS at NNLO. We thus conclude that the approximate NNLO corrections to be presented next apply to both the spin-averaged and the spin-dependent hard-scattering functions.

5.5 EXPANSION TO NNLO

We are now ready to present the NNLO ($\mathcal{O}(\alpha_s^2)$) expansion for the SIDIS quark hard-scattering function near threshold, which is the main result of this paper. We insert the NLP evolved parton distributions and fragmentation functions of Eq. (5.32) into Eq. (5.30) and expand. To write our formulas compactly, we introduce

$$\mathcal{L} \equiv \frac{1}{2}\left(\ln(\bar{N}) + \ln(\bar{M})\right). \tag{5.36}$$

We then find for the transverse hard-scattering function in the quark channel:

$$\tilde{\omega}_{qq}^T\left(N, M, \alpha_s(\mu_R), \frac{\mu_R}{Q}, \frac{\mu_F}{Q}\right) = \tilde{\omega}_{qq}^{T,(0)} + \frac{\alpha_s(\mu_R)}{\pi}\, \tilde{\omega}_{qq}^{T,(1)}$$
$$+ \left(\frac{\alpha_s(\mu_R)}{\pi}\right)^2 \tilde{\omega}_{qq}^{T,(2)} + \mathcal{O}(\alpha_s^3), \tag{5.37}$$

where

$$\tilde{\omega}_{qq}^{T,(1)}\left(N,M,\frac{\mu_R}{Q},\frac{\mu_F}{Q}\right) = e_q^2 C_F\left\{2\mathcal{L}^2+\frac{\pi^2}{6}-4+\left(-\frac{3}{2}+2\mathcal{L}\right)\ln\frac{\mu_F^2}{Q^2} + \mathcal{L}\left(\frac{1}{N}+\frac{1}{M}\right)\right\}. \tag{5.38}$$

The last term is the NLP contribution. We have kept "mixed" NLP corrections of the form $\ln(\bar{N})/M$ and $\ln(\bar{M})/N$. Equation (5.38) reproduces the dominant part of the full NLO results given in [20, 95], including the NLP terms. Its LP part is consistent with the results based on NLL threshold resummation presented in [20].

For the approximate NNLO terms we find

$$\begin{aligned}
\frac{1}{e_q^2}\tilde{\omega}_{qq}^{T,(2)}\left(N,M,\frac{\mu_R}{Q},\frac{\mu_F}{Q}\right) &= 2C_F^2\mathcal{L}^4+4C_F\mathcal{L}^3\left(\frac{\pi}{3}b_0+C_F\ln\frac{\mu_F^2}{Q^2}\right)\\
&+C_F\mathcal{L}^2\left[C_F\left(-8+\frac{\pi^2}{3}+2\ln^2\frac{\mu_F^2}{Q^2}-3\ln\frac{\mu_F^2}{Q^2}\right)+\left(\frac{67}{18}-\frac{\pi^2}{6}\right)C_A-\frac{5}{9}N_f\right]\\
&+C_F\mathcal{L}\left[\left(\frac{101}{27}-\frac{7}{2}\zeta(3)\right)C_A-\frac{14}{27}N_f+C_F\ln\frac{\mu_F^2}{Q^2}\left(-8+\frac{\pi^2}{3}-3\ln\frac{\mu_F^2}{Q^2}\right)\right.\\
&\left.+\left(\left(\frac{67}{18}-\frac{\pi^2}{6}\right)C_A-\frac{5}{9}N_f\right)\ln\frac{\mu_F^2}{Q^2}-\pi b_0\ln^2\frac{\mu_F^2}{Q^2}\right]\\
&+C_F^2\left[\frac{511}{64}-\frac{\pi^2}{16}-\frac{\pi^4}{60}-\frac{15}{4}\zeta(3)+\ln\frac{\mu_F^2}{Q^2}\left(\frac{9}{8}\ln\frac{\mu_F^2}{Q^2}+\frac{93}{16}-3\zeta(3)\right)\right]\\
&+C_FC_A\left[-\frac{1535}{192}-\frac{5\pi^2}{16}+\frac{7\pi^4}{720}+\frac{151}{36}\zeta(3)\right]+C_FN_f\left[\frac{127}{96}+\frac{\pi^2}{24}+\frac{\zeta(3)}{18}\right]\\
&+\frac{3}{4}C_F\pi b_0\ln^2\frac{\mu_F^2}{Q^2}-\frac{C_F\pi^3b_0}{3}\ln\frac{\mu_F^2}{Q^2}+C_F\left(-\frac{17}{48}C_A+\frac{3}{2}\zeta(3)C_A+\frac{N_f}{24}\right)\ln\frac{\mu_F^2}{Q^2}\\
&+\pi b_0\ln\frac{\mu_R^2}{Q^2}\,\frac{1}{e_q^2}\tilde{\omega}_{qq}^{T,(1)}\left(N,M,\frac{\mu_R}{Q},\frac{\mu_F}{Q}\right)+2C_F^2\mathcal{L}^3\left(\frac{1}{N}+\frac{1}{M}\right).
\end{aligned} \tag{5.39}$$

Again, the last term is the dominant NLP correction. Here, two of the three powers of $\mathcal{L}$ arise from the LP part in the first line of Eq. (5.38), which then multiplies the NLO expansion of the NLP factor given in Eq. (6.16).

The results for the spin-dependent quark hard-scattering function near threshold are identical:

$$\Delta\tilde{\omega}_{qq}^{(k)}\left(N,M,\frac{\mu_R}{Q},\frac{\mu_F}{Q}\right) = \tilde{\omega}_{qq}^{T,(k)}\left(N,M,\frac{\mu_R}{Q},\frac{\mu_F}{Q}\right), \tag{5.40}$$

for $k = 0, 1, 2$ and including NLP corrections. In fact, this will arguably hold to all orders of perturbation theory.

So far we have only addressed the $q \to q$ channel. As we discussed in the previous section, the off-diagonal evolution of parton distributions and fragmentation functions to NLP induces quark-gluon mixing. As a result, once we insert the NLP singlet evolution in (5.35) into the cross section (5.30), we also obtain terms with $\tilde{q}(N, \mu_F)\tilde{D}_g(M, \mu_F)$ or $\tilde{g}(N, \mu_F)\tilde{D}_q(M, \mu_F)$. Evidently, these approximate the quark-to-gluon and gluon-to-quark channel contributions to SIDIS. The terms are of course suppressed by $1/N$ or $1/M$, but they also carry logarithmic enhancement. We find, at NLO:

$$\begin{aligned} \tilde{\omega}_{gq}^{T,(1)}\left(N, M, \frac{\mu_R}{Q}, \frac{\mu_F}{Q}\right) &= -e_q^2\, C_F\, \frac{\mathcal{L}}{M}\,, \\ \tilde{\omega}_{qg}^{T,(1)}\left(N, M, \frac{\mu_R}{Q}, \frac{\mu_F}{Q}\right) &= -e_q^2\, T_R\, \frac{\mathcal{L}}{N}\,, \end{aligned} \tag{5.41}$$

with $T_R = 1/2$. These expressions reproduce the corresponding full NLO transverse hard-scattering functions of Refs. [20, 95] at large moment variable. Again the contributions to the respective spin-dependent hard-scattering functions $\Delta\tilde{\omega}_{gq}^{(1)}, \Delta\tilde{\omega}_{qg}^{(1)}$ are identical to the ones given in (5.41).

Unfortunately, the evolution method that we have used here to obtain the NLP corrections fails for the $q \to g$ and $g \to q$ channels beyond NLO. We have found this by inspecting related results for the Drell-Yan process at measured rapidity. Here, evolution gives the approximate result

$$\tilde{\omega}_{qg}^{\mathrm{DY},(2)}(N, M)\Big|_{\mathrm{evol}} = -\frac{T_R\mathcal{L}}{2M}\left(4C_F\mathcal{L}^2 - (C_F - C_A)\ln\bar{N}\ln\bar{M}\right), \tag{5.42}$$

whereas the correct result is known to be [22, 101, 152–156]

$$\begin{aligned} \tilde{\omega}_{qg}^{\mathrm{DY},(2)}(N, M) &= -\frac{T_R\mathcal{L}}{2M}\left(4C_F\mathcal{L}^2 - (C_F - C_A)\ln\bar{N}\ln\bar{M}\right) \\ &+ (C_F - C_A)\,\frac{\ln^3\bar{M}}{48M}\,. \end{aligned} \tag{5.43}$$

The difference of the two results is

$$\tilde{\omega}_{qg}^{\mathrm{DY},(2)}(N, M) - \tilde{\omega}_{qg}^{\mathrm{DY},(2)}(N, M)\Big|_{\mathrm{evol}} = (C_F - C_A)\,\frac{\ln^3(\bar{M})}{48M}\,. \tag{5.44}$$

Interestingly, it depends only on one of the two Mellin variables. In the inclusive case, where $N = M$, this difference may be understood from Ref. [137] where the all-order resummation of the leading large-N contributions to the quark-gluon

contribution to inclusive Drell-Yan was derived. In the light of this, it is clear that evolution cannot correctly produce the leading NNLO terms for the SIDIS $q \to g$ and $g \to q$ channels. When expanding our corresponding results, we obtain

$$\begin{aligned}\tilde{\omega}_{gq}^{T,(2)}(N,M)\Big|_{\text{evol}} &= -\frac{C_F\mathcal{L}}{2M}\left(4C_F\mathcal{L}^2-(C_F-C_A)\ln(\bar{N})\ln(\bar{M})\right), \\ \tilde{\omega}_{qg}^{T,(2)}(N,M)\Big|_{\text{evol}} &= -\frac{T_R\mathcal{L}}{2N}\left(4C_F\mathcal{L}^2-(C_F-C_A)\ln(\bar{N})\ln(\bar{M})\right).\end{aligned} \tag{5.45}$$

We note that the $1/N$ and $1/M$ terms in the NLO splitting functions contribute here. As already stated, the results in Eq. (5.45) are not expected to be complete, although it appears likely that a term identical to the one given in Eq. (5.44) (or with $M \to N$) would need to be added. It would be highly desirable to extend the work of [137] to the Drell-Yan process at measured rapidity and to SIDIS. This is of course beyond the scope of the present work. For now we therefore refrain from encouraging use of Eq. (5.45) in any phenomenological analysis. Our NNLO approximations given in this paper therefore only apply to the quark channel.

Appendix B.2 presents our NLO and NNLO near-threshold results as functions of $\hat{x}$ and $\hat{z}$. These are obtained by a straightforward inverse transform of the above Mellin-space results.

5.6 PHENOMENOLOGICAL PREDICTIONS

We now turn to a few illustrative phenomenological applications of our approximate NNLO results. Here we only consider the unpolarized transverse structure function. We reserve a more detailed numerical analysis to the work in Chapter 6, in which we will also investigate the phenomenology of NNLL resummation.

We first need to go back from Mellin space to x, z space. This is achieved by an inverse double-Mellin transform. The structure function $\mathcal{F}_i^h(x,z,Q^2)$ can be recovered from its moments $\tilde{\mathcal{F}}_i^h(N,M,Q^2)$ given in Eq. (6.6) in the following way:

$$\mathcal{F}_i^h(x,z,Q^2) = \int_{\mathcal{C}_N}\frac{dN}{2\pi i}\,x^{-N}\int_{\mathcal{C}_M}\frac{dM}{2\pi i}\,z^{-M}\,\tilde{\mathcal{F}}_i^h(N,M,Q^2), \tag{5.46}$$

where $\mathcal{C}_N$ and $\mathcal{C}_M$ denote integration contours in the complex plane, one for each Mellin inverse. They have to be chosen in such a way that all singularities of the integrand in N lie to the left of $\mathcal{C}_N$, and likewise for the poles in M and the contour $\mathcal{C}_M$. In the actual calculation, we obtained excellent numerical convergence by

setting $N = c_N + \zeta\, e^{i\phi_N}$ and $M = c_M + \xi\, e^{i\phi_M}$ (with $\zeta, \xi \in [0, \infty]$ as contour parameters), where $c_N = 1.8$ and $c_M = 3.3$ and where we tilt each contour by an angle $\phi_N = \phi_M = 3\pi/4$.

To be consistent with the NNLO approximation of the hard-scattering functions that we make, we also need to use NNLO parton distribution functions and fragmentation functions. For the former, we choose the CT18 NNLO set of Ref. [157], from which we also adopt the NNLO strong coupling. NNLO analyses of fragmentation functions are still scarce [110, 158], partly because only the process $e^+e^- \to h + X$ is available at NNLO. For the present study we use the set of Ref. [110]. In order to be able to examine the sizes of the various corrections to the cross section, we stick to the NNLO sets of parton distributions and fragmentation functions also when computing LO or NLO results. Unless stated otherwise, we choose the renormalization and factorization scales as $\mu_R = \mu_F = Q$. Technically, in order to obtain Mellin moments of the parton distributions and fragmentation functions as needed for Eq. (5.10) in (6.28), we perform fits of a functional form $P(x)$ to them, so that the Mellin moments of $P(x)$ can be taken analytically. We have checked that our fits are accurate to better than 1% over the kinematic domain we are interested in.

We present results appropriate for the COMPASS experiment at CERN with c.m. energy $\sqrt{s} = 17.3$ GeV, and for the EIC with $\sqrt{s} = 100$ GeV. For both, we consider the process $\ell p \to \ell \pi^+ X$. We compute the contribution by the transverse structure function to the SIDIS cross section, using Eq. (6.2) and dropping the longitudinal part. We focus on the z-dependence of the cross section and integrate over $y \in [0.1, 0.9]$ and $x \in [0.1, 0.8]$. Note that we choose both x and z to be rather large so that we are safely in the threshold regime. Because of the relation $Q^2 = xys$, our choice of kinematics implies $Q^2 > 3$ GeV^2 for COMPASS, and $Q^2 > 100$ GeV^2 for the EIC. We furthermore require $W > 7$ GeV, where $W^2 = Q^2(1-x)/x + m_p^2$.

We note in passing that SIDIS experiments typically quote hadron multiplicities, which are ratios of the SIDIS cross section over the fully inclusive DIS one, for given kinematics. For the present paper we are interested in the actual NNLO corrections to SIDIS, so we do not compute multiplicities here. It would be straightforward to do this by computing DIS to full NNLO.

We start by examining NLO, where the exact answer is of course known. In the following we normalize all results by the LO cross section. The top part of Fig. 15 presents results for COMPASS kinematics. The black line shows the ratio of the full transverse NLO cross section for the $q \to q$ channel to the LO one. As one can see, the NLO corrections show the expected strong increase toward large values of z. The dashed blue line shows the LP approximation to the NLO cross section,

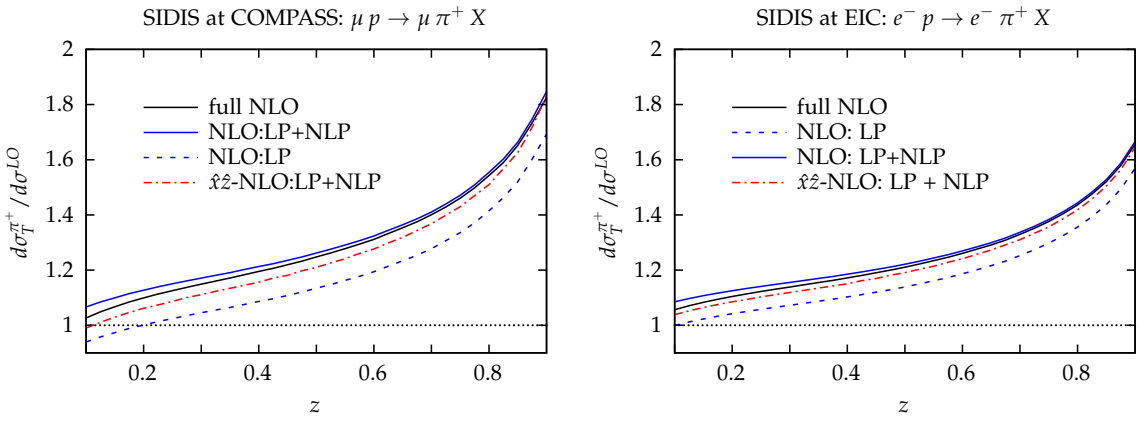

Figure 12: Left: Ratios of NLO results for the unpolarized $\ell p \to \ell \pi^+ X$ transverse cross section in the $q \to q$ channel to the LO cross section, for COMPASS kinematics with $x \in [0.1, 0.8]$. The black solid line shows the exact NLO result from Ref. [95], the dashed blue line the LP approximation in Mellin space, and the solid blue line the LP+NLP approximation. The red dash-dotted line shows the approximation obtained by Eq. (B.13) in $\hat{x}, \hat{z}$ space. Right: Same for EIC kinematics.

based on Eq. (5.38) but without the NLP term in the second line. The result shows overall good agreement with full NLO, indicating the dominance of the threshold regime, but has a nearly constant difference to the exact result. The agreement with full NLO becomes even much better when the dominant NLP corrections in the second line of Eq. (5.38) are included, as shown by the solid blue line. Clearly the full NLO is excellently approximated by this near-threshold result over the whole range in z, and especially so toward large z.

It is interesting to compare the NLO approximations based on the Mellin-space calculation (as shown so far) and on Eq. (B.13) in $\hat{x}, \hat{z}$ space. The two approximations differ by terms that are even more suppressed than the NLP terms. Nevertheless, their numerical difference is quite large, with the Mellin result yielding a far better approximation to the exact NLO result than the approximate $\hat{x}, \hat{z}$ space result. We thus conclude that Mellin space appears better suited for obtaining accurate approximations to the full result. Similar conclusions were obtained for other processes, such as for Higgs boson production [32].

The bottom part of Fig. 15 shows corresponding results for the EIC. They have a very similar trend as our COMPASS results, with a slightly reduced size of the corrections near threshold. This is expected due to the larger Q^2 relevant at the EIC. Again, the NLO corrections are extremely well reproduced by the approximate ones generated by Mellin-space LP+NLP resummation.

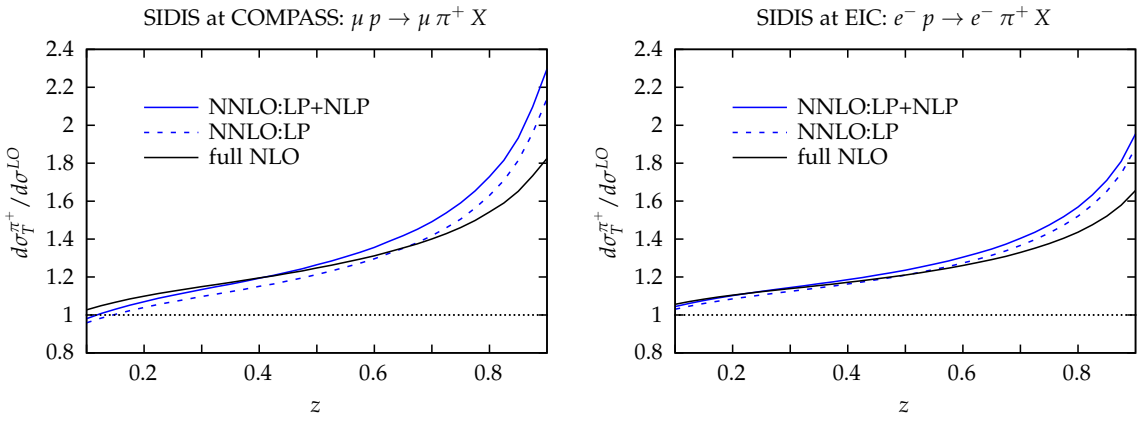

Figure 13: Left: Ratios of Mellin-space NNLO results for the unpolarized transverse cross section in the $q \to q$ channel to the LO cross section, with NLP corrections (blue solid) and without NLPs (blue dashed), for $\ell p \to \ell \pi^+ X$ at COMPASS. For comparison we also show the full NLO result again. Right: Same for EIC kinematics.

The findings in Fig. 15 provide confidence that our Mellin-space NNLO expansions based on resummation also provide an accurate approximation to the full NNLO corrections for the $q \to q$ channel. Figure 16 presents our NNLO results, again normalized to LO. Here we have included the exact NLO part of the cross section, so that the approximation only applies to the NNLO terms. The dashed line shows the result based on the LP terms at NNLO, while for the solid one we have included the dominant NLP terms as well. We also display again the curves for full NLO that were already shown in Fig. 15. One can see that the NNLO corrections become sizable as $z \to 1$, where the threshold logarithms grow in size. As in the NLO case, there is a rather significant positive contribution to the cross section by the NLP terms, both for COMPASS and the EIC. Inclusion of the dominant NNLO terms is expected to reduce the dependence of the cross section on the renormalization and factorization scales. Figure 14 shows the variation of the LO, full NLO and the (approximate) NNLO cross sections with scale. Here we vary independently $\mu_F = Q/2, Q, 2Q$ and $\mu_R = Q/2, Q, 2Q$. Among the nine combinations this results in, we discard the two with very disparate values, that is, $\mu_F = Q/2, \mu_R = 2Q$ and $\mu_F = 2Q, \mu_R = Q/2$. We then take the envelope of the remaining seven results. The figure shows the resulting bands. We present them in terms of the ratio $\big(d\sigma(\mu_F, \mu_R) - d\sigma(\mu_F = \mu_R = Q)\big)/d\sigma(\mu_F = \mu_R = Q)$, so that the cross section with $\mu_F = \mu_R = Q$ always produces the zero line in the plot. The result for COMPASS[4] (top figure) shows that around $z = 0.1$ the NNLO scale uncertainty is large, but does improve significantly toward higher z where it becomes better than the NLO

4 For COMPASS, we now increase the lower cut on Q^2 to $Q^2 > 5$ GeV^2, so that we can reasonably use the scale $\mu = Q/2$.

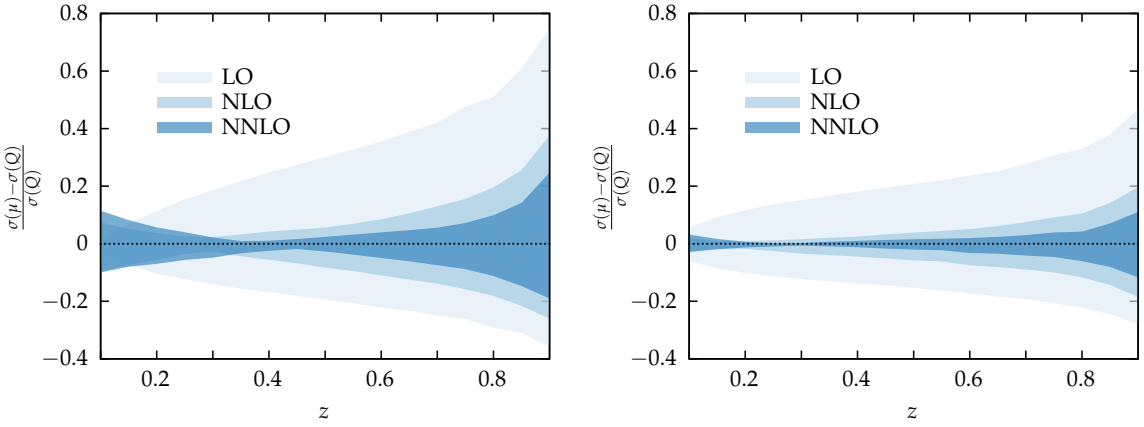

Figure 14: Left: Scale dependence of the NLO and approximate NNLO cross sections for COMPASS kinematics. We have varied μ_F and μ_R as described in the text. We have used $Q^2 > 5$ GeV^2 here. Right: Same for EIC kinematics.

one. It does, however, remain non-negligible even at large z. The main patterns are reproduced also for EIC kinematics (bottom part of the figure); however, here the scale uncertainty is overall very small at NNLO, showing a band that is much narrower than the NLO one at medium to large z. We note that we have included the NLO contributions by the qg subprocesses in the results shown in the figure, whose effects are however relatively small.

We finally note that we do not consider the SIDIS spin asymmetry here. Since the approximate NNLO corrections are identical for the spin-averaged and spin-dependent cross sections (even for the dominant NLP terms), the asymmetry is expected to be affected very little by the corrections. This was indeed already observed in the NLL study [21].

5.7 CONCLUSIONS AND OUTLOOK

We have presented approximate next-to-next-to-leading order corrections to semi-inclusive DIS, $\ell p \to \ell h X$. These corrections apply to the quark channel and are based on the threshold resummation formalism. We have first determined all ingredients for threshold resummation for SIDIS at next-to-next-to-leading logarithmic accuracy, extending previous work by one logarithmic order. As SIDIS is characterized by two "scaling" variables, $\hat{x} = Q^2/2p \cdot q$ and $\hat{z} = p \cdot p_c/P \cdot q$, the moment-space resummation is naturally formulated in terms of two Mellin moments N and M. Although these are separate variables, the SIDIS resummation formula may be obtained by that for the inclusive Drell-Yan cross section by a simple rescaling $N \to \sqrt{NM}$, up to differences associated with the fact that the virtual photon in

SIDIS is spacelike. These differences are accounted for by the hard factor in the resummed SIDIS cross section, which is related to the spacelike quark form factor rather than the timelike one contributing to Drell-Yan. We have subsequently expanded the resummed expressions to $\mathcal{O}(\alpha_s^2)$, to obtain the NNLO corrections.

To further improve the accuracy of the near-threshold NNLL and NNLO approximation we have determined also the dominant subleading terms which are suppressed by $1/N$ or $1/M$ near threshold, but still enhanced by logarithms. These "next-to-leading power" terms may be obtained by use of the DGLAP evolution of the parton distribution functions between scales Q and $Q/\sqrt{\bar{N}\bar{M}}$. We have found that the approximate NNLO corrections are identical for the spin-averaged (transverse) cross section and the longitudinally polarized one, even including the NLP corrections. This has important ramifications for phenomenology as it means that the SIDIS spin asymmetry will be largely unaffected even by NNLO corrections.

We have presented a few basic phenomenological results at approximate NNLO. These indicate a significant increase of the cross section at large z, as well as a still sizable contribution of the NLP corrections. Our results are readily suited for initial studies of SIDIS at NNLO in "global" fitting frameworks for fragmentation functions and/or parton distributions, especially polarized ones. Furthermore, the corrections we have derived will provide important benchmarks for future full NNLO calculations of SIDIS.

There are several avenues for future improvements on our work. Extension to approximate N^{3}LO near threshold and to N^{3}LL resummation would be quite straightforward (see Chapter 6). As already mentioned earlier, it will also be important to address the quark-gluon channels to SIDIS and to determine their dominant NLP corrections, following the lines in Ref. [137]. In the same vein, the longitudinal SIDIS structure function should be addressed at higher orders. For inclusive DIS, F_L receives corrections as large as $\alpha_s^2 \ln^2(1-x)$ at high x, which were derived and extended to all orders in Ref. [134]. Although these are again NLP corrections, it will be relevant to investigate the corresponding logarithmic structure of F_L in SIDIS. Finally, we note that the corrections we have derived here are really valid when both x and z are large. The recent study [107] considers the Drell-Yan cross section at measured rapidity and derives a factorization theorem that is valid when only *one* of the two kinematic variables $\sqrt{z}\,e^{\pm y}$ is large, while the other can have an arbitrary value. Extension of such a theorem to the SIDIS case when only x *or* z is large would be quite valuable as it would extend the validity of the threshold approximation for SIDIS.

6

THRESHOLD RESUMMATION AT N^{3}LL ACCURACY AND APPROXIMATE N^{3}LO CORRECTIONS

We advance the threshold resummation formalism for semi-inclusive deep-inelastic scattering (SIDIS) to next-to-next-to-next-to-leading logarithmic (N^{3}LL) order, including the three-loop hard factor. We expand the results in the strong coupling to obtain approximate next-to-next-to-next-to-leading order (N^{3}LO) corrections for the SIDIS cross section. In Mellin moment space, these corrections include all terms that are logarithmically enhanced at threshold, or that are constant. We also consider a set of corrections that are suppressed near threshold. Our numerical estimates show modest changes of the cross section by the approximate N^{3}LO terms, suggesting a very good perturbative stability of the SIDIS process. This Chapter is based on publication [ii].

6.1 INTRODUCTION

The semi-inclusive deep-inelastic scattering (SIDIS) process $\ell p \to \ell h X$ has become a widely used probe of hadronic structure and hadronization phenomena. Its main uses are extractions of (polarized) parton distribution and fragmentation functions or combinations thereof [18, 19, 113, 115, 116, 158–162]. In global analyses of these quantities SIDIS data can add useful information on, for example, the flavor structure of the sea quarks. The future Electron Ion Collider (EIC) will allow precise measurements of SIDIS observables over wide kinematic regimes [163].

In Chapter 5, we have studied higher-order QCD corrections to the SIDIS cross section. Our approach was to use the threshold resummation formalism for SIDIS and carry out fixed-order expansions of the resummed cross section. Threshold resummation for SIDIS was originally discussed in Ref. [121] and then further developed in more general terms in [20] and [21]. These papers formulated the resummation at next-to-leading logarithmic (NLL) accuracy. In [i] we extended the resummation to next-to-next-to-leading logarithm (NNLL), which also allowed us to obtain approximate fixed-order corrections to the hard scattering cross section for SIDIS at next-to-next-to-leading order (NNLO) level. These results were used

recently to obtain the first NNLO set of fragmentation functions fit "globally" to SIDIS and electron-positron annihilation data [19].

The purpose of the present paper is to advance our previous study to N^{3}LL and to again use the resummed cross section to derive approximate fixed-order corrections to the SIDIS cross section, in this case at N^{3}LO. Our main motivation for this analysis is to further improve the perturbative framework for SIDIS and to set the stage for precision analyses of SIDIS data from the future EIC in terms of parton distributions or fragmentation functions at high perturbative order. While such analyses at N^{3}LO may presently still seem far off, the study of the perturbative stability of the SIDIS cross section and its associated threshold resummation is in any case valuable. This becomes indeed possible by going to N^{3}LL and N^{3}LO and carrying out comparisons with lower orders. We also note that in our previous paper [i] we presented phenomenological results only for the fixed-order (NNLO) corrections. Here we wish to carry out numerical studies also for the resummed case, which provides another motivation for this study.

In Sec. 6.2 we give an overview of the kinematics of the process, introducing Mellin moments. Section 6.3 describes the threshold resummation framework. Section 6.4 is dedicated to the derivation of the three-loop hard factor to be used for obtaining N^{3}LL or N^{3}LO results. In Sec. 6.5 we carry out the expansion of the resummed results to N^{3}LO. Finally, Section 6.6 presents some numerical studies in the EIC kinematical regime.

6.2 PERTURBATIVE SIDIS CROSS SECTION

We consider the semi-inclusive deep-inelastic scattering (SIDIS) process $\ell(k)\, p(P) \to \ell'(k')\, h(P_h)\, X$ with the momentum transfer $q = k - k'$. It is described by the variables

$$\begin{aligned} Q^2 &= -q^2 = -(k-k')^2\,, \\ x &= \frac{Q^2}{2P\cdot q}\,, \\ y &= \frac{P\cdot q}{P\cdot k}\,, \\ z &= \frac{P\cdot P_h}{P\cdot q}\,. \end{aligned} \tag{6.1}$$

We have $Q^2 = xys$, with $\sqrt{s}$ the center-of-mass energy of the incoming electron and proton. We follow Ref. [20] to write the spin-averaged SIDIS cross section as

$$\frac{d^3\sigma^h}{dxdydz} = \frac{4\pi\alpha^2}{Q^2}\left[\frac{1+(1-y)^2}{2y}\mathcal{F}_T^h(x,z,Q^2) + \frac{1-y}{y}\mathcal{F}_L^h(x,z,Q^2)\right], \tag{6.2}$$

where α is the fine structure constant and $\mathcal{F}_T^h \equiv 2F_1^h$ and $\mathcal{F}_L^h \equiv F_L^h/x$ are the transverse and longitudinal structure functions. In what follows we will only treat the transverse structure function in the $q \to q$ or $\bar{q} \to \bar{q}$ channels, which is the only channel that appears already at the lowest order (LO) of perturbation theory. We write all equations for the spin-averaged case, although they will equally apply to the helicity-dependent one [21], [i].

Using factorization, the unpolarized structure functions may be written as double convolutions. For example, for the transverse one we have

$$\mathcal{F}_T^h(x,z,Q^2) = \sum_{f,f'}\int_x^1\frac{d\hat{x}}{\hat{x}}\int_z^1\frac{d\hat{z}}{\hat{z}}\,D_{f'}^h\left(\frac{z}{\hat{z}},\mu_F\right)\omega_{f'f}^T\left(\hat{x},\hat{z},\alpha_s(\mu_R),\frac{\mu_R}{Q},\frac{\mu_F}{Q}\right)f\left(\frac{x}{\hat{x}},\mu_F\right). \tag{6.3}$$

Here $f(\xi,\mu_F)$ is the distribution of parton $f = q,\bar{q},g$ in the nucleon at momentum fraction ξ and factorization scale μ_F, while $D_{f'}^h(\zeta,\mu_F)$ is the corresponding fragmentation function for parton f' going to the observed hadron h. For simplicity, the factorization scales are chosen to be equal in the initial and final state. μ_R is the renormalization scale entering also the strong coupling α_s. The functions $\omega_{f'f}^T$ are the transverse spin-averaged hard-scattering coefficient functions which can be computed in QCD perturbation theory. Their expansions read

$$\omega_{f'f}^T = \omega_{f'f}^{T,(0)} + \frac{\alpha_s(\mu_R)}{\pi}\omega_{f'f}^{T,(1)} + \left(\frac{\alpha_s(\mu_R)}{\pi}\right)^2\omega_{f'f}^{T,(2)} + \left(\frac{\alpha_s(\mu_R)}{\pi}\right)^3\omega_{f'f}^{T,(3)} + \mathcal{O}(\alpha_s^4). \tag{6.4}$$

At LO we have for the $q \to q$ and $\bar{q} \to \bar{q}$ channels

$$\omega_{qq}^{T,(0)}(\hat{x},\hat{z}) = e_q^2\,\delta(1-\hat{x})\delta(1-\hat{z}), \tag{6.5}$$

with the quark's fractional charge e_q. The well known first-order coefficient function $\omega_{f'f}^{T,(1)}$ is for example available in [20, 64].

In the following, it is convenient to take double Mellin moments of the SIDIS cross section, for which the convolutions in Eq. (6.3) turn into ordinary products. We define

$$\begin{aligned}\tilde{\mathcal{F}}_T^h(N,M,Q^2) &\equiv \int_0^1 dx\,x^{N-1}\int_0^1 dz\,z^{M-1}\,\mathcal{F}_T^h(x,z,Q^2)\\ &= \sum_{f,f'}\tilde{D}_{f'}^h(M,\mu_F)\,\tilde{\omega}_{f'f}^T\left(N,M,\alpha_s(\mu_R),\frac{\mu_R}{Q},\frac{\mu_F}{Q}\right)\tilde{f}(N,\mu_F),\end{aligned} \tag{6.6}$$

where

$$\tilde{f}(N,\mu_F) \equiv \int_0^1 dx\, x^{N-1} f(x,\mu_F),$$

$$\tilde{D}^h_{f'}(M,\mu_F) \equiv \int_0^1 dz\, z^{M-1} D^h_{f'}(z,\mu_F),$$

$$\tilde{\omega}^T_{f'f}\left(N,M,\alpha_s(\mu_R),\frac{\mu_R}{Q},\frac{\mu_F}{Q}\right) \equiv \int_0^1 d\hat{x}\,\hat{x}^{N-1}\int_0^1 d\hat{z}\,\hat{z}^{M-1}\omega^T_{f'f}\left(\hat{x},\hat{z},\alpha_s(\mu_R),\frac{\mu_R}{Q},\frac{\mu_F}{Q}\right). \tag{6.7}$$

As a result the structure functions can be obtained from the moments of the parton distribution functions and fragmentation functions, and the double-Mellin moments of the partonic hard-scattering functions.

For the perturbative expansion given in Eq. (6.4) we have in moment space at lowest order according to Eq. (6.5)

$$\tilde{\omega}^{T,(0)}_{qq}(N,M) \;=\; e_q^2. \tag{6.8}$$

The corresponding moments of the next-to-leading order (NLO) terms $\omega^{T,(1)}_{f'f}$ may be found in Refs. [20, 64]. In the following, we consider logarithmic higher-order corrections to the hard-scattering functions that arise at large values of $\hat{x}$ and $\hat{z}$ or, equivalently, at large N and M.

6.3 THRESHOLD RESUMMATION AT N^{3}LL ACCURACY

The resummation of threshold logarithms for SIDIS was extensively studied in Refs. [20, 89, 121], [i]. The NNLL resummation formula for the unpolarized SIDIS transverse structure function was discussed in Ref. [i]. The resummed partonic transverse structure function takes the form

$$\begin{aligned}\tilde{\omega}^{T,\mathrm{res}}_{qq}\left(N,M,\alpha_s(\mu_R),\frac{\mu_R}{Q},\frac{\mu_F}{Q}\right) &= e_q^2\, H^{\mathrm{SIDIS}}_{qq}\left(\alpha_s(\mu_R),\frac{\mu_R}{Q},\frac{\mu_F}{Q}\right)\widehat{C}_{qq}\left(\alpha_s(\mu_R),\frac{\mu_R}{Q}\right)\\ &\times\exp\left\{\int_{Q^2/(\bar{N}\bar{M})}^{Q^2}\frac{d\mu^2}{\mu^2}\left[A_q\big(\alpha_s(\mu)\big)\ln\left(\frac{\mu^2\bar{N}\bar{M}}{Q^2}\right)-\frac{1}{2}\widehat{D}_q\big(\alpha_s(\mu)\big)\right]\right.\\ &\left.+\ln\bar{N}\int_{Q^2}^{\mu_F^2}\frac{d\mu^2}{\mu^2}A_q\big(\alpha_s(\mu)\big)+\ln\bar{M}\int_{Q^2}^{\mu_F^2}\frac{d\mu^2}{\mu^2}A_q\big(\alpha_s(\mu)\big)\right\},\end{aligned} \tag{6.9}$$

which actually holds to any logarithmic order. As stated earlier, our goal is to set up the formalism for resummation to N^{3}LL. In Eq. (6.9) we have

$$\bar{N} \;=\; N\,\mathrm{e}^{\gamma_E} \quad\text{and}\quad \bar{M} \;=\; M\,\mathrm{e}^{\gamma_E}, \tag{6.10}$$

with the Euler constant γ_E. Each of the functions $A_q, \widehat{D}_q, H_{qq}^{\text{SIDIS}}, \widehat{C}_{qq}$ is a perturbative series in the strong coupling. We write the corresponding expansions generically as

$$\mathcal{Q} = \sum_{k=0}^{\infty} \left(\frac{\alpha_s(\mu_R)}{\pi}\right)^k \mathcal{Q}^{(k)}, \tag{6.11}$$

where $\mathcal{Q} = A_q, \widehat{D}_q, H_{qq}^{\text{SIDIS}}, \widehat{C}_{qq}$. We note that $A_q^{(0)} = \widehat{D}_q^{(0)} = \widehat{D}_q^{(1)} = 0$. To achieve N^{3}LL accuracy, we need A_q to order α_s^4 and all other functions to order α_s^3. The corresponding coefficients are collected in Appendix B.1. The main new ingredient not directly known from the literature is the $\bar{N}, \bar{M}$-independent coefficient $H_{qq}^{\text{SIDIS},(3)}$ whose derivation will be presented below in Sec. 6.4. The other prefactor $\widehat{C}_{qq}$ in Eq. (6.9) collects all moment-independent terms of the resummed exponent; see [32, 99], [i]. The formulas needed for its derivation to order α_s^3 may be found in Ref. [32].

In order to explicitly obtain the structure function resummed to N^{3}LL we now expand the exponents in Eq. (6.9) appropriately. The operations are quite standard. We obtain

$$\begin{aligned}\tilde{\omega}_{qq}^{T,\text{res}}\left(N, M, \alpha_s(\mu_R), \frac{\mu_R}{Q}, \frac{\mu_F}{Q}\right) &= e_q^2\, H_{qq}^{\text{SIDIS}}\left(\alpha_s(\mu_R), \frac{\mu_R}{Q}, \frac{\mu_F}{Q}\right) \widehat{C}_{qq}\left(\alpha_s(\mu_R), \frac{\mu_R}{Q}\right) \\ &\times \exp\left\{\frac{\lambda_{NM}}{2b_0\alpha_s(\mu_R)}\, h_q^{(1)}\left(\frac{\lambda_{NM}}{2}\right) + h_q^{(2)}\left(\frac{\lambda_{NM}}{2}, \frac{\mu_R}{Q}, \frac{\mu_F}{Q}\right)\right. \\ &\left. + \alpha_s(\mu_R)\, h_q^{(3)}\left(\frac{\lambda_{NM}}{2}, \frac{\mu_R}{Q}, \frac{\mu_F}{Q}\right) + \alpha_s^2(\mu_R)\, h_q^{(4)}\left(\frac{\lambda_{NM}}{2}, \frac{\mu_R}{Q}, \frac{\mu_F}{Q}\right)\right\},\end{aligned} \tag{6.12}$$

where

$$\lambda_{NM} \equiv b_0\, \alpha_s(\mu_R)\left(\ln \bar{N} + \ln \bar{M}\right). \tag{6.13}$$

The functions $h_q^{(k)}$ impart resummation to N^{k-1}LL accuracy. The first three are well known in the literature:

$$\begin{aligned} h_q^{(1)}(\lambda) &= \frac{A_q^{(1)}}{\pi b_0 \lambda}\left[2\lambda + (1-2\lambda)\ln(1-2\lambda)\right], \\ h_q^{(2)}(\lambda) &= -\frac{A_q^{(2)}}{\pi^2 b_0^2}\left[2\lambda + \ln(1-2\lambda)\right] \\ &\quad + \frac{A_q^{(1)} b_1}{\pi b_0^3}\left[2\lambda + \ln(1-2\lambda) + \frac{1}{2}\ln^2(1-2\lambda)\right] \\ &\quad + \frac{A_q^{(1)}}{\pi b_0} 2\lambda \ln\frac{\mu_F^2}{Q^2} - \frac{A_q^{(1)}}{\pi b_0}\left[2\lambda + \ln(1-2\lambda)\right]\ln\frac{\mu_R^2}{Q^2}, \end{aligned}$$

$$
\begin{aligned}
h_q^{(3)}(\lambda) = &-\frac{A_q^{(2)} b_1}{\pi^2 b_0^3}\frac{1}{1-2\lambda}[2\lambda + \ln(1-2\lambda) + 2\lambda^2] \\
&+ \frac{A_q^{(1)} b_1^2}{\pi b_0^4 (1-2\lambda)}\left[2\lambda^2 + 2\lambda\ln(1-2\lambda) + \frac{1}{2}\ln^2(1-2\lambda)\right] \\
&+ \frac{A_q^{(1)} b_2}{\pi b_0^3}\left[2\lambda + \ln(1-2\lambda) + \frac{2\lambda^2}{1-2\lambda}\right] + \frac{2A_q^{(3)}}{\pi^3 b_0^2}\frac{\lambda^2}{1-2\lambda} \\
&+ \frac{2A_q^{(2)}}{\pi^2 b_0}\lambda\ln\frac{\mu_F^2}{Q^2} - \frac{A_q^{(1)}}{\pi}\lambda\ln^2\frac{\mu_F^2}{Q^2} + \frac{2A_q^{(1)}}{\pi}\lambda\ln\frac{\mu_F^2}{Q^2}\ln\frac{\mu_R^2}{Q^2} \\
&- \frac{1}{1-2\lambda}\left(\frac{A_q^{(1)} b_1}{\pi b_0^2}[2\lambda + \ln(1-2\lambda)] - \frac{4A_q^{(2)}}{\pi^2 b_0}\lambda^2\right)\ln\frac{\mu_R^2}{Q^2} \\
&+ \frac{2A_q^{(1)}}{\pi}\frac{\lambda^2}{1-2\lambda}\ln^2\frac{\mu_R^2}{Q^2} - \frac{\widehat{D}_q^{(2)}}{\pi^2 b_0}\frac{\lambda}{1-2\lambda}\,. \qquad (6.14)
\end{aligned}
$$

The function $h_q^{(4)}$, needed for N^{3}LL resummation, is found to be

$$
\begin{aligned}
h_q^{(4)}(\lambda) = &\frac{1}{(1-2\lambda)^2}\left(\frac{A_q^{(2)} b_1^2}{\pi^2 b_0^4}\left[-\frac{8}{3}\lambda^3 - \lambda^2 + \lambda + \frac{1}{2}\ln^2(1-2\lambda) + \frac{1}{2}\ln(1-2\lambda)\right]\right. \\
&+ \frac{A_q^{(2)} b_2}{\pi^2 b_0^3}\frac{8}{3}\lambda^3 + \frac{A_q^{(1)} b_1^3}{\pi b_0^5}\left[\frac{8}{3}\lambda^3 + 2\lambda^2\ln(1-2\lambda) - \frac{1}{6}\ln^3(1-2\lambda)\right] \\
&+ \frac{A_q^{(1)} b_1 b_2}{\pi b_0^4}\left[-\frac{16}{3}\lambda^3 + 3\lambda^2 - \lambda - 4\lambda^2\ln(1-2\lambda) + 2\lambda\ln(1-2\lambda) - \frac{1}{2}\ln(1-2\lambda)\right] \\
&+ \frac{A_q^{(1)} b_3}{\pi b_0^3}\left[\frac{8}{3}\lambda^3 - 3\lambda^2 + \lambda + 2\lambda^2\ln(1-2\lambda) - 2\lambda\ln(1-2\lambda) + \frac{1}{2}\ln(1-2\lambda)\right] \\
&+ \frac{A_q^{(3)} b_1}{\pi^3 b_0^3}\left[\frac{8}{3}\lambda^3 - \lambda^2 - \lambda - \frac{1}{2}\ln(1-2\lambda)\right] + \frac{A_q^{(4)}}{\pi^4 b_0^2}\left[2\lambda^2 - \frac{8}{3}\lambda^3\right] \\
&\left.+ \frac{\widehat{D}_q^{(2)} b_1}{\pi^2 b_0^2}\left[\lambda - \lambda^2 + \frac{1}{2}\ln(1-2\lambda)\right] + \frac{\widehat{D}_q^{(3)}}{\pi^3 b_0}\left[\lambda^2 - \lambda\right]\right)\,. \qquad (6.15)
\end{aligned}
$$

This result is in agreement with that given in Ref. [164] for the Drell-Yan process. For simplicity, we have set the renormalization and factorization scales to Q. The results presented in Eq. (6.12) may be used to obtain N^{3}LO (that is, $\mathcal{O}(\alpha_s^3)$) expansions of the hard-scattering function $\tilde{\omega}_{qq}^T$. This expansion will be carried out in Sec. 6.5.

We stress that all terms generated by Eq. (6.12) are either logarithmic or constant near threshold. The full hard-scattering function in Mellin space will, at any order in perturbation theory, also contain terms that are suppressed by powers of $1/N$ and/or $1/M$. Such terms are often referred to as "next-to-leading power (NLP)" corrections. As discussed in Chapter 5 (see also references therein), one can straightforwardly account for the dominant NLP terms by multiplying the resummed cross section in Eq. (6.9) by the two factors

$$\exp\left\{-\int_{\mu_F^2}^{Q^2/(\bar{N}\bar{M})}\frac{d\mu^2}{\mu^2}\frac{\alpha_s(\mu)}{\pi}\frac{C_F}{2N}\right\}\exp\left\{-\int_{\mu_F^2}^{Q^2/(\bar{N}\bar{M})}\frac{d\mu^2}{\mu^2}\frac{\alpha_s(\mu)}{\pi}\frac{C_F}{2M}\right\}. \tag{6.16}$$

where the coefficients $-C_F/(2N)$ and $-C_F/(2M)$ in the exponents correspond to the NLP terms in the LO diagonal evolution kernels for the quark parton distributions and the quark fragmentation functions, respectively. At N^{3}LO the two exponential factors, when combined with the resummed exponents in Eq. (6.9), will generate all terms of the form $\alpha_s^3 \ln^n(N)\ln^m(M)(1/N+1/M)$, with $n+m=5$.

6.4 THE HARD FACTOR AT THREE LOOPS

The factor $H_{qq}^{\rm SIDIS}$ is derived from the finite part of the virtual corrections to the process $\gamma^* q \to q$. The basic ingredient is the renormalized spacelike form quark factor, from which one needs to subtract the infrared divergencies via a suitable method developed in Refs. [100, 124]. For our present purposes, we will need the renormalized three-loop form factor, which was derived in [50–52][1] and reads in dimensional regularization with $d = 4-2\epsilon$ space-time dimensions:

$$F_q(q^2) = F_q^{(0)} + \frac{\alpha_s}{\pi}F_q^{(1)} + \left(\frac{\alpha_s}{\pi}\right)^2 F_q^{(2)} + \left(\frac{\alpha_s}{\pi}\right)^3 F_q^{(3)} + \mathcal{O}(\alpha_s^4), \tag{6.17}$$

where $F_q^{(0)}$ and $F_q^{(1)}$ can be found in (5.21) and

1 We note that recently even the four-loop results were published [42].

$$
\begin{aligned}
F_q^{(3)} = {} & C_F^3\Bigg[-\frac{1}{48\epsilon^6}-\frac{3}{32\epsilon^5}+\frac{1}{\epsilon^4}\left(\frac{\pi^2}{192}-\frac{25}{64}\right)+\frac{1}{\epsilon^3}\left(\frac{25\zeta(3)}{48}-\frac{83}{64}-\frac{\pi^2}{128}\right) \\
& +\frac{1}{\epsilon^2}\left(\frac{69\zeta(3)}{32}-\frac{515}{128}-\frac{77\pi^2}{768}+\frac{71\pi^4}{7680}\right)+\frac{1}{\epsilon}\left(\frac{2119\zeta(3)}{192}-\frac{107\pi^2\zeta(3)}{576}\right. \\
& \left.+\frac{161\zeta(5)}{80}-\frac{9073}{768}-\frac{467\pi^2}{768}+\frac{487\pi^4}{15360}\right)+\frac{2669\zeta(3)}{64}+\frac{61\pi^2\zeta(3)}{384}-\frac{913\zeta(3)^2}{96} \\
& +\frac{2119\zeta(5)}{160}-\frac{53675}{1536}-\frac{13001\pi^2}{4608}+\frac{12743\pi^4}{92160}-\frac{9095\pi^6}{3483648}\Bigg] \\
& +C_F^2C_A\Bigg[-\frac{11}{64\epsilon^5}+\frac{1}{\epsilon^4}\left(-\frac{361}{1152}-\frac{\pi^2}{192}\right)+\frac{1}{\epsilon^3}\left(-\frac{13\zeta(3)}{32}-\frac{1703}{3456}+\frac{9\pi^2}{256}\right) \\
& +\frac{1}{\epsilon^2}\left(-\frac{241\zeta(3)}{288}+\frac{1705}{1296}+\frac{1487\pi^2}{13824}-\frac{83\pi^4}{11520}\right)+\frac{1}{\epsilon}\left(-\frac{4151\zeta(3)}{384}+\frac{215\pi^2\zeta(3)}{1152}\right. \\
& \left.-\frac{71\zeta(5)}{32}+\frac{374149}{31104}+\frac{31891\pi^2}{41472}-\frac{2975\pi^4}{165888}\right)-\frac{19933\zeta(3)}{384}-\frac{403\pi^2\zeta(3)}{576} \\
& +\frac{101\zeta(3)^2}{12}-\frac{3445\zeta(5)}{288}+\frac{11169211}{186624}+\frac{537803\pi^2}{124416}-\frac{723739\pi^4}{4976640}-\frac{18619\pi^6}{17418240}\Bigg] \\
& +C_F^2N_f\Bigg[\frac{1}{32\epsilon^5}+\frac{35}{576\epsilon^4}+\frac{1}{\epsilon^3}\left(\frac{139}{1728}-\frac{\pi^2}{128}\right)+\frac{1}{\epsilon^2}\left(-\frac{55\zeta(3)}{288}-\frac{775}{5184}-\frac{133\pi^2}{6912}\right) \\
& +\frac{1}{\epsilon}\left(\frac{469\zeta(3)}{1728}-\frac{24761}{15552}-\frac{2183\pi^2}{20736}-\frac{287\pi^4}{82944}\right)+\frac{21179\zeta(3)}{5184}+\frac{35\pi^2\zeta(3)}{1152} \\
& -\frac{193\zeta(5)}{288}-\frac{691883}{93312}-\frac{16745\pi^2}{31104}-\frac{8503\pi^4}{2488320}\Bigg]+C_FC_A^2\Bigg[-\frac{1331}{5184\epsilon^4} \\
& +\frac{1}{\epsilon^3}\left(\frac{1433}{7776}-\frac{55\pi^2}{5184}\right)+\frac{1}{\epsilon^2}\left(-\frac{451\zeta(3)}{864}+\frac{11669}{31104}+\frac{1625\pi^2}{31104}-\frac{11\pi^4}{12960}\right) \\
& +\frac{1}{\epsilon}\left(\frac{1763\zeta(3)}{864}-\frac{11\pi^2\zeta(3)}{432}-\frac{17\zeta(5)}{24}-\frac{139345}{559872}-\frac{7163\pi^2}{93312}-\frac{83\pi^4}{17280}\right) \\
& +\frac{505087\zeta(3)}{31104}+\frac{13\pi^2\zeta(3)}{36}-\frac{71\zeta(3)^2}{36}-\frac{217\zeta(5)}{288}-\frac{51082685}{3359232}-\frac{412315\pi^2}{279936} \\
& +\frac{22157\pi^4}{622080}-\frac{769\pi^6}{326592}\Bigg]+C_FN_f^2\Bigg[-\frac{11}{1296\epsilon^4}-\frac{1}{1944\epsilon^3}+\frac{1}{\epsilon^2}\left(\frac{23}{2592}+\frac{\pi^2}{864}\right)
\end{aligned}
$$

$$+\frac{1}{\epsilon}\left(-\frac{\zeta(3)}{648}+\frac{2417}{139968}-\frac{5\pi^2}{2592}\right)-\frac{13\zeta(3)}{486}-\frac{190931}{839808}-\frac{103\pi^2}{3888}-\frac{47\pi^4}{77760}\Bigg]$$

$$+C_FC_AN_f\left[\frac{121}{1296\epsilon^4}+\frac{1}{\epsilon^3}\left(\frac{5\pi^2}{2592}-\frac{47}{972}\right)+\frac{1}{\epsilon^2}\left(\frac{53\zeta(3)}{432}-\frac{517}{3888}-\frac{119\pi^2}{7776}\right)\right.$$

$$+\frac{1}{\epsilon}\left(-\frac{241\zeta(3)}{1296}-\frac{8659}{139968}+\frac{1297\pi^2}{46656}+\frac{11\pi^4}{8640}\right)-\frac{67\zeta(3)}{27}+\frac{\pi^2\zeta(3)}{288}-\frac{\zeta(5)}{48}$$

$$\left.+\frac{1700171}{419904}+\frac{115555\pi^2}{279936}+\frac{\pi^4}{31104}\right]+C_FN_{f,V}\left(\frac{C_A^2-4}{2C_A}\right)\left(\frac{7\zeta(3)}{48}-\frac{5\zeta(5)}{6}\right.$$

$$\left.+\frac{5\pi^2}{96}+\frac{1}{8}-\frac{\pi^4}{2880}\right)+\mathcal{O}(\epsilon)\,. \tag{6.18}$$

Here we have kept terms of higher order in ϵ in the one-loop and two-loop results since these turn out to make finite contributions in the end. In the above expressions, $\zeta(j)$ is the Riemann zeta function, N_f is the number of flavors, and $C_F = 4/3, C_A = 3$. For purely electromagnetic interactions the factor $N_{f,V=\gamma}$ becomes [51]

$$N_{f,\gamma} = \frac{\sum_q e_q}{e_q}\,. \tag{6.19}$$

As shown in Refs. [100, 124], the hard coefficient may be extracted from the form factor in the following way. Adapted to the case of SIDIS we have from [100]

$$H_{qq}^{\text{SIDIS}}(\alpha_s(Q)) \;=\; \left|\,\left[1-\tilde{I}_q(\epsilon,\alpha_s(Q))\right]F_q\,\right|^2\,, \tag{6.20}$$

where $\tilde{I}_q$ is an operator that removes the poles of the form factor and makes the necessary soft and collinear adjustments needed to extract the hard coefficient. It is given in [100] in terms of a convenient all-order form:

$$1-\tilde{I}_q(\epsilon,\alpha_s) \;=\; \exp\left\{R_q\left(\epsilon,\alpha_s\right)-i\Phi_q\left(\epsilon,\alpha_s\right)\right\}\,, \tag{6.21}$$

with functions R_q and Φ_q that each are perturbative series. The phase Φ_q does not contribute in our case since we take the absolute square in Eq. (6.20). The function R_q effects the cancelation of infrared divergences from the quark form factor. It can be expressed in terms of a soft and a collinear part:

$$R_q(\epsilon,\alpha_s) = R_q^{\text{soft}}(\epsilon,\alpha_s)+R_q^{\text{coll}}(\epsilon,\alpha_s)\,, \tag{6.22}$$

where for N^{3}LL accuracy

$$R_q^{\text{soft}}(\epsilon,\alpha_s) = C_F\left(\frac{\alpha_s}{\pi}R_q^{\text{soft}\,(1)}(\epsilon)+\left(\frac{\alpha_s}{\pi}\right)^2R_q^{\text{soft}\,(2)}(\epsilon)+\left(\frac{\alpha_s}{\pi}\right)^3R_q^{\text{soft}\,(3)}(\epsilon)+\mathcal{O}(\alpha_s^4)\right),$$

$$R_q^{\rm coll}(\epsilon,\alpha_s) = \frac{\alpha_s}{\pi} R_q^{\rm coll\,(1)}(\epsilon) + \left(\frac{\alpha_s}{\pi}\right)^2 R_q^{\rm coll\,(2)}(\epsilon) + \left(\frac{\alpha_s}{\pi}\right)^3 R_q^{\rm coll\,(3)}(\epsilon) + \mathcal{O}(\alpha_s^4)\,, \tag{6.23}$$

with $R_q^{\rm soft\,(1)}$, $R_q^{\rm soft\,(2)}$, $R_q^{\rm coll\,(1)}$ and $R_q^{\rm coll\,(2)}$ in (5.26) and

$$\begin{aligned}
R_q^{\rm soft\,(3)}(\epsilon) &= \frac{11(b_0\pi)^2}{36\epsilon^4} - \frac{2b_1\,\pi^2}{9\epsilon^3} - \frac{5}{36\epsilon^3} b_0\pi\,\frac{A_q^{(2)}}{C_F} + \frac{1}{18\epsilon^2}\,\frac{A_q^{(3)}}{C_F} \\
&+ \frac{1}{24\epsilon^2} b_0\pi \left[C_A\left(7\zeta(3) + \frac{11\pi^2}{36} - \frac{202}{27}\right) + N_f\left(\frac{28}{27} - \frac{\pi^2}{18}\right)\right] \\
&- \frac{1}{48\epsilon}\left[C_A^2\left(-\frac{136781}{5832} + \frac{6325}{1944}\pi^2 - \frac{11}{45}\pi^4 + \frac{329}{6}\zeta(3) - \frac{11}{9}\pi^2\zeta(3) - 24\zeta(5)\right)\right. \\
&+ C_A\,N_f\left(\frac{5921}{2916} - \frac{707}{972}\pi^2 + \frac{\pi^4}{15} - \frac{91}{27}\zeta(3)\right) + C_F\,N_f\left(\frac{1711}{216} - \frac{\pi^2}{12} - \frac{\pi^4}{45} - \frac{38}{9}\zeta(3)\right) \\
&\left.+ N_f^2\left(\frac{260}{729} + \frac{5}{162}\pi^2 - \frac{14}{27}\zeta(3)\right)\right] \\
&+ C_A^2\left(\frac{5211949}{1679616} - \frac{578479}{559872}\pi^2 + \frac{9457}{311040}\pi^4 + \frac{19}{326592}\pi^6 - \frac{64483}{7776}\zeta(3) + \frac{121}{192}\pi^2\zeta(3)\right. \\
&\left.+ \frac{67}{72}\zeta(3)^2 - \frac{121}{144}\zeta(5)\right) + C_A\,N_f\left(-\frac{412765}{839808} + \frac{75155}{279936}\pi^2 - \frac{79}{9720}\pi^4 + \frac{154}{81}\zeta(3)\right. \\
&\left.- \frac{11}{288}\pi^2\zeta(3) - \frac{1}{24}\zeta(5)\right) + C_F\,N_f\left(-\frac{42727}{62208} + \frac{605}{6912}\pi^2 + \frac{19}{12960}\pi^4 + \frac{571}{1296}\zeta(3)\right. \\
&\left.- \frac{11}{144}\pi^2\zeta(3) + \frac{7}{36}\zeta(5)\right) + N_f^2\left(-\frac{2}{6561} - \frac{101}{7776}\pi^2 + \frac{37}{77760}\pi^4 - \frac{185}{1944}\zeta(3)\right),
\end{aligned} \tag{6.24}$$

and

$$\begin{aligned}
R_q^{\rm coll\,(3)}(\epsilon) &= C_F\frac{(b_0\pi)^2}{4\epsilon^3} - C_F\frac{b_1\pi^2}{4\epsilon^2} - \frac{b_0\pi}{12\epsilon^2}\left[C_F^2\left(6\zeta(3) - \frac{\pi^2}{2} + \frac{3}{8}\right)\right. \\
&\left.+ C_A C_F\left(-3\zeta(3) + \frac{11\pi^2}{18} + \frac{17}{24}\right) + C_F N_f\left(-\frac{1}{12} - \frac{\pi^2}{9}\right)\right] \\
&+ \frac{1}{24\epsilon}\left[C_F^3\left(\frac{29}{16} + \frac{3}{8}\pi^2 + \frac{\pi^4}{5} + \frac{17}{2}\zeta(3) - \frac{2}{3}\pi^2\zeta(3) - 30\zeta(5)\right)\right. \\
&+ C_F^2 C_A\left(\frac{151}{32} - \frac{205}{72}\pi^2 - \frac{247}{1080}\pi^4 + \frac{211}{6}\zeta(3) + \frac{1}{3}\pi^2\zeta(3) + 15\zeta(5)\right) \\
&\left.+ C_A^2 C_F\left(-\frac{1657}{288} + \frac{281}{81}\pi^2 - \frac{\pi^4}{144} - \frac{194}{9}\zeta(3) + 5\zeta(5)\right)\right.
\end{aligned}$$

$$+ C_F^2 N_f \left(-\frac{23}{8} + \frac{5}{36}\pi^2 + \frac{29}{540}\pi^4 - \frac{17}{3}\zeta(3) \right)$$
$$+ C_F N_f^2 \left(-\frac{17}{72} + \frac{5}{81}\pi^2 - \frac{2}{9}\zeta(3) \right)$$
$$+ C_F C_A N_f \left(\frac{5}{2} - \frac{167}{162}\pi^2 + \frac{\pi^4}{360} + \frac{25}{9}\zeta(3) \right) \Bigg] . \tag{6.25}$$

The coefficients b_0 and b_1 can be found in Appendix B.1. Inserting all terms into Eq. (6.20) and expanding in α_s, all poles in powers of $1/\epsilon$ cancel. The final expression for H_{qq}^{SIDIS} up to three loops can be found in Appendix B.1.

6.5 EXPANSION TO N^{3}LO

We are now ready to present the N^{3}LO ($\mathcal{O}(\alpha_s^3)$) expansion for the SIDIS $q \to q$ hard-scattering function near threshold. To write our formulas compactly we introduce

$$\mathcal{L} \equiv \frac{1}{2} \left(\ln(\bar{N}) + \ln(\bar{M}) \right) . \tag{6.26}$$

The coefficients $\tilde{\omega}_{qq}^{T,(1)}$ and $\tilde{\omega}_{qq}^{T,(2)}$ in Eq. (6.4) were already given in Chapter 5, Eqs. (5.38) and (5.39). For the approximate N^{3}LO terms we find:

$$\frac{1}{e_q^2} \tilde{\omega}_{qq}^{T,(3)}(N, M, 1, 1) = \frac{4}{3} C_F^3 \mathcal{L}^6 + \frac{8}{3} C_F^2 \pi b_0 \mathcal{L}^5 + \mathcal{L}^4 \left[C_F^3 \left(-8 + \frac{\pi^2}{3} \right) - \frac{11}{27} C_F C_A N_f \right.$$
$$\left. + C_F^2 C_A \left(\frac{67}{9} - \frac{\pi^2}{3} \right) + \frac{121}{108} C_F C_A^2 - \frac{10}{9} C_F^2 N_f + \frac{1}{27} C_F N_f^2 \right]$$
$$+ \mathcal{L}^3 \left[C_F C_A N_f \left(\frac{\pi^2}{27} - \frac{289}{162} \right) + C_F^2 C_A \left(-7\zeta(3) + \frac{11\pi^2}{54} + \frac{70}{27} \right) \right.$$
$$\left. + C_F C_A^2 \left(\frac{445}{81} - \frac{11\pi^2}{54} \right) + C_F^2 N_f \left(-\frac{\pi^2}{27} - \frac{17}{54} \right) + \frac{10}{81} C_F N_f^2 \right]$$
$$+ \mathcal{L}^2 \left[C_F^3 \left(\frac{511}{32} - \frac{15}{2}\zeta(3) - \frac{\pi^2}{8} - \frac{\pi^4}{30} \right) + C_F C_A N_f \left(\frac{5\pi^2}{54} - \frac{2051}{648} \right) \right.$$
$$+ C_F^2 C_A \left(\frac{151}{18}\zeta(3) + \frac{143\pi^2}{216} - \frac{\pi^4}{120} - \frac{8893}{288} \right) + C_F^2 N_f \left(\frac{10}{9}\zeta(3) + \frac{67}{18} - \frac{\pi^2}{108} \right)$$
$$\left. + C_F C_A^2 \left(\frac{11\pi^4}{360} - \frac{11}{2}\zeta(3) - \frac{67\pi^2}{108} + \frac{15503}{1296} \right) + \frac{25}{162} C_F N_f^2 \right]$$
$$+ \mathcal{L} \left[C_F^2 C_A \left(14\zeta(3) - \frac{1}{12} 7\pi^2 \zeta(3) + \frac{101\pi^2}{162} - \frac{404}{27} \right) + C_F N_f^2 \left(\frac{\zeta(3)}{9} + \frac{58}{729} \right) \right.$$

$$
\begin{aligned}
&+ C_F C_A^2 \left(\frac{11\pi^2}{36}\zeta(3) - \frac{1541}{108}\zeta(3) + 6\zeta(5) - \frac{11\pi^4}{720} - \frac{799\pi^2}{1944} + \frac{297029}{23328} \right) \\
&+ C_F^2 N_f \left(\frac{19}{18}\zeta(3) + \frac{\pi^4}{180} + \frac{3}{32} - \frac{7\pi^2}{81} \right) + C_F C_A N_f \left(\frac{113}{108}\zeta(3) + \frac{103\pi^2}{1944} \right. \\
&\left. - \frac{\pi^4}{360} - \frac{31313}{11664} \right) \Big] + C_F^3 \left(\frac{\zeta(3)^2}{2} + \frac{5\pi^2}{6}\zeta(3) - \frac{115}{16}\zeta(3) + \frac{83}{4}\zeta(5) + \frac{761\pi^6}{136080} + \frac{37\pi^4}{2880} \right. \\
&\left. - \frac{5599}{384} - \frac{1663\pi^2}{1152} \right) + C_F^2 C_A \left(\frac{37}{12}\zeta(3)^2 - \frac{119\pi^2}{72}\zeta(3) - \frac{12877}{432}\zeta(3) - \frac{689}{72}\zeta(5) \right. \\
&\left. + \frac{40223\pi^2}{10368} + \frac{74321}{2304} - \frac{149\pi^6}{27216} - \frac{1147\pi^4}{38880} \right) + C_F^2 N_f \left(\frac{1181}{216}\zeta(3) - \frac{19}{18}\zeta(5) - \frac{421}{192} \right. \\
&\left. - \frac{559\pi^2}{1296} - \frac{29\pi^4}{9720} \right) + C_F N_f^2 \left(\frac{\zeta(3)}{324} - \frac{23\pi^2}{432} - \frac{7081}{15552} - \frac{17\pi^4}{19440} \right) + C_F C_A^2 \left(-\frac{25}{12}\zeta(3)^2 \right. \\
&\left. + \frac{569\pi^2}{864}\zeta(3) + \frac{139345}{5184}\zeta(3) - \frac{51}{16}\zeta(5) + \frac{17\pi^6}{34020} + \frac{3103\pi^4}{311040} - \frac{93889\pi^2}{31104} - \frac{1505881}{62208} \right) \\
&+ C_F C_A N_f \left(\frac{\pi^2}{216}\zeta(3) - \frac{383}{81}\zeta(3) - \frac{\zeta(5)}{8} + \frac{469\pi^4}{77760} + \frac{6493\pi^2}{7776} + \frac{110651}{15552} \right) \\
&+ C_F N_{f,V} \frac{(C_A^2 - 4)}{C_A} \left(\frac{7\zeta(3)}{48} - \frac{5\zeta(5)}{6} + \frac{5\pi^2}{96} + \frac{1}{8} - \frac{\pi^4}{2880} \right) + 2\, C_F^3\, \mathcal{L}^5 \left(\frac{1}{N} + \frac{1}{M} \right) .
\end{aligned}
\tag{6.27}
$$

As before, we have set $\mu_R = \mu_F = Q$ for simplicity. We stress that the corrections given by this expression include all terms that are logarithmically enhanced at threshold, or that are constant. In physical space these are terms with double distributions (that is, "plus" distributions and δ-functions) in $\hat{x}$ and $\hat{z}$.

The last term in Eq. (6.27) represents the dominant NLP contributions. Note that upon expansion beyond NLO the exponential factors in (6.16) will also generate terms with inverse powers $1/N^2, 1/M^2$ and higher, which we have discarded for consistency since they are far beyond the approximations we make. We will see later that these terms are numerically very small.

6.6 PHENOMENOLOGICAL PREDICTIONS

We will now present some phenomenological predictions for the transverse SIDIS cross section at NNLL and N^{3}LL, as well as for the expansion to N^{3}LO. We will also compare to our previous NNLO results of [i].

In order to obtain results for the transverse structure function $\mathcal{F}_T^h(x,z,Q^2)$ in physical x,z space we need to invert its Mellin moments $\tilde{\mathcal{F}}_T^h(N,M,Q^2)$ in Eq. (6.6). This is achieved by the inverse double-Mellin transform

$$\mathcal{F}_T^h(x,z,Q^2) \;=\; \int_{\mathcal{C}_N} \frac{dN}{2\pi i}\, x^{-N} \int_{\mathcal{C}_M} \frac{dM}{2\pi i}\, z^{-M}\, \tilde{\mathcal{F}}_T^h(N,M,Q^2)\,, \tag{6.28}$$

where $\mathcal{C}_N$ and $\mathcal{C}_M$ denote integration contours in the complex plane, one for each Mellin inverse. We adopt the minimal prescription of Ref. [98] to treat the Landau pole present in the resummed exponents in Eqs. (6.12),(6.14) at $\lambda_{NM} = 1$, or (see Eq. (6.13)),

$$\bar{N}\bar{M} \;=\; \mathrm{e}^{1/(b_0\,\alpha_s(\mu_R))}\,. \tag{6.29}$$

According to the minimal prescription, the two contours need to be chosen such that all singularities in the complex plane lie to their left, except for the Landau pole. We parameterize the two contours as

$$N = c_N \pm \zeta \mathrm{e}^{\pm i\phi_N}\,, \quad M = c_M + \xi \mathrm{e}^{i\phi_M}\,, \tag{6.30}$$

with $\zeta,\xi \in [0,\infty]$ as contour parameters, where $c_N = 1.8$ and $c_M = 3.3$. The precise values do not matter as long as c_N and c_M are chosen to the right of the poles of the PDFs and FFs, respectively, and their product is below the Landau pole. We found the values $c_N = 1.8$ and $c_M = 3.3$ (which reflect the slightly steeper behavior of the FFs compared to the PDFs at low momentum fractions) to be optimal for good convergence of the numerical integration in our code. We furthermore choose $\phi_N = 3\pi/4$; the two signs for the N-contour in (6.30) select the two branches in the complex plane. As N moves along its contour, the position of the Landau pole relevant for the M-integral will move as well, mapping out a trajectory in the plane. This implies that the angle ϕ_M needs to be chosen as a function of N, so that during the M integration this trajectory is never crossed. A more detailed description of the inverse double-Mellin transform can be found in Ref. [20].

We note that we only consider the transverse structure function in (6.2) here. The longitudinal one is suppressed near threshold, even beyond the dominant NLP terms we have included for $\mathcal{F}_T^h$. While it would be very interesting to also investigate higher-order corrections to $\mathcal{F}_L^h$, this is beyond the scope of this work. In what follows, we also discard the contributions by the $q \to g$ and $g \to q$ channels to the structure function. These are fully known only to NLO. We could include the contributions at NLO level in our approximate NNLO, N^{3}LO results to be presented below, but this would simply amount to a uniform shift of all results by a few per cent, which is not really relevant for our main goal of analyzing the structure of higher-order contributions in the $q \to q$ channel.

For the parton distribution functions and fragmentation functions we choose the NNLO sets of Ref. [157] and Ref. [110], respectively. Clearly, in order to present true

N^{3}LL or N^{3}LO results, we would need PDFs and FFs evolved at those same orders, which are currently not yet available. We therefore keep the renormalization and factorization scales at $\mu_R = \mu_F = Q$ and do not investigate the scale dependence of our results. In this sense we use the NNLO parton distributions and fragmentation functions as templates for the N^{3}LO ones, which should be adequate for a first analysis of the beyond-NNLO effects we are interested in. We note that the scale dependence of the transverse SIDIS cross section was anyway found to be rather small already at NNLO in Ref. [i]. Note that we "match" all results to NLO, so that the NLO corrections for the $q \to q$ channel are always included *exactly*.

Our predictions will refer to the unpolarized $\ell p \to \ell \pi^+ X$ process appropriate for the future EIC with $\sqrt{s} = 100$ GeV. We focus on the z-dependence of the cross section and, unless stated otherwise, integrate over $y \in [0.1, 0.9]$ and $x \in [0.1, 0.8]$. We choose x and z to be rather large so that we are safely in the threshold regime. Because of the relation $Q^2 = xys$, our choice of kinematics implies $Q^2 > 100$ GeV^2 for the EIC. We furthermore require $W > 7$ GeV, where $W^2 = Q^2(1-x)/x + m_p^2$, with m_p the proton mass.

We begin by comparing fully resummed results obtained at various different levels of logarithmic accuracy. The upper left part of Fig. 15 shows the NLL, NNLL, and N^{3}LL resummed cross sections as functions of z, normalized to the LO one. As one can see, the NNLL terms show an enhancement over NLL, and the additional terms arising at N^{3}LL lead to a very modest further increase of the cross section. This result demonstrates that the resummed SIDIS cross section has excellent perturbative stability. We can further investigate the improvements provided by going to NNLL and N^{3}LL. To this end, we note that even at a given logarithmic order the resummation formula in Eq. (6.9) may actually be used in various ways that are all equivalent in terms of their perturbative content, but differ numerically. Let us refer to the corresponding choices as *resummation schemes*. We consider three such schemes:

SCHEME (A) Here we use Eq. (6.9) as written. That is, we keep the functions H_{qq}^{SIDIS} and $\widehat{C}_{qq}$ as separate factors, each its own perturbative series of the form (6.11). Also, we use the Mellin moments N and M precisely in the form $\bar{N}$ and $\bar{M}$ as defined in (6.10). This scheme has been used for the first plot in Fig. 15.

SCHEME (B) Here we expand the product $H_{qq}^{\text{SIDIS}} \times \widehat{C}_{qq}$ in Eq. (6.9) strictly to the desired order. That is, suppose we are at NLL where $H_{qq}^{\text{SIDIS}} = 1 + \frac{\alpha_s}{\pi} H_{qq}^{\text{SIDIS},(1)}$ and $\widehat{C}_{qq} = 1 + \frac{\alpha_s}{\pi} \widehat{C}_{qq}^{(1)}$, then we use $H_{qq}^{\text{SIDIS}} \times \widehat{C}_{qq} = 1 + \frac{\alpha_s}{\pi} (H_{qq}^{\text{SIDIS},(1)} + \widehat{C}_{qq}^{(1)})$ and drop terms of $\mathcal{O}(\alpha_s^2)$. We continue to use the variables $\bar{N}$ and $\bar{M}$.

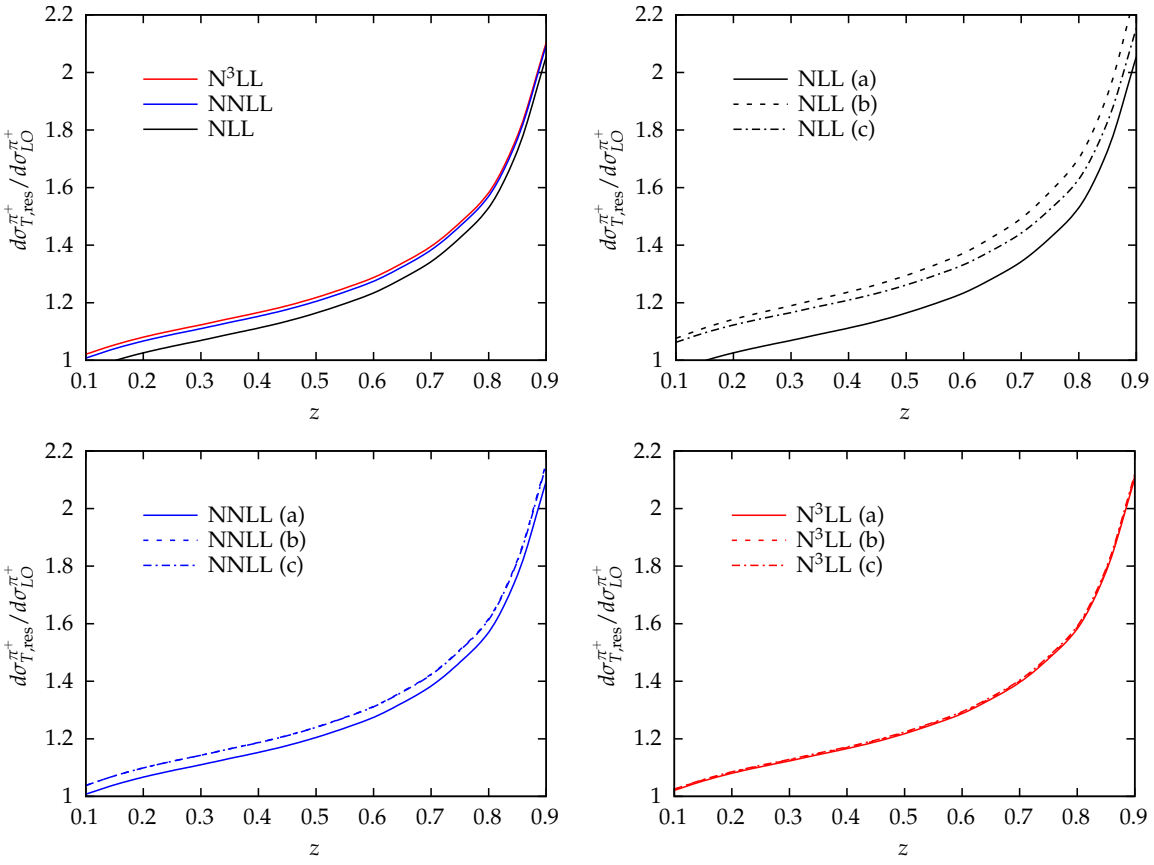

Figure 15: Ratios of resummed results for the unpolarized $\ell p \to \ell \pi^+ X$ transverse cross section in the $q \to q$ channel to the LO one, for EIC kinematics with $x \in [0.1, 0.8]$. Upper left: comparison of NLL (black), NNLL (blue), and N^3LL (red) resummation. Upper right and lower panel: Results for resummation schemes (a),(b),(c) as described in the text at NLL, NNLL, and N^{3}LL.

SCHEME (C) Here we first use the expansion of $H_{qq}^{\text{SIDIS}} \times \widehat{C}_{qq}$ as for scheme (b). In addition, we use (6.10),(6.13) to write

$$\lambda_{NM} = b_0 \alpha_s(\mu_R)\big(\ln N + \ln M\big) + 2\gamma_E b_0 \alpha_s(\mu_R)\,. \tag{6.31}$$

The terms with the Euler constant lead to modifications of the functions $h_q^{(k>1)}$ in Eq. (6.14) [32, 164]. They evidently also generate non-logarithmic corrections in the resummed exponent. These may be expanded out perturbatively, so that they migrate from the exponent to an N, M-independent prefactor. This prefactor is then expanded along with the factor $H_{qq}^{\text{SIDIS}} \times \widehat{C}_{qq}$ into a *single* perturbative function that now multiplies the resummed exponent, the latter now being a function of N and M rather than of $\bar{N}$ and $\bar{M}$.

It is immediately clear that the three resummation schemes are indeed equivalent for a given logarithmic accuracy. The remaining three plots in Fig. 15 compare the three schemes at NLL (upper right), NNLL (lower left), and N^{3}LL (lower right). It is striking to see how the difference among the three schemes is still rather large at NLL, then strongly decreases at NNLL, and finally becomes extremely small at N^{3}LL. (We note in passing that this means that the enhancement over NLL seen in the first plot in Fig. 15 is a feature only present in scheme (a) but does not really occur in the other two schemes). Of course, one does expect the details of how the expansions are performed to matter less and less with increasing logarithmic order. Nevertheless, the level at which the resummed predictions become independent of the resummation scheme at NNLL and especially at N^{3}LL is truly remarkable.

Encouraged by these observations, we now turn to fixed-order expansions of our resummed results. Figure 16 (left) shows again the NNLL-resummed result for scheme (a), along with its expansion to NNLO as given by Eqs. (5.38) and (5.39) (black solid line) and already obtained in Ref. [i]. All results are again normalized to the LO cross section. We note that finite-order expansions are independent of the resummation scheme chosen. We observe that resummation within scheme (a) leads to a suppression of the cross section at lower z and to the expected enhancement at high z where the threshold logarithms become particularly important. In addition to these two results, we also expand the resummed cross section numerically to orders α_s^2 and α_s^3. As expected, the result for the $\mathcal{O}(\alpha_s^2)$ expansion (dash-dotted line) is extremely close to the NNLO one. The only difference between these two results comes from the fact that the formal expansion of the NLP factors in (6.16) will produce also terms with higher inverse powers of N and M, as noted at the end of Sec. 6.5. These terms are not included in our explicit NNLO expansions, but do contribute to the numerical $\mathcal{O}(\alpha_s^2)$ expansion of the cross section. As one can see by comparing the two corresponding curves, they are of very small size. The dashed line in the left part of Fig. 16 shows the $\mathcal{O}(\alpha_s^3)$ expansion of the NNLL

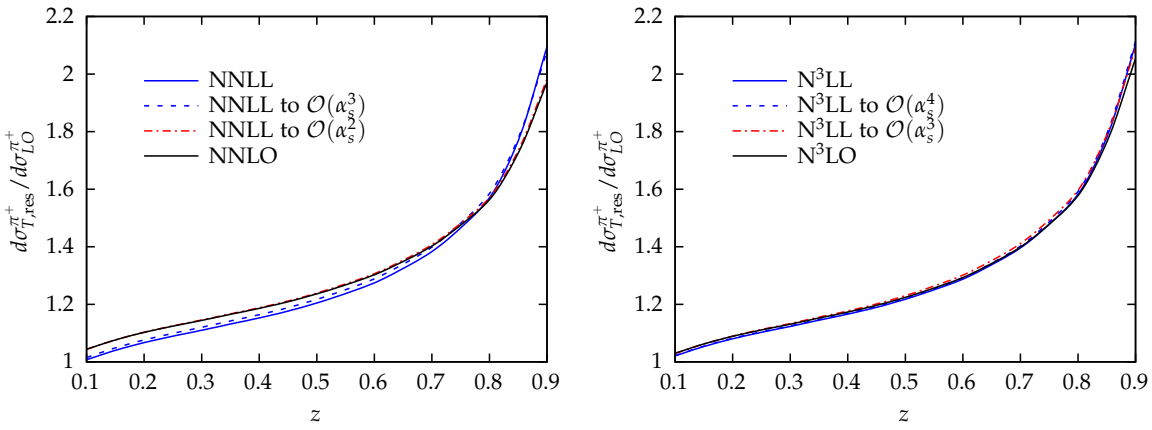

Figure 16: Left: NNLO and NNLL-resummed results for the unpolarized $\ell p \to \ell \pi^+ X$ transverse cross section in the $q \to q$ channel normalized to the LO one, for EIC kinematics with $x \in [0.1, 0.8]$. We also show numerical expansions of the NNLL result to $\mathcal{O}(\alpha_s^2)$ and $\mathcal{O}(\alpha_s^3)$. Right: Same as left, but for N^{3}LL, N^{3}LO and expansions to $\mathcal{O}(\alpha_s^3)$ and $\mathcal{O}(\alpha_s^4)$.

resummed cross section. We observe that this result is already very close to the full NNLL one, indicating that terms of order $\mathcal{O}(\alpha_s^4)$ or higher are small.

The right part of Fig. 16 presents the same analysis one order higher. We show the N^{3}LL-resummed cross section for scheme (a), and now the expansion to N^{3}LO as given by Eqs. (5.38),(5.39) and (6.27). This time, we numerically expand the N^{3}LL result to orders α_s^3 and α_s^4. Again the numerical expansion to $\mathcal{O}(\alpha_s^3)$ essentially coincides with the approximate N^{3}LO one, up to tiny corrections suppressed as $1/N^2, 1/M^2$ or higher. The result at $\mathcal{O}(\alpha_s^3)$ is almost indistinguishable from the full N^{3}LL-resummed one, demonstrating again that corrections beyond third order are all but negligible. We note that the $\mathcal{O}(\alpha_s^3)$ expansion obtained from the N^{3}LL-resummed result is more complete than the $\mathcal{O}(\alpha_s^3)$ expansion shown in the left part of Fig. 16: It contains all *seven* "towers" of threshold logarithms, that is, terms of the form $\alpha_s^3 \ln^n(N) \ln^m(M)$ with $0 \leq n + m \leq 6$, whereas NNLL resummation can only correctly reproduce the five towers with $2 \leq n + m \leq 6$.

We also briefly consider the x dependence of the resummed results, integrating over the region $z \in [0.2, 0.9]$. Figure 17 shows on the left the corresponding results obtained at NLO and for NLL, NNLL, and N^{3}LL resummation within our scheme (a). One can observe that, as before for the z dependence, resummation leads to a strong enhancement of the cross section, especially so at large values of x. Compared to the upper left plot of Fig. 15, the various resummed curves tend to lie closer to one another. This may in part be due to the fact that larger x kinematically correspond to larger values of $Q^2 = xys$, where the strong coupling becomes

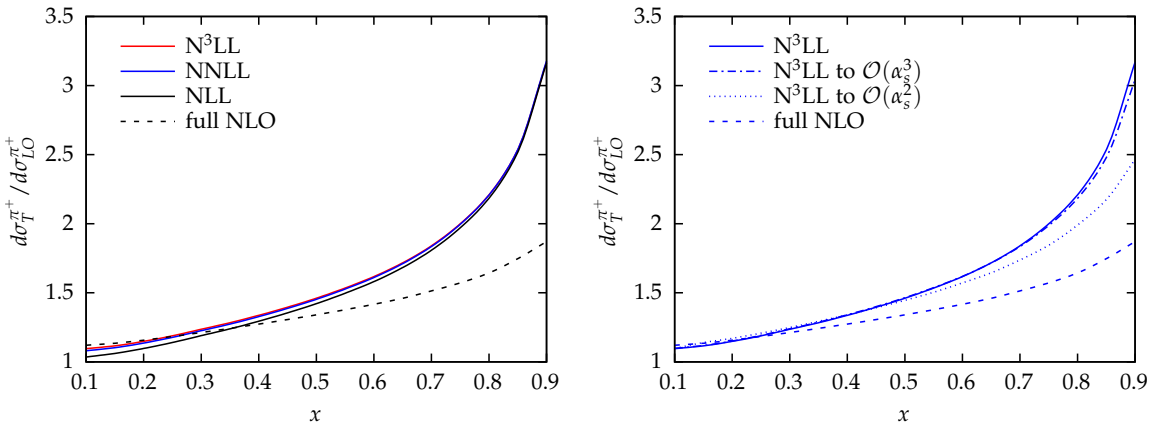

Figure 17: Left: NLO, NLL, NNLL and N^{3}LL-resummed results for the unpolarized $\ell p \to \ell \pi^+ X$ transverse cross section in the $q \to q$ channel, as functions of x, normalized to LO. Right: same as on the left, N^{3}LL resummed results expanded to orders $\mathcal{O}(\alpha_s^3)$ and $\mathcal{O}(\alpha_s^2)$ are shown as well. The plos are for EIC kinematics with $z \in [0.2, 0.9]$.

smaller and hence the threshold variable λ_{NM} as well. This effect is not present in case of the z dependence of the cross sections.

We at last show the N^{3}LL resummed results on the right of Fig. 17, expanded to different orders in α_s. We notice that the fully resummed curve is well approximated by the $\mathcal{O}(\alpha_s^3)$ expansion. Yet higher logarithmic orders in the exponent are therefore not expected to significantly improve the N^{3}LL resummed prediction.

6.7 CONCLUSIONS AND OUTLOOK

We have explored higher-order QCD corrections to the quark-to-quark hard-scattering cross section relevant for semi-inclusive DIS. We have developed the threshold resummation framework for SIDIS to N^{3}LL accuracy, hereby extending previous work carried out at NNLL [i]. Among the main tasks to be completed for achieving N^{3}LL resummation was the derivation of the three-loop hard factor from the spacelike form factor. We have used our N^{3}LL results to derive approximate N^{3}LO corrections for SIDIS. These corrections contain all seven "towers" of threshold logarithms that are present at this order. We have also included dominant subleading logarithmic terms that are suppressed near threshold.

We have presented phenomenological results for resummed and approximate fixed-order SIDIS cross sections for EIC kinematics. These show an excellent perturbative stability of the cross section in the sense that the N^{3}LL cross section is only mod-

estly enhanced over the NNLL one, and that generally corrections beyond $\mathcal{O}(\alpha_s^3)$ seem unimportant. A particularly striking result is that the actual treatment of resummation, in terms of how the relevant expansions are carried out in practice, matters less and less when the logarithmic accuracy of resummation increases, so that the N^{3}LL result is essentially insensitive to the resummation scheme adopted. Clearly, our results show that the SIDIS cross section may serve as an excellent testbed for studies of higher orders in perturbation theory. We believe that our results are a valuable addition to the general "library" of QCD observables that are known to NNLO and beyond.

Future extensions of this work should also address non-perturbative power corrections to the SIDIS cross section, very little about which is currently known. It would be an interesting phenomenlogical study to confront experimental data with our perturbative results at various high orders ranging from NLO to N^{3}LL, ascertaining how the size of phenomenlogically extracted power corrections depends on the order of perturbation theory that is employed.

We finally note that while we have focused our studies entirely on the spin-averaged SIDIS cross section, all our results equally apply to the helicity-dependent one. More precisely, the N^{3}LL result and hence its approximate N^{3}LO expansion are identical in the spin-averaged and the spin-dependent cases. This further corroborates the finding of Ref. [21] that the SIDIS spin asymmetry is insensitive to higher-order perturbative QCD corrections.

7

T-ODD PROTON-HELICITY ASYMMETRY

We compute the single-spin asymmetry A_{UL} in semi-inclusive deep-inelastic scattering of unpolarized leptons and longitudinally polarized protons at large transverse momentum of the produced hadron. Our calculation is performed in collinear factorization at the lowest order of QCD perturbation theory. For photon exchange the asymmetry is T-odd and receives contributions from the interference of the tree level and one-loop absorptive amplitudes. We consider the behavior of the spin asymmetry at low transverse momentum where contact to the formalism based on transverse-momentum dependent distribution functions can be made. We also present some phenomenological results relevant for the COMPASS and HERMES experiments and the future Electron-Ion Collider. This Chapter is based on publication [iii].

7.1 INTRODUCTION

T-odd effects in semi-inclusive deep-inelastic scattering (SIDIS) have been a focus of numerous theoretical and experimental studies in recent years [165]. These studies were motivated by the discovery [166–168] that a proton can in fact have intrinsic T-odd parton distribution functions, associated with the interplay of transverse polarization of the proton or its partons with the partonic transverse momenta. Here the term "T-odd" refers to a "naive" time-reversal operation, which corresponds to ordinary time reversal without the interchange of initial and final states of the reaction considered.

T-odd effects can, however, also be generated in perturbation theory. They are absent at tree level, but the seminal papers [169–174] described how they can arise from absorptive parts of loop amplitudes at $\mathcal{O}(\alpha_s^2)$ in QCD hard scattering, where α_s is the strong coupling. Initially proposed as tests of QCD and its gluon self-coupling [170, 171, 173], T-odd effects in perturbative QCD have remained a subject of interest ever since [175–185]. In regards to SIDIS, the early studies [174, 180, 181] have addressed neutrino scattering as well as scattering of longitudinally polarized leptons off unpolarized protons [180, 181].

In the present Chapter, we extend the previous work and compute the leading perturbative T-odd effects for SIDIS with unpolarized leptons colliding with longitudinally polarized protons via photon exchange [25, 186, 187], which to our knowledge have not been investigated by other authors. Calculating the relevant absorptive parts of one-loop amplitudes, and using collinear factorization, we derive the corresponding azimuthal terms in the spin asymmetry A_{UL} when the proton beam helicity is flipped. Our calculation is to be seen in the same spirit as other approaches that aim to obtain the phase required for (in their case, transverse) single-spin asymmetries through a hard-scattering mechanism [184, 185, 188]. In particular, Ref. [185] has investigated perturbative T-odd effects for the single- *transverse* SIDIS spin asymmetry A_{UT} via the structure function g_T and, as we shall see, there are interesting connections of that study to our present work.

There are several aspects of this observable that motivate us to carry out this study. First, and perhaps foremost, perturbative T-odd effects in QCD have remained elusive so far, and given their unique property of arising from loop effects in QCD, any observable sensitive to them is valuable. In this context it is also worth mentioning that for A_{UL} the effects are sensitive to the proton's helicity parton distributions *despite* the fact that an unpolarized lepton beam is used. This is quite unique as well, since usually conservation of parity in strong interactions prohibits such single-longitudinal spin asymmetries.

Second, measurements of the relevant azimuthal terms have been carried out in various fixed-target experiments by the HERMES [189–192], CLAS [193] and COMPASS [194–196] collaborations, albeit in kinematic regions that are not clearly in the perturbative regime. Nevertheless, it is interesting to see whether the perturbative calculations give results that are roughly consistent with data at the highest transverse momenta $P_{h\perp}$ of the produced hadron accessed so far. Much higher $P_{h\perp}$ should become available at the future Electron-Ion Collider (EIC), where SIDIS studies with exquisite precision will be feasible [163]. It is therefore valuable to extend the "library" of observables relevant at the EIC.

Finally, as mentioned above, most studies of T-odd effects in QCD have addressed the non-perturbative regime in terms of parton distributions and fragmentation functions. For SIDIS, this approach becomes particularly useful when the transverse momentum of the outgoing hadron is relatively low, $P_{h\perp}^2 \ll Q^2$, with Q^2 the virtuality of the exchanged photon. In this case one can describe SIDIS in terms of "Transverse Momentum Dependent" (TMD) parton distributions and fragmentation functions [197, 198]. As has been shown [199, 200], TMDs can indeed generate the SIDIS spin asymmetry A_{UL}, and numerous phenomenological studies have been performed [201–208]. Having also a perturbative calculation of A_{UL}, for which

the observed transverse momentum is acquired by the recoil against a hard parton in the scattering process, one can address the question in how far the TMD formalism is recovered as one takes the limit $P_{h\perp}^2 \ll Q^2$. General statements about the high-transverse-momentum tail of TMDs were developed in [26], which also make predictions for the behavior of A_{UL} that may be directly compared to our results. In this context also the T-odd beam-spin asymmetry A_{LU} is interesting [180, 181, 209, 210], for which the initial lepton is polarized, and we will briefly discuss this asymmetry as well. We note that additional insights into the matching of TMDs to perturbative calculations have become available in recent years [211–220].

This Chapter is organized as follows. In Sec. 7.2 we introduce the kinematic variables and the main ingredients for the perturbative description of the spin-dependent SIDIS cross section. In Sec. 7.3, we briefly review the main properties of T-odd asymmetries and describe the strategy for our calculation. Section 7.4 presents our perturbative results for the T-odd contributions to the SIDIS spin asymmetry. Next, in Sec. 7.5, we consider the limit of small transverse momenta and compare to known results in the TMD regime. Phenomenological results are presented in Sec. 7.6. Here we consider the spin asymmetry A_{UL} at the EIC and also compare to the COMPASS [196] and HERMES data [189, 192]. Section 7.7 concludes this Chapter.

We note that the T-odd asymmetry has already been the subject of Ref. [25], where we calculated the lowest order pQCD corrections to it. In Sections 7.3, 7.4 & 7.6, which are based on [25], we review this calculation. In the present Chapter however we go far beyond that, while taking steps towards the TMD formalism in Sec. 7.5, which is the new contribution to the T-odd asymmetry within this dissertation.

7.2 PERTURBATIVE SIDIS CROSS SECTION

We consider the SIDIS process

$$\ell(k) + p(P,S) \to \ell'(k') + h(P_h) + X\,,$$

where we have indicated the four-momenta of the participating particles, and where S is the proton spin vector. We set $q \equiv k - k'$ and $Q^2 \equiv -q^2$ for the exchanged virtual gauge boson, for which we will consider only a virtual photon, thus excluding parity-violating effects. The usual kinematical variables relevant for SIDIS are defined as

$$x = \frac{Q^2}{2P\cdot q}\,, \quad y = \frac{P\cdot q}{P\cdot k}\,, \quad z = \frac{P\cdot P_h}{P\cdot q}\,. \tag{7.1}$$

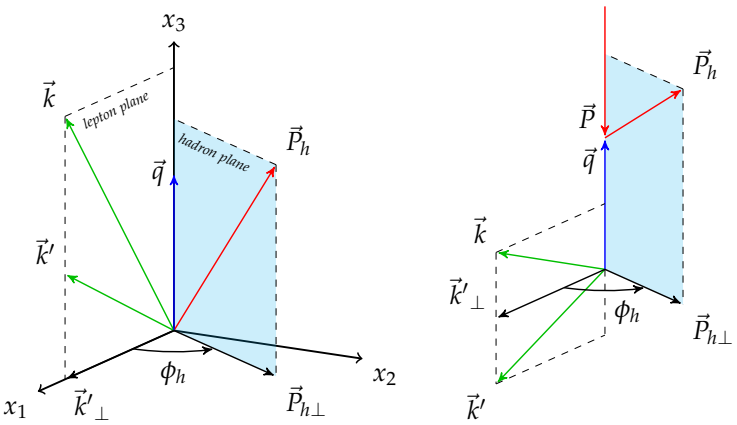

Figure 18: *Left: kinematics of the SIDIS process in the rest frame of the proton. Right: same in the Breit frame.*

In the following, we will consider the transverse momentum $P_{h\perp}$ and its azimuthal angle ϕ_h with respect to the lepton plane, defined in a suitable reference frame. For SIDIS phenomenology one usually adopts the proton rest frame. The kinematics of the process in this frame are depicted on the left side of Fig. 18. The x_3 axis is defined by the direction of the photon three-momentum $\vec{q}$. Our actual calculations will be performed in the Breit frame in which the photon four-momentum has a vanishing energy component, $q = (0, 0, 0, Q)$, which simplifies the calculations. This frame is related to the rest frame by a longitudinal boost along the x_3 axis so that all transverse components remain unchanged. The situation in the Breit frame is shown on the right side of Fig. 18.

As discussed in the Introduction, we consider longitudinal polarization for the proton. In the proton rest frame, this is defined by choosing the proton's spin vector along (or opposite to) the direction of the virtual photon. Here $\vec{S} \parallel \vec{q}$ will correspond to negative longitudinal polarization of the proton. We note that in actual experiments one will define longitudinal polarization in the proton rest frame by choosing the spin parallel or antiparallel to the *lepton* beam direction rather than the photon one. The two cases are, of course, related; all details may be found in Ref. [221] (see also [192]). Specifically, they differ by admixtures related to the corresponding transverse single-spin asymmetry A_{UT}, which can be taken into account in the experimental analysis. Note that the case with polarization along the lepton beam direction readily extends to the situation at an ℓp collider, where a longitudinally polarized proton will be in a helicity state. In the following we will therefore consider protons with either positive or negative helicity.

For an incoming unpolarized lepton scattering off a longitudinally polarized proton two independent structure functions contribute to the proton helicity-dependent part of the cross section [26, 200, 222], entering with dependences of the form $\sin(\phi_h)$ or $\sin(2\phi_h)$, respectively. Explicitly, we have

$$\begin{aligned}\frac{d^5\Delta\sigma^h}{dx\,dy\,dz\,dP_{h\perp}^2\,d\phi_h} &= \frac{1}{2}\left(\frac{d^5\sigma_+^h}{dx\,dy\,dz\,dP_{h\perp}^2\,d\phi_h} - \frac{d^5\sigma_-^h}{dx\,dy\,dz\,dP_{h\perp}^2\,d\phi_h}\right) \\ &= \frac{\pi\alpha^2}{xQ^2}\frac{y}{1-\varepsilon}\left\{\sqrt{2\varepsilon(1+\varepsilon)}\,F_{UL}^{\sin\phi_h}\sin(\phi_h) + \varepsilon\,F_{UL}^{\sin 2\phi_h}\sin(2\phi_h)\right\},\end{aligned} \tag{7.2}$$

where the subscripts $\pm$ denote proton helicities and ε is defined as the ratio of longitudinal and transverse photon fluxes,

$$\varepsilon \equiv \frac{1-y}{1-y+y^2/2}\,. \tag{7.3}$$

The structure functions $F_{UL}^{\sin\phi_h}, F_{UL}^{\sin 2\phi_h}$ depend on x, z, Q^2 and $P_{h\perp}^2$, which we will usually not write out. In the following, we will compute them in collinear factorization, where they become double convolutions of helicity parton distribution functions, fragmentation functions, and perturbative partonic coefficient functions. We will only consider the lowest order (LO) in perturbation theory, at which the structure functions may be cast into the forms

$$\begin{aligned}F_{UL}^{\sin\phi_h} &= \left(\frac{\alpha_s(\mu^2)}{2\pi}\right)^2 \frac{x}{Q^2z^2} \\ &\times \sum_{\substack{a,b \\ =q,\bar{q},g}} \int_x^1 \frac{d\hat{x}}{\hat{x}} \int_z^1 \frac{d\hat{z}}{\hat{z}}\,\Delta f_a\left(\frac{x}{\hat{x}},\mu^2\right) C_{UL}^{\sin\phi_h,a\to b}(\hat{x},\hat{z})\,D_b^h\left(\frac{z}{\hat{z}},\mu^2\right) \\ &\times \delta\left(\frac{q_T^2}{Q^2} - \frac{(1-\hat{x})(1-\hat{z})}{\hat{x}\hat{z}}\right),\end{aligned} \tag{7.4}$$

and likewise for $F_{UL}^{\sin 2\phi_h}$. The factor $(\alpha_s/(2\pi))^2\,x/(Q^2z^2)$ has been introduced for convenience; it explicitly exhibits the leading power of α_s of the structure functions and also makes the coefficient functions $C_{UL}^{\sin\phi_h,a\to b}$, $C_{UL}^{\sin 2\phi_h,a\to b}$ dimensionless functions of only the two partonic variables

$$\hat{x} \equiv \frac{Q^2}{2p_a\cdot q}\,, \quad \hat{z} \equiv \frac{p_a\cdot p_b}{p_a\cdot q}\,, \tag{7.5}$$

which are the partonic counterparts of the hadronic variables in Eq. (7.1). The coefficient functions are to be derived for each $2\to 2$ partonic channel $\gamma^* + a \to$

$b + c$, where parton b fragments into the observed hadron and parton c remains unobserved. These processes are $\gamma^* q(\bar{q}) \to q(\bar{q})g$, $\gamma^* q(\bar{q}) \to gq(\bar{q})$, $\gamma^* g \to q\bar{q}$, and $\gamma^* g \to \bar{q}q$.

In Eq. (7.4) $\Delta f_a(\xi, \mu^2)$ is the helicity distribution of parton $a = q, \bar{q}, g$ in the proton at momentum fraction ξ and factorization scale μ (which, for simplicity, we choose equal to the renormalization scale μ appearing in the strong coupling constant α_s). Furthermore, $D_b^h(\zeta, \mu^2)$ is the corresponding fragmentation function for parton b going to the observed hadron h, at momentum fraction ζ and, again, at factorization scale μ. All functions in Eq. (7.4) are tied together by the δ function in the second line which expresses the fact that at LO the recoiling partonic system consists of a single massless parton c. For convenience, we have introduced the variable

$$q_T^2 \equiv \frac{P_{h\perp}^2}{z^2}\,. \tag{7.6}$$

7.3 T-ODD SINGLE-SPIN ASYMMETRY AT LOWEST ORDER

The terms proportional to $\sin(\phi_h)$ and $\sin(2\phi_h)$ represent correlations of the forms $\vec{S} \cdot (\vec{k}'_\perp \times \vec{P}_{h\perp})$ and $\vec{S} \cdot (\vec{k}'_\perp \times \vec{P}_{h\perp})(\vec{k}'_\perp \cdot \vec{P}_{h\perp})$, respectively, which already suggests that they are "naively" time-reversal odd. This sets a constraint on the partonic scattering processes that may contribute to the corresponding asymmetries in perturbation theory. To set the stage for our derivations, we briefly review how this constraint can be exploited to simplify the calculations.

Denoting as S_{fi} the scattering matrix element between an initial state i and a final state f, a
textitnaive time-reversal transformation corresponds to a time-reversal without interchange of initial and final states. Hence a T-odd observable is characterized by [174, 223, 224]

$$\left|S_{fi}\right|^2 \neq \left|S_{\tilde{f}\tilde{i}}\right|^2, \tag{7.7}$$

where $\tilde{i}(\tilde{f})$ is obtained from $i(f)$ by reversing momenta and spins. T-odd effects can also be present in theories which are invariant under
textittrue time-reversal, fulfilling

$$\left|S_{fi}\right|^2 = \left|S_{\tilde{i}\tilde{f}}\right|^2. \tag{7.8}$$

This is easily understood by considering the reaction matrix T:

$$S_{fi} \equiv \delta_{fi} + i(2\pi)^4 \delta^{(4)}\left(P_f - P_i\right) T_{fi}\,, \tag{7.9}$$

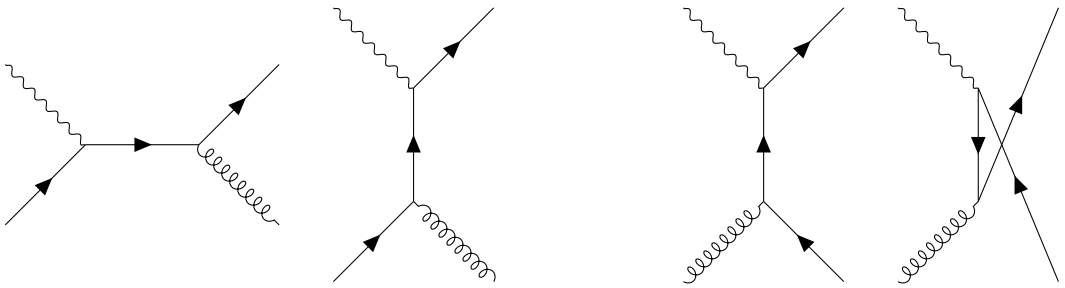

Figure 19: *Tree-level diagrams for* $\gamma^* + q \to q + g$ *and* $\gamma^* + g \to q + \bar{q}$.

and the unitarity condition for the scattering matrix

$$T_{fi} - T_{if}^* = i \sum_X T_{Xf}^* T_{Xi} \delta^{(4)} (P_X - P_i) \equiv i\alpha_{fi} \,, \tag{7.10}$$

where in the last equation we introduced the absorptive part α_{fi} of the reaction amplitude. Eq. (7.10) can be rewritten as $T_{if}^* = T_{fi} - i\alpha_{fi}$. Taking the square modulus of both sides we find

$$\left|T_{if}\right|^2 = \left|T_{fi}\right|^2 + 2\,\mathrm{Im}\left(T_{fi}^* \alpha_{fi}\right) + \left|\alpha_{fi}\right|^2 . \tag{7.11}$$

True time reversal invariance, Eq. (7.8), implies $\left|T_{if}\right|^2 = \left|T_{\tilde{f}\tilde{i}}\right|^2$ (leaving aside the case $i = f$). Thus, if only QED and QCD interactions are present, Eq. (7.11) gives an expression for T-odd terms:

$$\left|T_{\tilde{f}\tilde{i}}\right|^2 - \left|T_{fi}\right|^2 = 2\,\mathrm{Im}\left(T_{fi}^* \alpha_{fi}\right) + \left|\alpha_{fi}\right|^2 . \tag{7.12}$$

If we consider the partonic processes underlying semi-inclusive DIS, the LO contributions to T_{fi} are the tree-level diagrams for $\gamma^* + q \to q + g$ and $\gamma^* + g \to q + \bar{q}$ shown in Fig. 19. The leading terms for the absorptive amplitude α_{fi} arise from loop corrections already at one-loop order. The one-loop diagrams shown in Fig. 20 for the initial-quark channel and in Fig. 21 for the initial-gluon channel all have the property that they have an imaginary part and hence produce a phase relative to the corresponding tree-level amplitudes. As a result, the term $2\,\mathrm{Im}(\,T_{fi}^* \alpha_{fi})$ in Eq. (7.12) is non-vanishing already due to the interferences of the one-loop and tree amplitudes. We conclude that LO contributions to T-odd effects in SIDIS come precisely from these interferences and are of order $\mathcal{O}(\alpha_s^2)$ [174].

Let us briefly describe the strategy we have adopted in computing the T-odd interference contributions. Introducing the amplitudes $\mathcal{M}_{ab}^{\pm}$ for positive and negative helicity of parton a in the channel $\gamma^* + a \to b + c$, we write the difference of their squares as

$$|\mathcal{M}_{ab}^{+}|^2 - |\mathcal{M}_{ab}^{-}|^2 \;=\; L^{\mu\nu}\left(\hat{W}_{\mu\nu}^{+} - \hat{W}_{\mu\nu}^{-}\right) \;\equiv\; L^{\mu\nu}\Delta\hat{W}_{\mu\nu} \,, \tag{7.13}$$

where

$$L_{\mu\nu} = 2\left(k_\mu k'_\nu + k_\nu k'_\mu - \frac{Q^2}{2} g_{\mu\nu}\right) \tag{7.14}$$

is the leptonic tensor, and

$$\begin{aligned}\Delta\hat{W}_{\mu\nu} \equiv\ & \langle p_a, +|J_\mu(0)|p_b\, p_c\rangle \langle p_b\, p_c|J_\nu(0)|p_a, +\rangle \\ & - \langle p_a, -|J_\mu(0)|p_b\, p_c\rangle \langle p_b\, p_c|J_\nu(0)|p_a, -\rangle\end{aligned} \tag{7.15}$$

is the partonic tensor for a polarized parton a in the initial state and a fragmenting parton b in the final state (at LO, the final state is completely fixed by a and b). Since, as discussed above, only interferences between tree-level and one-loop amplitudes contribute to the order we are considering, we have

$$\begin{aligned}\Delta\hat{W}_{\mu\nu} = & \Big[\langle p_a, +|J_{\mu,\text{tree}}(0)|p_b\, p_c\rangle \langle p_b\, p_c|J_{\nu,\text{loop}}(0)|p_a, +\rangle \\ & + \langle p_a, +|J_{\mu,\text{loop}}(0)|p_b\, p_c\rangle \langle p_b\, p_c|J_{\nu,\text{tree}}(0)|p_a, +\rangle\Big] \\ & - \Big[\langle p_a, -|J_{\mu,\text{tree}}(0)|p_b\, p_c\rangle \langle p_b\, p_c|J_{\nu,\text{loop}}(0)|p_a, -\rangle \\ & + \langle p_a, -|J_{\mu,\text{loop}}(0)|p_b\, p_c\rangle \langle p_b\, p_c|J_{\nu,\text{tree}}(0)|p_a, -\rangle\Big]\,.\end{aligned} \tag{7.16}$$

The phase required for a non-vanishing imaginary part is generated by analytic continuation of logarithms in the loop integrals, e.g.,

$$\ln\left(-\frac{\mu^2}{\hat{s}+\mathrm{i}\epsilon}\right) \quad \longrightarrow \quad \ln\left(\frac{\mu^2}{\hat{s}}\right) + \mathrm{i}\pi\,, \tag{7.17}$$

where $\hat{s} = (q+p)^2 = Q^2(1-\hat{x})/\hat{x}$. As mentioned, such phases only appear in the s-channel diagrams and the two box-diagrams in Fig. 20, for initial quarks (or antiquarks). For initial gluons, they appear in the two box diagrams in Fig. 21.

It is quite straightforward to compute the partonic tensor $\Delta\hat{W}_{\mu\nu}$. The only subtlety is related to the use of the Dirac matrix γ_5 and the Levi-Civita tensor $\varepsilon_{\mu\nu\rho\sigma}$ in dimensional regularization in $d = 4-2\epsilon$ dimensions. Here we have used the scheme of Refs. [79, 80] which is known to be algebraically consistent. We have used the Mathematica package `Tracer` [225] to compute the Dirac traces and contractions and `Package-X` [226] for the evaluation of the loop integrals and their imaginary parts. We note that poles at $\epsilon = 0$ arise at various intermediate stages of the calculation; these all have to cancel in the end since, at the lowest order, the T-odd part of the hadronic tensor must not have any ultraviolet or infrared or collinear singularities. This provides a useful check on our calculation. The partonic coefficient functions are found from the final result for $L^{\mu\nu}\Delta\hat{W}_{\mu\nu}$ as the coefficients of the terms $\sim \sin(\phi_h)$ and $\sim \sin(2\phi_h)$. No other angular dependences appear.

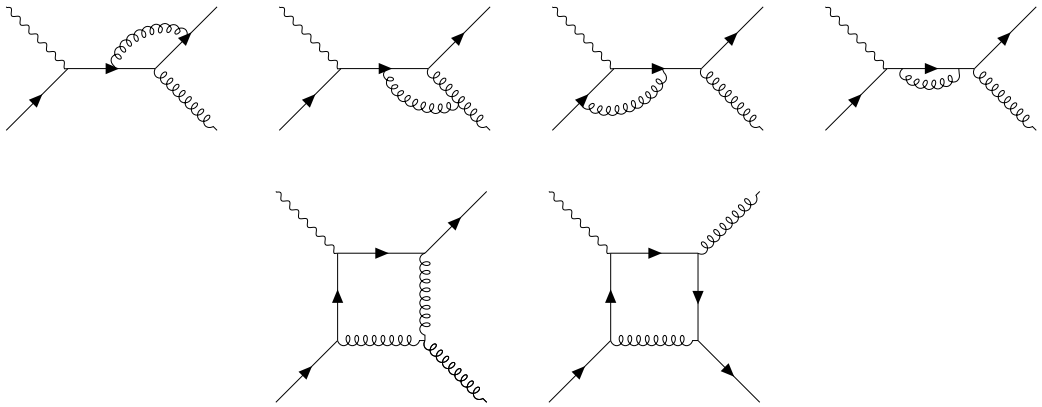

Figure 20: One-loop diagrams for $\gamma^* + q \to q + g$ that provide a phase relative to the tree-level amplitude. We note that there are additional one-loop diagrams that do not produce a phase.

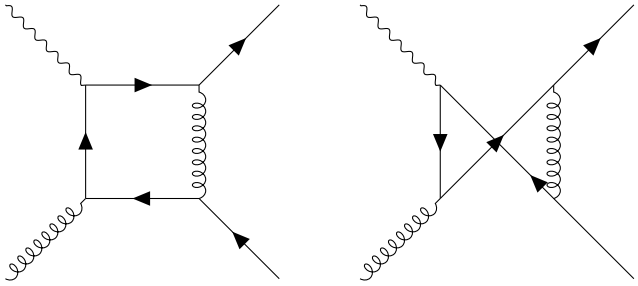

Figure 21: One-loop diagrams for $\gamma^* + g \to q + \bar{q}$ that provide a phase relative to the tree-level amplitude.

7.4 ANALYTICAL RESULTS

For the partonic coefficient functions for $F_{UL}^{\sin\phi_h}$ we find [25, 187]:

$$\begin{aligned}
C_{UL}^{\sin\phi_h,q\to q}(\hat{x},\hat{z}) &= e_q^2 C_F \Big(C_A(1-\hat{x}) + C_F(\hat{x}-1-\hat{z}+3\hat{x}\hat{z}) \\
&\quad + (C_A - 2C_F)(1-2\hat{x})\frac{\hat{z}\ln\hat{z}}{1-\hat{z}} \Big) \frac{Q}{q_T}\,, \\
C_{UL}^{\sin\phi_h,q\to g}(\hat{x},\hat{z}) &= -e_q^2 C_F \frac{(1-\hat{z})}{\hat{z}} \Big(C_A(1-\hat{x}) + C_F(-3\hat{x}\hat{z}+4\hat{x}+\hat{z}-2) \\
&\quad + (C_A - 2C_F)(1-2\hat{x})\frac{(1-\hat{z})\ln(1-\hat{z})}{\hat{z}} \Big) \frac{Q}{q_T}\,, \\
C_{UL}^{\sin\phi_h,g\to q}(\hat{x},\hat{z}) &= e_q^2 (C_A - 2C_F)(1-\hat{x})\frac{1}{2\hat{z}^2} \Big(\hat{x}\hat{z}(1-2\hat{z}) - (1-\hat{x})\ln(1-\hat{z}) \\
&\quad + (1-\hat{x})\frac{\hat{z}\ln(\hat{z})}{1-\hat{z}} \Big) \frac{Q}{q_T}\,,
\end{aligned} \tag{7.18}$$

while for the coefficients for $F_{UL}^{\sin 2\phi_h}$ we have [25, 187]

$$\begin{aligned}
C_{UL}^{\sin 2\phi_h,q\to q}(\hat{x},\hat{z}) &= e_q^2 C_F(1-\hat{x}) \Big((C_A - 2C_F)\frac{(1-2\hat{z})\ln\hat{z}}{1-\hat{z}} \\
&\quad - (C_A + (1-3\hat{z})C_F) \Big) \frac{Q^2}{q_T^2}\,, \\
C_{UL}^{\sin 2\phi_h,q\to g}(\hat{x},\hat{z}) &= -e_q^2 C_F(1-\hat{x})\frac{(1-\hat{z})^2}{\hat{z}^2} \Big((C_A - 2C_F)\frac{(1-2\hat{z})\ln(1-\hat{z})}{\hat{z}} \\
&\quad + (C_A - (2-3\hat{z})C_F) \Big) \frac{Q^2}{q_T^2}\,, \\
C_{UL}^{\sin 2\phi_h,g\to q}(\hat{x},\hat{z}) &= e_q^2 (C_A - 2C_F)(1-\hat{x})^2\frac{1}{2\hat{z}^3} \Big(\hat{z}(2(1-\hat{z})\hat{z}-1) - (1-\hat{z})\ln(1-\hat{z}) \\
&\quad - \frac{\hat{z}^2\ln\hat{z}}{1-\hat{z}} \Big) \frac{Q^2}{q_T^2}\,.
\end{aligned} \tag{7.19}$$

Note that the ratio q_T/Q in the above expressions is fixed by $\hat{x}$ and $\hat{z}$ through the δ-function in (7.4). The $q \to q$ and $q \to g$ coefficients are related by crossing symmetry in the following way:

$$\begin{aligned}
C_{UL}^{\sin\phi_h,q\to g}(\hat{x},\hat{z}) &= -C_{UL}^{\sin\phi_h,q\to q}(\hat{x},1-\hat{z})\,, \\
C_{UL}^{\sin 2\phi_h,q\to g}(\hat{x},\hat{z}) &= C_{UL}^{\sin 2\phi_h,q\to q}(\hat{x},1-\hat{z})\,.
\end{aligned} \tag{7.20}$$

Furthermore, because of charge conjugation and parity invariance the results for the antiquark channels $\bar{q} \to \bar{q}$ and $\bar{q} \to g$ are identical to those for $q \to q$ and $q \to g$, respectively. In addition, we have

$$C_{UL}^{\sin\phi_h, g\to\bar{q}}(\hat{x},\hat{z}) = -C_{UL}^{\sin\phi_h, g\to q}(\hat{x},1-\hat{z})\,,$$
$$C_{UL}^{\sin 2\phi_h, g\to\bar{q}}(\hat{x},\hat{z}) = C_{UL}^{\sin 2\phi_h, g\to q}(\hat{x},1-\hat{z})\,. \tag{7.21}$$

In Ref. [186] we have also derived these results via crossing of the corresponding T-odd asymmetries in e^+e^- annihilation in [181]. Our results given above correct the sign of the results in [186]. For the case of quark-initiated processes, an independent cross check is provided by the SIDIS beam asymmetries A_{LU} calculated in Ref. [174]. Indeed, for the charged-current case considered in these papers, the interaction mediated by W-bosons selects left-handed quarks, so that even if the target is unpolarized, the partonic matrix elements are the same as in our Eq. (7.16), albeit with reversed helicity. For instance, by looking at the functions F_8 and F_9 in Eqs. (3.14) of [181], in the case of quark-initiated diagrams, one can verify that they correspond to our $C_{UL}^{\sin\phi_h}$ and $C_{UL}^{\sin 2\phi_h}$ functions with a reversed sign. Clearly, this reasoning does not allow comparisons in the case of incoming gluons.

As we mentioned in the Introduction, there are interesting connections of our work to the recent study [185] on a two-loop perturbative mechanism for the single-transverse SIDIS spin asymmetry A_{UT} involving the structure function g_T. A well-known feature of g_T is that its Wandzura-Wilczek [227] part is proportional to an integral over the quark and gluon helicity parton distributions. This part of the calculation of [185] therefore involves hard-scattering cross sections with definite helicities of the incoming partons. Remarkably, these turn out to be the same as the ones we have presented above (apart, of course, from normalization which is necessarily different for A_{UL} and A_{UT}). This feature deserves further investigation in the future.

7.5 LOW-q_T LIMIT

As discussed in the Introduction, it is interesting to expand the above results for the structure functions for low values of q_T/Q, in order to make contact with results

predicted by the TMD formalism. When $q_T^2/Q^2 \to 0$ we can expand the delta condition in (7.4) as described, for example, in [228–230]:

$$\frac{1}{\hat{x}\hat{z}}\,\delta\left(\frac{q_T^2}{Q^2}-\frac{(1-\hat{x})(1-\hat{z})}{\hat{x}\hat{z}}\right)=\delta(1-\hat{z})\delta(1-\hat{x})\ln\left(\frac{Q^2}{q_T^2}\right)+\frac{\delta(1-\hat{z})}{(1-\hat{x})_+}+\frac{\delta(1-\hat{x})}{(1-\hat{z})_+}+\mathcal{O}\left(\frac{q_T^2}{Q^2}\right). \tag{7.22}$$

Here the "plus" distribution is defined in the usual way upon integration with a regular function as in (3.17). To simplify notation, we write the double convolution integral as (we omit the scale dependence of the parton distributions and fragmentation functions here):

$$\left(\Delta f\otimes\mathcal{C}\otimes D\right)(x,z)\equiv\int_x^1\frac{d\hat{x}}{\hat{x}}\int_z^1\frac{d\hat{z}}{\hat{z}}\delta\left(\frac{q_T^2}{Q^2}-\frac{(1-\hat{x})(1-\hat{z})}{\hat{x}\hat{z}}\right)\Delta f\left(\frac{x}{\hat{x}}\right)\mathcal{C}(\hat{x},\hat{z})D\left(\frac{z}{\hat{z}}\right). \tag{7.23}$$

From the $\sin(\phi_h)$ terms in (7.18) we then find the following contribution to the $q\to q$ coefficient at low q_T/Q:

$$\begin{aligned}\left(\Delta f_q\otimes C_{UL}^{\sin\phi_h,q\to q}\otimes D_q^h\right)(x,z)&\\ =e_q^2\frac{Q}{q_T}\frac{C_A}{2}\Bigg\{&-C_F\left(2\ln\left(\frac{q_T^2}{Q^2}\right)+3\right)\Delta f_q(x)\,D_q^h(z)\\ &+D_q^h(z)\int_x^1 d\hat{x}\,\delta P_{qq}(\hat{x})\,\Delta f_q\left(\frac{x}{\hat{x}}\right)+\Delta f_q(x)\int_z^1 d\hat{z}\,\delta P_{qq}(\hat{z})\,D_q^h\left(\frac{z}{\hat{z}}\right)\Bigg\}\\ &-e_q^2\frac{Q}{q_T}\frac{C_F}{C_A}\Delta f_q(x)\int_z^1 d\hat{z}\,\frac{\hat{z}}{1-\hat{z}}\left(1+\frac{\ln\hat{z}}{1-\hat{z}}\right)D_q^h\left(\frac{z}{\hat{z}}\right),\end{aligned} \tag{7.24}$$

where

$$\delta P_{qq}(x)\equiv C_F\left[\frac{2x}{(1-x)_+}+\frac{3}{2}\delta(1-x)\right] \tag{7.25}$$

is the LO splitting function for the scale evolution of the transversity distributions. In the $q\to g$ channel we obtain

$$\begin{aligned}&\left(\Delta f_q\otimes C_{UL}^{\sin\phi_h,q\to g}\otimes D_g^h\right)(x,z)\\ &\quad=e_q^2\frac{Q}{q_T}C_F\,\Delta f_q(x)\int_z^1 d\hat{z}\,\frac{1-\hat{z}}{\hat{z}^2}\left((C_A-2C_F)\ln(1-\hat{z})-2C_F\hat{z}\right)D_g^h\left(\frac{z}{\hat{z}}\right).\end{aligned} \tag{7.26}$$

For the process $\gamma^* g \to q\bar{q}$ the coefficient function diverges logarithmically for $\hat{z} \to 1$. In addition to the expansion (7.22) we therefore also need

$$\frac{\ln(1-\hat{z})}{\hat{x}\hat{z}}\,\delta\left(\frac{q_T^2}{Q^2}-\frac{(1-\hat{x})(1-\hat{z})}{\hat{x}\hat{z}}\right) = -\frac{1}{2}\ln^2\left(\frac{Q^2}{q_T^2}\right)\delta(1-\hat{x})\delta(1-\hat{z}) - \frac{\delta(1-\hat{z})}{(1-\hat{x})_+}\ln\left(\frac{Q^2}{q_T^2}\right) + \delta(1-\hat{x})\left(\frac{\ln(1-\hat{z})}{1-\hat{z}}\right)_+ - \delta(1-\hat{z})\left(\left(\frac{\ln(1-\hat{x})}{1-\hat{x}}\right)_+ - \frac{\ln\hat{x}}{1-\hat{x}}\right). \quad (7.27)$$

Details of the derivation of this equation are given in Appendix C.1. We then find

$$\begin{aligned}&\left(\Delta f_g \otimes C_{UL}^{\sin\phi_h, g\to q} \otimes D_q^h\right)(x,z)\big] \\ &= \frac{e_q^2}{2}\frac{Q}{q_T}(C_A - 2C_F)D_q^h(z)\int_x^1 d\hat{x}\,\Delta f_g\left(\frac{x}{\hat{x}}\right)\left[(1-\hat{x})\ln\left(\frac{Q^2}{q_T^2}\right)\right. \\ &\qquad \left. +(1-\hat{x})\ln\left(\frac{1-\hat{x}}{\hat{x}}\right) - 1\right]. \end{aligned} \quad (7.28)$$

The results in Eqs. (7.24),(7.26),(7.28) are valid up to terms of order q_T/Q. Keeping in mind the overall factor $1/Q^2$ in Eq. (7.4), we see that the structure function $F_{UL}^{\sin\phi_h}$ is predicted to have the leading power

$$F_{UL}^{\sin\phi_h} \propto \frac{1}{Qq_T} + \mathcal{O}\left(\frac{1}{Q^2}\right) \quad (7.29)$$

at low q_T, modulo logarithms. The behavior found for $\gamma^* q \to qg$ in Eq. (7.24) is particularly interesting. The term $-C_F(2\ln(q_T^2/Q^2)+3)$ is the well-known first-order contribution to the Sudakov form factor. The next two terms both contain the LO transversity splitting function δP_{qq}, convoluted with either the helicity parton distribution or the fragmentation function. A generic low-q_T structure with the Sudakov form factor and splitting functions is familiar from the spin-averaged case (see Ref. [230]). However, the appearance of the transversity splitting function in combination with Δf_q or D_q^h, and along with an overall factor C_A, is quite remarkable. This feature must be related to the fact that in the TMD framework the leading part of $A_{UL}^{\sin\phi_h}$ receives contributions from the T-even function h_L, which is twist-three and describes the distribution of transversely polarized quarks in a longitudinally polarized hadron, convoluted with the Collins function probing the fragmentation of transversely polarized quarks [200]. The last term in (7.24) and the results in Eqs. (7.26),(7.28) do not appear to have a straightforward structure. Another striking feature is the appearance of a logarithm of q_T/Q in the result for the

$g \to q$ channel in Eq. (7.28): such logarithms do not usually appear in off-diagonal contributions at lowest order.

Similarly, we can consider the low-q_T/Q limit for the $\sin(2\phi_h)$ terms. Here we find for the $q \to q$ channel:

$$\begin{aligned}
&\left(\Delta f_q \otimes C_{UL}^{\sin 2\phi_h, q\to q} \otimes D_q^h\right)(x,z) \\
&= -e_q^2 \frac{3}{4} C_A \left\{ -C_F \left(2 \ln\left(\frac{q_T^2}{Q^2}\right) + 3\right) \Delta f_q(x)\, D_q^h(z) \ln\left(\frac{q_T^2}{Q^2}\right) \right. \\
&\left. + D_q^h(z) \int_x^1 d\hat{x}\, \delta P_{qq}(\hat{x})\, \Delta f_q\left(\frac{x}{\hat{x}}\right) + \Delta f_q(x) \int_z^1 d\hat{z}\, \delta P_{qq}(\hat{z}) D_q^h\left(\frac{z}{\hat{z}}\right) \right\} \\
&+ \frac{C_F}{2C_A} \Delta f_q(x) \int_z^1 d\hat{z}\, \frac{\hat{z}}{(1-\hat{z})^2} \left(1 - 3\hat{z} - 2(2\hat{z}-1)\frac{\ln \hat{z}}{1-\hat{z}}\right) D_q^h\left(\frac{z}{\hat{z}}\right) . \qquad (7.30)
\end{aligned}$$

Apart from normalization, the first three terms are identical to the corresponding ones in Eq. (7.24). We note that, despite first appearances, the integrand of the last term is regular as $\hat{z} \to 1$.

In the $q \to g$ channel we have

$$\begin{aligned}
&\left(\Delta f_q \otimes C_{UL}^{\sin 2\phi_h, q\to g} \otimes D_g^h\right)(x,z) = -e_q^2 C_F \Delta f_q(x) \\
&\times \int_z^1 \frac{d\hat{z}}{\hat{z}} \left((C_A - 2C_F) \frac{(1-2\hat{z})\ln(1-\hat{z})}{\hat{z}} + (C_A - (2-3\hat{z})C_F) \right) D_g^h\left(\frac{z}{\hat{z}}\right) . \qquad (7.31)
\end{aligned}$$

For the channel $\gamma^* g \to q\bar{q}$ we again need the expansion (7.27) and obtain

$$\begin{aligned}
\left(\Delta f_g \otimes C_{UL}^{\sin 2\phi_h, g\to q} \otimes D_q^h\right)(x,z) = \frac{e_q^2}{2} (C_A - 2C_F) D_q^h(z) \\
\int_x^1 d\hat{x}\, \Delta f_g\left(\frac{x}{\hat{x}}\right) \hat{x} \left[\ln\left(\frac{Q^2}{q_T^2}\right) + \ln\left(\frac{1-\hat{x}}{\hat{x}}\right) + \frac{3}{2} \right] . \qquad (7.32)
\end{aligned}$$

The results in Eqs. (7.31),(7.32) receive corrections of order q_T^2/Q^2, so that

$$F_{UL}^{\sin 2\phi_h} \propto \frac{1}{Q^2} + \mathcal{O}\left(\frac{q_T^2}{Q^4}\right) , \qquad (7.33)$$

again up to logarithms.

Our low-q_T expansions fill two of the gaps reported in Table 2 of Ref. [26] providing the missing perturbative expressions for the ϕ_h-dependent T-odd cross sections. From the point of view of TMD factorization, they correspond to the leading part

of the "high-q_T calculation". As discussed in [26], the TMD framework predicts the same behavior $\propto 1/(Qq_T)$ of the $\sin(\phi_h)$ terms as we find in Eq. (7.29). In this sense the TMD calculation matches the collinear one. At this point, however, one cannot decide whether this matching is really quantitative in the sense that not just the overall power counting matches, but also the full combination of hard-scattering coefficients, parton distributions and fragmentation functions. Currently, despite enormous progress in recent years [211–220], the high-transverse-momentum tails of TMDs are not understood at a sufficient level to obtain definitive results for A_{UL}, especially in the case of the fragmentation correlators. Clearly, it will be very interesting to explore this issue more deeply in the future, also in the light of TMD factorization theorems extending beyond leading twist proposed recently [217, 219].

For the $\sin(2\phi_h)$ terms, we find in Eq. (7.33) that the perturbative structure function becomes constant at low q_T. Including the factors of the strong coupling, $F_{UL}^{\sin 2\phi_h}$ behaves in total as α_s^2/Q^2. This result is not in accordance with the TMD prediction [26] that the high-q_T tail of this structure function should behave as α_s/q_T^4. In the TMD framework, $F_{UL}^{\sin 2\phi_h}$ is leading twist, being a convolution of the longitudinal worm-gear functions with Collins functions [200]. As one can see, even the powers of the strong coupling differ between the TMD prediction and our perturbative result.

In the context of this discussion, it is also interesting to recall the corresponding results for the T-odd beam spin asymmetry A_{LU} [180, 181], for which the initial lepton is polarized. The relevant results are given in Appendix C.2. Interestingly, at low q_T, the same features as described above for A_{UL} are encountered.

7.6 PHENOMENOLOGICAL RESULTS

We now present some simple phenomenology of the T-odd effects in SIDIS with longitudinally polarized protons. We will not carry out any full-fledged study; rather, we wish to explore the overall size of the $\sin\phi_h$ and $\sin(2\phi_h)$ modulations.

The quantities of interest in polarization experiments are typically spin asymmetries. In the present case, the longitudinal proton helicity single spin asymmetry in SIDIS is defined as

$$A_{UL}(\phi_h) \equiv \frac{d\sigma_+^h(\phi_h) - d\sigma_-^h(\phi_h)}{d\sigma_+^h(\phi_h) + d\sigma_-^h(\phi_h)}, \tag{7.34}$$

where as in Sec. 7.2 $d\sigma_\pm^h$ represents the (differential) cross section for positive (negative) proton helicity. The denominator of the asymmetry is just twice the spin-averaged cross section as a function of the azimuthal angle ϕ_h. As is well

known [200, 228], this cross section has a ϕ_h independent piece as well as terms proportional to $\cos(\phi_h)$ and $\cos(2\phi_h)$. Dividing numerator and denominator by the ϕ_h independent term, we may write

$$A_{UL}(\phi_h) = \frac{A_{UL}^{\sin\phi_h}\sin\phi_h + A_{UL}^{\sin 2\phi_h}\sin 2\phi_h}{1 + A_{UU}^{\cos\phi_h}\cos\phi_h + A_{UU}^{\cos 2\phi_h}\cos 2\phi_h}\,. \tag{7.35}$$

The various angular modulations $A_{UL}^{\sin\phi_h}$ etc. are also known as analyzing powers. The ones of interest to us here, $A_{UL}^{\sin\phi_h}$ and $A_{UL}^{\sin 2\phi_h}$, may be extracted from the full cross section as follows:

$$A_{UL}^{\sin n\phi_h} = \frac{\int_0^{2\pi} d\phi_h \sin(n\phi_h)\left[d\sigma_+^h(\phi_h) - d\sigma_-^h(\phi_h)\right]}{\frac{1}{2}\int_0^{2\pi} d\phi_h \left[d\sigma_+^h(\phi_h) + d\sigma_-^h(\phi_h)\right]} \qquad (n = 1, 2)\,. \tag{7.36}$$

In this way, the terms with $\cos(\phi_h)$ and $\cos(2\phi_h)$ in the spin-averaged cross section do not contribute. Experimental data are commonly reported in terms of the $A_{UL}^{\sin n\phi_h}$, and accordingly these are the quantities that we will consider for our numerical predictions.

As stated earlier, in the present Chapter we restrict ourselves to LO predictions for the T-odd terms, keeping the leading contribution $\propto \alpha_s^2$ in the numerator. For consistency, we therefore also need to use only the LO term in the denominator, which is only of order α_s and is easily computed [222]. (We note that the NLO corrections for the spin-averaged cross section in the denominator are available [231–233].) Because of this mismatch of perturbative orders in the numerator and denominator, the analyzing powers $A_{UL}^{\sin\phi_h}, A_{UL}^{\sin 2\phi_h}$ are themselves of order α_s, which is in contrast to most other spin asymmetries for which the leading power of α_s cancels. We therefore expect $A_{UL}^{\sin\phi_h}, A_{UL}^{\sin 2\phi_h}$ to be quite sensitive to the choice of scale and to higher-order corrections.

For our numerical studies we use the DSSV [17, 18] set for the helicity parton distributions and the DSS14 [160] set of fragmentation functions. We note that only pion fragmentation is considered in this set. We set the renormalization and factorization scales equal to Q. For the denominator of the asymmetries we use the NNPDF31 [234] set of unpolarized parton distributions. We call this set from the LHAPDF library [235].

We start by presenting estimates for the future Electron-Ion Collider (EIC) with a center-of-mass energy of 140 GeV. At this fairly high energy, the $\sin\phi_h$ and $\sin(2\phi_h)$ modulations are overall quite strongly suppressed. The reason is that at high energies rather low momentum fractions in the parton distribution functions are probed, where the polarized distributions are much smaller than the unpolarized ones. The left part of Fig. 22 shows x-dependence of the analyzing powers

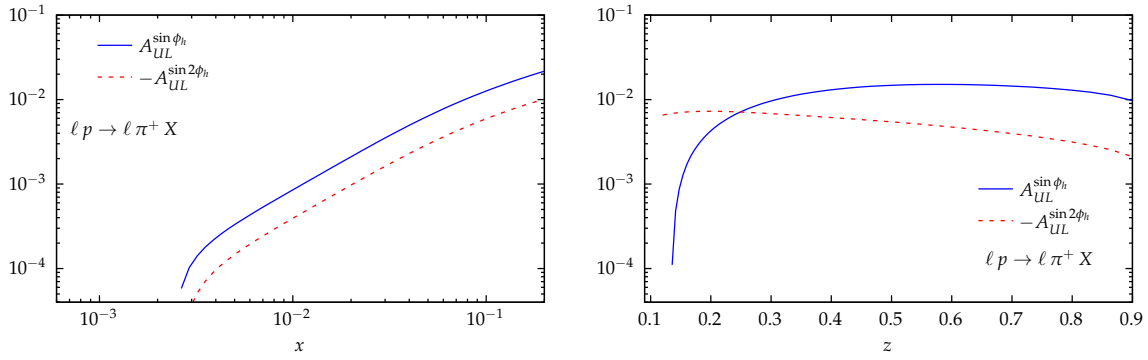

Figure 22: Left: x-dependence and Right: z-dependence of the analyzing powers for $\ell p \to \ell\, \pi^+ X$ at the future EIC. The $\sin(2\phi_h)$ analyzing power has been multiplied by (-1). For the left graph, $z = 0.4$, while for the right graph $x = 0.1$. In both cases we use $\sqrt{s} = 140$ GeV, $Q^2 = 50$ GeV^2 and $P_{h\perp} = 2$ GeV.

$A_{UL}^{\sin\phi_h}$ (blue solid line) and $-A_{UL}^{\sin 2\phi_h}$ (red dashed line) for π^+ production, at a set of fixed values of z, Q^2 and $P_{h\perp}$. These values have been chosen by considering the "projected EIC data" shown in Ref. [163]. We observe that the asymmetries indeed rapidly decrease toward low values of x. The right part of the figure shows the z-dependence of the asymmetries, which is much more moderate through most of the range considered.

In the following we show results integrated over large bins in z and Q^2, but differential in $P_{h\perp}$ and x. To this end, we define

$$A_{UL,\mathrm{int}}^{\sin n\phi_h} \equiv \frac{\int_{z_{\min}}^{z_{\max}} dz \int_{Q^2_{\min}}^{Q^2_{\max}} dQ^2 \int_0^{2\pi} d\phi_h \sin(n\phi_h)\left[d\sigma^+(\phi_h) - d\sigma^-(\phi_h)\right]}{\frac{1}{2}\int_{z_{\min}}^{z_{\max}} dz \int_{Q^2_{\min}}^{Q^2_{\max}} dQ^2 \int_0^{2\pi} d\phi_h \left[d\sigma^+(\phi_h) + d\sigma^-(\phi_h)\right]} \quad (n = 1, 2)\,. \tag{7.37}$$

Figure 23 shows $A_{UL,\mathrm{int}}^{\sin\phi_h}$ and $A_{UL,\mathrm{int}}^{\sin 2\phi_h}$ as functions of $P_{h\perp}$ at the EIC, for fixed values $x = 0.1$ (blue solid) and $x = 0.01$ (red dashed), for production of positive and negative pions. As expected for an $\mathcal{O}(\alpha_s)$ effect, and because of the suppression of the polarized parton distributions already mentioned, the asymmetries are quite small, especially for $x = 0.01$. Also, $A_{UL,\mathrm{int}}^{\sin 2\phi_h}$ is generally smaller than $A_{UL,\mathrm{int}}^{\sin\phi_h}$ because of its stronger suppression at low q_T/Q discussed in the previous section. We also observe that the asymmetries for positively and negatively charged pions tend to have opposite signs, which is due to the dominance of the (positive) up-quark helicity parton distribution for π^+ production, and of the (negative) down-quark helicity distribution in case of π^-. We note that detailed studies of the uncertainties to be expected for such measurements at the EIC will evidently require a full analysis that also incorporates efficiencies and detector effects, which is beyond the scope of this Chapter. A ballpark estimate based on the spin-averaged SIDIS rates expected

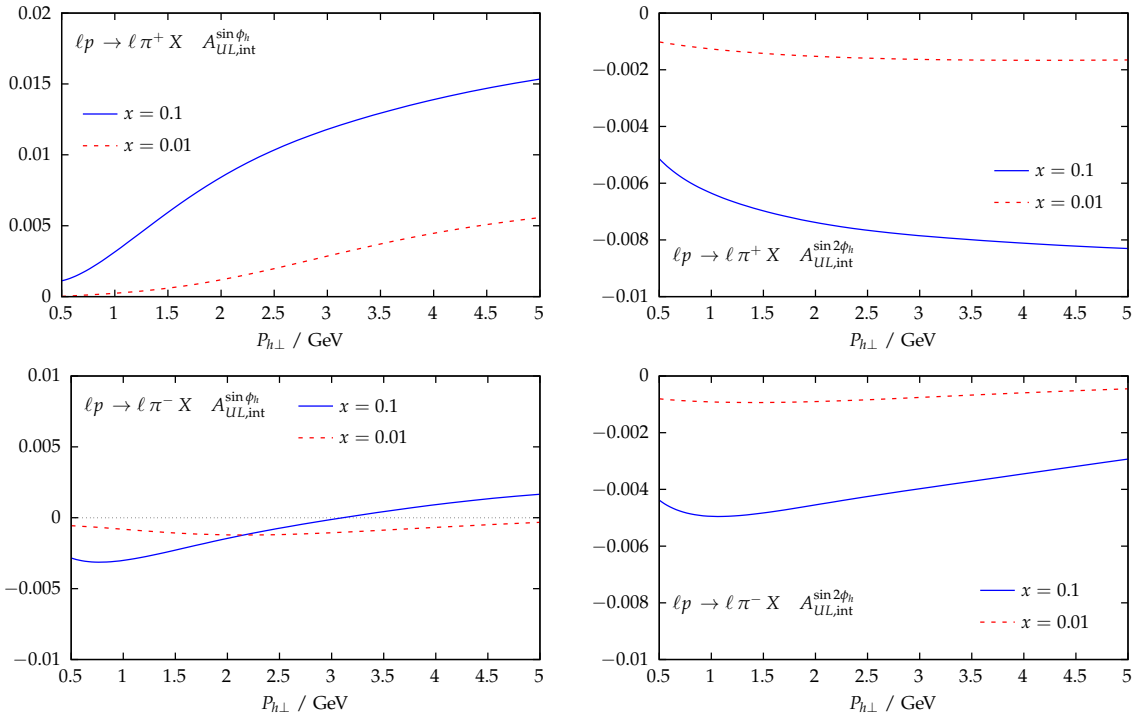

Figure 23: T-odd asymmetries as functions of $P_{h\perp}$ for $x = 0.1$ and $x = 0.01$ for $\ell p \to \ell \pi^+ X$ and $\ell p \to \ell \pi^- X$ at the EIC. We have integrated the cross sections over $Q^2/(\text{GeV})^2 \in [10, 100]$ for $x = 0.1$ (blue solid) and $Q^2/(\text{GeV})^2 \in [2, 10]$ for $x = 0.01$ (red dashed), and in both cases over $z \in [0.05, 0.8]$.

at the EIC (as reported in [163]) provides confidence that even asymmetries of the small size as in Fig. 23 should be resolvable at the EIC.

We proceed by presenting a comparison to data from COMPASS [196] where the asymmetry A_{UL} has been measured in muon scattering off longitudinally polarized deuterons at $\sqrt{s} = 17.4$ GeV. Such a comparison is of course somewhat precarious as the hadron transverse momenta accessed in the COMPASS SIDIS data are typically below 1 GeV. Even though Q^2 extends to values well in the perturbative regime and $q_T = P_{h\perp}/z$ is typically significantly larger than 1 GeV, it is clear that the use of perturbation theory is questionable. Arguably a TMD description would appear to be more appropriate here. Related to this, for a valid perturbative description, one should address the Sudakov logarithms we have found at low q_T (see Sec. 7.5) and resum them to all orders of perturbation theory. Such an analysis is presently not possible since the evolution of all TMD functions contributing to A_{UL} is not yet available. In any case, our main interest here is to explore the rough size of the perturbative predictions for A_{UL} and to see whether there is broad consistency with the experimental data.

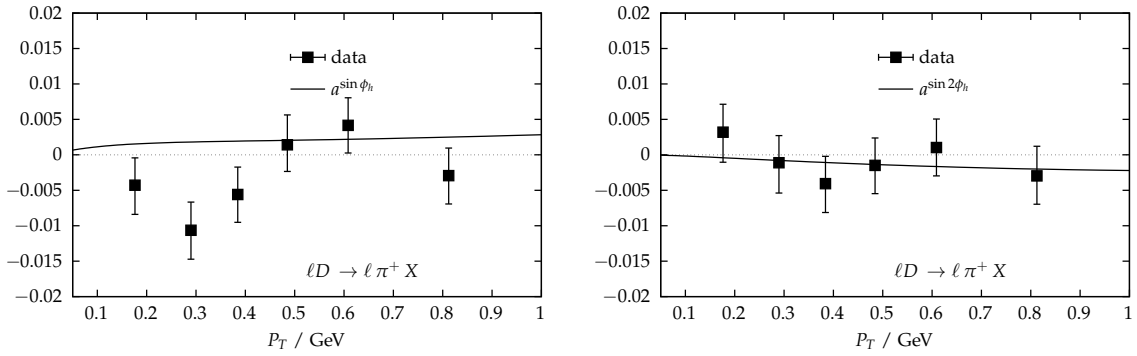

Figure 24: Comparison of our numerical estimates for $A_{UL}^{\sin\phi_h}$ and $A_{UL}^{\sin 2\phi_h}$ with data from the COMPASS collaboration [196] in hadron production off longitudinally polarized deuterons at $\sqrt{s} = 17.4$ GeV. We show the $P_{h\perp}$ distribution of the asymmetry integrated over $x \in [0.004, 0.7]$, $z \in [0.01, 1]$ and $Q^2/(\text{GeV})^2 \in [1, 100]$.

We note that COMPASS has considered the production of arbitrary charged hadrons. Sets of fragmentation functions for $h^\pm$ are not available in DSS14, so we continue to use the pion fragmentation functions. Given that pions dominate the spectrum of produced hadrons and that fragmentation effects cancel to some extent in the spin asymmetry, this should be more than sufficient for a first comparison. We consider the π^+-channel: $\mu d \to \mu\,\pi^+\,X$. As in [196] we integrate over $x \in [0.004, 0.7]$, $z \in [0.01, 1]$ and $Q^2/(\text{GeV})^2 \in [1, 100]$ and divide by the value $|P_L| = 0.8$ of the muon beam polarization. Figure 24 shows the comparisons both for $A_{UL}^{\sin\phi_h}$ and for $A_{UL}^{\sin 2\phi_h}$. We observe reasonable agreement, given the rather large uncertainties of the data, and keeping in mind that the $P_{h\perp}$ values are such that a TMD description would appear to be more appropriate, as discussed above.

We finally also show a comparison to data from the HERMES experiment [189, 192] taken for $\pi^\pm$ production at $\sqrt{s} = 7.25$ GeV. As we discussed in Sec. 7.2, in an actual experiment the target is polarized along (or opposite to) the lepton beam direction. This means that the measured asymmetry A_{UL} receives contributions from both the longitudinal and transverse spin asymmetries with respect to the direction of the virtual photon [192, 221], so that $A_{UL}(l) \neq A_{UL}(q)$ (where the arguments l and q denote target polarization defined relative to the lepton or photon direction, respectively). For HERMES with its relatively modest Q^2 values, the difference between $A_{UL}(l)$ and $A_{UL}(q)$ – which is of subleading twist – is expected to be potentially more pronounced. Combining with data taken with a transversely polarized target, HERMES has in fact been able to provide an extraction of $A_{UL}(q)$ [192]. Figure 25 shows both sets of HERMES data, $A_{UL}^{\sin\phi_h}(l)$ and $A_{UL}^{\sin\phi_h}(q)$, compared to our calculations of $A_{UL}^{\sin\phi_h}(q)$. We show the comparisons as functions of x and z, using the mean values of x, z, Q^2 and $P_{h\perp}$ for each point reported in Table 1 of [192]. One can see that for positively charged pions the differences between $A_{UL}^{\sin\phi_h}(l)$ and

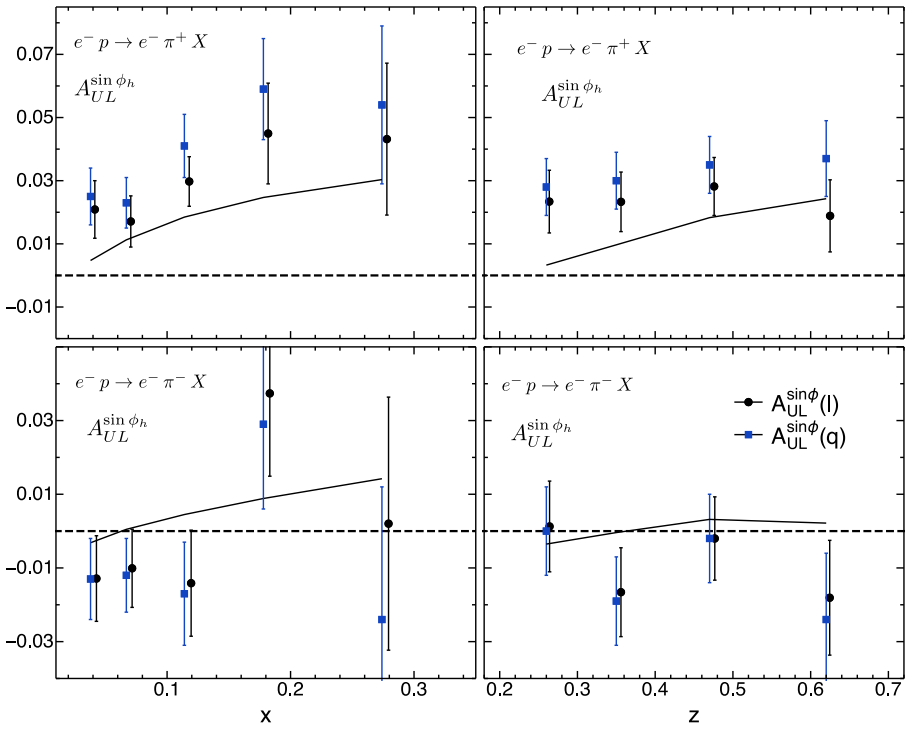

Figure 25: Comparison of our calculations of $A_{UL}^{\sin\phi_h}$ with data from the HERMES collaboration [192] in $\pi^{\pm}$ production off longitudinally polarized protons, as functions of x (left) and z (right). $A_{UL}^{\sin\phi_h}(l)$ and $A_{UL}^{\sin\phi_h}(q)$ represent the asymmetries for target polarization defined relative to the lepton or photon direction, respectively, taken from [187].

$A_{UL}^{\sin\phi_h}(q)$ are quite large, while they are small for π^- production. We also notice that our calculations reproduce the trend of the data rather well overall, despite the fact that HERMES accessed only rather small transverse momenta.

HERMES data for the $\sin 2\phi_h$ asymmetry are available only without correction for the polarization direction [189]. The right part of Fig. 26 shows the data for $A_{UL}^{\sin 2\phi_h}(l)$ for π^+ production, compared to our calculations. Here we have used the mean values of x and Q^2 for each point as given in [189], while adopting $\langle z \rangle$ and $\langle P_{h\perp} \rangle$ from [192]. To facilitate comparison with the $\sin\phi_h$ asymmetry, we show the corresponding results for $A_{UL}^{\sin\phi_h}$ on the left side of Fig. 26. As before, the $\sin 2\phi_h$ asymmetry is smaller. Our calculations are overall in fair agreement with the data for both asymmetries; in particular, they nicely capture the difference in magnitude between the $\sin\phi_h$ and $\sin 2\phi_h$ components. The situation thus appears to be different from that for the $\cos 2\phi_h$ unpolarized structure function $F_{UU}^{\cos 2\phi_h}$ analyzed in [236], for which the perturbative $\mathcal{O}(\alpha_s)$ prediction for HERMES kinematics was shown to be negligible compared to higher-twist effects. It should be stressed again,

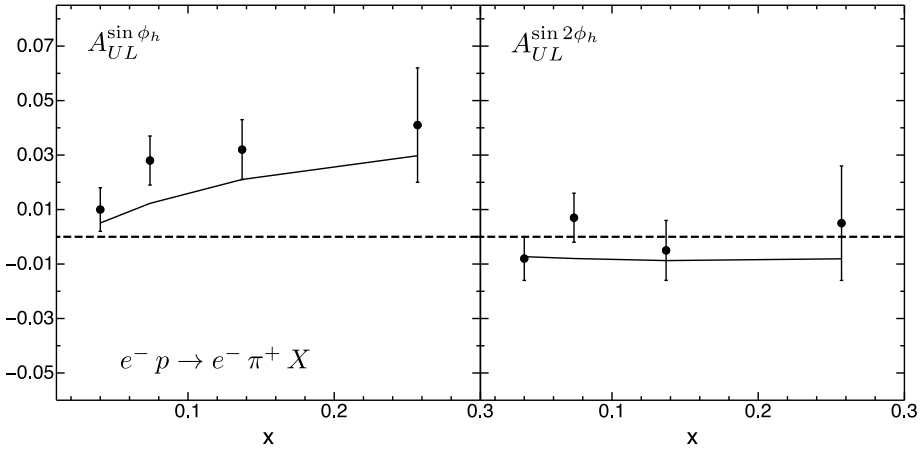

Figure 26: Numerical results for $A_{UL}^{\sin\phi_h}$ and $A_{UL}^{\sin 2\phi_h}$ compared to HERMES data [189] for π^+ production off longitudinally polarized protons. The data have not been corrected for the polarization direction, taken from [187].

however, that the data shown in Fig. 26 have not been corrected for the polarization direction, and according to Fig. 25 such correction effects are expected to be particularly important in the case of π^+ production.

7.7 CONCLUSIONS

We have presented a perturbative calculation for the single-spin asymmetry A_{UL} in semi-inclusive deep-inelastic scattering, which may be measured by scattering unpolarized leptons off longitudinally polarized nucleons. This asymmetry is interesting because, in the absence of parity violation, it is T-odd and receives perturbative contributions only via QCD loop effects. Also, it is sensitive to the proton's helicity parton distributions, despite the fact that it is measured with an unpolarized lepton beam. Our calculation builds on the large body of previous work on T-odd effects in hard scattering, opening a new avenue for future measurements at the EIC.

We have provided compact expressions for the T-odd contributions in the various partonic channels. We have used these to derive the low-transverse-momentum behavior of the T-odd terms, which shows striking features. Our results add new information on the relations between TMDs and perturbative hard scattering which had been missing so far. They may be used for comparisons to detailed quantitative predictions to be obtained in the future within the TMD formalism.

Our phenomenological calculations reveal the expected relatively small size of the T-odd asymmetries. We have made predictions for the asymmetries at the future electron-ion-collider, where it should be possible to explore them. Our results are also broadly consistent with available COMPASS and HERMES data, although the applicability of a purely hard-scattering picture is questionable here. All in all we hope that this Chapter will contribute to the long-standing quest to establish and understand T-odd effects in QCD.

A

APPENDIX

Here we show the QCD Feynman rules in the covariant gauge, [237, 238].

$$= \frac{i\delta^{ab}}{q^2+i\varepsilon}\left(-g^{\mu\nu}+(1-\xi)\frac{q^\mu q^\nu}{q^2+i\varepsilon}\right)$$

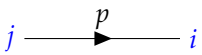

$$= i\delta^{ij}\frac{\not{p}+m}{p^2-m^2+i\varepsilon}$$

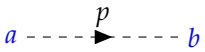

$$= \frac{i\delta^{ab}}{p^2+i\varepsilon}$$

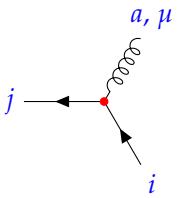

$$= -ig\gamma^\mu[T^a]_{ij}$$

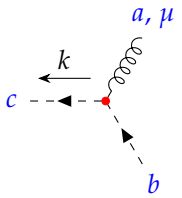

$$= -gf^{abc}k^\mu$$

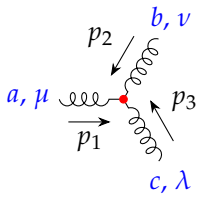

$$= -gf^{abc}\left[g^{\mu\nu}(p_1-p_2)^\lambda+g^{\nu\lambda}(p_2-p_3)^\mu+g^{\lambda\mu}(p_3-p_1)^\nu\right]$$

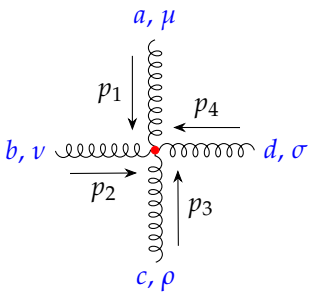

$$= ig^2\left\{\begin{array}{l} f^{eab}f^{ecd}\left(g^{\mu\rho}g^{\nu\sigma}-g^{\mu\sigma}g^{\nu\rho}\right) \\ \quad +f^{eac}f^{edb}\left(g^{\mu\sigma}g^{\rho\nu}-g^{\mu\nu}g^{\rho\sigma}\right) \\ \quad\quad +f^{ead}f^{ebc}\left(g^{\mu\nu}g^{\sigma\rho}-g^{\mu\rho}g^{\sigma\nu}\right) \end{array}\right.$$

B

APPENDIX

B.1 COEFFICIENTS FOR RESUMMATION

In the expansion of the running strong coupling (2.23) we use the following coefficients [31, 32]

$$
\begin{aligned}
b_0 &= \frac{1}{12\pi}\left(11C_A - 2N_f\right) , \qquad b_1 = \frac{1}{24\pi^2}\left(17C_A^2 - 5C_A N_f - 3C_F N_f\right) , \\
b_2 &= \frac{1}{64\pi^3}\left(\frac{2857}{54}C_A^3 - \frac{1415}{54}C_A^2 N_f - \frac{205}{18}C_A C_F N_f + C_F^2 N_f + \frac{79}{54}C_A N_f^2 + \frac{11}{9}C_F N_f^2\right) , \\
b_3 &= \frac{1}{256\pi^4}\left[\left(\frac{149753}{6} + 3564\zeta(3)\right) - \left(\frac{1078361}{162} + \frac{6508}{27}\zeta(3)\right) N_f \right. \\
&\quad \left. + \left(\frac{50065}{162} + \frac{6472}{81}\zeta(3)\right) N_f^2 + \frac{1093}{729}N_f^3\right] ,
\end{aligned}
\tag{B.1}
$$

with N_f the number of flavors and

$$
C_F = \frac{N_c^2 - 1}{2N_c} = \frac{4}{3} , \quad C_A = N_c = 3 . \tag{B.2}
$$

For the b_3 coefficient we have inserted the values of C_F, C_A; the full expression can be found in [239].

The functions A_q, $\widehat{D}$ and $\widehat{B}$ appearing in Eqs. (4.29) & (4.59) are perturbative series in the strong coupling

$$
\begin{aligned}
A_q(\alpha_s) &= \frac{\alpha_s}{\pi}A_q^{(1)} + \left(\frac{\alpha_s}{\pi}\right)^2 A_q^{(2)} + \left(\frac{\alpha_s}{\pi}\right)^3 A_q^{(3)} + \mathcal{O}(\alpha_s^4) \\
\widehat{D}_q(\alpha_s) &= \left(\frac{\alpha_s}{\pi}\right)^2 \widehat{D}_q^{(2)} + \mathcal{O}(\alpha_s^3) \\
\widehat{B}_q(\alpha_s) &= \frac{\alpha_s}{\pi}\widehat{B}_q^{(1)} + \left(\frac{\alpha_s}{\pi}\right)^2 \widehat{B}_q^{(2)} + \mathcal{O}(\alpha_s^3) .
\end{aligned}
\tag{B.3}
$$

The relevant expansion coefficients for A_q in Eq. (6.11) read [31, 85, 240–245]:

$$A_q^{(1)} = C_F\,, \qquad A_q^{(2)} = \frac{1}{2}\,C_F\left[C_A\left(\frac{67}{18}-\frac{\pi^2}{6}\right)-\frac{5}{9}N_f\right]\,,$$

$$\begin{aligned}A_q^{(3)} = {}& \frac{1}{4}C_F\left[C_A^2\left(\frac{245}{24}-\frac{67}{9}\zeta(2)+\frac{11}{6}\zeta(3)+\frac{11}{5}\zeta(2)^2\right)+C_FN_f\left(-\frac{55}{24}+2\zeta(3)\right)\right.\\ &\left.+C_AN_f\left(-\frac{209}{108}+\frac{10}{9}\zeta(2)-\frac{7}{3}\zeta(3)\right)-\frac{1}{27}N_f^2\right]\end{aligned}$$

$$\begin{aligned}A_q^{(4)} = {}& C_F\left[C_A^3\left(\frac{1309\zeta_3}{432}-\frac{11\pi^2\zeta_3}{144}-\frac{\zeta_3^2}{16}-\frac{451\zeta_5}{288}+\frac{42139}{10368}-\frac{5525\pi^2}{7776}\right.\right.\\ &\left.+\frac{451\pi^4}{5760}-\frac{313\pi^6}{90720}\right)+N_fT_FC_A^2\left(-\frac{361\zeta_3}{54}+\frac{7\pi^2\zeta_3}{36}+\frac{131\zeta_5}{72}-\frac{24137}{10368}+\frac{635\pi^2}{1944}\right.\\ &\left.-\frac{11\pi^4}{2160}\right)+N_fT_FC_FC_A\left(\frac{29\zeta_3}{9}-\frac{\pi^2\zeta_3}{6}+\frac{5\zeta_5}{4}-\frac{17033}{5184}+\frac{55\pi^2}{288}-\frac{11\pi^4}{720}\right)\\ &+N_fT_FC_F^2\left(\frac{37\zeta_3}{24}-\frac{5\zeta_5}{2}+\frac{143}{288}\right)+(N_fT_F)^2C_A\left(\frac{35\zeta_3}{27}-\frac{7\pi^4}{1080}-\frac{19\pi^2}{972}+\frac{923}{5184}\right)\\ &+(N_fT_F)^2C_F\left(-\frac{10\zeta_3}{9}+\frac{\pi^4}{180}+\frac{299}{648}\right)+(N_fT_F)^3\left(-\frac{1}{81}+\frac{2\zeta_3}{27}\right)\Big]\\ &+\frac{d_F^{abcd}d_A^{abcd}}{N_c}\left(\frac{\zeta_3}{6}-\frac{3\zeta_3^2}{2}+\frac{55\zeta_5}{12}-\frac{\pi^2}{12}-\frac{31\pi^6}{7560}\right)\\ &+N_f\frac{d_F^{abcd}d_F^{abcd}}{N_c}\left(\frac{\pi^2}{6}-\frac{\zeta_3}{3}-\frac{5\zeta_5}{3}\right)\,,\end{aligned} \tag{B.4}$$

with

$$\frac{d_F^{abcd}d_A^{abcd}}{N_c^2-1}=\frac{N_c(N_c^2+6)}{48}, \quad \frac{d_F^{abcd}d_F^{abcd}}{N_c^2-1}=\frac{N_c^4-6N_c^2+18}{96N_c^2}, \quad T_F=\frac{1}{2}\,. \tag{B.5}$$

Furthermore for the expansion of the function $\widehat{D}_q$ we have [31, 32, 99, 100, 246],

$$\widehat{D}_q^{(2)} = C_F\left[C_A\left(-\frac{101}{27}+\frac{7}{2}\,\zeta(3)\right)+\frac{14}{27}\,N_f\right]\,,$$

$$\begin{aligned}\widehat{D}_q^{(3)} = {}& C_F\left[C_A^2\left(-\frac{1}{36}11\pi^2\zeta(3)+\frac{1541\zeta(3)}{108}-6\zeta(5)+\frac{11\pi^4}{720}+\frac{799\pi^2}{1944}-\frac{297029}{23328}\right)\right.\\ &+C_AN_f\left(-\frac{113\zeta(3)}{108}+\frac{\pi^4}{360}-\frac{103\pi^2}{1944}+\frac{31313}{11664}\right)+N_f^2\left(-\frac{\zeta(3)}{9}-\frac{58}{729}\right)\\ &\left.+C_FN_f\left(-\frac{19\zeta(3)}{18}-\frac{\pi^4}{180}+\frac{1711}{864}\right)\right]\,.\end{aligned} \tag{B.6}$$

The coefficients for the $\widehat{B}_q$ function are given by using $B_q^{(1)}$ and $B_q^{(2)}$ from [106, 164]

$$\begin{aligned}
\widehat{B}_q^{(1)} &= -\frac{3}{4} C_F \,, \\
\widehat{B}_q^{(2)} &= C_F \left[C_A \left(\frac{5\zeta(3)}{2} + \frac{11\pi^2}{144} - \frac{3155}{864} \right) + N_f \left(\frac{247}{432} - \frac{\pi^2}{72} \right) \right] .
\end{aligned} \tag{B.7}$$

The expansion coefficients for $\widehat{C}_{qq}$ in Eq. (6.9) read [32]

$$\begin{aligned}
\widehat{C}_{qq}^{(1)} &= \frac{\pi^2}{3} A_q^{(1)} \,, \\
\widehat{C}_{qq}^{(2)} &= \frac{\pi^4}{18} \left(A_q^{(1)}\right)^2 + A_q^{(1)} \pi b_0 \left(\frac{\pi^2}{3} \ln \frac{\mu_R^2}{Q^2} + \frac{8}{3}\zeta(3) \right) + \frac{\pi^2}{3} A_q^{(2)} \,, \\
\widehat{C}_{qq}^{(3)} &= \frac{\pi^6}{162} \left(A_q^{(1)}\right)^3 - \frac{1}{3}\pi^3 b_0 \widehat{D}_q^{(2)} + \frac{1}{9} \left(A_q^{(1)}\right)^2 b_0 \pi^3 \left(\pi^2 \ln \frac{\mu_R^2}{Q^2} + 8\zeta(3) \right) \\
&+ A_q^{(1)} b_1 \left(\frac{\pi^4}{3} \ln \frac{\mu_R^2}{Q^2} + \frac{8\pi^2\zeta(3)}{3} \right) + A_q^{(1)} b_0^2 \left(\frac{\pi^4}{3} \ln^2 \frac{\mu_R^2}{Q^2} + \frac{16}{3}\pi^2\zeta(3) \ln \frac{\mu_R^2}{Q^2} - \frac{\pi^6}{45} \right) \\
&+ \frac{2}{3} A_q^{(2)} \pi b_0 \left(\pi^2 \ln \frac{\mu_R^2}{Q^2} + 8\zeta(3) \right) + \frac{\pi^4}{9} A_q^{(1)} A_q^{(2)} + \frac{\pi^2}{3} A_q^{(3)} \,.
\end{aligned} \tag{B.8}$$

Finally, for H_{qq}^{SIDIS} we find for an arbitrary renormalization scale μ_R, but for $\mu_F = Q$:

$$\begin{aligned}
H_{qq}^{\text{SIDIS},(1)} &= C_F \left(-4 - \frac{\pi^2}{6} \right) , \\
H_{qq}^{\text{SIDIS},(2)} &= C_F^2 \left(-\frac{15\zeta(3)}{4} + \frac{61\pi^2}{48} + \frac{511}{64} - \frac{\pi^4}{60} \right) + C_F N_f \left(\frac{\zeta(3)}{2} + \frac{29\pi^2}{216} + \frac{127}{96} \right) \\
&+ C_F C_A \left(\frac{7\zeta(3)}{4} + \frac{3\pi^4}{80} - \frac{1535}{192} - \frac{403\pi^2}{432} \right) + H_{qq}^{\text{SIDIS},(1)} \, \pi b_0 \ln \frac{\mu_R^2}{Q^2} \,,
\end{aligned} \tag{B.9}$$

and, in Sec. 6.4, the three-loop contribution

$$
\begin{aligned}
H_{qq}^{\mathrm{SIDIS},(3)} = {} & C_F^3 \left(\frac{\zeta(3)^2}{2} + \frac{25\pi^2\zeta(3)}{12} - \frac{115\zeta(3)}{16} + \frac{83\zeta(5)}{4} \right. \\
& \left. + \frac{1937\pi^6}{136080} - \frac{5599}{384} - \frac{181\pi^4}{960} - \frac{4729\pi^2}{1152} \right) \\
& + C_F^2 C_A \left(\frac{37\zeta(3)^2}{12} - \frac{571\pi^2\zeta(3)}{216} - \frac{8653\zeta(3)}{432} - \frac{689\zeta(5)}{72} \right. \\
& \left. + \frac{2603\pi^4}{38880} + \frac{93581\pi^2}{10368} + \frac{74321}{2304} - \frac{227\pi^6}{17010} \right) \\
& + C_F C_A^2 \left(-\frac{25\zeta(3)^2}{12} + \frac{571\pi^2\zeta(3)}{288} + \frac{82385\zeta(3)}{5184} - \frac{51\zeta(5)}{16} \right. \\
& \left. + \frac{41071\pi^4}{311040} - \frac{51967\pi^2}{10368} - \frac{125\pi^6}{27216} - \frac{1505881}{62208} \right) \\
& + C_F^2 N_f \left(-\frac{1}{27}7\pi^2\zeta(3) + \frac{869\zeta(3)}{216} - \frac{19\zeta(5)}{18} - \frac{421}{192} - \frac{1363\pi^2}{1296} - \frac{157\pi^4}{4860} \right) \\
& + C_F C_A N_f \left(-\frac{1}{72}5\pi^2\zeta(3) - \frac{94\zeta(3)}{81} - \frac{\zeta(5)}{8} + \frac{10595\pi^2}{7776} + \frac{110651}{15552} \right. \\
& \left. - \frac{1259\pi^4}{77760} \right) + C_F N_f^2 \left(-\frac{79\zeta(3)}{324} - \frac{\pi^4}{3888} - \frac{307\pi^2}{3888} - \frac{7081}{15552} \right) \\
& + C_F N_{f,V} \left(\frac{C_A^2 - 4}{C_A} \right) \left(\frac{7\zeta(3)}{48} - \frac{5\zeta(5)}{6} + \frac{5\pi^2}{96} + \frac{1}{8} - \frac{\pi^4}{2880} \right) \\
& + \left[C_F C_A \left(\frac{7\zeta(3)}{2} + \frac{3\pi^4}{40} - \frac{1535}{96} - \frac{403\pi^2}{216} \right) + C_F N_f \left(\zeta(3) + \frac{29\pi^2}{108} \right. \right. \\
& \left. + \frac{127}{48} \right) + C_F C_A N_f \left(\frac{\zeta(3)}{3} + \frac{767\pi^2}{1296} - \frac{\pi^4}{80} + \frac{853}{144} \right) \\
& \left. + C_F^2 \left(-\frac{15\zeta(3)}{2} + \frac{61\pi^2}{24} - \frac{\pi^4}{30} + \frac{511}{32} \right) \right] \pi b_0 \ln \frac{\mu_R^2}{Q^2} \\
& + C_F \left(-4 - \frac{\pi^2}{6} \right) \pi^2 b_1 \ln \frac{\mu_R^2}{Q^2} + C_F \left(-4 - \frac{\pi^2}{6} \right) \pi^2 b_0^2 \ln^2 \frac{\mu_R^2}{Q^2} \,. \qquad \text{(B.10)}
\end{aligned}
$$

B.2 NEAR-THRESHOLD RESULTS IN x, z-SPACE

Performing a double-inverse Mellin transform of the results given in Eqs. (5.38) and (5.39) we obtain approximate results for the quark-to-quark hard-scattering function $\omega_{qq}^T(\hat{x}, \hat{z}, \alpha_s(\mu_R), \mu_R/Q, \mu_F/Q)$ in Eq. (6.3), valid near threshold. To obtain compact expressions, we introduce the following abbreviations:

$$\begin{aligned}
\delta_x &\equiv \delta(1-\hat{x}), \quad \delta_z \equiv \delta(1-\hat{z}), \\
\mathcal{D}_x^i &\equiv \left[\frac{\ln^i(1-\hat{x})}{1-\hat{x}}\right]_+, \quad \mathcal{D}_z^i \equiv \left[\frac{\ln^i(1-\hat{z})}{1-\hat{z}}\right]_+, \\
\ell_x^i &\equiv \ln^i(1-\hat{x}), \quad \ell_z^i \equiv \ln^i(1-\hat{z}).
\end{aligned} \tag{B.11}$$

We write

$$\begin{aligned}
&\frac{1}{e_q^2}\,\omega_{qq}^T\left(\hat{x}, \hat{z}, \alpha_s, \frac{\mu_R}{Q}, \frac{\mu_F}{Q}\right) \\
&\quad= \delta_x\,\delta_z + \frac{\alpha_s}{\pi}\,C_F\,\Delta_{qq}^{(1)} \\
&\quad+ \left(\frac{\alpha_s}{\pi}\right)^2 C_F\left[C_F\,\Delta_{qq}^{(2),C_F} + C_A\,\Delta_{qq}^{(2),C_A} + N_f\,\Delta_{qq}^{(2),N_f}\right] \\
&\quad+ \left(\frac{\alpha_s}{\pi}\right)^2 \pi b_0\,C_F\,\Delta_{qq}^{(1)}\,\ln\frac{\mu_R^2}{Q^2} + \mathcal{O}(\alpha_s^3).
\end{aligned} \tag{B.12}$$

The NLO term reads

$$\begin{aligned}
\Delta_{qq}^{(1)} &= \delta_x\mathcal{D}_z^1 + \delta_z\mathcal{D}_x^1 + \mathcal{D}_x^0\,\mathcal{D}_z^0 - 4\delta_x\delta_z \\
&- \delta_x\left(\mathcal{D}_z^0 + \frac{3}{4}\delta_z\right)\ln\frac{\mu_F^2}{Q^2} - \delta_z\left(\mathcal{D}_x^0 + \frac{3}{4}\delta_x\right)\ln\frac{\mu_F^2}{Q^2} \\
&- \mathcal{D}_x^0 - \mathcal{D}_z^0 - \delta_x\,\ell_z^1 - \delta_z\,\ell_x^1.
\end{aligned} \tag{B.13}$$

Note that we have included the NLP contributions, which are given in the third line. They show up as terms that carry only a single distribution, in either $\hat{x}$ or $\hat{z}$.

Since the NNLO C_F^2 contribution is quite lengthy, we split it into its LP and NLP contributions and write it as

$$\Delta_{qq}^{(2),C_F} = \Delta_{qq,\mathrm{LP}}^{(2),C_F} + \Delta_{qq,\mathrm{NLP}}^{(2),C_F}. \tag{B.14}$$

We then have for the leading-power part:

$$\begin{aligned}
\Delta^{(2),C_F}_{qq,\mathrm{LP}} &= \frac{1}{2}\left(\delta_x\,\mathcal{D}^3_z+\delta_z\,\mathcal{D}^3_x\right)+\frac{3}{2}\left(\mathcal{D}^0_x\mathcal{D}^2_z+\mathcal{D}^0_z\mathcal{D}^2_x+2\,\mathcal{D}^1_x\mathcal{D}^1_z\right)\\
&- \left(4+\frac{\pi^2}{3}\right)\left(\mathcal{D}^0_x\mathcal{D}^0_z+\delta_x\,\mathcal{D}^1_z+\delta_z\mathcal{D}^1_x\right)+2\zeta(3)\left(\delta_x\,\mathcal{D}^0_z+\delta_z\,\mathcal{D}^0_x\right)\\
&+ \delta_x\,\delta_z\left(\frac{511}{64}-\frac{15\zeta(3)}{4}+\frac{29\pi^2}{48}-\frac{7\pi^4}{360}\right)\\
&+ \Bigg[\delta_x\,\mathcal{D}^1_z+\delta_z\,\mathcal{D}^1_x+\mathcal{D}^0_x\,\mathcal{D}^0_z\\
&\quad+\frac{3}{2}\left(\delta_x\,\mathcal{D}^0_z+\delta_z\,\mathcal{D}^0_x\right)+\delta_x\,\delta_z\left(\frac{9}{8}-\frac{\pi^2}{6}\right)\Bigg]\ln^2\frac{\mu_F^2}{Q^2}\\
&+ \Bigg[-\frac{3}{2}\Big(\delta_x\,\mathcal{D}^2_z+\delta_z\,\mathcal{D}^2_x+2\,\mathcal{D}^0_x\,\mathcal{D}^1_z\\
&\qquad+2\,\mathcal{D}^0_z\,\mathcal{D}^1_x+\mathcal{D}^0_x\,\mathcal{D}^0_z+\delta_x\,\mathcal{D}^1_z+\delta_z\,\mathcal{D}^1_x\Big)\\
&\quad+\left(4+\frac{\pi^2}{3}\right)\left(\delta_x\,\mathcal{D}^0_z+\delta_z\,\mathcal{D}^0_x\right)\\
&\quad+\delta_x\,\delta_z\left(-5\zeta(3)+\frac{\pi^2}{4}+\frac{93}{16}\right)\Bigg]\ln\frac{\mu_F^2}{Q^2}\,,
\end{aligned}\tag{B.15}$$

while the dominant NLP terms are given by

$$\begin{aligned}
\Delta^{(2),C_F}_{qq,\mathrm{NLP}} &= -\frac{3}{2}\left(\mathcal{D}^2_x+\mathcal{D}^2_z+2\,\mathcal{D}^1_x\,\ell^1_z+2\,\mathcal{D}^1_z\,\ell^1_x+\mathcal{D}^0_x\,\ell^2_z+\mathcal{D}^0_z\,\ell^2_x\right)\\
&- \frac{1}{2}\left(\delta_x\,\ell^3_z+\delta_z\,\ell^3_x\right).
\end{aligned}\tag{B.16}$$

The $C_F C_A$ and $C_F N_f$ parts do not possess any dominant NLP contributions (see Eq. (5.39)). They read:

$$\begin{aligned}
\Delta_{qq}^{(2),C_A} &= -\frac{11}{24}\left(\delta_x\,\mathcal{D}_z^2+\delta_z\,\mathcal{D}_x^2+2\,\mathcal{D}_x^0\,\mathcal{D}_z^1+2\,\mathcal{D}_z^0\,\mathcal{D}_x^1\right)\\
&+\left(\frac{67}{36}-\frac{\pi^2}{12}\right)\left(\mathcal{D}_x^0\,\mathcal{D}_z^0+\delta_x\,\mathcal{D}_z^1+\delta_z\,\mathcal{D}_x^1\right)\\
&+\left(\delta_x\,\mathcal{D}_z^0+\delta_z\,\mathcal{D}_x^0\right)\left(\frac{7\zeta(3)}{4}+\frac{11\pi^2}{72}-\frac{101}{54}\right)\\
&+\delta_x\,\delta_z\left(\frac{43\zeta(3)}{12}+\frac{17\pi^4}{720}-\frac{1535}{192}-\frac{269\pi^2}{432}\right)\\
&+\frac{11}{24}\left[\delta_x\,\mathcal{D}_z^0+\delta_z\,\mathcal{D}_x^0+\frac{3}{2}\,\delta_x\,\delta_z\right]\ln^2\frac{\mu_F^2}{Q^2}\\
&+\left[-\left(\delta_x\,\mathcal{D}_z^0+\delta_z\,\mathcal{D}_x^0\right)\left(\frac{67}{36}-\frac{\pi^2}{12}\right)\right.\\
&\qquad\left.+\,\delta_x\,\delta_z\left(\frac{3\zeta(3)}{2}-\frac{11\pi^2}{36}-\frac{17}{48}\right)\right]\ln\frac{\mu_F^2}{Q^2}\,.
\end{aligned}\tag{B.17}$$

and

$$\begin{aligned}
\Delta_{qq}^{(2),N_f} &= \frac{1}{12}\left(\delta_x\,\mathcal{D}_z^2+\delta_z\,\mathcal{D}_x^2+2\,\mathcal{D}_x^0\,\mathcal{D}_z^1+2\,\mathcal{D}_z^0\,\mathcal{D}_x^1\right)\\
&-\frac{5}{18}\left(\mathcal{D}_x^0\,\mathcal{D}_z^0+\delta_x\,\mathcal{D}_z^1+\delta_z\,\mathcal{D}_x^1\right)\\
&+\left(\delta_x\,\mathcal{D}_z^0+\delta_z\,\mathcal{D}_x^0\right)\left(\frac{7}{27}-\frac{\pi^2}{36}\right)\\
&+\delta_x\,\delta_z\left(\frac{\zeta(3)}{6}+\frac{19\pi^2}{216}+\frac{127}{96}\right)\\
&-\frac{1}{12}\left[\delta_x\,\mathcal{D}_z^0+\delta_z\,\mathcal{D}_x^0+\frac{3}{2}\,\delta_x\,\delta_z\right]\ln^2\frac{\mu_F^2}{Q^2}\\
&+\left[\frac{5}{18}\left(\delta_x\,\mathcal{D}_z^0+\delta_z\,\mathcal{D}_x^0\right)+\delta_x\,\delta_z\left(\frac{1}{24}+\frac{\pi^2}{18}\right)\right]\ln\frac{\mu_F^2}{Q^2}\,.
\end{aligned}\tag{B.18}$$

We stress that the results in Eqs. (B.15),(B.17),(B.18) collect *all* double distributions in $\hat{x}$ and $\hat{z}$ that arise at NNLO. We also note that the Mellin-space and the x, z-space expressions near threshold are not strictly identical, but differ by terms that are suppressed near threshold. These terms are generically of the form $\ln^m(\bar{N})/N^2$ or $1/N$ (without logarithms) in Mellin space (and likewise with N replaced by M),

and of the form $(1-\hat{x})\ln^m(1-\hat{x})$ or constant (and also with $\hat{x}$ replaced by $\hat{z}$) in x,z-space.

C

APPENDIX

C.1 DERIVATION OF EQ. (7.27)

Setting $\rho \equiv q_T^2/Q^2$ we consider the expression

$$\begin{aligned}
&\int_x^1 \frac{d\hat{x}}{\hat{x}} \int_z^1 \frac{d\hat{z}}{\hat{z}} \ln(1-\hat{z})\, \delta\left(\rho - \frac{(1-\hat{x})(1-\hat{z})}{\hat{x}\hat{z}}\right) \Delta f\left(\frac{x}{\hat{x}}\right) D\left(\frac{z}{\hat{z}}\right) \\
&= \int_x^{\frac{1-z}{1-z(1-\rho)}} d\hat{x} \left\{ \frac{\ln(1-\hat{z})}{1-\hat{x}(1-\rho)} \Delta f\left(\frac{x}{\hat{x}}\right) D\left(\frac{z}{\hat{z}}\right) \right\}_{\hat{z}=\frac{1-\hat{x}}{1-\hat{x}(1-\rho)}} \\
&= \int_x^{\frac{1-z}{1-z(1-\rho)}} d\hat{x}\, \frac{\ln\left(\frac{\rho\hat{x}}{1-\hat{x}(1-\rho)}\right)}{1-\hat{x}(1-\rho)} \Bigg[\left(\Delta f\left(\frac{x}{\hat{x}}\right) - \Delta f(x)\right) \left(D\left(\frac{z}{\hat{z}}\right) - D(z)\right) \\
&+ D(z)\left(\Delta f\left(\frac{x}{\hat{x}}\right) - \Delta f(x)\right) + \Delta f(x)\left(D\left(\frac{z}{\hat{z}}\right) - D(z)\right) + \Delta f(x)\, D(z) \Bigg]_{\hat{z}=\frac{1-\hat{x}}{1-\hat{x}(1-\rho)}} .
\end{aligned} \tag{C.1}$$

In the second equality we have added and subtracted terms in such a way that four types of contributions arise. The first one with $(\Delta f(x/\hat{x}) - \Delta f(x))\,(D(z/\hat{z}) - D(z))$ is easily seen to vanish for $q_T/Q \to 0$ since $\hat{z} \to 1$ in that limit. The second term becomes, at small ρ:

$$\begin{aligned}
&D(z) \int_x^{\frac{1-z}{1-z(1-\rho)}} d\hat{x}\, \frac{\ln\left(\frac{\rho\hat{x}}{1-\hat{x}(1-\rho)}\right)}{1-\hat{x}(1-\rho)} \left(\Delta f\left(\frac{x}{\hat{x}}\right) - \Delta f(x)\right) \\
&= D(z) \int_x^1 d\hat{x} \left[\left(\frac{\ln\rho - \ln(1-\hat{x})}{1-\hat{x}}\right)_+ + \frac{\ln\hat{x}}{1-\hat{x}} \right] \Delta f\left(\frac{x}{\hat{x}}\right) \\
&+ D(z)\, \Delta f(x) \left(\frac{1}{2}\ln^2(1-x) - \ln\rho\, \ln(1-x) + \mathrm{Li}_2(1-x)\right) + \mathcal{O}(\rho)\,,
\end{aligned} \tag{C.2}$$

where the plus distribution is defined as in Eq. (3.17) and where Li_2 denotes the dilogarithm function. For the third term we go back to $\hat{z}$ as integration variable. We then find

$$\Delta f(x) \int_z^{\frac{1-x}{1-x(1-\rho)}} d\hat{z}\, \frac{\ln(1-\hat{z})}{1-\hat{z}(1-\rho)} \left(D\left(\frac{z}{\hat{z}}\right) - D(z) \right)$$

$$= \Delta f(x) \int_z^1 d\hat{z} \left(\frac{\ln(1-\hat{z})}{1-\hat{z}} \right)_+ D\left(\frac{z}{\hat{z}}\right) - \frac{1}{2} \ln^2(1-z)\, \Delta f(x)\, D(z) + \mathcal{O}(\rho)\,. \quad \text{(C.3)}$$

Finally, for the last term in (C.1) we obtain

$$\Delta f(x)\, D(z) \int_x^{\frac{1-z}{1-z(1-\rho)}} d\hat{x}\, \frac{\ln\left(\frac{\rho\hat{x}}{1-\hat{x}(1-\rho)}\right)}{1-\hat{x}(1-\rho)} = \Delta f(x)\, D(z) \left\{ -\frac{1}{2} \ln^2(\rho) + \ln\rho\, \ln(1-x) \right.$$

$$\left. - \frac{1}{2} \ln^2(1-x) + \frac{1}{2} \ln^2(1-z) - \mathrm{Li}_2(1-x) \right\} + \mathcal{O}(\rho)\,. \quad \text{(C.4)}$$

Combining all terms in (C.2)–(C.4) and expressing them in terms of distributions, we directly recover Eq. (7.27). Note that all terms involving logarithms or dilogarithms of the lower integration limits x, z cancel in the final answer, as they should, since we have defined our plus distributions by integrations from 0 to 1 (see Eq. (3.17)).

C.2 PERTURBATIVE RESULTS FOR THE BEAM-SPIN ASYMMETRY A_{LU}

The cross section for the beam-spin asymmetry A_{LU} may be written as [200]:

$$\frac{d^5\Delta\sigma^h}{dx\, dy\, dz\, dP_{h\perp}^2\, d\phi_h} = \frac{1}{2} \left(\frac{d^5\sigma_+^h}{dx\, dy\, dz\, dP_{h\perp}^2\, d\phi_h} - \frac{d^5\sigma_-^h}{dx\, dy\, dz\, dP_{h\perp}^2\, d\phi_h} \right)$$

$$= \frac{\pi\alpha^2 y}{xQ^2} \sqrt{\frac{2\varepsilon}{1-\varepsilon}}\, F_{LU}^{\sin\phi_h} \sin(\phi_h)\,. \quad \text{(C.5)}$$

As is well-known, there is no term with $\sin(2\phi_h)$ for single-photon exchange. Writing the structure function $F_{LU}^{\sin\phi_h}$ as

$$F_{LU}^{\sin\phi_h} = \left(\frac{\alpha_s(\mu^2)}{2\pi} \right)^2 \frac{x}{Q^2 z^2} \sum_{\substack{a,b \\ = q,\bar{q},g}} \int_x^1 \frac{d\hat{x}}{\hat{x}} \int_z^1 \frac{d\hat{z}}{\hat{z}}\, \Delta f_a\left(\frac{x}{\hat{x}}, \mu^2\right) C_{LU}^{\sin\phi_h, a\to b}(\hat{x}, \hat{z})\, D_b^h\left(\frac{z}{\hat{z}}, \mu^2\right)$$

$$\times\, \delta\left(\frac{q_T^2}{Q^2} - \frac{(1-\hat{x})(1-\hat{z})}{\hat{x}\hat{z}} \right)\,, \quad \text{(C.6)}$$

we have from Refs. [174, 181]:

$$
\begin{aligned}
C_{LU}^{\sin\phi_h,q\to q}(\hat{x},\hat{z}) &= -e_q^2 C_F \left(C_A(1-\hat{x}) - C_F(1-\hat{x}+\hat{z}+\hat{x}\hat{z}) + (C_A - 2C_F)\frac{\hat{z}\ln\hat{z}}{1-\hat{z}} \right) \frac{Q}{q_T}, \\
C_{LU}^{\sin\phi_h,q\to g}(\hat{x},\hat{z}) &= e_q^2 C_F \frac{(1-\hat{z})}{\hat{z}} \Bigg(C_A(1-\hat{x}) + C_F(\hat{x}\hat{z}+\hat{z}-2) \\
&\quad + (C_A - 2C_F)\frac{(1-\hat{z})\ln(1-\hat{z})}{\hat{z}} \Bigg) \frac{Q}{q_T}, \\
C_{LU}^{\sin\phi_h,g\to q}(\hat{x},\hat{z}) &= -e_q^2 (C_A - 2C_F)\frac{1-\hat{x}}{2\hat{z}^2} \Bigg(-\hat{x}\hat{z}(1-2\hat{z}) - (1-\hat{x})\ln(1-\hat{z}) \\
&\quad + (1-\hat{x})\frac{\hat{z}\ln(\hat{z})}{1-\hat{z}} \Bigg) \frac{Q}{q_T}.
\end{aligned}
\tag{C.7}
$$

Carrying out the expansions for low q_T/Q we find, up to corrections of order q_T/Q:

$$
\begin{aligned}
&\left(f_q \otimes C_{LU}^{\sin\phi_h,q\to q} \otimes D_q^h\right)(x,z) \\
&= e_q^2 \frac{Q}{q_T}\frac{C_A}{2} \Bigg\{ -C_F \left(2\ln\left(\frac{q_T^2}{Q^2}\right) + 3 \right) f_q(x)\, D_q^h(z) \\
&+ D_q^h(z) \int_x^1 d\hat{x}\, \delta P_{qq}(\hat{x})\, f_q\left(\frac{x}{\hat{x}}\right) + f_q(x) \int_z^1 d\hat{z}\, \delta P_{qq}(\hat{z})\, D_q^h\left(\frac{z}{\hat{z}}\right) \Bigg\} \\
&- e_q^2 \frac{Q}{q_T}\frac{C_F}{C_A} f_q(x) \int_z^1 d\hat{z}\, \frac{\hat{z}}{1-\hat{z}} \left(1 + \frac{\ln\hat{z}}{1-\hat{z}} \right) D_q^h\left(\frac{z}{\hat{z}}\right), \\
&\left(f_q \otimes C_{LU}^{\sin\phi_h,q\to g} \otimes D_g^h\right)(x,z) \\
&= e_q^2 \frac{Q}{q_T} C_F f_q(x) \int_z^1 d\hat{z}\, \frac{1-\hat{z}}{\hat{z}^2} \left((C_A - 2C_F)\ln(1-\hat{z}) - 2C_F\hat{z} \right) D_g^h\left(\frac{z}{\hat{z}}\right), \\
&\left(f_g \otimes C_{LU}^{\sin\phi_h,g\to q} \otimes D_q^h\right)(x,z)] \\
&= -\frac{e_q^2}{2}\frac{Q}{q_T}(C_A - 2C_F) D_q^h(z) \int_x^1 d\hat{x}\, f_g\left(\frac{x}{\hat{x}}\right) \left[(1-\hat{x})\ln\left(\frac{Q^2}{q_T^2}\right) + (1-\hat{x})\ln\left(\frac{1-\hat{x}}{\hat{x}}\right) + 2x - 1 \right],
\end{aligned}
\tag{C.8}
$$

where the convolution has been defined in (7.23) and the transversity splitting function in (7.25).

ACKNOWLEDGEMENTS

I thank Werner Vogelsang. He is a great teacher who taught me so many things about Physics during my time in his group. His enormous patience and kindness supported me whenever I had difficulties with my work. It was a great pleasure to work with him. The collaboration with him was a very fascinating, exciting and enriching experience. Thank you!

I thank Thomas Gutsche for being a great source of knowledge in physics and for interesting conversations during lunch or coffee breaks about traveling around the world. I thank him as well for being my second supervisor. I thank Daniel de Florian and my friend Fulvio Piacenza for a nice collaboration, Valery Lyubovitskij for always having an open door when I had a question, Marc Schlegel, Marco Stratmann, my office mate Felix Kunzelmann, Patrick, Bommel, Johannes, Markus Loechner, Felix Reichenbach, Fabian Kraus and Daniel. I thank Stefano Forte and Felix Hekhorn for inviting me to Milano which was the only opportunity to travel during my PhD.

In particular I would like to thank Juliane Haug helping me with the NLO computation of SIDIS and Fabian Wunder who I could always bother with questions concerning many different topics of QCD. Both always had an open ear for my questions. I am especially grateful to my friends and colleagues Christoph, Santiagio, Felix Battran, Robin, Oli and Martin from our Jazza Banda! We spend some memorable evenings in the Franz Viertel making music. It was a pleasure to jam with you! I thank Christoph for helping me delve into the world of resummation and with the C++ code I used for the A_{UL} predictions.

I thank Sabine and Ingrid for the office management and their support whenever I was unsure about administrative questions. I thank Susanne Hempel from the Mathematics & Physics Library in the C-building. She is a very kind person and created a warm and welcoming atmosphere which I frequently appreciated during my time at campus Auf der Morgenstelle.

Finally, I thank my beloved Juliette for being a constant support in my life.

BIBLIOGRAPHY

[1] Y. Nagashima, *Elementary Particle Physics: Quantum Field Theory and Particles*. Wiley, 2011, vol. 1. [Online]. Available: https://onlinelibrary.wiley.com/doi/book/10.1002/9783527630097 (visited on Dec. 8, 2022).

[2] Y. Nagashima, *Elementary Particle Physics: Foundations of the Standard Model*. Wiley, 2013, vol. 2. [Online]. Available: https://onlinelibrary.wiley.com/doi/book/10.1002/9783527648887 (visited on Dec. 8, 2022).

[3] F. Halzen and A. D. Martin. 1984, ISBN: 978-0-471-88741-6.

[4] H. Yukawa, *Proc. Phys. Math. Soc. Jap.*, vol. 17, pp. 48–57, 1935.

[5] C. M. G. Lattes, H. Muirhead, G. P. S. Occhialini, and C. F. Powell, *Nature*, vol. 159, pp. 694–697, 1947.

[6] R. Brown, U. Camerini, P. H. Fowler, H. Muirhead, C. F. Powell, and D. M. Ritson, *Nature*, vol. 163, p. 82, 1949.

[7] G. D. Rochester and C. C. Butler, *Nature*, vol. 160, pp. 855–857, 1947.

[8] C. Powell, *Nobel Lectures*, 1950. [Online]. Available: https://www.nobelprize.org/prizes/physics/1950/powell/lecture/ (visited on Dec. 23, 2022).

[9] LBNL, *Introduction to the Detection of Nuclear Particles in a Bubble Chamber*, 7th ed. The Ealing Corporation, 1977.

[10] V. E. Barnes *et al.*, *Phys. Lett.*, vol. 12, pp. 134–136, 1964.

[11] M. Gell-Mann, *Phys. Rev.*, vol. 125, pp. 1067–1084, 1962.

[12] V. E. Barnes *et al.*, *Phys. Rev. Lett.*, vol. 12, pp. 204–206, 1964.

[13] M. Gell-Mann, *Phys. Lett.*, vol. 8, pp. 214–215, 1964.

[14] H. L. Anderson, E. Fermi, E. A. Long, and D. E. Nagle, *Phys. Rev.*, vol. 85, p. 936, 1952.

[15] R. D. Field. 1989, vol. 77, ISBN: 978-0-201-48362-8.

[16] R. L. Workman *et al.*, *PTEP*, vol. 2022, p. 083C01, 2022.

[17] D. de Florian, R. Sassot, M. Stratmann, and W. Vogelsang, *Phys. Rev. Lett.*, vol. 101, p. 072 001, 2008. arXiv: 0804.0422 [hep-ph].

[18] D. de Florian, R. Sassot, M. Stratmann, and W. Vogelsang, *Phys. Rev. D*, vol. 80, p. 034 030, 2009. arXiv: 0904.3821 [hep-ph].

[19] I. Borsa, D. de Florian, R. Sassot, M. Stratmann, and W. Vogelsang, *Phys. Rev. Lett.*, vol. 129, no. 1, p. 012 002, 2022. arXiv: 2202.05060 [hep-ph].

[20] D. P. Anderle, F. Ringer, and W. Vogelsang, *Phys. Rev. D*, vol. 87, no. 3, p. 034 014, 2013. arXiv: 1212.2099 [hep-ph].

[21] D. P. Anderle, F. Ringer, and W. Vogelsang, *Phys. Rev. D*, vol. 87, p. 094 021, 2013. arXiv: 1304.1373 [hep-ph].

[22] R. Hamberg, W. L. van Neerven, and T. Matsuura, *Nucl. Phys. B*, vol. 359, pp. 343–405, 1991, [Erratum: Nucl.Phys.B 644, 403–404 (2002)].

[23] E. B. Zijlstra and W. L. van Neerven, *Nucl. Phys. B*, vol. 383, pp. 525–574, 1992.

[24] P. J. Rijken and W. L. van Neerven, *Nucl. Phys. B*, vol. 487, pp. 233–282, 1997. arXiv: hep-ph/9609377.

[25] M. Abele, M.S. thesis, Tübingen University, 2019.

[26] A. Bacchetta, D. Boer, M. Diehl, and P. J. Mulders, *JHEP*, vol. 08, p. 023, 2008. arXiv: 0803.0227 [hep-ph].

[27] C.-N. Yang and R. L. Mills, *Phys. Rev.*, vol. 96, J.-P. Hsu and D. Fine, Eds., pp. 191–195, 1954.

[28] R. Brock *et al.*, *Rev. Mod. Phys.*, vol. 67, pp. 157–248, 1995. [Online]. Available: https://www.physics.smu.edu/scalise/cteq/handbook/v1.1/handbook.pdf (visited on Jan. 7, 2023).

[29] J. Schwichtenberg, *Physics from Symmetry*, Undergraduate Lecture Notes in Physics. 2018. [Online]. Available: https://link.springer.com/book/10.1007/978-3-319-19201-7 (visited on Dec. 8, 2022).

[30] S. Catani, *Introduction to QCD*, Lecture series for postgraduate students. CERN, 1998. [Online]. Available: http://cds.cern.ch/record/377090 (visited on Dec. 8, 2022).

[31] A. Vogt, *Phys. Lett. B*, vol. 497, pp. 228–234, 2001. arXiv: hep-ph/0010146.

[32] S. Catani, D. de Florian, M. Grazzini, and P. Nason, *JHEP*, vol. 07, p. 028, 2003. arXiv: hep-ph/0306211.

[33] D. J. Gross and F. Wilczek, *Phys. Rev. Lett.*, vol. 30, J. C. Taylor, Ed., pp. 1343–1346, 1973.

[34] H. D. Politzer, *Phys. Rept.*, vol. 14, pp. 129–180, 1974.

[35] P. A. Zyla *et al.*, *PTEP*, vol. 2020, no. 8, p. 083C01, 2020.

[36] G. F. Sterman and S. Weinberg, *Phys. Rev. Lett.*, vol. 39, p. 1436, 1977.

[37] Y. L. Dokshitzer, D. Diakonov, and S. I. Troian, *Phys. Rept.*, vol. 58, pp. 269–395, 1980.

[38] T. Kinoshita, *J. Math. Phys.*, vol. 3, pp. 650–677, 1962.

[39] T. D. Lee and M. Nauenberg, *Phys. Rev.*, vol. 133, G. Feinberg, Ed., B1549–B1562, 1964.

[40] V. V. Sudakov, *Sov. Phys. JETP*, vol. 3, pp. 65–71, 1956.

[41] L. Magnea and G. F. Sterman, *Phys. Rev. D*, vol. 42, pp. 4222–4227, 1990.

[42] R. N. Lee, A. Manteuffel, R. M. Schabinger, A. V. Smirnov, V. A. Smirnov, and M. Steinhauser, *Phys. Rev. Lett.*, vol. 128, no. 21, p. 212 002, 2022. arXiv: 2202.04660 [hep-ph].

[43] G. Kramer and B. Lampe, *Z. Phys. C*, vol. 34, p. 497, 1987, [Erratum: Z.Phys.C 42, 504 (1989)].

[44] T. Matsuura and W. L. van Neerven, *Z. Phys. C*, vol. 38, p. 623, 1988.

[45] T. Matsuura, S. C. van der Marck, and W. L. van Neerven, *Nucl. Phys. B*, vol. 319, pp. 570–622, 1989.

[46] R. V. Harlander, *Phys. Lett. B*, vol. 492, pp. 74–80, 2000. arXiv: hep-ph/0007289.

[47] S. Moch, J. A. M. Vermaseren, and A. Vogt, *JHEP*, vol. 08, p. 049, 2005. arXiv: hep-ph/0507039.

[48] S. Moch, J. A. M. Vermaseren, and A. Vogt, *Phys. Lett. B*, vol. 625, pp. 245–252, 2005. arXiv: hep-ph/0508055.

[49] T. Gehrmann, T. Huber, and D. Maitre, *Phys. Lett. B*, vol. 622, pp. 295–302, 2005. arXiv: hep-ph/0507061.

[50] P. A. Baikov, K. G. Chetyrkin, A. V. Smirnov, V. A. Smirnov, and M. Steinhauser, *Phys. Rev. Lett.*, vol. 102, p. 212 002, 2009. arXiv: 0902.3519 [hep-ph].

[51] T. Gehrmann, E. W. N. Glover, T. Huber, N. Ikizlerli, and C. Studerus, *JHEP*, vol. 06, p. 094, 2010. arXiv: 1004.3653 [hep-ph].

[52] R. N. Lee, A. V. Smirnov, and V. A. Smirnov, *JHEP*, vol. 04, p. 020, 2010. arXiv: 1001.2887 [hep-ph].

[53] J. C. Collins, *Phys. Rev. D*, vol. 22, p. 1478, 1980.

[54] A. Sen, *Phys. Rev. D*, vol. 24, p. 3281, 1981.

[55] G. P. Korchemsky and A. V. Radyushkin, *Nucl. Phys. B*, vol. 283, pp. 342–364, 1987.

[56] L. Magnea, *Nucl. Phys. B*, vol. 593, pp. 269–288, 2001. arXiv: hep-ph/0006255.

[57] G. Altarelli, R. K. Ellis, and G. Martinelli, *Nucl. Phys. B*, vol. 157, pp. 461–497, 1979.

[58] J. Kubar-Andre and F. E. Paige, *Phys. Rev. D*, vol. 19, p. 221, 1979.

[59] K. Harada, T. Kaneko, and N. Sakai, *Nucl. Phys. B*, vol. 155, pp. 169–188, 1979, [Erratum: Nucl.Phys.B 165, 545 (1980)].

[60] J. C. Collins, *Perturbative Quantum Chromodynamics*, Advanced Series on Directions in High Energy Physics, A. H. Mueller, Ed. 1989, vol. 5.

[61] G. Altarelli, R. K. Ellis, G. Martinelli, and S.-Y. Pi, *Nucl. Phys. B*, vol. 160, pp. 301–329, 1979.

[62] W. Furmanski and R. Petronzio, *Z. Phys. C*, vol. 11, p. 293, 1982.

[63] D. de Florian, M. Stratmann, and W. Vogelsang, in *Workshop on Physics with Polarized Protons at Hera: 1st Meeting*, Oct. 1997. arXiv: hep-ph/9710410.

[64] D. de Florian, M. Stratmann, and W. Vogelsang, *Phys. Rev. D*, vol. 57, pp. 5811–5824, 1998. arXiv: hep-ph/9711387.

[65] P. Nason and B. R. Webber, *Nucl. Phys. B*, vol. 421, pp. 473–517, 1994, [Erratum: Nucl.Phys.B 480, 755 (1996)].

[66] D. Graudenz, *Nucl. Phys. B*, vol. 432, pp. 351–376, 1994. arXiv: hep-ph/9406274.

[67] D. de Florian and Y. Rotstein Habarnau, *Eur. Phys. J. C*, vol. 73, no. 3, p. 2356, 2013. arXiv: 1210.7203 [hep-ph].

[68] R. P. Feynman, *Phys. Rev. Lett.*, vol. 23, L. M. Brown, Ed., pp. 1415–1417, 1969.

[69] J. D. Bjorken and E. A. Paschos, *Phys. Rev.*, vol. 185, pp. 1975–1982, 1969.

[70] J. D. Bjorken, *Phys. Rev.*, vol. 179, pp. 1547–1553, 1969.

[71] J. C. Collins, D. E. Soper, and G. F. Sterman, *Adv. Ser. Direct. High Energy Phys.*, vol. 5, pp. 1–91, 1989. arXiv: hep-ph/0409313.

[72] J. Haug, M.S. thesis, Tübingen University, 2021.

[73] G. Altarelli and G. Parisi, *Nucl. Phys. B*, vol. 126, pp. 298–318, 1977.

[74] M. A. Ahmed and G. G. Ross, *Nucl. Phys. B*, vol. 111, pp. 441–460, 1976.

[75] R. Mertig and W. L. van Neerven, *Z. Phys. C*, vol. 70, pp. 637–654, 1996. arXiv: hep-ph/9506451.

[76] W. Vogelsang, *Phys. Rev. D*, vol. 54, pp. 2023–2029, 1996. arXiv: hep-ph/9512218.

[77] W. Vogelsang, *Nucl. Phys. B*, vol. 475, pp. 47–72, 1996. arXiv: hep-ph/9603366.

[78] M. S. Chanowitz, M. Furman, and I. Hinchliffe, *Nucl. Phys. B*, vol. 159, pp. 225–243, 1979.

[79] G. 't Hooft and M. J. G. Veltman, *Nucl. Phys. B*, vol. 44, pp. 189–213, 1972.

[80] P. Breitenlohner and D. Maison, *Commun. Math. Phys.*, vol. 52, pp. 11–38, 1977.

[81] W. Furmanski and R. Petronzio, *Phys. Lett. B*, vol. 97, pp. 437–442, 1980.

[82] G. Curci, W. Furmanski, and R. Petronzio, *Nucl. Phys. B*, vol. 175, pp. 27–92, 1980.

[83] E. G. Floratos, C. Kounnas, and R. Lacaze, *Nucl. Phys. B*, vol. 192, pp. 417–462, 1981.

[84] S. Moch, J. A. M. Vermaseren, and A. Vogt, *Nucl. Phys. B*, vol. 889, pp. 351–400, 2014. arXiv: 1409.5131 [hep-ph].

[85] S. Moch, J. A. M. Vermaseren, and A. Vogt, *Nucl. Phys. B*, vol. 688, pp. 101–134, 2004. arXiv: hep-ph/0403192.

[86] A. Vogt, S. Moch, and J. A. M. Vermaseren, *Nucl. Phys. B*, vol. 691, pp. 129–181, 2004. arXiv: hep-ph/0404111.

[87] S. Moch, B. Ruijl, T. Ueda, J. A. M. Vermaseren, and A. Vogt, *JHEP*, vol. 10, p. 041, 2017. arXiv: 1707.08315 [hep-ph].

[88] S. Moch, B. Ruijl, T. Ueda, J. A. M. Vermaseren, and A. Vogt, *Phys. Lett. B*, vol. 825, p. 136853, 2022. arXiv: 2111.15561 [hep-ph].

[89] G. F. Sterman and W. Vogelsang, *Phys. Rev. D*, vol. 74, p. 114002, 2006. arXiv: hep-ph/0606211.

[90] G. F. Sterman, *AIP Conf. Proc.*, vol. 74, D. W. Duke and J. F. Owens, Eds., pp. 22–40, 1981.

[91] J. G. M. Gatheral, *Phys. Lett. B*, vol. 133, pp. 90–94, 1983.

[92] J. Frenkel and J. C. Taylor, *Nucl. Phys. B*, vol. 246, pp. 231–245, 1984.

[93] C. F. Berger, Other thesis, May 2003. arXiv: hep-ph/0305076.

[94] E. Laenen, G. F. Sterman, and W. Vogelsang, *Phys. Rev. D*, vol. 63, p. 114018, 2001. arXiv: hep-ph/0010080.

[95] M. Stratmann and W. Vogelsang, *Phys. Rev. D*, vol. 64, p. 114007, 2001. arXiv: hep-ph/0107064.

[96] G. F. Sterman, *Nucl. Phys. B*, vol. 281, pp. 310–364, 1987.

[97] E. Laenen, G. F. Sterman, and W. Vogelsang, *Phys. Rev. Lett.*, vol. 84, pp. 4296–4299, 2000. arXiv: hep-ph/0002078.

[98] S. Catani, M. L. Mangano, P. Nason, and L. Trentadue, *Nucl. Phys. B*, vol. 478, pp. 273–310, 1996. arXiv: hep-ph/9604351.

[99] P. Hinderer, F. Ringer, G. Sterman, and W. Vogelsang, *Phys. Rev. D*, vol. 99, no. 5, p. 054 019, 2019. arXiv: 1812.00915 [hep-ph].

[100] S. Catani, L. Cieri, D. de Florian, G. Ferrera, and M. Grazzini, *Nucl. Phys. B*, vol. 888, pp. 75–91, 2014. arXiv: 1405.4827 [hep-ph].

[101] V. Ravindran, J. Smith, and W. L. van Neerven, *Nucl. Phys. B*, vol. 767, pp. 100–129, 2007. arXiv: hep-ph/0608308.

[102] S. Catani and L. Trentadue, *Nucl. Phys. B*, vol. 327, pp. 323–352, 1989.

[103] H. Contopanagos, E. Laenen, and G. F. Sterman, *Nucl. Phys. B*, vol. 484, pp. 303–330, 1997. arXiv: hep-ph/9604313.

[104] S. Catani, M. L. Mangano, and P. Nason, *JHEP*, vol. 07, p. 024, 1998. arXiv: hep-ph/9806484.

[105] R. Baier and K. Fey, *Z. Phys. C*, vol. 2, pp. 339–349, 1979.

[106] S. Moch and A. Vogt, *Phys. Lett. B*, vol. 680, pp. 239–246, 2009. arXiv: 0908.2746 [hep-ph].

[107] G. Lustermans, J. K. L. Michel, and F. J. Tackmann, Aug. 2019. arXiv: 1908.00985 [hep-ph].

[108] L. De Ros, M.S. thesis, Università di Milano, 2022.

[109] D. de Florian, M. Epele, R. J. Hernandez-Pinto, R. Sassot, and M. Stratmann, *Phys. Rev. D*, vol. 95, no. 9, p. 094 019, 2017. arXiv: 1702.06353 [hep-ph].

[110] D. P. Anderle, T. Kaufmann, M. Stratmann, and F. Ringer, *Phys. Rev. D*, vol. 95, no. 5, p. 054 003, 2017. arXiv: 1611.03371 [hep-ph].

[111] E. Leader, A. V. Sidorov, and D. B. Stamenov, *Phys. Rev. D*, vol. 93, no. 7, p. 074 026, 2016. arXiv: 1506.06381 [hep-ph].

[112] V. Bertone, N. P. Hartland, E. R. Nocera, J. Rojo, and L. Rottoli, *Eur. Phys. J. C*, vol. 78, no. 8, p. 651, 2018. arXiv: 1807.03310 [hep-ph].

[113] R. A. Khalek, V. Bertone, and E. R. Nocera, *Phys. Rev. D*, vol. 104, no. 3, p. 034 007, 2021. arXiv: 2105.08725 [hep-ph].

[114] D. De Florian, G. A. Lucero, R. Sassot, M. Stratmann, and W. Vogelsang, *Phys. Rev. D*, vol. 100, no. 11, p. 114 027, 2019. arXiv: 1902.10548 [hep-ph].

[115] J. J. Ethier, N. Sato, and W. Melnitchouk, *Phys. Rev. Lett.*, vol. 119, no. 13, p. 132 001, 2017. arXiv: 1705.05889 [hep-ph].

[116] E. Moffat, W. Melnitchouk, T. C. Rogers, and N. Sato, *Phys. Rev. D*, vol. 104, no. 1, p. 016 015, 2021. arXiv: 2101.04664 [hep-ph].

[117] A. Daleo, C. A. Garcia Canal, and R. Sassot, *Nucl. Phys. B*, vol. 662, pp. 334–358, 2003. arXiv: hep-ph/0303199.

[118] A. Daleo and R. Sassot, *Nucl. Phys. B*, vol. 673, pp. 357–384, 2003. arXiv: hep-ph/0309073.

[119] D. Anderle, D. de Florian, and Y. Rotstein Habarnau, *Phys. Rev. D*, vol. 95, no. 3, p. 034 027, 2017. arXiv: 1612.01293 [hep-ph].

[120] R. Abdul Khalek *et al.*, Mar. 2021. arXiv: 2103.05419 [physics.ins-det].

[121] M. Cacciari and S. Catani, *Nucl. Phys. B*, vol. 617, pp. 253–290, 2001. arXiv: hep-ph/0107138.

[122] D. Westmark and J. F. Owens, *Phys. Rev. D*, vol. 95, no. 5, p. 056 024, 2017. arXiv: 1701.06716 [hep-ph].

[123] P. Banerjee, G. Das, P. K. Dhani, and V. Ravindran, *Phys. Rev. D*, vol. 98, no. 5, p. 054 018, 2018. arXiv: 1805.01186 [hep-ph].

[124] S. Catani, L. Cieri, D. de Florian, G. Ferrera, and M. Grazzini, *Nucl. Phys. B*, vol. 881, pp. 414–443, 2014. arXiv: 1311.1654 [hep-ph].

[125] M. Kramer, E. Laenen, and M. Spira, *Nucl. Phys. B*, vol. 511, pp. 523–549, 1998. arXiv: hep-ph/9611272.

[126] R. Akhoury, M. G. Sotiropoulos, and G. F. Sterman, in *6th International Workshop on Deep Inelastic Scattering and QCD (DIS 98)*, Jun. 1998, pp. 774–776. arXiv: hep-ph/9806388.

[127] A. Kulesza, G. F. Sterman, and W. Vogelsang, *Phys. Rev. D*, vol. 66, p. 014 011, 2002. arXiv: hep-ph/0202251.

[128] H. Shimizu, G. F. Sterman, W. Vogelsang, and H. Yokoya, *Phys. Rev. D*, vol. 71, p. 114 007, 2005. arXiv: hep-ph/0503270.

[129] E. Laenen, L. Magnea, and G. Stavenga, *Phys. Lett. B*, vol. 669, pp. 173–179, 2008. arXiv: 0807.4412 [hep-ph].

[130] G. Grunberg and V. Ravindran, *JHEP*, vol. 10, p. 055, 2009. arXiv: 0902.2702 [hep-ph].

[131] E. Laenen, L. Magnea, G. Stavenga, and C. D. White, *JHEP*, vol. 01, p. 141, 2011. arXiv: 1010.1860 [hep-ph].

[132] D. Bonocore, E. Laenen, L. Magnea, L. Vernazza, and C. D. White, *Phys. Lett. B*, vol. 742, pp. 375–382, 2015. arXiv: 1410.6406 [hep-ph].

[133] D. Bonocore, E. Laenen, L. Magnea, S. Melville, L. Vernazza, and C. D. White, *JHEP*, vol. 06, p. 008, 2015. arXiv: 1503.05156 [hep-ph].

[134] S. Moch and A. Vogt, *JHEP*, vol. 04, p. 081, 2009. arXiv: 0902.2342 [hep-ph].

[135] A. Vogt, *Phys. Lett. B*, vol. 691, pp. 77–81, 2010. arXiv: 1005.1606 [hep-ph].

[136] A. A. Almasy, G. Soar, and A. Vogt, *JHEP*, vol. 03, p. 030, 2011. arXiv: 1012.3352 [hep-ph].

[137] N. A. Lo Presti, A. A. Almasy, and A. Vogt, *Phys. Lett. B*, vol. 737, pp. 120–123, 2014. arXiv: 1407.1553 [hep-ph].

[138] A. A. Almasy, N. A. Lo Presti, and A. Vogt, *JHEP*, vol. 01, p. 028, 2016. arXiv: 1511.08612 [hep-ph].

[139] V. Del Duca, E. Laenen, L. Magnea, L. Vernazza, and C. D. White, *JHEP*, vol. 11, p. 057, 2017. arXiv: 1706.04018 [hep-ph].

[140] I. Moult, I. W. Stewart, G. Vita, and H. X. Zhu, *JHEP*, vol. 08, p. 013, 2018. arXiv: 1804.04665 [hep-ph].

[141] M. A. Ebert, I. Moult, I. W. Stewart, F. J. Tackmann, G. Vita, and H. X. Zhu, *JHEP*, vol. 04, p. 123, 2019. arXiv: 1812.08189 [hep-ph].

[142] N. Bahjat-Abbas, D. Bonocore, J. Sinninghe Damsté, E. Laenen, L. Magnea, L. Vernazza, and C. D. White, *JHEP*, vol. 11, p. 002, 2019. arXiv: 1905.13710 [hep-ph].

[143] M. van Beekveld, W. Beenakker, R. Basu, E. Laenen, A. Misra, and P. Motylinski, *Phys. Rev. D*, vol. 100, no. 5, p. 056 009, 2019. arXiv: 1905.11771 [hep-ph].

[144] M. van Beekveld, W. Beenakker, E. Laenen, and C. D. White, *JHEP*, vol. 03, p. 106, 2020. arXiv: 1905.08741 [hep-ph].

[145] A. H. Ajjath, P. Mukherjee, and V. Ravindran, *Phys. Rev. D*, vol. 105, no. 9, p. 094 035, 2022. arXiv: 2006.06726 [hep-ph].

[146] A. H. Ajjath, P. Mukherjee, V. Ravindran, A. Sankar, and S. Tiwari, *JHEP*, vol. 04, p. 131, 2021. arXiv: 2007.12214 [hep-ph].

[147] A. H. Ajjath, P. Mukherjee, V. Ravindran, A. Sankar, and S. Tiwari, *Phys. Rev. D*, vol. 103, p. L111502, 2021. arXiv: 2010.00079 [hep-ph].

[148] A. H. Ajjath, P. Mukherjee, V. Ravindran, A. Sankar, and S. Tiwari, *Eur. Phys. J. C*, vol. 82, no. 3, p. 234, 2022. arXiv: 2107.09717 [hep-ph].

[149] M. Beneke, A. Broggio, S. Jaskiewicz, and L. Vernazza, *JHEP*, vol. 07, p. 078, 2020. arXiv: 1912.01585 [hep-ph].

[150] A. Broggio, S. Jaskiewicz, and L. Vernazza, *JHEP*, vol. 10, p. 061, 2021. arXiv: 2107.07353 [hep-ph].

[151] Z. L. Liu, B. Mecaj, M. Neubert, and X. Wang, *Phys. Rev. D*, vol. 104, no. 1, p. 014 004, 2021. arXiv: 2009.04456 [hep-ph].

[152] C. Anastasiou, L. J. Dixon, K. Melnikov, and F. Petriello, *Phys. Rev. D*, vol. 69, p. 094 008, 2004. arXiv: hep-ph/0312266.

[153] C. Anastasiou, L. J. Dixon, K. Melnikov, and F. Petriello, *Phys. Rev. Lett.*, vol. 91, p. 182 002, 2003. arXiv: hep-ph/0306192.

[154] S. Catani, L. Cieri, G. Ferrera, D. de Florian, and M. Grazzini, *Phys. Rev. Lett.*, vol. 103, p. 082 001, 2009. arXiv: 0903.2120 [hep-ph].

[155] R. Gavin, Y. Li, F. Petriello, and S. Quackenbush, *Comput. Phys. Commun.*, vol. 182, pp. 2388–2403, 2011. arXiv: 1011.3540 [hep-ph].

[156] X. Chen, T. Gehrmann, N. Glover, A. Huss, T.-Z. Yang, and H. X. Zhu, *Phys. Rev. Lett.*, vol. 128, no. 5, p. 052 001, 2022. arXiv: 2107.09085 [hep-ph].

[157] T.-J. Hou *et al.*, *Phys. Rev. D*, vol. 103, no. 1, p. 014 013, 2021. arXiv: 1912.10053 [hep-ph].

[158] H. Abdolmaleki, M. Soleymaninia, H. Khanpour, S. Amoroso, F. Giuli, A. Glazov, A. Luszczak, F. Olness, and O. Zenaiev, *Phys. Rev. D*, vol. 104, no. 5, p. 056 019, 2021. arXiv: 2105.11306 [hep-ph].

[159] E. Leader, A. V. Sidorov, and D. B. Stamenov, *Phys. Rev. D*, vol. 82, p. 114 018, 2010. arXiv: 1010.0574 [hep-ph].

[160] D. de Florian, R. Sassot, M. Epele, R. J. Hernández-Pinto, and M. Stratmann, *Phys. Rev. D*, vol. 91, no. 1, p. 014 035, 2015. arXiv: 1410.6027 [hep-ph].

[161] V. Bertone, S. Carrazza, N. P. Hartland, E. R. Nocera, and J. Rojo, *Eur. Phys. J. C*, vol. 77, no. 8, p. 516, 2017. arXiv: 1706.07049 [hep-ph].

[162] I. Borsa, D. de Florian, R. Sassot, and M. Stratmann, *Phys. Rev. D*, vol. 105, no. 3, p. L031502, 2022. arXiv: 2110.14015 [hep-ph].

[163] E. C. Aschenauer, I. Borsa, R. Sassot, and C. Van Hulse, *Phys. Rev. D*, vol. 99, no. 9, p. 094 004, 2019. arXiv: 1902.10663 [hep-ph].

[164] S. Moch, J. A. M. Vermaseren, and A. Vogt, *Nucl. Phys. B*, vol. 726, pp. 317–335, 2005. arXiv: hep-ph/0506288.

[165] M. Grosse Perdekamp and F. Yuan, *Ann. Rev. Nucl. Part. Sci.*, vol. 65, pp. 429–456, 2015. arXiv: 1510.06783 [hep-ph].

[166] D. W. Sivers, *Phys. Rev. D*, vol. 41, p. 83, 1990.

[167] S. J. Brodsky, D. S. Hwang, and I. Schmidt, *Phys. Lett. B*, vol. 530, pp. 99–107, 2002. arXiv: hep-ph/0201296.

[168] J. C. Collins, *Phys. Lett. B*, vol. 536, pp. 43–48, 2002. arXiv: hep-ph/0204004.

[169] A. De Rujula, J. M. Kaplan, and E. De Rafael, *Nucl. Phys. B*, vol. 35, pp. 365–389, 1971.

[170] A. De Rujula, R. Petronzio, and B. E. Lautrup, *Nucl. Phys. B*, vol. 146, pp. 50–62, 1978.

[171] K. Fabricius, I. Schmitt, G. Kramer, and G. Schierholz, *Phys. Rev. Lett.*, vol. 45, p. 867, 1980.

[172] J. G. Körner, G. Kramer, G. Schierholz, K. Fabricius, and I. Schmitt, *Phys. Lett. B*, vol. 94, pp. 207–210, 1980.

[173] K. Hagiwara, K.-i. Hikasa, and N. Kai, *Phys. Rev. Lett.*, vol. 47, p. 983, 1981.

[174] K. Hagiwara, K.-i. Hikasa, and N. Kai, *Phys. Rev. D*, vol. 27, p. 84, 1983.

[175] B. Pire and J. P. Ralston, *Phys. Rev. D*, vol. 28, p. 260, 1983.

[176] K. Hagiwara, K.-i. Hikasa, and N. Kai, *Phys. Rev. Lett.*, vol. 52, p. 1076, 1984.

[177] A. Bilal, E. Masso, and A. De Rujula, *Nucl. Phys. B*, vol. 355, pp. 549–602, 1991.

[178] R. D. Carlitz and R. S. Willey, *Phys. Rev. D*, vol. 45, pp. 2323–2348, 1992.

[179] A. Brandenburg, L. J. Dixon, and Y. Shadmi, *Phys. Rev. D*, vol. 53, pp. 1264–1281, 1996. arXiv: hep-ph/9505355.

[180] M. Ahmed and T. Gehrmann, *Phys. Lett. B*, vol. 465, pp. 297–302, 1999. arXiv: hep-ph/9906503.

[181] J. G. Körner, B. Melic, and Z. Merebashvili, *Phys. Rev. D*, vol. 62, p. 096 011, 2000. arXiv: hep-ph/0002302.

[182] K. Hagiwara, K. Mawatari, and H. Yokoya, *JHEP*, vol. 12, p. 041, 2007. arXiv: 0707.3194 [hep-ph].

[183] R. Frederix, K. Hagiwara, T. Yamada, and H. Yokoya, *Phys. Rev. Lett.*, vol. 113, p. 152 001, 2014. arXiv: 1407.1016 [hep-ph].

[184] S. Benic, Y. Hatta, H.-n. Li, and D.-J. Yang, *Phys. Rev. D*, vol. 100, no. 9, p. 094 027, 2019. arXiv: 1909.10684 [hep-ph].

[185] S. Benić, Y. Hatta, A. Kaushik, and H.-n. Li, *Phys. Rev. D*, vol. 104, no. 9, p. 094 027, 2021. arXiv: 2109.05440 [hep-ph].

[186] M. Aicher, Ph.D. dissertation, Regensburg University, 2011. [Online]. Available: https://epub.uni-regensburg.de/21656/.

[187] F. Piacenza, Ph.D. dissertation, Pavia University, 2020. [Online]. Available: http://hdl.handle.net/11571/1318351.

[188] J.-w. Qiu and G. F. Sterman, *Phys. Rev. D*, vol. 59, p. 014 004, 1999. arXiv: hep-ph/9806356.

[189] A. Airapetian *et al.*, *Phys. Rev. Lett.*, vol. 84, pp. 4047–4051, 2000. arXiv: hep-ex/9910062.

[190] A. Airapetian *et al.*, *Phys. Rev. D*, vol. 64, p. 097 101, 2001. arXiv: hep-ex/0104005.

[191] A. Airapetian *et al.*, *Phys. Lett. B*, vol. 562, pp. 182–192, 2003. arXiv: hep-ex/0212039.

[192] A. Airapetian *et al.*, *Phys. Lett. B*, vol. 622, pp. 14–22, 2005. arXiv: hep-ex/0505042.

[193] H. Avakian *et al.*, *Phys. Rev. Lett.*, vol. 105, p. 262 002, 2010. arXiv: 1003.4549 [hep-ex].

[194] M. G. Alekseev *et al.*, *Eur. Phys. J. C*, vol. 70, pp. 39–49, 2010. arXiv: 1007.1562 [hep-ex].

[195] I. A. Savin, *J. Phys. Conf. Ser.*, vol. 678, no. 1, p. 012 063, 2016.

[196] C. Adolph *et al.*, *Eur. Phys. J. C*, vol. 78, no. 11, p. 952, 2018, [Erratum: Eur.Phys.J.C 80, 298 (2020)]. arXiv: 1609.06062 [hep-ex].

[197] T. C. Rogers, *Eur. Phys. J. A*, vol. 52, no. 6, p. 153, 2016. arXiv: 1509.04766 [hep-ph].

[198] R. Angeles-Martinez *et al.*, *Acta Phys. Polon. B*, vol. 46, no. 12, pp. 2501–2534, 2015. arXiv: 1507.05267 [hep-ph].

[199] A. Bacchetta, P. J. Mulders, and F. Pijlman, *Phys. Lett. B*, vol. 595, pp. 309–317, 2004. arXiv: hep-ph/0405154.

[200] A. Bacchetta, M. Diehl, K. Goeke, A. Metz, P. J. Mulders, and M. Schlegel, *JHEP*, vol. 02, p. 093, 2007. arXiv: hep-ph/0611265.

[201] M. Boglione and P. J. Mulders, *Phys. Lett. B*, vol. 478, pp. 114–120, 2000. arXiv: hep-ph/0001196.

[202] B.-Q. Ma, I. Schmidt, and J.-J. Yang, *Phys. Rev. D*, vol. 63, p. 037 501, 2001. arXiv: hep-ph/0009297.

[203] B.-Q. Ma, I. Schmidt, and J.-J. Yang, *Phys. Rev. D*, vol. 65, p. 034 010, 2002. arXiv: hep-ph/0110324.

[204] A. V. Efremov, K. Goeke, and P. Schweitzer, *Phys. Lett. B*, vol. 568, pp. 63–72, 2003. arXiv: hep-ph/0303062.

[205] S. Boffi, A. V. Efremov, B. Pasquini, and P. Schweitzer, *Phys. Rev. D*, vol. 79, p. 094 012, 2009. arXiv: 0903.1271 [hep-ph].

[206] J. Zhu and B.-Q. Ma, *Phys. Lett. B*, vol. 696, pp. 246–251, 2011. arXiv: 1104.4564 [hep-ph].

[207] Z. Lu, B.-Q. Ma, and J. She, *Phys. Rev. D*, vol. 84, p. 034 010, 2011. arXiv: 1104.5410 [hep-ph].

[208] H. Li and Z. Lu, Nov. 2021. arXiv: 2111.03840 [hep-ph].

[209] F. Yuan, *Phys. Lett. B*, vol. 589, pp. 28–34, 2004. arXiv: hep-ph/0310279.

[210] A. V. Afanasev and C. E. Carlson, *Phys. Rev. D*, vol. 74, p. 114 027, 2006. arXiv: hep-ph/0603269.

[211] X. Ji, J.-W. Qiu, W. Vogelsang, and F. Yuan, *Phys. Rev. Lett.*, vol. 97, p. 082 002, 2006. arXiv: hep-ph/0602239.

[212] X. Ji, J.-W. Qiu, W. Vogelsang, and F. Yuan, *Phys. Lett. B*, vol. 638, pp. 178–186, 2006. arXiv: hep-ph/0604128.

[213] F. Yuan and J. Zhou, *Phys. Rev. Lett.*, vol. 103, p. 052 001, 2009. arXiv: 0903.4680 [hep-ph].

[214] K. Kanazawa, Y. Koike, A. Metz, D. Pitonyak, and M. Schlegel, *Phys. Rev. D*, vol. 93, no. 5, p. 054 024, 2016. arXiv: 1512.07233 [hep-ph].

[215] I. Scimemi, A. Tarasov, and A. Vladimirov, *JHEP*, vol. 05, p. 125, 2019. arXiv: 1901.04519 [hep-ph].

[216] V. Moos and A. Vladimirov, *JHEP*, vol. 12, p. 145, 2020. arXiv: 2008.01744 [hep-ph].

[217] A. Vladimirov, V. Moos, and I. Scimemi, *JHEP*, vol. 01, p. 110, 2022. arXiv: 2109.09771 [hep-ph].

[218] I. Scimemi and A. Vladimirov, *Eur. Phys. J. C*, vol. 78, no. 10, p. 802, 2018. arXiv: 1804.08148 [hep-ph].

[219] M. A. Ebert, A. Gao, and I. W. Stewart, *JHEP*, vol. 06, p. 007, 2022. arXiv: 2112.07680 [hep-ph].

[220] S. Rodini and A. Vladimirov, Apr. 2022. arXiv: 2204.03856 [hep-ph].

[221] M. Diehl and S. Sapeta, *Eur. Phys. J. C*, vol. 41, pp. 515–533, 2005. arXiv: hep-ph/0503023.

[222] A. Mendez, *Nucl. Phys. B*, vol. 145, pp. 199–220, 1978.

[223] G. Karpman, R. Leonardi, and F. Strocchi, *Phys. Rev.*, vol. 174, pp. 1957–1968, 1968.

[224] F. Cannata, R. Leonardi, and F. Strocchi, *Phys. Rev. D*, vol. 1, pp. 191–199, 1970.

[225] M. Jamin and M. E. Lautenbacher, *Comput. Phys. Commun.*, vol. 74, pp. 265–288, 1993.

[226] H. H. Patel, *Comput. Phys. Commun.*, vol. 218, pp. 66–70, 2017. arXiv: 1612.00009 [hep-ph].

[227] S. Wandzura and F. Wilczek, *Phys. Lett. B*, vol. 72, pp. 195–198, 1977.

[228] R.-b. Meng, F. I. Olness, and D. E. Soper, *Nucl. Phys. B*, vol. 371, pp. 79–110, 1992.

[229] R. Meng, F. I. Olness, and D. E. Soper, *Phys. Rev. D*, vol. 54, pp. 1919–1935, 1996. arXiv: hep-ph/9511311.

[230] D. Boer and W. Vogelsang, *Phys. Rev. D*, vol. 74, p. 014 004, 2006. arXiv: hep-ph/0604177.

[231] A. Daleo, D. de Florian, and R. Sassot, *Phys. Rev. D*, vol. 71, p. 034 013, 2005. arXiv: hep-ph/0411212.

[232] B. A. Kniehl, G. Kramer, and M. Maniatis, *Nucl. Phys. B*, vol. 711, pp. 345–366, 2005, [Erratum: Nucl.Phys.B 720, 231 (2005)]. arXiv: hep-ph/0411300.

[233] B. Wang, J. O. Gonzalez-Hernandez, T. C. Rogers, and N. Sato, *Phys. Rev. D*, vol. 99, no. 9, p. 094 029, 2019. arXiv: 1903.01529 [hep-ph].

[234] R. D. Ball *et al.*, *Eur. Phys. J. C*, vol. 77, no. 10, p. 663, 2017. arXiv: 1706.00428 [hep-ph].

[235] A. Buckley, J. Ferrando, S. Lloyd, K. Nordström, B. Page, M. Rüfenacht, M. Schönherr, and G. Watt, *Eur. Phys. J. C*, vol. 75, p. 132, 2015. arXiv: 1412.7420 [hep-ph].

[236] V. Barone, A. Prokudin, and B.-Q. Ma, *Phys. Rev. D*, vol. 78, p. 045 022, 2008. arXiv: 0804.3024 [hep-ph].

[237] R. K. Ellis, W. J. Stirling, and B. R. Webber. Cambridge University Press, Feb. 2011, vol. 8, ISBN: 978-0-511-82328-2, 978-0-521-54589-1.

[238] G. Altarelli, *Collider Physics within the Standard Model*, Lectures Notes in Physics, J. Wells, Ed. Springer, 2017, vol. 937. [Online]. Available: https://link.springer.com/book/10.1007/978-3-319-51920-3 (visited on Dec. 8, 2022).

[239] T. van Ritbergen, J. A. M. Vermaseren, and S. A. Larin, *Phys. Lett. B*, vol. 400, pp. 379–384, 1997. arXiv: hep-ph/9701390.

[240] J. Kodaira and L. Trentadue, *Phys. Lett. B*, vol. 123, pp. 335–338, 1983.

[241] R. V. Harlander and W. B. Kilgore, *Phys. Rev. D*, vol. 64, p. 013 015, 2001. arXiv: hep-ph/0102241.

[242] T. O. Eynck, E. Laenen, and L. Magnea, *JHEP*, vol. 06, p. 057, 2003. arXiv: hep-ph/0305179.

[243] S. Moch, B. Ruijl, T. Ueda, J. A. M. Vermaseren, and A. Vogt, *Phys. Lett. B*, vol. 782, pp. 627–632, 2018. arXiv: 1805.09638 [hep-ph].

[244] A. von Manteuffel, E. Panzer, and R. M. Schabinger, *Phys. Rev. Lett.*, vol. 124, no. 16, p. 162 001, 2020. arXiv: 2002.04617 [hep-ph].

[245] J. M. Henn, G. P. Korchemsky, and B. Mistlberger, *JHEP*, vol. 04, p. 018, 2020. arXiv: 1911.10174 [hep-th].

[246] S. Catani, D. de Florian, and M. Grazzini, *JHEP*, vol. 05, p. 025, 2001. arXiv: hep-ph/0102227.

COLOPHON

This document was typeset using the typographical look-and-feel `classicthesis` developed by André Miede. The style was inspired by Robert Bringhurst's seminal book on typography "*The Elements of Typographic Style*". `classicthesis` is available for both LaTeX and LyX:

https://bitbucket.org/amiede/classicthesis/

Final Version as of September 9, 2023 (`classicthesis` version 4.1).